EXPLORING ASTROCYTES IN THE MOUSE LATERAL SEPTUM: DECIPHERING SEX RELATED ASTROCYTE CONTRIBUTION TO SOCIAL FEAR

DISSERTATION ZUR ERLANGUNG DES DOKTORGRADES DER NATURWISSENSCHAFTEN (DR. RER. NAT.) DER FAKULTÄT FÜR BIOLOGIE UND VORKLINISCHE MEDIZIN DER UNIVERSITÄT REGENSBURG.

vorleget von

Laura Boi

aus

Sorgono, Italien

im Jahr

2024

EXPLORING ASTROCYTES IN THE MOUSE LATERAL SEPTUM: DECIPHERING SEX RELATED ASTROCYTE CONTRIBUTION TO SOCIAL FEAR

DISSERTATION ZUR ERLANGUNG DES DOKTORGRADES DER NATURWISSENSCHAFTEN (DR. RER. NAT.) DER FAKULTÄT FÜR BIOLOGIE UND VORKLINISCHE MEDIZIN DER UNIVERSITÄT REGENSBURG.

vorleget von

Laura Boi

aus

Sorgono, Italien

im Jahr

2024

Das Promotionsgesuch wurde eingereicht am:

24.10.2024

Die Arbeit wurde angeleitet von:

Prof. Dr. Inga D. Neumann

Unterschrift:

It takes fear to find courage

The present is here, don´t be shy.
Embrace your fear, let it enlight.
Turn it into fuel, it´s finally all right.
Now face your fear and open your eyes.
It´s the time for your courage to rise.

Laura Boi

Illustration by Martino Pietropoli

Abbreviations

ACC	Anterior Cingulate Cortex
AAV	Adeno Associated Virus
aCSF	artificial Cerebrospinal Fluid
AMY	Amygdala
ANS	Autonomic Nervous System
AVP	Arginine Vasopressin
BNST	Bed Nucleus of the Stria Terminalis
CA1	Cornu Ammonis region 1
CA2	Cornu Ammonis region 2
CA3	Cornu Ammonis region 3
cAMP	Cyclic Adenosine Monosphophate
CBT	Cognitive Behavioral Therapy
CeA	Central Amygdala
CRH	Corticotropin Release Hormone
CNS	Central Nervous System
CS	Conditioned Stimulus
Cx	Connexin
Cx30	Connexin 30
Cx43	Connexin 43
pCx43	phosphorylated Connexin 43
DSM-V	Diagnostic and Statistical Manual of Mental Disorders - Fifth Edition
EAAT1	Excitatory Amino Acid Transporter 1
EAAT2	Excitatory Amino Acid Transporter 2
E	Estrogen
ERE	Estrogen Response Element
GABA	Gamma-Aminobutyric Acid
GFAP	Glial Fibrillary Acidic Protein
$GFAP^+$	Glial Fibrillary Acidic Protein expressing
GLU	Glutamate
GLUT1	Glutamate Transporter
GPCR	G Protein Coupled Receptor
GS	Glutamine Synthetase
HIP	Hippocampus
HPA	Hypothalamic-Pituitary-Adrenal

HYP	Hypothalamus
icv	intracerebroventricular
ip	intraperitoneal
LS	Lateral Septum
LSc	LS caudal region
LSd	LS dorsal region
LSr	LS rostral region
LSv	LS ventral region
MAOI	Monoamine Oxydase Inhibitor
mRNA	messenger Ribonucleic Acid
NAc	Nucleus Accumbens
OB	Olfactory Bulb
OGB1	Oregon Green 488 Bapta 1
OXT	Oxytocin
OXTR	Oxytocin Receptor
$OXTR^+$	Oxytocin Receptor expressing
PBS	Phosphate Buffer Saline
PFA	Paraformaldehyde
PFC	Prefrontal Cortex
PVN	Paraventricular Nucleus
ROI	Region Of Interest
S100β	S100 calcium-binding protein β
SAD	Social Anxiety Disorder
scr	scramble
SAM	Sympathetic-Adreno-Medullary
SEM	Standard Error of the Mean
SR101	Sulforhodamine 101
SFC	Social Fear Conditioning
SFC^-	Social Fear Conditioning Unconditioned animal
SFC^+	Social Fear Conditioning Conditioned animal
SNRI	Serotonin Noradrenaline Reuptake Inhibitor
SON	Supraoptic Nucleus
SSRI	Selective Serotonin Reuptake Inhibitor
US	Unconditioned stimulus
Veh	Vehicle
VTA	Ventral Tegmental Area

Contents

Abstract

Astrocytes, once considered passive support cells in the central nervous system, are now recognized as key modulators of synaptic plasticity and emotional behaviors. Recent studies highlight their significant involvement in anxiety- and depressive-like behaviors, particularly through astrocytic oxytocin (OXT) signaling. While the specific contributions of astrocytes remain largely unexplored, research has extensively characterized the role of OXT in regulating social behavior, particularly in the lateral septum (LS). OXT protective effects against social fear, as seen in animal models of social anxiety disorder (SAD), one of the most prevalent anxiety disorders, underscore its therapeutic potential. Social interactions are vital for the survival and well-being of individual. However, when responses to social cues become maladaptive, as in SAD, it poses a pathological challenge. Given the high prevalence of SAD and the limited efficacy of current treatments, there is an urgent need for a deeper exploration of these underlying mechanisms.

To better understand the neuronal and molecular mechanisms underlying SAD, the social fear conditioning (SFC) paradigm has been developed. In this paradigm, social fear is induced through operant conditioning, leading to avoidance of social stimuli, followed by repeated social exposure, which mirrors cognitive behavioral therapy (CBT) in humans. Research using the SFC paradigm has demonstrated that OXT signaling reverses social fear in mice. Moreover, alterations in OXTR binding in the LS during repeated exposure to social cues suggest that OXTR-mediated signaling plays a key role in both the expression and extinction of social fear.

Given the limited treatment options for SAD and the growing evidence of astrocytes involvement in modulating emotional behaviors through OXT signaling further exploration of astrocytic mechanisms is urgently needed. Investigating astrocytic OXT signaling could reveal new insights into the regulation of social behaviors and identify novel therapeutic targets for anxiety disorders like SAD.

In this thesis, I demonstrated the involvement of astrocytes in the learning processes associated with social fear acquisition and their subsequent influence on social behaviors. Additionally, I identified a potential role for astrocytic OXT signaling in modulating social behaviors during the extinction phase of fear responses, although this signaling did not appear to impact the initial acquisition of social fear itself. To account for possible sex differences in responses, both male and female mice were included to characterize the distinct effects observed.

Considering the multifaceted and heterogeneous functions associated with the LS, an initial characterization of astrocytic cells and $OXTR^{+}$ astrocytes throughout the LS was conducted. The

results revealed a greater density of both astrocytic cells and $OXTR^+$ astrocytes in the caudal part of the LS (LSc), with females exhibiting higher expression levels than males. Given their emerging role in learning processes, a morphological analysis was performed to investigate their responses to social fear acquisition and extinction within both the hippocampus (HIP) and the various subdivisions of the LS.

In male mice, astrocytes demonstrated a response to social fear acquisition in both the HIP and LSc, indicating their role in remodeling synaptic signaling during the learning process. This astrocytic activity could significantly influence behavior during the social fear extinction phase. To further explore this hypothesis, I induced structural depletion of astrocytes in the LSc using L-AAA, an inhibitor of glutamine synthetase, and assessed social behavior during the social fear conditioning paradigm in both male and female mice. The findings indicated that while male mice properly acquired social fear, they exhibited heightened fear responses during the extinction phase. Conversely, females displayed impaired social fear acquisition but exhibited behavior comparable to control groups during the extinction phase. This suggests that astrocytes contribute differentially to social behaviors in male and female mice.

To deepen the investigation into astrocytic activity during social fear acquisition, I employed calcium imaging techniques in both male and female mice. Social fear conditioning led to an increase in baseline astrocytic Ca^{2+} activity in both sexes, with males exhibiting higher baseline activity. Given the known prosocial and anxiolytic effects of OXT, I also examined the impact of TGOT (a selective OXT receptor agonist) on astrocytic Ca^{2+} activity. Notably, social fear acquisition enhanced astrocytic Ca^{2+} activity in response to TGOT, with females demonstrating a more pronounced Ca^{2+} response compared to males across the astrocytic population. This finding suggests a potential "ceiling effect" in female mice under baseline conditions, leading to heightened astrocytic activity induced by social fear conditioning compared to their male counterparts.

Lastly, I found that downregulating astrocytic OXTR resulted in faster extinction of social fear in both male and female mice, as evidenced by reduced fear responses during the extinction phase. This underscores the critical role of astrocytic OXT signaling in regulating social behaviors during the extinction process.

Collectively, these findings highlight the intricate relationship between astrocytes, OXT signaling, and social behavior, emphasizing the need for further exploration of astrocytic mechanisms in the context of social anxiety disorder. Understanding these dynamics may pave the way for novel therapeutic approaches aimed at addressing the complexities of social anxiety and related behavioral challenges.

Introduction

"It is not the strongest of the species that survives, nor the most intelligent, but rather the one most responsive to change."

(Charles Darwin)

Emotions define us through the feelings they evoke. They result from how our brain processes stimuli received from the surrounding environment, aiding in the maintenance for a good coexistence with the world for both our physical and mental health. Although the emotional process is largely unconscious, its outcome is represented by our feelings. We often label these feelings as happiness, fear, anger, sadness, contempt, disgust, and surprise. Every feeling matters, contributing collectively to our psychological resilience as human beings. Emotions have been a crucial aspect of human evolution and continue to play vital roles in stress-coping, communication, and decision-making today. The importance of emotional reactions in facilitating organisms to adapt to various stimuli and environmental situations was recognized probably for the first time by Charles Darwin in the late 19th century. Since then, the significance of emotions has continued to expand over time. Emotions are central to maintaining balance with our surroundings, and their influence on well-being is particularly evident in modern society, where the pressures of daily life require constant emotional adaptation to finding and maintain mental and physical equilibrium.

Significant disturbances in emotional regulation can lead to the development of mental health conditions. In 2019, approximately 12.5% of the global population was living with a mental disorder (World Health Organization, WHO). Over the past few years, dramatic events such as COVID-19 pandemic, and cultural and military conflicts, have indeed triggered widespread psychological distress (Gryksa and Neumann 2022). These circumstances have not only impacted physical condition but have deep impact on mental health and overall well-being. Meta-analysis studies, for instance, have shown that the number of people living with anxiety has tripled within one year of the onset of the COVID-19 pandemic (Santabárbara et al. 2021). These findings underline the pressing need to implement strategies in order to preserve the mental well-being of vulnerable individuals and reduce the impact of various factors linked to anxiety.

1. Fear and anxiety

When we run, we experience accelerated breathing, tense muscles, reddening skin, and sweat. These are the typical physiological stress responses following a physical challenge. Nowadays, running is often used to improve physical and mental wellness. However, our ancestors ran to escape predators or to hunt, translated into the fight-or-flight response today (Cannon 1915; Engel and Schmale 1972), as a typical physiological and adaptive reaction of the body when it feels threatened. Although fear is often considered a negative emotion, it is a natural and adaptive reaction to overcome threatening and imminent situations (Ekman 1992; LeDoux 2012). The fight-or-flight response can be seen as a continuous and equally balanced dance between fear and courage, orchestrated by the hypothalamus (HYP), a brain region that integrates autonomic, endocrine, and behavioral responses to overcome life-threatening situations (Kandel and Mack 2013).

Essentially, while fear is the emotional response to real and impending threats, preparing the body to fight or flight, anxiety is the feeling for the anticipation of future threats characterized by features such as muscle tension and vigilance behavior (Eilam et al. 2011; Kozlowska et al. 2015).

1.1. Emotional process and stress response

The neuronal network of emotional processing is broad and complex, involving different brain regions of the central nervous system (CNS), that exert actions either in the emotion regulation process and/or in the emotion responding process (Kandel and Mack 2013). The emotion processing starts with the perception of environmental stimuli through the sensory nervous system (visual, auditory, olfactory or tactile). This sensory information is transmitted to thalamic regions, including the lateral geniculate nucleus and the medial geniculate nucleus, as well as to the somatosensory cortex. From there, the information is processed in key brain regions associated with emotion, such as the striatum, amygdala (AMY), insula, and anterior cingulate cortex (ACC) (LeDoux 2000; Kandel and Mack 2013). The AMY, a key region in the detection of fear and formation and retrieval of the fear-related memories, interacts with both the autonomic and neuroendocrine system (LeDoux 2000; LeDoux 2003). It does so via direct or indirect projections to the paraventricular nucleus (PVN), and the brain stem, leading to the activation of the hypothalamic-pituitary-adrenal (HPA) axis (LeDoux 1992; LeDoux 2003; Kandel and Mack 2013) and the sympathetic-adreno-medullary (SAM) axis, respectively. The HPA axis represents a vital neuroendocrine system in the regulation of the stress response (Hackney 2006). However, the stress response results from a significant interplay between the, the HPA axis, the SAM and the immune system (McEwen 2004; Hackney 2006). The physiological stress response is divided into two main phases. The first phase reflects a rapid response of the SAM axis, with a release of catecholamines that prepare the body for immediate

action (fight-or-flight), enhancing alertness, vigilance, arousal and reducing pain perception with physiological symptoms such as (Chrousos 1998; Ulrich-Lai and Herman 2009).

In parallel, the second and slower response involves the activation of the HPA axis (see Figure 1 for details): i) the HYP and the anterior pituitary are triggered to produce and release corticotropin release hormone (CRH) and adrenocorticotropic hormone (ACTH), respectively; ii) once released in the bloodstream, ACTH stimulates the zona fasciculata of the adrenal gland to release glucocorticoids, particularly cortisol in humans (corticosterone in rodents); iii) cortisol enhances the activity of the autonomous nervous system (i.e. increasing heart rate) and exerts significant effects on the immune and metabolic systems (Sapolsky et al. 2000; Holsboer and Ising 2010; Joëls et al. 2018). To ensure a proper reestablishment of basal homeostasis, the HPA axis is inhibited trough multiple mechanisms: i) via the efficient negative feedback exerted by cortisol at the level of both HYP and hippocampus (HIP): ii) via the aminergic systems of norephinephrine and serotonin, which send projections to the HPA axis from the locus coeruleus and raphe nuclei, respectively (Martin et al. 2009; Holsboer and Ising 2010; Tafet and Nemeroff 2016).

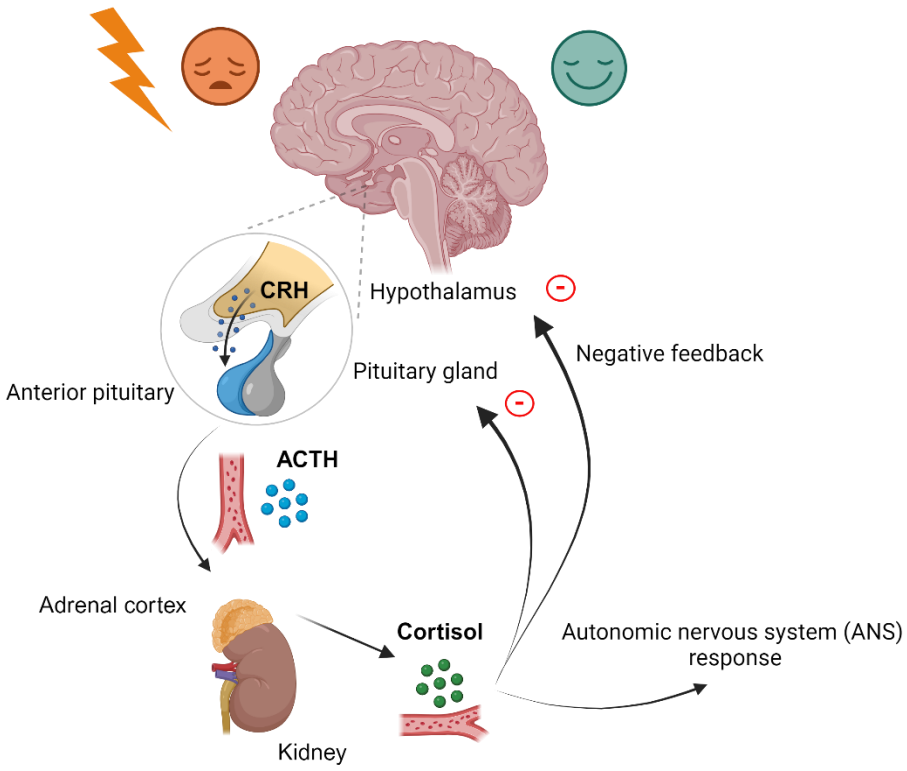

Figure 1. Schematic illustration of the hypothalamus-pituitary-adrenal (HPA) axis. *The activation of the HPA axis initiates with the release of corticotropin-releasing hormone (CRH) from the hypothalamus into the median eminence. CRH then travels through the portal capillary system that vascularize the anterior pituitary, to stimulate the release of the adrenocorticotropic hormones (ACTH) into the bloodstream. ACTH reaches the adrenal cortex, where it induces the release of cortisol (or corticosterone in rodents) into the blood. The HPA axis response is terminated through a negative feedback loop by cortisol at both the pituitary gland and the hypothalamus, restoring the homeostasis. Additionally, once released into the blood, cortisol exerts significant effects on the autonomic nervous system (ANS), regulating involuntary physiological functions such as cardiovascular, metabolic, immune system and reproductive systems to help cope with stress. Illustration created using Biorender.com.*

However, in the case of a prolonged stressful experiences (chronic stress), the persistent activation of the HPA axis results in elevated cortisol levels under basal conditions (McEwen 2004; Kloet et al. 2005; Lupien et al. 2009) and is accompanied by feelings of anxiety and arousal, shifting the response from adaptive to maladaptive (Campion et al. 1975; Kloet et al. 2005; Lupien et al. 2009; McEwen 2004; Uschold-Schmidt et al. 2012), and can lead to the development of anxiety-related pathologies (Tafet and Nemeroff 2016; Duval et al. 2015; Penninx et al. 2021; Martin et al. 2009).

In summary, a transient state of fear and anxiety is a physiological adaptation to acute stressor exposure, essential for survival. It triggers active defense mechanisms (fight or flight), passive responses (freezing behavior), or precautionary responses (vigilance behavior) in humans and rodents (Bracha 2004; Eilam et al. 2011; Kozlowska et al. 2015). In contrast, excessive and prolonged feelings of anxiety, fear and worry can lead to the development of anxiety disorders, causing persistent stress and/or impair of social, occupational, or other important area of functioning (Chrousos and Gold 1992; Charmandari et al. 2005; Neumann and Slattery 2016)(Gray and McNaughton 1996).

2. Anxiety disorders

Currently anxiety disorders represent the most prevalent class of psychological diseases, affecting 4% of the global population, followed by depressive disorders (3.8%) (WHO, World Health Organization).

2.1. Diagnosis and classification

As previously mentioned, symptoms of anxiety, such as fear and worry, often overlap with physiological responses to stressful situations, including muscle tension, palpitations, and shortness of breath. Consequently, recognizing the need for treatment and accurately diagnosing anxiety disorders can be challenging due to their overlap with acute stress responses, often leading to continuous underdiagnosis.(Alonso et al. 2018). The distinguishing factor lies in the frequency, severity, and persistence of a set of symptoms, along with subsequent impact on daily functioning (Hackney 2006; Goldstein and Kopin 2007). Compared to other mental disorders, anxiety disorders have typically an earlier developmental onset, often manifesting during childhood and adolescence (DSM-V, American Psychiatric Association 2013). If not treated, these disorders can persist into adulthood (DSM-V). Generally, girls and women are more affected than boys and men (around 2:1 ratio) (DSM-V), and are more likely to be diagnosed in comorbidity with an another anxiety or depressive disorder (McLean et al. 2011). Although anxiety disorders share features of avoidance, anxiety, and fear, they differ for the age of onset, duration criteria (which may be shorter in children),

and the specific objects or situations that trigger emotional and behavioral states. As a result, the DSM-V lists the following different types of anxiety disorders:

- Separation anxiety disorders: feeling anxious and fearful about being separated from affectionate people.
- Selective mutism: inability to speak in social situation in specific environments (e.g. school).
- Generalized anxiety disorder: persistent and excessive worry about daily activities or events.
- Panic disorder: panic attacks and fear to experience more panic attacks.
- Phobia-related disorder: intense, irrational fears of specific objects or situations.
- Social anxiety disorder (SAD): extreme levels of fear and worry related to social situations during which the person feels humiliated and embarrassed.

Pathological anxiety can coexist with various mental disorders, such as depression, bipolar disorder, and substance abuse, as well as somatic illnesses including cardiac, thyroid, respiratory diseases (Penninx et al. 2021) increasing the risk of diagnostic confusion. Therefore, when patients show symptoms of other health conditions or effects of substance abuse, it is essential to conduct both psychiatric and somatic evaluations to ensure accurate diagnosis and treatment.

2.1. Risk factors

Like almost all other mental disorders, anxiety disorders are characterized by an intricate pathogenesis that embrace genetic, epigenetic, environmental, and individual risk factors (Meier and Deckert 2019; Penninx et al. 2021). Genetic factors represent a substantial component in the predisposition to anxiety disorders, with this risk being further modulated by epigenetic mechanisms, induced by environmental stressors and regulation of neuroendocrine system (Schiele and Domschke 2018; Gottschalk and Domschke 2017). Heritability factor indicate a contribution of around 50% for SAD, panic disorder and agoraphobia, and around 35% for generalized anxiety disorder (Kendler and Myers 2014; Gottschalk and Domschke 2017; Meier and Deckert 2019). Additionally, anxiety disorders share genetic components with other mental and stress-related, which explains their high comorbidity (Meier et al. 2019; Penninx et al. 2021). Early life stressful experiences, age of onset and sex differences are crucial vulnerability factors. These factor are significant due to the structural, functional and differentiation processes that the brain undergoes across the lifespan in males and females (Bale and Epperson 2015; Oyola and Handa 2017; Kaufman et al. 2000), leading to different susceptibility risk across the lifespan. Lastly, anxiety disorder prevalence is highest in high-income countries (Penninx et al. 2021), highlighting the influence of cultural and social aspects on human health.

3. Social anxiety disorder

With a lifetime prevalence rate of 12.1%, SAD represents one of the most common anxiety disorders (DSM-V, (Kessler et al. 2012). Also known as social phobia, it is characterized by an intense and persistent fear and anxiety of various social situations, involving both performance-related and interpersonal interactions. Individuals with SAD experience an overwhelming fear of being scrutinized and judged by others, leading to significant anxiety and avoidance behaviors. This pervasive fear is often accompanied by physiological symptoms such as sweating and shortness of breath, which exacerbate avoidance behaviors and result in increased social isolation (DSM-V). SAD has a typically early onset, starting during adolescence and often continuing into adulthood, significantly affecting individuals' psychosocial functioning. This disorder is linked to substantial socio-economic and functional impairments, as evidenced by the 90% of those with SAD experiencing disruptions in their daily lives (Stein and Stein 2008; Leichsenring and Leweke 2017). Consequently, it is not surprising that SAD frequently coexists and increases the risk of other psychological conditions, including substance abuse disorders, depressive disorders and other anxiety disorders (Leichsenring and Leweke 2017).

A significant challenge in treating SAD is the low rate of treatment-seeking behavior among patients. (Lecrubier et al. 2000; Stein and Stein 2008). Even among those who do seek treatment, only 32% receive adequate care, often due to underrecognition or misdiagnosis, with some cases mistakenly attributed to ordinary shyness (Davidson et al. 1993; Schneier 2006; Stein and Stein 2008; Leichsenring and Leweke 2017). Several studies have shown a higher prevalence in women than men (Figure 2), across areas such as United States, Europe, and Asia (Cho et al. 2007; Ohayon and Schatzberg 2010; McLean et al. 2011). As reviewed in (Asher et al. 2017), women tend to report more severe symptoms and are more likely to suffer from comorbid mood and anxiety disorders, compared to men, who more likely suffer from comorbid externalizing disorder, like substance abuse. Interestingly, despite these differences in prevalence and symptomatology, men are more likely than women to seek treatment for SAD, as noted in the DSM-V.

3.1. Treatment and prevention

An intervention is needed whenever a negative state persists for an extensive period, causing persistent distress and/or impairing social, occupational, or other important areas of functioning. The treatment of SAD typically involves a combination of psychotherapeutic and pharmacotherapeutic approaches (Ipser et al. 2008; Rodebaugh et al. 2004; Acarturk et al. 2009).

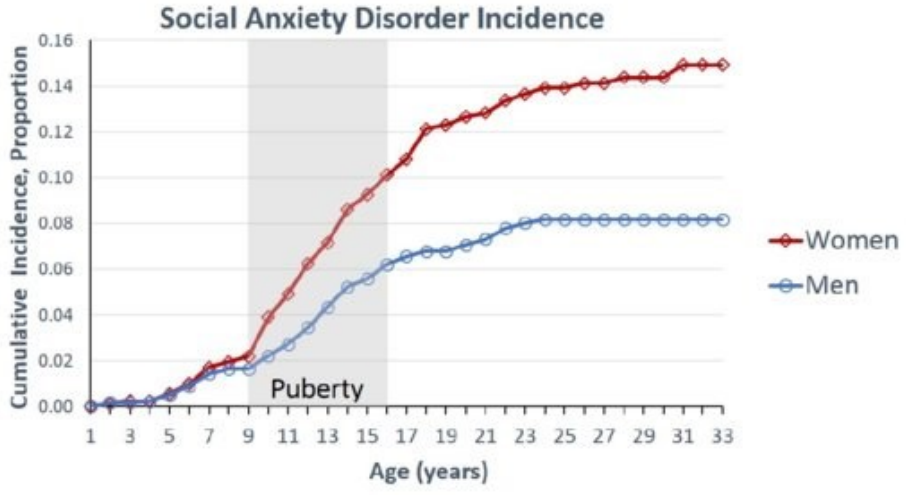

***Figure 2**. **Lifetime prevalence of Social Anxiety Disorder in men and women.** Image from Wright et al., 2020.*

The first-line of treatment for SAD is psychotherapy, specifically cognitive behavioral therapy (CBT), which includes disorder-specific protocols of psychoeducation, exposure, and cognitive reconstruction (Acarturk et al. 2009; Biagianti et al. 2023). Despite the challenge some patients face with exposure therapy, CBT is a well-established treatment that provides educational support and disease-related knowledge to help patients identify the source of their emotions and understands how these emotions influence their behaviors (Acarturk et al. 2009; Thomas 2014; Biagianti et al. 2023). This approach helps patients cope with their irrational and self-defeating thoughts and actions. Studies show varying treatment responses to CBT, ranging from 8% to 65% (Taylor et al. 2012; Leichsenring and Leweke 2017), with stable effects observed as early as 1 to 6 months post-treatment (Acarturk et al. 2009), and enduring effects over the years (Zhang et al. 2019).

To overcome CBT treatment limitations in both access and responsiveness (Collins et al. 2004; Taylor et al. 2012), pharmacotherapy is prioritized in severity case, providing faster relief (Leichsenring and Leweke 2017). Antidepressants such as selective serotonin reuptake inhibitors (SSRIs) and serotonin-norepinephrine reuptake inhibitors (SNRIs) are the most recommended pharmacotherapy approach, due to their positive benefit/risk balance (Szuhany and Simon 2022; Kent et al. 1998; Szuhany and Simon 2022; Bandelow 2020). Indeed, similarly to CBT treatment effects (Taylor and Liberzon 2007; Goldin et al. 2013), SSRIs enhance serotonin availability in brain networks involved in emotion regulation, leading to a decrease in limbic neural response to aversive stimuli and improved prefrontal cortex functioning, resulting in normalization of the HPA system (Ma 2015; Tafet and Nemeroff 2020). Although SSRI and SSNI treatment shows low relapse rates,

the non-response rate is still very high, between 30 to 50% (Ipser et al. 2008; Leichsenring and Leweke 2017).

Benzodiazepines, a class of anxiolytic which enhance GABAergic function, are prescribed for their efficacy in rapidly reducing anxiety symptoms (Balon and Starcevic, 2020; Engin, 2022). However, their long-term used is contraindicated due to the high risk of physiological dependency and withdrawal symptoms associated with these medications (Balon and Starcevic 2020; Engin 2022). The choice to prefer antidepressants over anxiolytics depends on several individual-related factors, such as the speed of onset of the disorder, comorbidities or history of substance abuse, depressive symptoms and side effects (Ipser et al. 2008; Kimmel et al. 2015; Tafet and Nemeroff 2020; Balon and Starcevic 2020). Additionally, beta-blockers are occasionally prescribed to alleviate performance anxiety symptoms by blocking the release of stress hormones like adrenaline and noradrenaline, particularly useful when taken about an hour before a stressful event (Leichsenring and Leweke 2017). Monoamine oxidase inhibitors, which inhibit enzymes responsible for degrading neurotransmitters such as serotonin, norepinephrine and serotonin, are prescribed as third-line treatment due to their serious adverse effects (Ipser et al. 2008). Recently, psychodynamic therapy (PDT) has gained attention. Influenced by Sigmund Freud´s idea from over 100 years ago, which proposed that human behaviors is influenced by experiences beyond conscious awareness (Freud, Richards 1953-74), PDT targets multiple domains of experience and functioning. It aims to understand interpersonal and intrafamilial dynamics to address the root causes of psychological distress (Pitman and Knauss 2020; Busch 2024).

Since no treatments leads to a complete remission and cure, the goal is to improve psychological well-being by reducing symptoms. In this context, psychodynamic, mindfulness-based interventions and physical exercise, can be also implemented either as an integration or a prevention approach (Kandola et al. 2016; Hofmann and Gómez 2017; Leichsenring and Leweke 2017). Several studies show how exercise promote hippocampal functioning and plasticity (Kandola et al. 2016), and increase cortisol levels (Hill et al. 2008), contributing to the modulation of physiological responses, particularly in the HPA axis (Kandola and Stubbs 2020). Exercise acts similarly to exposure therapy in CBT, conditioning the neuroendocrine system to handle future stressors (Hackney 2006; Kandola and Stubbs 2020).

Considering overarching trends such as diversity, urbanization, and social inequality that characterize the contemporary society, it is crucial to understand the neurobiological mechanisms these conditioning. This understanding aims to improve the well-being and functioning of affected people, promoting inclusivity and social equality.

2.1. Animal models for social fear

To develop effective therapeutic treatments in clinical research, basic neuroscience plays a crucial role in uncovering the underlying mechanisms of psychiatric disorders. For this purpose, animal models that replicate the key features of the disorder in humans are essential. Although skepticism about the reliability of animal models has grown over the years, researchers have continually refined and improved their approaches to developing animal models (Belzung and Lemoine 2011). First defined early in 1969 (McKinney and Bunney 1969), subsequently adapted and optimized, Willner proposed three validation criteria for animal models: face validity, predictive validity and construct validity (Willner 1984). More recently, ethological validity and biomarker validity have been integrated as crucial aspects of face validity, as they represent observable criteria (Belzung and Lemoine 2011; Cryan and Slattery 2007). The criteria are as follows:

- Face validity. Animal models should mimic behavioral and physiological characteristics of the disease. This is essential to establish a phenotype as similar as possible to the clinical case. This includes ethological validity, where the animal´s natural behavior is reflected, providing insights into how the disorders manifests within its ecological and evolutionary context.
- Predictive validity. The animal model should reliably predict the efficacy and safety of treatments intended for human use. Consistency between responses in the animal model and clinical outcomes in humans is essential for this criterion.
- Constructive validity. To accurately reconstruct the human disorder, the animal model needs to be based on theoretical and rational constructs representing the biological processes underlying the clinical disease.

Rodent models are preferred in neuroscience research for ethical, practical, and scientific reasons. Their evolutionary similarities with humans in neurofunction, developmental processes, and behavior, make them particularly valuable for studying complex neural mechanisms Given the strong cross-species similarities in the fear physiology, animal models of fear conditioning have been used as form of associative learning (Shechner et al. 2014). This associative learning task involves the association of a neutral conditioned stimulus (CS), like a tone, with an aversive unconditioned stimulus (US), like an electric shock, leading to a CS-US association and the production of fear-related responses (LeDoux 2000; Maren 2001). One specific model relevant to SAD is the social fear conditioning (SFC) paradigm (Toth et al. 2012). Addressing all three validity criteria, this model relies on social operant conditioning, during which animals learn to associate the voluntary action of interacting with another mouse with the consequence of receiving an electric foot shock. This induces the expression of social fear state and social fear-related behaviors, like freezing and social avoidance (Toth et al. 2012). During the extinction process, mice are re-exposed to different conspecifics

without receiving electrical foot shocks, leading to the extinction of fear-related behaviors by creating new memories where the CS is associated with the absence of the US (Toth et al. 2012; Shechner et al. 2014). SFC is considered a valid animal model of social anxiety due to the consistent positive outcomes following anxiolytic treatments, and the absence of changes in other behaviors such as general anxiety, locomotor activity or anhedonia (Toth et al. 2012, 2013). This contrasts with other models of SAD, such social isolation, which can induce broader behavioral changes (Toth and Neumann 2013; Hol et al. 1999). Another model of SAD is social defeat stress, where animals are subordinated by an aggressive conspecific. While this model induces SAD-like phenotype, it differs from SFC since it generates social avoidance specifically directed towards the defeater. In contrast, SFC induces social avoidance towards all conspecifics. Furthermore, chronic social defeat induces generalized changes in anxiety and depressive-like behavior (Franklin et al. 2017; Toth and Neumann 2013).

It is important to remember that all animal models have inherent limitations, particularly in capturing the unique human sphere of hypersensitivity, criticism and negativity (Réus et al. 2014). Nevertheless, these models remain invaluable tools for unraveling the cellular and molecular mechanisms underlying fear and anxiety-related disorders. Understanding these mechanisms is critical for developing more targeted and effective treatments for individuals affected by SAD and related conditions.

3. Neurocircuitry of social fear

Fear and anxiety, beyond their symptomatic manifestations, share overlapping neurocircuitry that orchestrates behavioral and physiological responses to threatening stimuli. Brain regions implicated in stress responses also significantly contribute to anxiety symptoms. A neurocircuitry, in essence, comprises interconnected brain regions forming a complex network via numerous neural connections. Investigating the neurobiological underpinnings of SAD has gained prominence over the years, aiming to unravel its intricate complexity encompassing emotional, neuroendocrine, motivational, and cognitive networks (Cremers and Roelofs 2016).

Neuroimaging studies have revealed hyperactivation of the amygdala and the hippocampus in response to aversive faces in patients with generalized SAD (Stein et al. 2002; Evans et al. 2008; Phan et al. 2006). Additionally, the anticipation of public speaking in social phobia activates regions involved in the automatic processing of emotions, such as pons, striatum, insula and temporal lobe (Lorberbaum et al. 2004; Engel et al. 2009). While neuroimaging helps to uncover connections from a broad perspective, basic research helps to identify latent factors contributing to SAD.

Animal studies have pinpointed the basolateral amygdala (BLA) as critical for the social fear acquisition through associative processes like long-term potentiation (LTP), with synapse enhancement from BLA to central amygdala (CeA) during repeated conditioned stimulus exposure (Kim and Jung 2006; Fanselow and LeDoux 1999). The amygdala interconnects with other brain regions involved in the acquisition of the fear memory, such as HIP and prefrontal cortex (PFC) (Sierra-Mercado et al. 2011; Diaz and Lin 2020). Moreover, inactivation studies using muscimol have demonstrated the involvement of the ventral hippocampus (vHIP) in social fear acquisition following social defeat (Markham et al. 2010), and the PFC in social avoidance in conditioned animals (Xu et al. 2019). The vHIP appears to be involved in the contextual fear memory, as evidenced by the correlation between vHIP lesions and impairments in contextual fear memory (Diaz and Lin 2020). In line with the roles played by AMY, HIP and PFC in social defeat, an increase of neuronal cFos was found in these regions following social stress (Matsuda et al. 1996; Bourne et al. 2013). The nucleus accumbens (NAc) and the BNST, receiving projections from the AMY, ultimately mediate social fear-related behaviors such as active avoidance (Diaz and Lin 2020; Jasnow et al. 2004; Ramirez et al. 2015).

From a translational perspective, understanding the mechanisms behind erasing fear association is essential to develop appropriate therapeutic approaches. The process of fear extinction, whether through new learning or inhibition of existing CS-US associations, remains incompletely understood, indicating overlaps in brain regions and circuits implicated in both fear acquisition and extinction. The PFC has been proposed as a key player in the extinction process, inhibiting maladaptive behaviors by projecting influences to the amygdala and hypothalamus (Kim and Jung 2006). The dorsal hippocampus (dHIP) was found to participate in the context-specific learning of fear extinction (Corcoran and Maren 2004; Corcoran et al. 2005; Sierra-Mercado et al. 2011)

Another interesting aspect to take in consideration is that the above mentioned brain regions involved in the fear circuits (AMY, HIP, PFC), have been shown to be sexually dimorphic and to be activated differently in learning paradigms, including fear acquisition and extinction (Velasco et al. 2019; Lebron-Milad et al. 2012). For example, it was shown that males and females perform differently depending on the type of learning task the estrous phase females were on that day. Particularly, in operant conditioning studies, females outperformed males by being more actively response to aversive stimuli compared to higher freezing behavior observed in males (Dalla and Shors 2009; van Haaren et al. 1990; Beatty and Beatty 1970; Steenbergen et al. 1990). The differences could depend on gonadal hormones in complex and interactive way, including hormonal cycles as well as hormonal fluctuations across development with their subsequent different behavioral outcome (Dalla and Shors 2009). Starting from the determination of XX or XY genotype, sex hormones shape brain structure by influencing gene expression, cellular formation, and overall neural architecture (Woolley 1998; Vries et al. 2002; McCarthy and Arnold 2011) . Sex-dimorphic influences persist throughout sex-

hormonal cycles and various stages of neurodevelopment (McCarthy et al. 2009; Kundakovic and Tickerhoof 2024). Additionally, environmental factors play a role in shaping these differences (Velasco et al. 2019).

Despite considerable gaps in our understanding of the circuits and mechanisms involved in the fear acquisition and extinction, the disparities between males and females are even more pronounced. Research specifically focused on females remains limited, partly due to the erroneous assumption of similarities with males and the complexity of monitoring the estrous cycle. However, the pressure to increase studies on sex-differences has grown in recent years, driven by the need for better understanding of pathophysiology and development of anxiety disorders.

3.1. Lateral septum: from septal rage to social fear extinction

In addition to the previously discussed brain regions, i.e., the AMY, HIP and PFC, the lateral septum (LS) is another pivotal structure influencing social behavior. Located in the lower posterior forebrain between the lateral ventricles, the LS along with the medial septum (MS) forms the septum complex. The LS gained significant attention in 1980, when studies revealed its role in modulating aggression, often leading to the phenomenon known as “septal rage” following its lesions in rats (Albert and Chew 1980). Over the years mounting evidences has highlighted the role of the LS in emotional and motivational behaviors, positioning it as a key regulator of social behaviors (Menon et al. 2022; Rizzi-Wise and Wang 2021). Strategically positioned, the LS integrates inputs related to internal states from limbic regions and transmits signals to hypothalamic and midbrain structures to regulate behavioral responses. Anatomically and neurochemically, the LS is quite heterogenous. Its anatomy is organized along rostral-caudal and dorsal-ventral axes, each associated with distinct input and functions (Figure 3), although exact differences between these areas are not completely defined (Wirtshafter and Wilson 2021). Along the dorsal-ventral axis, the LS is divided into dorsal (LSd) and ventral (LSv) regions. The LSv, innervated by the ventral HIP, appears rather involved in regulating emotional behaviors, while the LSd receives inputs from the dorsal HIP and primarily processes spatial information. Functional differences also exist along the rostral-caudal axis, with the rostral LS (LSr) being likely involved in cue processing and the caudal LS (LSc) implicated in contextual behaviors. The LS maintains reciprocal connections with various brainstem regions and basal ganglia circuits associated with locomotor behavior, integrating movement-related inputs. Moreover, LSr exhibits bidirectional projections with the hypothalamus and supramammillary nucleus, influencing arousal and defensive behaviors. Conversely, LSc receives significant inputs from structures like the VTA, locus coeruleus and raphe known to be involved in reinforcement and motivation. Additionally, intraseptal microcircuits reciprocally connect with the MS (Risold and Swanson

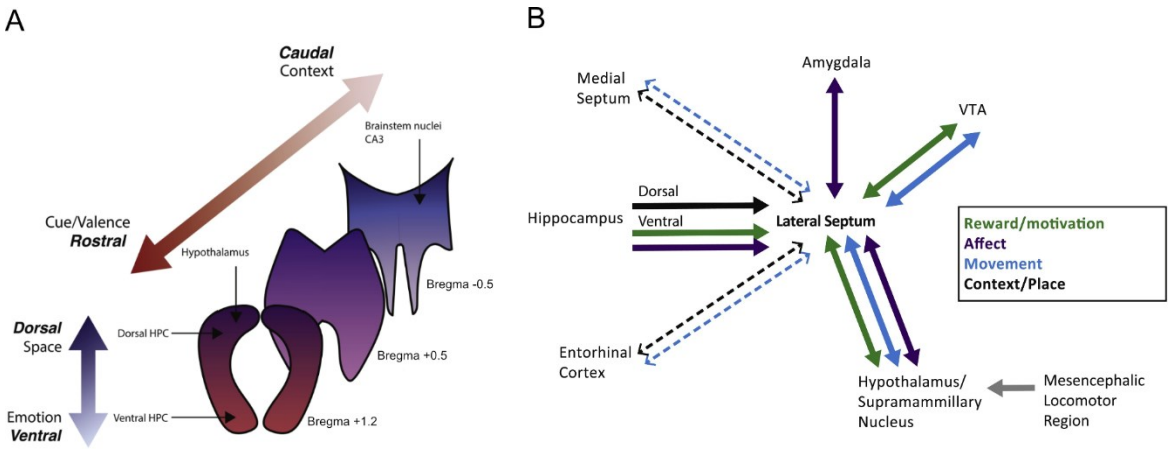

Figure 3. Schematic of the major lateral septum (LS) inputs and functionality. *The diagram on the left (A) shows the LS at different coordinates (dorsal/ventral and rostral/caudal) with diverse functionality depending on the gradient considered. The dorsal LS (LSd), primarily receiving inputs from the dorsal hippocampus, is mainly responsible for processing spatial information. The ventral LS (LSv) is more involved in the processing emotional and affective information, with inputs from the more ventral regions of the hippocampus. Considering the rostral/caudal gradient, the rostral (LSr), which receives projections form the hypothalamus, is likely involved in regulating affect and emotions. In contrast, the caudal LS (LSc), primarly innervated by the hippocampus and the ventral tegmental area, may play a role in pattern separation and reward-seeking behaviors. On the right (B) the diagram illustrates partial connectivity of the LS. The arrows indicate whether the connection is an input or bidirectional; dotted lines indicate debated projections, and the colors denote the type of information processed. Image adapted from (Wirtshafter and Wilson 2021).*

1997b). Within the LS itself, the presence of interneurons form local microcircuits that can autoinhibit and regulate signaling output (Sheehan et al. 2004).

Neurochemically, LS is predominantly composed of GABAergic neurons, accounting for over 90% (Zhao et al. 2013; Risold and Swanson 1997a). These GABAergic neurons establish reciprocal connections ith regions such as the HYP and periaqueductal gray. Additionally, the LS contains cholinergic and monoaminergic neurons (Risold and Swanson 1997a) which are associated with reward and motivational pathways. A small population of glutamatergic neurons is also present in the most ventral part of the LS (Lin et al. 2003). The functional complexity of LS is also reflected by its peculiar expression of various receptors, including receptors for oxytocin (OXT), arginine vasopressin (AVP), serotonin (5-HT), dopamine (DA), estrogen (E), CRH (Menon et al. 2022; Sheehan and Numan).

This complex and heterogeneous anatomy of LS elucidates its role as a central hub implicated in multifaceted functions ranging from emotional and motivational behaviors to spatial behaviors (Rizzi-Wise and Wang 2021; Menon et al. 2022)Moreover, the LS has been recognized for its influence on social behaviors, including aggression (Oliveira et al. 2021; Wong et al. 2016), maternal behavior, mating, social fear (Menon et al. 2022; Grossmann et al. 2024), reward, feeding and anxiety behaviors (Rizzi-Wise and Wang 2021). Interestingly, the LS may exert opposing roles in the regulation of fear and anxiety-like behaviors depending on the specifically activated pathways (Rizzi-Wise and Wang 2021). For example, activation of type 2 CRH receptor-expressing neurons and the hippocampus→lateral septal pathway (particularly from the dorsal cornu ammonis region 1

of the HIP, dCA1→LS), appears to promote anxiety-like behavior and fear (Opalka and Wang 2020; Hunsaker et al. 2009). In contrast, the ventral CA1/CA3→LS pathway likely suppresses fear and anxiety-like behaviors (Parfitt et al. 2017; Besnard et al. 2019; Besnard et al. 2020). Recent research has highlighted the pivotal role of the LS in memory processes related to fear and social interactions, including the acquisition, consolidation (conversion of short-term to long-term memory), and extinction of fear and social memories (Rizzi-Wise and Wang 2021). Disruption of LS activity has been shown to impair fear conditioning acquisition (Opalka and Wang 2020), a mechanism that appears to depend on hippocampal projections (Opalka and Wang 2020; Calandreau et al. 2007; Hunsaker et al. 2009). Similarly, disrupting LS inputs from the HIP during memory expression also leads to comparable outcomes (Hunsaker et al. 2009; Opalka and Wang 2020). Given the abundance of local OXT and AVP receptors, it is not surprising that these neuropeptides play a significant role in social memory processes mediated by LS (Rizzi-Wise and Wang 2021; Menon et al. 2022). For instance, infusion of AVP into the LS enhances social memory in male rats (Dantzer et al. 1988), however intracerebroventricular (icv) AVP does not affect social fear expression (Zoicas et al. 2014). Both icv and local OXT infusions in the LS facilitates social fear extinction in males (Zoicas et al., 2014), and local OXT infusions in the LS have similar effects in virgin female mice (Menon et al. 2018).

While abundant evidence highlights the involvement of the LS in a variety of behaviors, several aspects of social fear mechanisms, particularly those related to OXT, remain to be further elucidated. To gain a deeper understanding of the pivotal role of OXT in regulating social behaviors, the next section will be dedicated to the description of this neuropeptide system.

4. The brain oxytocin system

OXT is a highly conserved nonapeptide found in all vertebrates, which has increasingly attracted attention for its physiological and behavioral functions (Jurek and Neumann 2018). Traditionally known for its functions in milk ejection, uterine contractions, sexual arousal, OXT also plays crucial roles in a range of reproductive and non-reproductive social behaviors (Menon and Neumann 2023).

In mammals, OXT is synthetized by neurons distributed in the PVN, supraoptic (SON) and accessory nuclei of the hypothalamus, with additional production also in the BNST (Althammer and Grinevich 2017; Duque-Wilckens et al. 2020). Magnocellular neurons, located in the PVN and SON, project via the pituitary stalk to the posterior pituitary gland (neurohypophysis). Here, they form neuro-hemal contacts with fenestrated capillaries to release OXT directly into the bloodstream as a hormone (Grinevich and Neumann 2021). Despite being the source of peripheral OXT that acts as hormone, magnocellular neurons also project to various brain regions for central release of OXT in

the CNS (Althammer and Grinevich 2017). Additionally, another significant source of brain OXT are parvocellular neurons, which constitute a smaller neuronal population localized within the PVN, and the accessory nuclei of hypothalamus (Althammer and Grinevich 2017; Grinevich and Neumann 2021). Other than to coordinate the activity of magnocellular neurons (Eliava et al. 2016), OXT parvocellular neurons project to the midbrain, brain stem and spinal cord to control several physiological functions, such as feeding, cardiovascular reactions and erection (Althammer and Grinevich 2017; Swanson et al. 1980; Althammer and Grinevich 2017). OXT synthesis and central release are triggered by classical physiological stimuli like birth, suckling during lactation, and mating (Grinevich and Neumann 2021; Menon and Neumann 2023).

Brain OXT is released as a neuromodulator from the dendrites, cell bodies, and axonal projections of hypothalamic neurons, within the HYP and extrahypothalamic brain regions (Landgraf and Neumann 2004; Althammer and Grinevich 2017). In mammals, OXT neurons extend long-range axonal collaterals to various brian areas, including PFC, septum, HIP, olfactory nucleus, AMY and NAc (Grinevich et al. 2016; Knobloch and Grinevich 2014).

OXT exerts its effects by binding to its receptor (OXTR), which is expressed both in neurons and and glial cells, including astrocytes (Jurek and Neumann 2018; Althammer et al. 2022c). The OXTR is a G-protein-coupled receptor (GPCR), with 7 transmembrane domains and is encoded by the single gene (Oxtr). In rodents, the transcription of Oxtr may be promoted by estrogens, as an estrogen regulated element () is located in the Oxtr gene, or it can be decreased trough methylation of the Oxtr promoter (Jurek and Neumann 2018). Upon binding of OXT to OXTR, the G-protein β/γ subunits dissociate from the α-subunit, initiating distinct intracellular signaling cascades depending on the type of α-subunit involved. Specifically, OXTR can couple with two types of α-subunits, Gαi/o and Gαq/11 (Busnelli and Chini 2018), which can modulate synaptic transmission and plasticity (Gαi/o) or decrease neuronal activity (Gαq/11). Particularly, activation of Gαq/11 leads to the activation of the second messenger phospholipase C (PLC), which increases intracellular calcium (Ca^{2+}) levels. In contrast, activation of Gαi/o decreases the levels of the second messenger cyclic adenosine monophosphate (cAMP), resulting in membrane hyperpolarization. The downstream effects following the activation of these pathways, have been explored using selective agonists, such as atosiban, carbetocin or TGOT, which selectively activate Gαi or Gαq, or both respectively (Busnelli and Chini 2018). The same research group found that prolonged stimulation of OXTR with OXT or carbetocin leads to the internalization of the receptor (Busnelli and Chini 2018). Research has revealed sex-differences in OXTR expression in both neurons and astrocytes across various brain regions (Smith et al. 2017; Althammer et al. 2022c), as well developmental differences (Smith et al. 2017). OXTR expression tends to be higher in brain regions associated with reward, social and spatial memory (Jurek and Neumann 2018). In adulthood, elevated OXTR expression is particularly prominent in areas involved in social decision-making (Smith et al. 2017; Jurek and Neumann 2018).

These findings underscore the co-evolution of the OXT system with complex social and emotional behaviors, highlighting its crucial role in modulating these conserved responses.

4.1. Oxytocin implications in anxiety and social fear behaviors

Pituitary extracts were initially discovered to stimulate uterine contractions facilitating the birth process (Dale 1909) and, therefore, OXT received its name from the Greek words for “quick” and “birth”, as it acts as a neurohormone acting on peripheral OXTR.

A few decades later, research highlighted its influence as a brain neuromodulator on maternal behavior (Pedersen and Prange 1979), learning and memory processes (Wied 1965), and sexual behavior (Melin and Kihlstroem 1963). However, it was not until 1990´s (Bale et al. 2001; Neumann et al. 2000) that the scope of OXT´s effects expanded significantly, revealing its role in reducing anxiety and stress, as well as enhancing prosocial-behavior (Neumann and Slattery 2016; Jurek and Neumann 2018). Studies have demonstrated that OXT´s anxiolytic effects become particularly pronounced during periods of heightened OXT system activity such as lactation (Neumann et al. 1993; Neumann et al. 2000; Jurek et al. 2012) and mating in both males and females (Waldherr and Neumann 2007; Waldherr et al. 2010; Nyuyki et al. 2011). Behavioral tests have confirmed the robust anxiolytic effect of OXT when administered icv or locally within brain regions such as PVN, AMY, PFC (Bale et al. 2001; Ring et al. 2006; Blume et al. 2008). Besides its anxiolytic effects, OXT plays a peculiar role in regulating fear and social behaviors, including social fear and social memory (Figure 4) (Menon and Neumann 2023). Early studies demonstrated that icv infusion of OXT promotes pro-social behaviors and prevents social avoidance in male rats (Lukas et al. 2011). Further research revealed that intra-LS application of OXT mediates social memory in male rats, particularly in interactions with juveniles and adult females (Lukas et al. 2013). Additionally, the increase in OXT release in the LS observed during repeated exposure to social stimuli (extinction training) was blocked in social fear conditioned male and virgin female mice (Zoicas et al. 2014; Menon et al. 2018). Notably, local OXT infusion into the LS has been shown to facilitate social fear extinction in both male and female mice (Menon et al. 2018; Zoicas et al. 2014). Interestingly, lactating female mice, following SFC, did not show social fear during extinction training, suggesting that the heightened activity of OXT system during lactation may promote the investigation of same-sex conspecifics and highlighting a potential shift in social behavior facilitated by OXT (Menon et al. 2018).

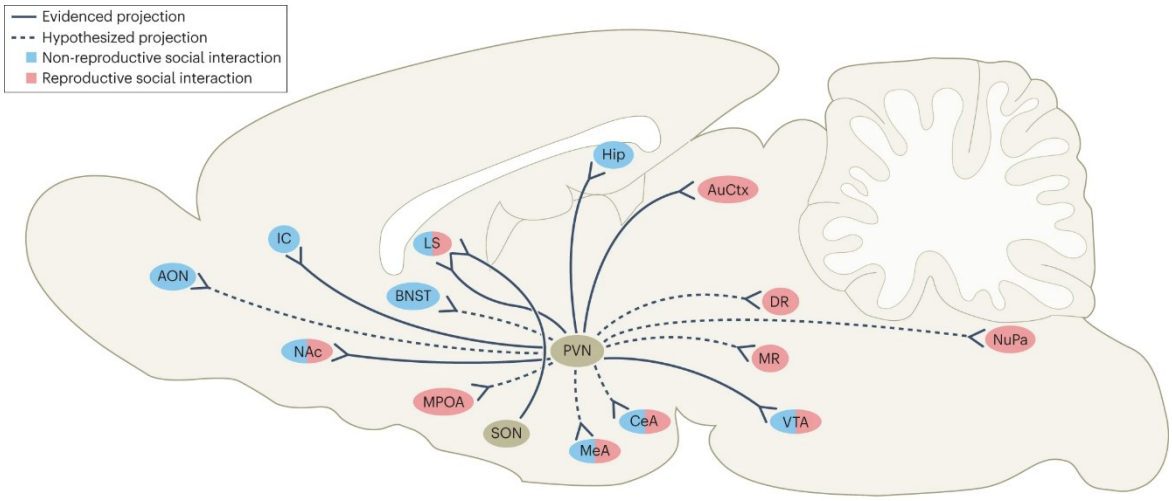

Figure 4. Illustration of the intracerebral projections of oxytocin (OXT) neurons from the hypothalamic paraventricular (PVN) and supraoptic (SON) nuclei to different brain regions. *Colors indicate when the innervated areas are activated or involved in the regulation of: non-productive social behaviors (blue) (e.g. social preference, social reward, social memory, social discrimination, inter-male and -female aggression) and reproductive social interactions (red) (e.g. mating preference, sexual behavior, pair bonding, maternal care and aggression), or both (blue and red). Solid lines indicate known projections, while dotted line represent hypothesized projections. AON, anterior olfactory nucleus; NAc, nucleus accumbens; IC, insular cortex; BNST, bed nucleus of the stria terminalis; MPOA, medial preoptic area; LS, lateral septum; MeA, medial amygdala; CeA, central amygdala; Hip, hippocampus; AuCtx, auditory cortex; DR, dorsal raphe nucleus; MR, median raphe nucleus; VTA, ventral tegmental area; NuPa, nucleus paragigantocellularis. Image from (Menon and Neumann 2023).*

Additionally, it was found that social fear acquisition influences OXTR binding in various brain regions, with an increase observed in the LSd 48 hrs after social fear acquisition (Zoicas et al. 2014). In contrast, overexpression of OXTR in the LS has been shown to increase social avoidance induced by social-defeat (Guzmán et al. 2013). This aligns with findings from other studies indicating that in the BNST, OXT can induce stress, anxiogenic effects, and social fear/avoidance (Duque-Wilckens et al. 2020; Luo et al. 2022). Similar contradictory outcomes have also been observed in humans studies, where intranasal OXT had both prosocial and anxiolytic effects (Meyer-Lindenberg et al. 2011), yet also increased startle response to stressful stimuli (Grillon et al. 2013) and heightened recollection of aversive events (Bartz et al. 2010; MacDonald and Feifel 2014). These mixed results suggest that OXT effects in both humans and rodents may vary depending on a range of factors, including brain region, context, sex, and early life experiences (MacDonald and Feifel 2014; Maroun and Wagner 2016; Jurek and Meyer 2020).

While much of the research has traditionally focused on neuronal mechanisms of OXT, recent studies have begun to explore the role of astrocytes in mediating its anxiolytic effects. Emerging evidence suggest that the anxiolytic effects of OXT within the CeA and PVN are significantly mediated through astrocytes (Wahis et al. 2021, Meinung et al., *in revision*). This shift in focus underscores the need for a broader investigation into not just neuronal pathways but also the potential contributions of astrocytic pathways to OXT effects. Given the critical importance of social interactions for psychological well-being, and the emerging role of astrocytes in mediating socio-

emotional behaviors (Kofuji and Araque 2021b; Shigetomi et al. 2016; Zhou et al. 2019; Cho et al. 2022; Bender et al. 2017), these findings offer a promising avenue for further investigation to understand how astrocytes contribute to socio-emotional dysfunctions and OXT-mediated effects. Therefore, the following section will provide an overview of astroglial cells to better understand their potential role in this context.

5. Astrocytes

"We are all now connected by the Internet,
like neurons in a giant brain [connected by the glia]"

adapted from Stephen Hawking

Representing the most complex and age-resilient system of the human body, the brain is composed of about 10^{11} of neurons and an equal number of glial cells (Bartheld et al. 2016). Derived from the Greek word for "glue", the term glia was originally used by Virchow in 1846 to describe what was then thought to be a connective structure within the brain (Somjen 1988). However, Ramon y Cajal challenged this concept in 1909, predicting that glia had more significant roles beyond being static bystanders (Ramón y Cajal 1909). Today, it is understood that glia are critical for maintaining brain function throughout the lifetime, encompassing specialized cells such as oligodendrocytes, microglia, and astrocytes (Allen and Lyons 2018). Oligodendrocytes represent the source of the myelin sheaths that wrap around axons, crucial for enhancing the conduction velocity of action potential in the CNS (Allen and Lyons 2018). Microglia, primarily known as immune cells of the brain, also play a roles in diverse developmental and functional processes, such as synaptic pruning, clearance of apoptotic neurons, and interactions with various cell types in the CNS (Allen and Lyons 2018). Astrocytes, the most abundant type of glial cells in the CNS (Bartheld et al. 2016), were initially recognized as supportive elements of the nervous system (Somjen 1988). Over the years, they have been found to exert diverse and essential functions, ranging from regulating synapses and providing metabolic support to maintaining homeostasis and modulating circuits function (Verkhratsky et al. 2021; Allen and Lyons 2018).

Evolutionarily, neuroglia first appeared in response to the increased energy demands of an evolved central nervous system (Verkhratsky et al. 2019; Falcone 2022). In invertebrates with a centralized nervous system, such as flatworms, ancestral glial cells with basic supportive functions were found. As the complexity and functionality of the CNS increased in higher taxa like Annelida and Insects, more complex and structured "proto-astrocytes" emerged (Robertson 2014; Verkhratsky et al. 2019). The typical radiated morphology of astrocytes finally appeared in Chordata and low vertebrates, with radial glial cells becoming the main type of neuroglia in the CNS of vertebrates (Verkhratsky et al.

2019). Astroglia became increasingly complex in parallel with the evolution of higher intellectual functions and increased support demands, achieving significant complexity, heterogeneity, and functionality in higher vertebrates, including higher primates and humans (Verkhratsky and Nedergaard 2018). Functionally, astroglia have progressed at each phylogenetic stage, adapting to support the expanding cognitive and metabolic needs of the CNS (Falcone 2022; Verkhratsky et al. 2019; Robertson 2014).

Similar to neurons and oligodendrocytes, astrocytes originate from radial glia during early embryonic development within the neuroepithelium (Verkhratsky and Nedergaard 2016). Representing the precursor neural cells, radial glia underdo differentiation processes guided by complex molecular signaling pathways, leading to their transformation into astrocyte and subsequent migration (Verkhratsky and Nedergaard 2016). Unlike neurons, the astrocyte population at birth is relatively small, but expands substantially throughout life, ultimately reaching a 1:1 ratio with neurons in the adult brain (Verkhratsky and Nedergaard 2018; Bartheld et al. 2016). This strong glia-neuronal connection in relation to increased energy demands, underlies the pivotal contribution of astrocytes in the CNS functionality, particularly in response to heightened neuronal energy demands observed in complex mammalian CNS, including those of rodents and humans (Falcone 2022). The specialization of astrocytes in the mammalian brain, coupled with their heterogeneity and plasticity across various brain regions, physiological states, functions, and pathological conditions, highlights the complexity of these cells and underscore their crucial role in maintaining CNS function (Verkhratsky and Nedergaard 2016, 2018; Falcone 2022).

5.1. Astrocyte functions

As glial cells, astrocytes fulfill their traditional "glue" function by sustaining and regulating the neuronal network of the CNS, comparable to how rails support and direct high-speed trains. Despite their initial perception as having a superficial role, they play a pivotal role in maintaining homeostasis across all levels, from the molecular and cellular scale to the overall functioning of the synaptic transmission (Verkhratsky and Nedergaard 2016). Through phylogeny, astrocytes have consistently fulfilled a vital role in supporting and maintaining the central nervous system (CNS), providing structural nutritional support to neurons through various mechanisms (Verkhratsky et al. 2019). Firstly, astrocytes are integral components of the blood-brain barrier (BBB), a diffusion barrier formed by cerebral capillaries, endothelial tight junctions, perivascular pericytes, and astrocyte endfeet. (Ballabh et al. 2004; Daneman 2012; Daneman and Prat 2015). This barrier allows essential nutrients to pass into the brain while simultaneously preventing in harmful substances from entering (Zlokovic 2008; Daneman 2012; Daneman and Prat 2015). Beyond their role in the BBB, astrocytes play integral roles in regulating ion concentrations and metabolite flow to maintain optimal neuronal

function and signaling (Verkhratsky and Nedergaard 2018). Astrocytes manage to regulate ion balance and neurotransmitter levels through their intricate, ramified processes and the expression of various ion channels and transporters on their membranes (Verkhratsky et al. 2020). For example, they actively uptake excess potassium ions (K+) from the extracellular space to prevent disruptions in neuronal signaling, subsequently releasing them into nearby blood vessels (Verkhratsky and Nedergaard 2018; Verkhratsky et al. 2020). Equally crucial is their role in modulating neurotransmitter levels within the synaptic cleft, including glutamate, GABA, and glycine, essential for regulating neuronal connectivity (Sofroniew and Vinters 2010). Excess glutamate in the synaptic cleft can lead to excitotoxicity, where overactivation of N-methyl-D-aspartate (NMDA) receptors on neurons triggers harmful cascades that may result in cell death (Mark et al. 2001; Verkhratsky 2007). To prevent this, astrocytes express specific transporters to take up glutamate from the synaptic cleft and convert it into glutamine via the enzyme glutamine synthetase (Bak et al. 2006). Glutamine is then released back into the synapses for recycling, maintaining appropriate levels of glutamate and protecting neurons from excitotoxic damage (Sattler and Rothstein 2006; Bak et al. 2006) (Figure 5).

In response to neuronal activity, astrocytes release gliotransmitters such as ATP, glutamate, D-serine, GABA, and lactate (Parpura et al. 1994; Oliet and Mothet 2006; Koizumi 2010; Yoon and Lee 2014; Tang et al. 2014). These neuroactive substances bind to neuronal receptors, thus influencing overall synaptic function (Araque et al. 2014; Harada et al. 2015; Kofuji and Araque 2021b, 2021a). This bidirectional communication between astrocytes and neurons underscores the intricate interaction within the tripartite synapse model (Araque et al. 1999). The concept of tripartite synapses refers to the structural and functional interaction among three key components: the presynaptic neuron, the postsynaptic neuron, and the surrounding astrocytes (Araque et al. 1999). This model highlights the role of astrocytes as active participants in synaptic transmission, rather than merely passive support cells, highlights their critical involvement in regulating behavior and cognitive functions. Astrocytes owe their ability to actively participate in synaptic functionality to their elaborate morphology and structure, characterized by numerous processes, including the finest ones known as peripheral astrocytic processes (PAPs) (Lavialle et al. 2011; Bernardinelli et al. 2014; Verkhratsky and Nedergaard 2018). These astrocytic processes embrace synapses, integrating neuronal information and thereby enhancing synaptic activity and transmission for efficient signaling (Bernardinelli et al. 2014; Baldwin et al. 2024).

The crucial role played by astrocytes in improving signaling transmission through the integration of neuronal information includes not only synaptic function, but also extends to their involvement in synaptic development, maintenance, and elimination, as demonstrated in previous research (Nishida and Okabe 2007; Perea et al. 2009; Lippman Bell et al. 2010). Additionally, due to their proximity to both synapses and blood vessel, astrocytes can regulate blood flow response to synaptic activity

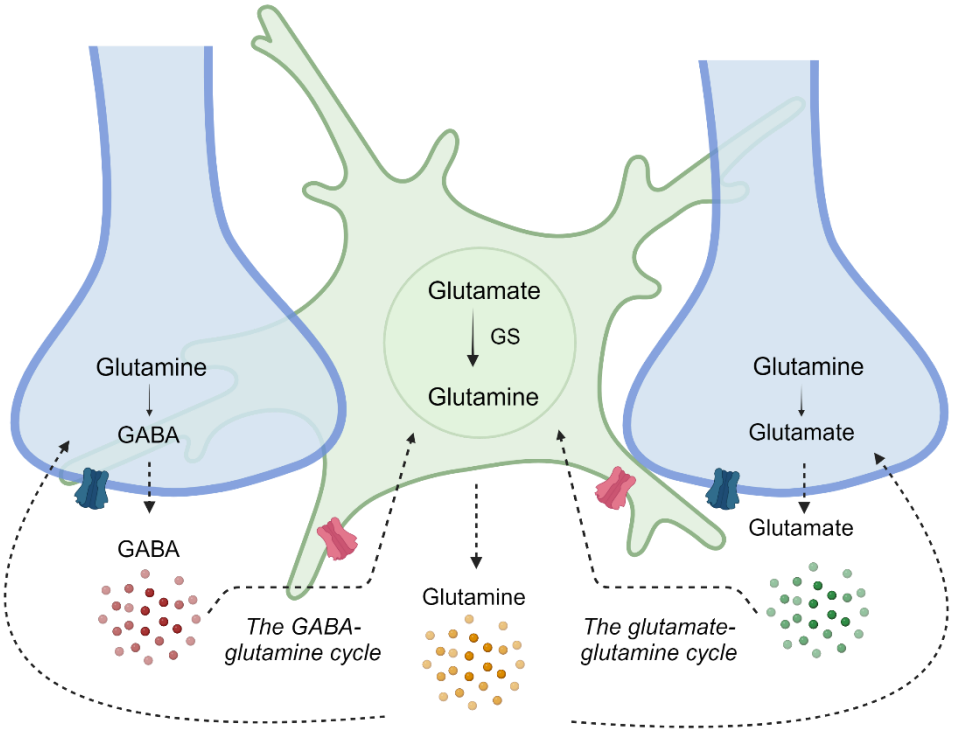

Figure 5. Schematic of the glutamate/GABA-glutamine cycle involving astrocytes and neurons. *Astrocytes play a certain role by taking up the majority of glutamate and a significant portion of GABA from the synaptic cleft, converting them into glutamine through the enzyme glutamine synthetase. Glutamine is then released back into the synaptic cleft where it is taken up by neurons to restock the neurotransmitter pool, facilitating ongoing neuronal signaling and maintaining optimal neurotransmitter levels. This cycle facilitates ongoing neuronal signaling and maintains optimal neurotransmission levels, protecting neurons from potential excitotoxicity caused by excessive neurotransmitter accumulation. Illustration created using Biorender.com.*

by producing and releasing various mediators such as prostaglandins and nitric oxide (Iadecola and Nedergaard 2007).

Fundamentally, neuron-astrocyte communication, gliotransmitter release, and general astrocytic function depend heavily on Ca^{2+} signaling (Verkhratsky and Nedergaard 2018). Although astrocytes were traditionally viewed as non-excitable cells incapable of generating action potentials in response to changes in membrane potential, they exhibit Ca^{2+}-based excitability in specific contexts (Charles et al. 1991). This excitability involves the release of Ca^{2+} from the endoplasmic reticulum in response to stimuli. Unlike neuronal electrical signals, which occur within milliseconds, astrocytic Ca^{2+} activity unfolds over minutes to hours (Bazargani and Attwell 2016), potentially explaining their involvement in slower processes within neural circuits. Intracellular Ca^{2+} fluctuations in astrocytes can be triggered indirectly from neuronal activity (Aguado et al. 2002; Perea et al. 2009), or directly through the activation of a wide variety of GPCR expressed in the astrocytic membrane (Araque et al. 1999; Kofuji and Araque 2021b). Interestingly, GPCR activation induces a rise in Ca^{2+} levels regardless on the type of the G protein activated (Durkee et al. 2019), although G_i proteins initially cause a transient Ca^{2+} increase followed by a decrease (Kol et al. 2020). Different types of Ca^{2+} permeable channels, transporters and exchangers expressed on the membrane of astrocytic processes,

contribute to the generation of Ca^{2+} signal (Shigetomi et al. 2016). Ca^{2+} elevations can occur locally as “microdomains” in specific thin area of astrocytic processes, and eventually, analogous to electrical signals in neurons, they may propagate to the main processes or soma (Pasti et al. 1997; Lia et al. 2021). Ultimately, Ca^{2+} waves can spread to adjacent astrocytes due to intercellular communication facilitated by connexin channels, which form gap junctions between astrocytes (Theis and Giaume 2012; Fujii et al. 2017). The opening of these gap channels can be triggered by an increase of intracellular Ca^{2+} signals, or even low external Ca^{2+} concentration (Suadicani et al. 2004; Scemes and Spray 2012; Khakh and McCarthy 2015). Forming astrocytic gap junctions, connexins are crucial for facilitating direct exchange of ions, metabolites, and signaling molecules between adjacent astrocytes (Verkhratsky and Nedergaard 2018). Through this extensive intercellular communication mediated by gap junctions, astrocytes coordinate their activities effectively, not only within the astrocytic networks but also supporting neuronal function and synaptic activity (Giaume and Venance 1998; Weiss et al. 2022). For instance, recent studies have highlighted connexins involvement in processes such as glutamate clearance and synaptic invasion (Pannasch et al. 2014; Pannasch et al. 2019). Ca^{2+} signals represent a remarkable aspect of intercellular communication within the astrocytic network and the interplay between astrocyte and other cells, including neurons (Khakh and McCarthy 2015; Verkhratsky and Nedergaard 2018; Eitelmann et al. 2023). The involvement of astrocytic Ca^{2+} transmission and connexins has been implicated in various aspects of neuronal function (Pannasch and Rouach 2013) and in the pathophysiology of neuronal diseases (Kuchibhotla et al. 2009; Torres et al. 2012).

Putting everything in a broader view, astrocytes emerge as dynamic and “social” cells within the brain´s intricate network. They can dynamically adjust their activity to environmental cues, meeting metabolic and signaling needs of neurons. In addition, they show remarkable abilities to interact with different components of the nervous system, including neurons, blood vessels, and other glial cells. They are not just supportive cells, but active participants in regulating brain functions.

5.2. Astrocyte morphology and identification

Undoubtedly, the astrocytic ability to coordinate and support neuronal function and synaptic activity stems from their developmental origins and unique morphology. In 1895, Lenhossék named them "astrocytes" due to their star-like shape, characterized by multiple branches extending from the soma. This morphological diversity is particularly fascinating, reaching greater complexity and size

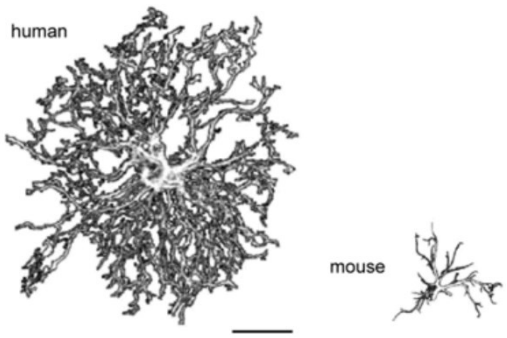

Figure 6. Graphical representation and GFAP immunostaining of human (left) and mouse (right) cortical astrocytes. *Illustration adapted from (Vasile et al. 2017).*

in humans compared to rodents (Figure 6) (Vasile et al. 2017). Among the various types, such as fibrous astrocytes and pericytes, protoplasmic astrocytes are the most abundant in the grey matter. They are distinguished by a small soma (~10 μm) from which 4-10 branches emerge, further branching into fine processes that form an elaborate arborization (Ogata and Kosaka 2002; Reeves et al. 2011; Verkhratsky and Nedergaard 2018). This extensive branching allows each astrocyte to embrace and contact approximately 100,000 synapses (Halassa et al. 2007).

As mentioned above, due to the noteworthy morphological heterogeneity, visualizing and identifying astrocytes is challenging, especially considering the absence of a universal marker that targets all types of astrocytic cells (Verkhratsky and Nedergaard 2018). Besides genetic profiling and the genetically controlled expression of astroglia-specific markers, or incubation with fluorescent probes with glial affinity, the most common techniques used to identify astrocytes are histochemical staining and immunocytochemistry (Verkhratsky and Nedergaard 2016). The most widely used astrocytic marker is glial fibrillary acidic protein (GFAP), an intermediate filament that, together with other proteins such as vimentin, forms the astroglial cytoskeleton (Hol and Pekny 2015). However, GFAP staining for morphology is limited as it reveals only the major branches, leaving the finer processes unstained (Connor and Berkowitz 1985). Another astrocytic marker is S100β protein, a Ca^{2+} binding protein acting as both a buffer and sensor for Ca^{2+} (Donato et al. 2013). Although it is widely used in both pathology and physiology, its specificity towards astrocytes is lower than that of GFAP since it is also expressed in oligodendrocytes, ependymal cells, vascular cells, and some neurons (Steiner et al. 2007; Rickmann and Wolff 1995). Markers linked to glutamate turnover are also widely used, including glutamine synthetase, whose cytosolic localization allows full visualization of the cell (Norenberg and Martinez-Hernandez 1979; Derouiche and Frotscher 1991), and glutamate transporters, such as EAAT-1 (GLAST) and EAAT2 (GLT-1), which are expressed exclusively in astrocytes, though is a region-specific manner (Williams et al. 2005). Relevant for the intercellular connectivity and the maintenance of a functional astrocytic network are the astrocyte homocellular

gap junctions composed from connexins (Cx), such as Cx26, Cx30 and Cx43 (Giaume et al. 1991; Nagy et al. 2001). In addition to the astrocytic markers, astrocyte activity can be visualized by monitoring Ca^{2+} transients due to the crucial role Ca^{2+} signals play in many astrocytic functions (Reeves et al. 2011; Khakh and McCarthy 2015; Semyanov et al. 2020). These transients can be detected by applying calcium indicators to astrocytes, which could be fluorescent dyes such as Oregon Green, or genetically encoded calcium indicator (GECIs) (Semyanov et al. 2020).

The morphological heterogeneity, functional peculiarities in different parts of the brain depending on neuronal activity, and their evolution in higher primates make astrocytes particularly challenging to study and characterize.

5.3. Astrocyte implications in memory and emotional behaviors

Although much has been discovered about the molecular basis of astrocyte structure diversity and plasticity, many questions remain about their involvement in synaptic and neural circuits, particularly in modulating higher cognitive functions and behaviors. As mentioned earlier, astrocytes respond to synaptic activity and contribute to synaptic connectivity and plasticity, which fine-tunes synaptic transmission and influences processes associated with memory and learning, such as long-term potentiation (LTP) and long-term depression (LTD) (Araque et al. 2014). Using highly selective chemogenetic and optogenetic approaches, recent studies have shown that activating the Gq pathway in astrocytes within the CA1 induces neuronal activity and LTP, subsequently improving memory performance in hippocampal-dependent tasks such as contextual fear memory (Adamsky and Goshen 2018; Mederos et al. 2019). Conversely, activation of the G_i pathway during memory consolidation did not affect short-term memory but impaired the retrieval of memories one month later (Kol et al. 2020).

Given their active involvement in synaptic dynamics, astrocytes are likely to contribute to the pathology of depression and anxiety disorders. Animal studies have demonstrated that astrocyte dysfunction is associated with the manifestation of depressive and anxiety phenotypes (Zhou et al. 2019). For instance, a depressive-like phenotype was observed following the application of the gliotoxin L-alpha-amino adipic acid (L-AAA) within the PFC and prelimbic cortex (Banasr and Duman 2008; David et al. 2019). L-AAA, a glutamate analogue, is taken up by astrocytic glutamate transporters and by binding to the glutamine synthetase, blocks the glutamine synthesis, leading to a disruption of the glutamate-glutamine cycle with a consequent reduced astrocytic function (McBean 1994; Brown and Kretzschmar 1998). Similar depressive-like phenotypes were observed following the disruption of glutamate transporters and gap junctional networks of astrocytes within the PFC (John et al. 2012; Sun et al. 2012).

In addition to their roles in the HIP and PFC, recent studies have identified astrocytes as integral components of fear circuits. Specifically, chemogenetic activation of astrocytes within the CeA reduced fear expression in a fear-conditioning paradigm in mice, suggesting an astrocytic fine-tune mechanism of synaptic activity (Martin-Fernandez et al. 2017). Interestingly, blocking Cx43 channel activity within the basolateral amygdala (BLA) prevented the acquisition of fear memories (Stehberg et al. 2012), indicating a role for gliotransmitters and astrocyte-astrocyte communication in modulating fear learning circuits (Orellana and Stehberg 2014). Furthermore, the role of astrocytes in remodeling synaptic transmission was demonstrated in a Pavlovian fear conditioning test, where astroglial process retraction was observed during memory consolidation, concomitant with an increase in synapses (Ostroff et al. 2014). This underscores the dynamic nature of astrocytes, illustrating their ability to adapt in response to the activation of specific brain regions.

Due to their heterogeneity, multifunctional aspects, and unique roles in regulating synaptic transmission, astrocytes have garnered increasing interest. Research groups are now investigating their involvement in emotional behaviors, particularly in relation to neuropeptides like OXT, which is known to influence these behaviors.

6. Astrocytic oxytocin signaling in anxiety-related behavior

As described, OXT has been extensively studied and associated with a wide range of emotional and social behaviors. While many studies have focused on neuronal effects of OXT, or without distinguishing between the precise target cell of OXT, the effects of OXT on astrocytes have gained increasing attention in recent decades. Pioneering studies starting in the 1980s reported that OXT influences astrocytic morphology in the PVN and the SON following infusions of synthetic OXT or during heightened OXT activity, such as lactation (Theodosis et al. 1986a; Theodosis et al. 1986b). Among other receptor types, astrocytes express OXTRs across the soma and processes in various brain regions, including the HIP, HYP, CeA, and LS (Wang and Hatton 2006; Wahis et al. 2021; Althammer et al. 2022b; Althammer et al. 2022c). By activating astrocytic GPCRs, OXT initiates a signaling cascade that results in the alteration of protein expression associated with cytoskeletal dynamics, such as beta-tubulin, elements of the ROCK pathway, and GFAP (Baudon et al. 2022). Recently, we could recently reveal (Meinung et al., *in revision*) that OXT remodels astrocytic cytoskeletal mainly via the PKC pathway.

OXT influences astrocytic roles in regulating synaptic transmission and plasticity from multiple perspectives. First, as already mentioned, OXT-induced morphological changes include the retraction of astroglial processes and increased neuronal somata contacts in the PVN and SON, leading to synapse reshaping (Langle et al. 2003; Theodosis et al. 1986a; Theodosis et al. 1986b). In

line with this, we observed), an increase in the spatial relationship between astrocytes and neurons in OXT-treated hippocampal slices, which could facilitate the formation of new synapses (Meinung et al., *in revision*), as already observed in the HYP (Hatton et al. 1984). Second, Meinung et al., (*in revision*) found that OXT induced cytoskeletal changes through the regulation of Cx43, a protein already known to affect the cytoskeleton of various cell types (Kameritsch et al. 2012; Matsuuchi and Naus 2013). Particularly, OXT-induced astrocytic cytoskeletal remodeling was prevented in Cx43 knockout (KO) mice, but not in Cx30 KO mice, suggesting a selective involvement of Cx43 in OXT-induced cytoskeletal dynamics and therefore on astrocytic intercellular communication. (Meinung et al., *in revision*). Lastly, the role of astrocytic calcium activity in overall astrocytic function was previously mentioned, especially in the release of gliotransmitters and remodeling of cellular structure (Kofuji and Araque 2021b). It has been found that the activation of oxytocin GPCR triggers astrocytic calcium transients by increasing calcium from intracellular stores (Di Scala-Guenot et al. 1994). Additionally, the activation of OXTR-expressing astrocytes within the CeA increased calcium activity, which subsequently triggered the electrical activity of nearby neurons through NMDAR activation, likely due to the release of the gliotransmitter D-serine (Wahis et al. 2021),. This highlights the importance of gliotransmitter function in modulating nearby synapses by releasing gliotransmitters into the synaptic cleft and activating presynaptic or extrasynaptic receptors such as NMDAR (Oliet et al. 2008; Baudon et al. 2022). Interestingly, Wahis et al. also found that this astrocyte-neuron communication in the CeA mediates the anxiolytic effects of oxytocin in pain-related anxiety (Wahis et al. 2021). Similarly, we found that the well-known anxiolytic effect exerted by OXT within the PVN (Blume et al. 2008; van den Burg et al. 2015; Jurek and Neumann 2018) was abolished following a viral-induced reduction of astrocytic OXTR expression in rats (Meinung et al., *in revision*).

Although many underlying mechanisms related to astrocytic synaptic regulation, gliotransmission release, and OXT-induced effects on astrocytes are yet to be unraveled, the potential roles of astrocytes and oxytocin in emotional behaviors are still ripe for discovery.

7. Aim of the study

Social interactions are fundamental in our interconnected society, and severe social deficits, such as those seen in SAD, can be profoundly debilitating. SAD frequently co-occurs with other psychological disorders, including substance abuse, and the limitations of current treatment options highlight an urgent need for further investigation. While much research has focused on neuronal mechanisms, my thesis explores the potential involvement of astrocytes in social fear in mice to expand our understanding of the underlying mechanisms of SAD.

Considering the critical role of OXT in regulating social behaviors, my study also investigates whether astrocytes may contribute to these effects. With the higher prevalence of SAD in women and the influence of sex steroids on cellular mechanisms, an additional objective is to examine sex-based differences in astrocytic function and social fear response. Finally, my research focuses on the astrocytic impact within the LS, a brain region known to modulate social behaviors, particularly social fear.

To sum up, this research aims to investigate the roles of astrocytes and astrocytic OXT signaling in influencing the phenotype of SAD in male and female mice, with a particular focus on understanding sex differences within the LS. Specifically, this thesis will:

a) Characterize the distribution of astrocytes and OXTR$^+$ astrocytes within the LS in male and female mice

To understand the distribution of astrocytes and specifically those expressing OXTR in the LS, I first aimed to map both the overall presence of astrocytes and the specific localization of OXTR-expressing (OXTR$^+$) astrocytes in male and female mice. This will provide a detailed profile of astrocyte distribution across sexes in the LS and its subregions, i.e., the rostral and caudal LS.

b) Analyze the effects of social fear acquisition and extinction on astrocytic morphology and protein expression in the LS

Given the emerging role of astrocytes in memory and fear-related processes, I aimed to investigate whether the acquisition and extinction of social fear influence astrocytic morphology and the expression of key astrocytic proteins, such as GFAP, connexins, and glutamate transporters in the LS of male mice.

c) Determine whether LS astrocytic structural depletion induced by L-AAA affects socio-emotional behaviors, including responses to the SFC paradigm in male and female mice

Recognizing the role of astrocytes in synaptic regulation, I hypothesized that dysfunctions in astrocytic activity within the LS might disrupt neuronal circuits involved in socio-emotional behaviors, particularly those related to social trauma. To test this, I aimed to analyze social behaviors in male and female mice after astrocytic structural depletion infusing L-AAA in the LS.

d) Explore the influence of OXT on LS astrocytic function in relation to the SFC paradigm in male and female mice

Given the significant role of OXT in social behaviors and its emerging influence on astrocytic function, I aimed to analyze Ca^{2+} signaling in LS brain slices taken after SFC under basal

conditions and in response to TGOT (an OXT agonist) in both male and female mice *ex vivo*. Based on these results, I will further explore whether reduced expression of astrocytic OXTR affects the regulation of social fear behaviors in both male and female mice.

Overall, this thesis aimed to elucidate the potential contribution of astrocytes and specifically astrocytic OXT signaling in the LS in social fear memory and extinction.

In this section, a detailed description is provided of the methods used during the current thesis. For a better understanding, behavioral techniques are followed by molecular methods.

1. Animals and husbandry

Wildtype female (Charles River, Sulzfeld, Germany, 8-12 weeks of age at the start of experiments) were kept group-housed under standard laboratory conditions (12/12 h light/dark cycle, lights on at 06:00, 22°C, 60 humidity, food, and water ad libitum) in polycarbonate cages (16 x 22 x 14 cm). Three days prior to the start of the experiment, they were transferred to individual housing. Wildtype lactating CD1 mice (8-9 weeks old) were housed under the same conditions until three days before their expected delivery, after which they were also single-housed. Wildtype CD1 male mice (8-9 weeks old) were kept single-housed under same standard laboratory conditions until described otherwise. Age and sex-matched CD1 mice were used as social stimuli in the SFC paradigm and the social preference test (SPT). All experimental procedures were performed between 08:00 and 14:00 hrs in accordance with the Guide for the Care and Use of Laboratory Animals by the National Institutes of Health, Bethesda, MD, USA, approved by the government of Oberpfalz and performed according to international guidelines on the ethical use of animals and ARRIVE guidelines (Kilkenny et al. 2010). All efforts were made to minimize the number of animals used and their suffering.

2. Behavioral testing

2.1. Social Fear Conditioning (SFC) Paradigm

SFC was performed as previously described on three consecutive days (Toth et al. 2012). Three days before starting the paradigm all animals were transferred to observational cages and were single-housed.

Social fear acquisition (Day 1). On the first day of social fear acquisition, the experimental mouse was transferred from its home cage to the conditioning chamber (a transparent perspex box with a stainless-steel grid floor, measuring 45 x 23 x 36 cm). Here, after a 30 s adaptation period, the mouse was exposed to an empty wire mesh cage (7 x 7 x 6 cm) as a non-social stimulus for a duration of 3 min. The empty cage was then replaced by an identical small cage containing an unfamiliar sex- and age-matched conspecific. The control group of mice that was not socially conditioned (SFC^-) and allowed to freely investigate the social stimulus in the conditioning chamber for a duration of 3 min,

without receiving any foot shocks. The socially fear conditioned group (SFC^+) was given a mild 1-second electric foot shock (0.7 mA, 1 s) each time they investigated the social stimulus. If the experimental animal made no more contacts for 6 min after the first shock, or 2 min after receiving 2 or more shocks, it was considered successful conditioned and was returned to its home cage. On average, SFC^+ mice received 2-3 foot-shocks. A small empty wired cage, similar to the one used during conditioning, was placed inside the home cage overnight to prevent fear manifestation towards the object during extinction training.

Social fear extinction (Day 2). The day after SFC, social fear extinction training was performed in the home cage of each mouse. Specifically, the mouse was exposed first to 3 non-social stimuli (empty cages) to access non-social investigation as a parameter of non-social fear and general anxiety-related behavior. It was then exposed to 6 different unfamiliar social stimuli, 6 age- and sex-matched mice. Each stimulus was presented for 3 min, with a 3 min inter-exposure interval. During the session, two key behaviors were analyzed: investigation time, defined as the time the mouse spent interacting and making direct contact with the stimulus (Toth et al. 2012), and vigilance time, defined as the time spent moving or stationary (e.g. behaviors such as freezing, stretch-attend posture, tail rattling) with the head oriented toward the stimulus (Williams et al. 2018; Williams et al. 2020). These behaviors were recorded and later analyzed by a trained observer, blind to the treatment conditions, using the JWatcher program (V 1.0, Macquarie University and UCLA). Successful social fear conditioning was indicated by reduced social investigation during the first social stimulus exposure when compared to the SFC^- group. A gradual increase in social investigation throughout the extinction training indicated successful extinction of social fear.

Recall (Day 3). The day after social fear extinction, a recall of the extinction was performed in the home cage. As the day before, each mouse was exposed to 6 different unfamiliar social stimuli (age- and sex-matched mice) for 3 min, with a 3 min inter-exposure interval. Animal behavior, specifically investigation and vigilance time, was videotaped and analyzed by a trained observer, blind to treatment, using the JWatcher program (V 1.0, Macquarie University and UCLA).

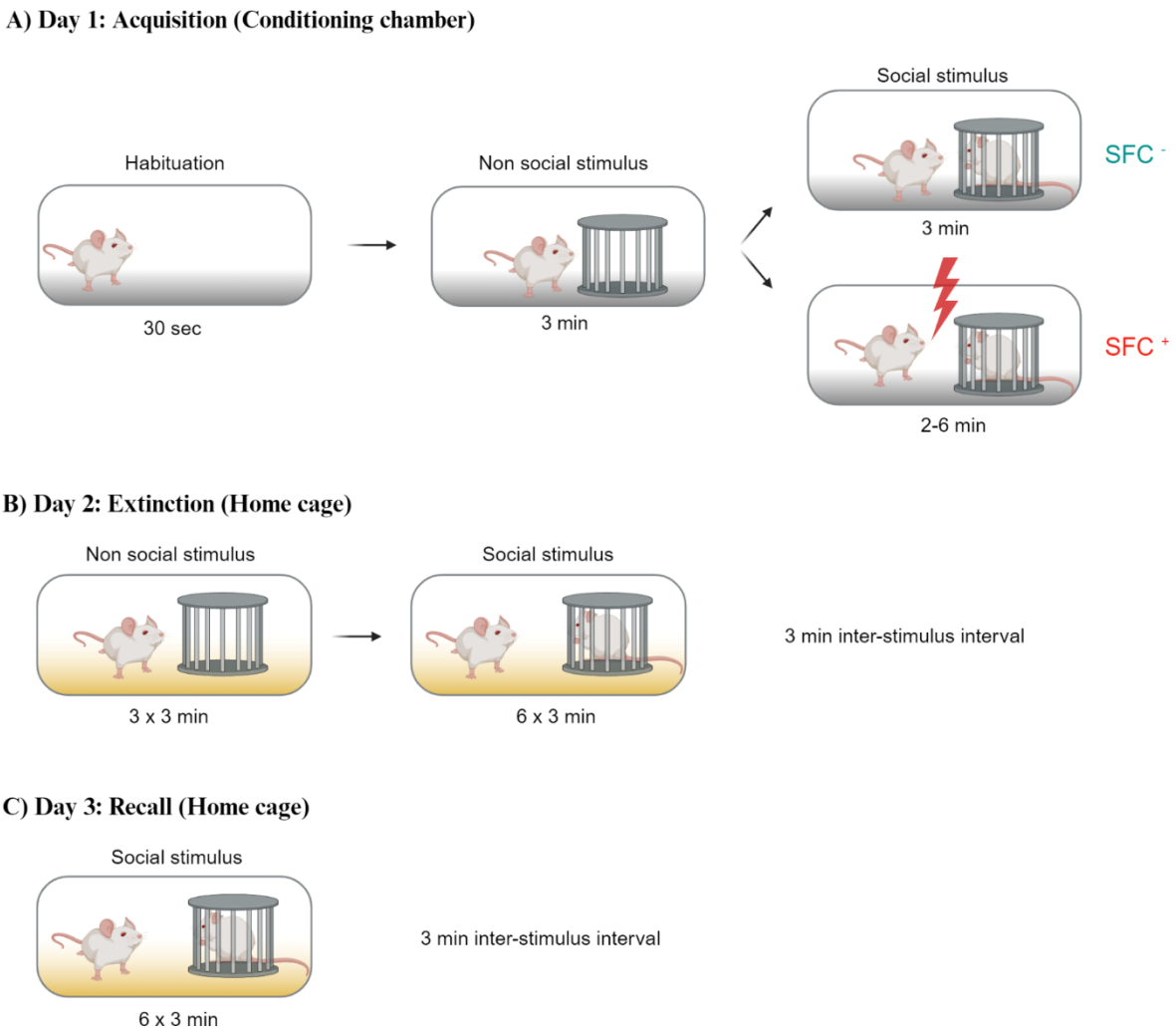

Figure 7. Schematic illustration of the Social Fear Conditioning (SFC) Paradigm. *A) On day 1 during acquisition of social fear, after 30 s of habituation in the conditioning chamber, mice were exposed for 3 min to a non-social stimulus. Unconditioned mice (SFC$^-$) were allowed to explore freely the social stimulus, while conditioned mice (SFC$^+$) received a foot shock when investigating the social stimulus. B) On day 2 during social fear extinction, mice were exposed to 3 non-social stimuli and 6 social stimuli, each for 3 min, with 3 min interval between exposure. C) On day 3 during social fear recall, mice were exposed again to 6 social stimuli to evaluate successful social fear extinction. Image adapted from (Menon et al. 2018).*

2.2. Social Preference Test (SPT)

To test naturally occurring of social approach-avoidance behaviors, the social preference test was performed as previously described (Lukas et al. 2011) with minor modifications. The apparatus consisted of three adjacent chambers, connected by small opening that allowed the mouse access. The test consisted of three phases:

- Habituation. The mouse was placed in the central (neutral) chamber, from which had the access to investigate the entire apparatus freely for 5 min.
- Social stimulus. An empty wired caged (7 x 7 x 6 cm) was placed as a non-social stimulus in one of the outer chambers, while a wired cage containing a conspecific was placed as

social stimulus in the other outer chamber. The experimental mouse was allowed to freely explore both stimuli for 5 min.

- Novel social stimulus versus familiar mouse. The empty wired cage was replaced with a similar one containing another conspecific, representing the novel social stimulus. The experimental mouse was allowed to freely explore the known and the unknown conspecific for 5 min.

Animal behavior was videotaped and analyzed by a trained observer blind to the treatment using the BORIS software (http://www.boris.unito.it). As a measure of social preference, the amount of time spent interacting with the social contact versus non-social contact was calculated. In addition, the investigation time between the familiar and the novel mouse was measured and recognized as social recognition. Other kind of behaviors such as rearing, self-grooming and stretched approaches were also measured.

2.3. Elevated plus maze (EPM)

In order to address general anxiety-related behavior, mice were tested on the EPM as previously described (Lister 1987; Menon et al. 2018). The maze consisted of two opened (6 x 30 x 0.2 cm, 100 lx) and two closed (6 x 30 x 16 cm, 30 lx) arms departing from a central and neutral area (6 x 6 cm) at an elevation of 35 cm above the ground. The test started by placing the animal on the central area facing a closed arm and allowed to freely explore the apparatus for 5 min. Animal behavior was videotaped and analyzed by a trained observer blind to treatment using the lab-owned plus maze DOS program. The number of entries and time in opened arms was an indicator of anxiety-related behavior.

2.4. Forced swim test (FST)

Depressive-related behavior was tested on mice, by performing FST as previously described (Porsolt et al. 1977; Slattery et al. 2012) with minor adaptations. The mouse was placed for 5 min in an acryl glass cylinder (25 cm of diameter) filled with water at a temperature of 23 +/- 1 °C and. Floating, swimming and struggling behavior was videotaped and analyzed by a trained observer blind to treatment using the JWatcher program (V 1.0, Macquarie University and UCLA). Floating or immobility was defined as the absence of active, escape-oriented behaviors such as struggling and swimming. An increase in immobility time in this test indicates a depressive-like phenotype.

3. Surgical procedures

All surgeries were preceded by a one-week habituation phase after the animal´s arrival. Surgery was performed under isoflurane anesthesia (4% Isoflurane, Abbott Gmbh Germany) and semi-sterile conditions (Toth et al. 2012; Menon et al. 2018). Mice received a subcutaneous injection of the analgesic Buprenorphine (0.05 mg/kg, Buprenovet, Bayer, Germany). Thirty minutes later they were positioned in a stereotactic frame (Kopf Instruments, Canada). To protect their eyes, an ophthalmic ointment (Bepathen, Bayer, Germany) was applied. Local anesthesia was provided by lidocaine application (Lidocaine hydrochloride 2%, Bela-pharm, Germany) on the top of the skull. All coordinates used are based on the mouse brain atlas (Franklin and Paxinos 2019).

3.1. Cannula implantation

To perform local intracerebral drug infusion, guide cannulae (8 mm long 23 G, Injecta Gmbh, Germany) were stereotaxically implanted bilaterally 2 mm above the target LSc based on the following coordinates: anterior-posterior (AP) +0.15 mm, medio-lateral (ML) ± 0.5 mm and dorso-ventral (DV) -1.6 mm from the bregma, as adapted from previous research (Menon et al. 2018). The cannulae were then fixed by using two stainless screws and dental cement (Kallocryl, Speiko-Dr. Speier Gmbh, Germany) and closed with a stainless-steel stylet (27 G) to prevent infections by contact with the external environment. After surgery mice were single housed and given at least five days to recover, during which time they were handled (holding, cleaning of stylets) daily to habituate them to the experimental procedure and minimize non-specific stress responses during the behavioral testing.

3.2. Intracerebral microinfusions

To specifically knockdown OXTR mRNA in astrocytes of the LSc, an adeno-associated virus (AAV) expressed under the GFAP promoter, combined with short hairpin RNA (shRNA) and mCherry fluoroprotein was used (AAV6-GFAP-*Oxtr*-mCherry-shRNA constructs (10^{12}), VectorBuilder). Animals received either AAV6-GFAP::shRNA (shRNA) vector or a control vector (scrRNA) (custom designed, VectorBuilder) microinfusions. The microinfusions were administered using a 5-µl micropipette (VWR, Darmstadt, Germany, inner diameter of 0.3 mm), pulled to create a long, narrow shank and calibrated so that 1-mm on a scale on the tubing corresponded to a volume of ~ 70 nl. A total volume of 280 nl / hemisphere of the shRNA or scrRNA vector was slowly infused into the LSc at AP +0.15 mm, ML ±0.5 mm and DV -3.2 mm from bregma by pressure infusion. To ensure proper diffusion of the virus within the target area, the infusions were performed in two different dorso-ventral positions: after the first infusion (AP +0.15 mm, ML ±0.5 mm and DV -3.2

mm from the bregma), the micropipette was kept in place for 2 min to guarantee appropriate distribution. After that, the micropipette was kept for other 3 min at the second position (AP +0.15 mm, ML ±0.5 mm and DV -2.9 mm from the bregma) to prevent the virus from diffusing to other regions while removing the micropipette. The wound was sutured using sterile nylon material and treated with Lidocaine (Lidocaine hydrochloride 2%, Bela-pharm, Germany). During the three-week post-surgical period, male mice were kept single-housed to avoid fighting. Female mice were kept single housed for 5 days to prevent injuries at the wound by grooming each other and to allow them to recover. After this initial period, female mice were group-housed until the end of the three-week post-surgical period. Behavioral experiments were performed three weeks after stereotaxic surgery.

4. Intracerebral infusions

4.1. L-AAA infusion

To determine the effect of the gliotoxin L-alpha-aminoadipic acid (L-AAA, Santa Cruz Biotechnology sc-202200A) within the LSc on socio-emotional behaviors, two concentrations of L-AAA (10 µg/µl and 25 µg/µl) were tested and adapted from previous studies (Banasr and Duman 2008; David et al. 2019). The stock solution of L-AAA (100 µg/µl) was prepared dissolving L-AAA powder in phosphate-buffered saline (PBS, 10 x) solution, using alternating sonification and vortexing steps. Once a homogenous solution was obtained, it was diluted by adding PBS (10x) to the desired concentrations. Mice received either L-AAA infusions (10 µg/µl or 25µg/µl; 0.2 µl/hemisphere) or PBS as control (0.2 µl/hemisphere) for two consecutive days. The infusions were performed by using an infusion cannula (27G, 10 mm long) inserted into the intracerebral guide cannula, which was connected via a polyethylene tube to a Hamilton syringe (Hamilton Company, Switzerland) to ensure the precise volume infusion. After the infusions, the cannula was kept in place for ~ 30 s to ensure proper local substance diffusion. To assess the effects of L-AAA-induced astrocytic structural depletion, behavioral tests were performed three days after the last infusion.

4.2. OXT infusion

To study OXT effects on astrocyte morphology in the LSc, an OXT dilution (5 ng/ 0.2 µl; Sigma Aldrich O6379) was freshly prepared from concentrated stock solution on the same day of the experiment, by adding sterile Ringer´s solution (0.9% NaCl, B. Braun, Melsungen AG, Germany). Mice received bilateral infusions of either OXT (0.2 µl/hemisphere) or sterile Ringer´s solution as control (0.2 µl/hemisphere), using the same infusion system already described above. 10 min after the infusions, animals were anesthetized for subsequent perfusion and brain harvesting (see section 5.1.).

5. Perfusion, tissue collection and slice preparation

5.1. Intracardial perfusion

Animals were anesthetized by intraperitoneal (ip) administration of a mixture of ketamine (10% 1 ml/kg, Medistar Arzneimitter GmbH, Germany) and xylazine (2%, 0.5 mL/kg, Serumwerk Bernburg AG, Germany). Mice were then intracardially perfused using ice-cold 0.01 M phosphate buffered saline (1x PBS) and 1x PBS supplemented with 4% PFA (Sigma Aldrich, Germany, pH 7.4) at a speed of 19 mL/min for 3 min. Brains were subsequently harvested and postfixed for 24 h at 4 °C in 4% PFA solution, and cryoprotected in 30% sucrose in 1 x PBS for 48 h. Afterwards brains were rapidly flash-frozen in N-methylbutane pre-cooled in dry ice and stored at -80 °C until further analysis (see sections 6.4. for immunohistochemistry and 6.5. for RNA scope).

5.2. Snap frozen tissue

To analyze changes in protein or gene expression, animals were deeply anesthetized using CO_2. Afterwards their brains were rapidly removed, flash-frozen in N-methylbutane pre-cooled in dry ice and stored at -80 °C. The brains were cryo-sliced in 300 µm-thickness coronal sections (Bregma +0.38 to -1.82), from which micro punches from caudal septum and hippocampus were obtained using a stainless-steel cannula (1 µm-diameter). These punches underwent different procedures depending on the subsequent steps, either for protein expression analysis (see section 6.2.) or gene expression analysis (see section 6.3.).

6. Molecular methods

6.1. Protein expression analysis

To study the SFC effects on astrocytic protein expression, male mice were sacrificed at a specific time point after the last behavioral test (either 1.5 or 24 hrs after the last experiment) and the tissue collection was performed as described above (see section 5.2.).

6.1.1. Protein extraction and quantification

The fresh brain tissue punches obtained were suspended in RIPA lysis buffer (Sigma Aldrich) and incubated on ice for 45 min under regular vortexing. After a 20-min centrifugation (13200 g, 4 °C), the supernatant containing the protein lysate was then transferred into fresh tubes. Prior to further characterization, the protein concentration was measured using a colorimetric BCA protein assay kit (Pierce ™ BCA Protein Assay Kit, Thermo scientific) following the manufacturer´s instructions. This consisted in preparing a standard curve with seven solutions with known protein concentrations (2 µg – 0.025 Albumin) mixed with 200 µl of BCA solution. In parallel, 2 µl of protein lysate was treated similarly. After 30-min of incubation at 37 °C, the resulting luminescent reaction was photometrically measured at 570 nm using a Fluorescent reader (FLUOstar OPTIMA, BMG Labtech). The values were the mean result of sample duplicates.

6.2. SDS-PAGE and Western blot analysis

To assess protein expression, 25 µg of the protein sample were mixed with 4x Laemmli Buffer (Table 6), then denatured at high temperature (either 70 °C for 15 min or at 95 °C for 5 min, for detailed blotting protocols see Table 3). Ultimately, they were loaded onto 12.5% Criterion ™ TGX Stain-Free ™ Gel (Bio-Rad, Germany) for electrophoretic separation at 70 V for 20 min, followed by 1.5 h at 140 V. A pre-stained protein ladder (Fermentas Inc., Glen Bumie, USA) was used as a marker to determine the size of the proteins. After electrophoresis, the gel was activated via UV-induction, and the proteins were transferred onto a nitrocellulose membrane for 30 min using Trans-Blot® Turbo™ Mini Nitrocellulose Transfer Packs (Bio-Rad). To measure the amount of total protein, which represents the internal reference control during subsequent analysis, the membrane was exposed for 2.5 min to UV-light using the ChemiDoc XRS+ Imager (Bio-Rad). Afterwards, the membrane was blocked for 90 min at RT with an appropriate blocking solution, followed by incubation with the primary antibody over night at 4 °C (see Table 3). Subsequently, the membrane was washed three times in Tris-buffered saline with 0.1 % Tween-20 (TBS-T, pH 7.6) for 5 min to remove unbound residues of the primary antibody and incubated for 30 min at RT with the secondary antibody conjugated with horseradish peroxidase (see Table 3). After three additional washing steps for 5 min in TBS-T, the membrane was incubated with the detection reagents Super Signal™ West Dura Extended Duration Substrate (Thermo Fisher Scientific) or Clarity Max™ Western ECL Substrate (for Cx30, Bio-Rad). Protein bands were then visualized via image acquisition using ChemiDoc XRS+ System (Bio-Rad). All images were analyzed with Image Lab Software (Bio-Rad) and the amount of the target protein was normalized to the respective amount of total protein. If needed, the membrane was re-used to detect additional proteins. For this purpose, a Restore Western Blot Stripping Buffer (#21059, Thermo Fisher Scientific) was applied to the membrane for 15-20 min to remove the primary-antibody complexes. The blot was then blocked in the appropriate blocking solution for 30 min and subjected to the antibody staining protocol as described above.

Table 3: List of antibodies with their respective application protocols used in immunoblotting experiments.

Target	Denaturation	Blocking solution (1 h, RT)	Primary AB (o.n., 4 °C)	Secondary AB (30 min, RT)
GFAP	95 °C for 5 min	5% BSA in TBS-T	GFAP cs123895 1:2000 5% BSA in TBS-T	Anti-rabbit IgG, 7074S 1:1000 in TBS-T
Cx30	70 °C for 15 min	5% MP in TBS-T	Cx30 Thermo 71-2200 1:250 5% MP in TBS-T	Anti-rabbit IgG, 7074S 1:1000 2% MP in TBS-T
Cx43	70 °C for 15 min	5% BSA in TBS-T	Cx43 cs3512S 1:1000 5% BSA in TBS-T	Anti-rabbit IgG, 7074S 1:1000 in TBS-T
pCx43	95 °C for 5 min	5% BSA in TBS-T	pCx43 cs3511S 1:1000 5% BSA in TBS-T	Anti-rabbit IgG, 7074S 1:1000 in TBS-T
EAAT1	95 °C for 5 min	5% MP in TBS-T	EAAT sc123895 1:400 5% MP in TBS-T	mIgGκ, BP-HRP sc-516102 1:1000 2% MP in TBS-T
EAAT2	70 °C for 15 min	5% BSA in TBS-T	EAAT2 sc515839 1:10 000 5% BSA in TBS-T	mIgGκ, BP-HRP sc-516102 1:1000 in TBS-T

RT: room temperature; o.n.: over night.

6.3. Gene expression analysis

To quantify OXTR mRNA expression following the short harpin-induced knockdown (see 3.2), mice were sacrificed, and brain tissue was collected following the above described protocol (see 5.2).

6.3.1. RNA isolation

Brain punches from the septum were collected in 1.5 ml Eppendorf tubes and maintained on ice throughout the whole procedure to prevent RNA degradation. The tissue was lysed in 500 µl of peqGold® TriFast (peqLab, Erlangen, Germany) and after homogenization, the lysate was mixed with 100 µl of Chloroform. Next, the homogenous solution was centrifuged for 20 min at 17000g and at 4 °C, the supernatant containing the RNA was collected, and the RNA was precipitated by adding approximately 200 µl of isopropanol (45% of the final volume), before storing at -20 °C overnight. After centrifugation (30 min at 17000g, 4 °C), the supernatant was discarded, and the RNA pellet was washed twice with 500 µl of ice-cold 80% ethanol, while centrifugating for 15 min

(17000g, at 4 °C) in between. Afterwards the pellet was dried for 5-10 min. The RNA was resuspended in 7 µl of nuclease-free H_2O and heated for 5 min at 70 °C (1000rpm) while shaking. RNA quantity and quality were assessed at 260/280 nm and 230/260 nm, respectively, using a NanoDrop spectrophotometer (Thermo Scientific, Waltham, USA), before the samples were utilized for reverse transcription and PCR amplification of cDNA.

6.3.2. Reverse Transcription (RT)

To reversely transcribe mRNA into complementary deoxyribonucleic acid (cDNA), 300 ng of mRNA sample was adjusted to a final volume of 20 µl with RNase-free H_2O and mixed with 4 µl of UltraScript Butter 5x (final concentration 1x, PCR Biosystem Inc., USA) and 1 µl of Random Hexamers 100 µlM (final concentration 5 µM, PCR Biosystem Inc., USA). Tubes containing only RNase-free H_2O were used as negative control (-RT) to verify the absence of genomic DNA contamination in the master mix. Following primer annealing for 2 min at 70 °C, 1 µl of each mix reaction was removed into the negative control tubes (-RT), while 1 µl of UltraScript 2.0 (UltraScript 2.0 cDNA Synthesis Kit, PCR Biosynthesis Inc., USA) was added at the rest of the mix to reach a final volume of 20 µl. All the samples were then incubated at 25 °C, 50 °C, 80 °C and 95°C for 10 min each using the Mastercycler® nexus X2 (Eppendorf, Wesseling-Berzdorf, Germany). The cDNA was stored at -20 °C until further analysis.

6.3.3. Quantitative Polymerase Chain Reaction (qPCR)

To quantify the expression of *Oxtr* mRNA, the target primers were amplified by using the quantitative polymerase chain reaction (qPCR) procedure. The dye SYBR Green (QuantiFast SYBR® Green PCR Kit, Qiagen) was applied, which binds the double stranded DNA. During the elongation phase of the PCR, the fluorescence emitted at 522 nm by the dye SYBR Green is proportional to the amount of double-stranded DNA of the gene of interest. For each sample, 5 µl of SYBR Green, 2 µl of the *Oxtr* forward and reverse primers (see Table 4; Metabion, Germany), 2 µl of RNase-free H_2O were added per well, in a 96-well plate. Additionally, 2 µl of the respective cDNA sample (previously diluted 1:3 in RNase-free H_2O) were added in triplicates. To ensure the absence of contamination, RNase-free H_2O was added instead of cDNA as a negative control. The housekeeping gene *Gapdh* served as internal control for further quantification of the gene of interest. The plates were sealed using a clear foil, centrifuged for 1 min a 1000g and incubated for the qPCR cycle (see Table 5) using the QuantStudio 5 Real-Time PCR System (Thermo Fisher Scientific). Only the detection of a single peak was considered, as the presence of multiple melting points indicates amplification of non-specific products.

Table 4: Primer sequences used for the quantification of targeted genes in mouse used in PCR experiments.

Gene	Forward Primer	Reverse Primer	Product length (bp)
Oxtr	CTGGAGTGTCGAGTT GGACC	AGCCAGGAACAGAAT GAGGC	136
Gpadh	TGATGACATCAAGAA GGTGG	CATTGTCATACCAGG AAA TGAG	185

Table 5: Cycler program used in qPCR experiments.

Step	Description	Temperature	Time	Cycles
1	Activation	95 °C	5 min	x 1
2	Denaturation	95 °C	3 sec	x 60
3	Elongation	60 °C	30 sec	
4	Cooling	∞	--	--

6.4. Immunohistochemistry

To study morphological changes in astrocytes, brains were cut in 40 µm-thickness coronal slices using a Cryostat (CM3000, Leica, Germany), focusing on slices containing the brain regions of interest, LS and HIP (Bregma +1.18 to -1.82). The slices were preserved in a cryopreservation solution (see Table 6) at -20 °C until further analysis. For immunohistochemistry, brain slices were then washed three times in 1 x PBS for 20 min each and blocked in 1x PBS containing 5% normal goat serum (NGS, Vector Laboratories) and 0.5% TritonX-100 for 1 h at room temperature (RT). Afterwards slices were incubated for 48 h at 4°C with primary antibody diluted in blocking solution (see Table 1). After 3 washes with 1x PBS, the slices were incubated for 2 h at RT with the appropriate secondary antibody (see Table 1), which was diluted in 1x PBS. Ultimately the brain slices were mounted on SuperFrost slides using Roti® Mount FluorCare DAPI (Carl Roth, Germany) and allowed to dry before being imaged (see section 7.1.).

Table 1: List of primary antibodies with their respective dilutions and secondary antibodies used in the immunohistochemistry and experiments.

Primary Antibody	Secondary Antibody
GFAP Cell Signaling D1F4Q XP (1:200)	goat-anti rabbit Alexa Fluor 488 (1:1000)
GFAP Sigma G3893 (1:500)	goat-anti mouse Alexa Fluor 594 (1:1000)
cFos sc-52 (1:10 000)	goat-anti rabbit Alexa Fluor 488 (1:1000)
cFos abcam 190289 (1:1000)	goat-anti rabbit Alexa Fluor 488 (1:1000)

6.5. RNA scope

To visualize single OXTR RNA molecules in the LS, an *in situ* hybridization method known as RNAscope was employed. RNA scope was performed according to the protocol described in (Althammer et al. 2022a), using the RNAscope Multiplex Fluorescent V2 kit, Advanced Cell Diagnostic, Acdbio) Briefly, tissue collection was conducted as outlined above (see 5.1.) and brain slices were cryo-sectioned into 20 µm-thick coronal slices (Bregma +1.18 to -0.10). Free-floating brain slices were initially treated with H_2O_2 for 10 min at RT, followed by three washed in 1x PBS (pH 7.4), and mounted on Superfrost Plus slides (AB00000112E01MNZ50, Thermofisher Scientific, Germany). A hydrophobic barrier was created around the slice using a PAP pen, and the sections were dehydrated in 100% ethanol before letting them air-dry. Slices were then permeabilized by incubating for 20 min at RT with Protease III (Acdbio), followed by three washes with dH_2O. The sections were then incubated with the OXTR probe (483671-C3) for 2 h at 40 °C. After hybridization, sections were washed twice for 2 min with RNAscope Wash Buffer (Acdbio) and subsequently incubated with Amp-1 and then Amp-2 (Amplification solution, Acdbio) for 30 min each at 40 °C, followed by an incubation with Amp-3 for 15 min at 40 °C. Each of these steps were preceded by 2 washing steps with RNAscope Wash Buffer. OXTR mRNA signal was then developed by incubating the sections with TSA Plus Fluorophore Cy3 (1:1000; FP1168, Perkin Elmer) for 30 min at 40 °C. After blocking with horseradish peroxidase (HRP, Acdbio) for 15 min at 40°C, the sections were washed three times in dH_2O for 2 min before proceeding with the immunohistochemical staining. Similarly, to the procedure described above (see 6.1.), sections were blocked for 1 h with the blocking solution (5% NGS, 0.5% Triton in 1x PBS), before being incubated for 48 h at 4 °C with primary antibodies diluted in blocking solution (Table 2), targeting astrocytic and neuronal marker (GFAP/S100b and NeuN, respectively). After three washing steps with 1x PBS, the sections were incubated for 1 h at RT with secondary antibodies diluted in 1x PBS (see Table 2). Following three final washing steps, slices were mounted with Roti-Mount DAPI and air-dried before being subjected to image acquisition (see section 7.3.)

Table 2: List of primary antibodies with their respective dilutions and secondary antibodies used in the immunohistochemical experiment combined with the RNAscope.

Primary Antibody	Secondary Antibody
GFAP Sigma G3893 (1:500)	goat-anti mouse Alexa Fluor 488 (1:1000)
S100 beta Sigma S2532 (1:1000)	goat-anti mouse Alexa Fluor 488 (1:1000)
NeuN MAB 377 (1:500)	goat-anti rabbit Alexa Fluor 647 (1:1000)

7. Image analysis

To ensure consistency during analysis, both microscopy settings as well as image analysis were maintained identical within each experiment.

7.1. Morphological analysis of astrocytes

To analyze morphological changes in astrocytes induced by SFC, brain slices from the region of interest were stained for GFAP and DAPI as described above (see 6.4.). Pictures were acquired using a confocal laser scanning microscope (CLSM, Zeiss LSM 980 Airyscan, Germany). To ensure capturing the entire astrocytic structure, three z-sections (each 30 µm-thick, with a 0.5 µm/z section interval, and acquired at 1024x1024 resolution using a 63x objective) were taken per animal for both LS and HIP (CA1) brain regions. These images were then analyzed using ImageJ software (Version 1.53c). First, the 3D stack was "flattened" through Z-projection at max intensity to emphasize details within the stacks. A merged channel with GFAP and DAPI was generated to facilitate visualization of the astrocyte soma. Finally, three parameters were analyzed: the number of primary processes, the length of the longest process and the area covered by each astrocyte (see Figure 8).

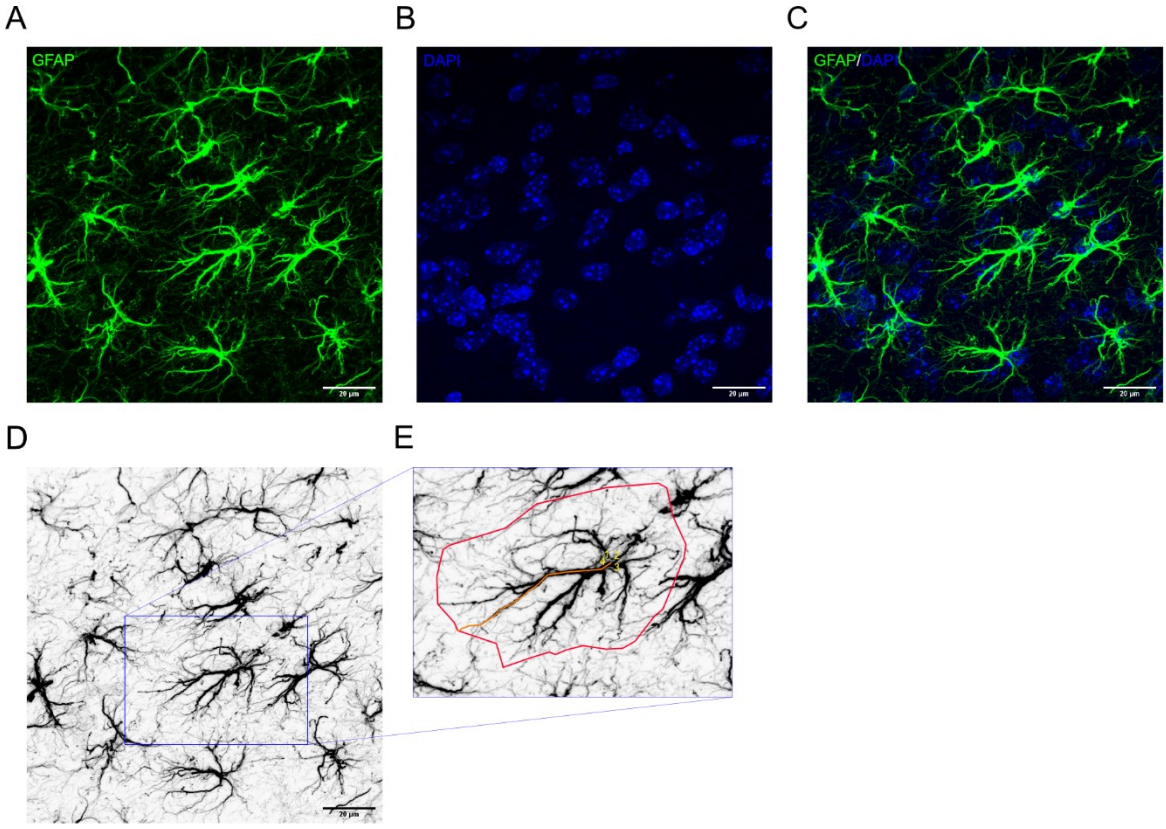

Figure 8. Analysis of astrocyte morphology with GFAP and DAPI staining. *Confocal images of astrocytes from the lateral septum (LS) of either social fear conditioned (SFC+) or unconditioned (SFC-) mice are taken containing GFAP (green) and DAPI (blue), which label respectively the astrocyte cytoskeleton and nucleus (A, B, C). Using ImageJ, astrocyte morphology is analyzed (D, E) by counting the number of primary processes (number in yellow), measure the length of the longest process (orange) and the area covered by each astrocyte (red). Scale bar = 20 µm.*

7.2. Immunofluorescence intensity measurements

To assess changes in the astrocyte structure in response to L-AAA-induced decreased functional activity (see section 4.1.), brain slices of the LS from animals injected with L-AAA were stained for GFAP and DAPI as described previously (see section 6.4.). Images of LS were acquired using a confocal laser scanning microscope (CLSM, Zeiss LSM 980 Airyscan, Germany), similarly as described above (see 6.5.1): three z-sections (each 30 µm-thick, with a 0.5 µm/z section interval, and acquired at 1024x1024 resolution with a 40x objective) were taken per animal. Using ImageJ (Version 1.53c), a sum z-projection was generated followed by background subtraction. Next, a square region of interest (ROI) measuring 600 µm was selected and analyzed for fluorescence intensity within it. Due to the tissue quality around the infusion site, the ROI was deliberately chosen adjacent to it.

7.3. Analysis of colocalization analysis of cFos, OXTR mRNA and GFAP

To determine the degree of overlap between astrocytes and cFos or OXTR mRNA in astrocytes, pictures from brain slices treated for immunohistochemistry and RNAscope (see sections 6.4. and 6.5.) were captured using a confocal laser scanning microscope (CLSM, Zeiss LSM 980 Airyscan, Germany; for details see section 7.3.). Finally, the number of colocalized cFos-GFAP$^+$ cells or OXTR mRNA$^+$--GFAP/S100β$^+$ and -NeuN$^+$ cells was manually counted to determine the colocalization of the astrocytic marker and the target molecules.

8. Calcium imaging of LS astrocytes following social fear acquisition in male and female mice

This experiment was performed at the University of Strasbourg in collaboration with Dr. Alexandre Charlet (INCI, *Institut des Neurosciences Cellulaires et Intégratives*, Strasbourg, France) providing calcium imaging material and expertise, and Prof. Dr. Inga Neumann (*University of Regensburg*, Germany) providing behavioral expertise for this project. Experiments were carried out by Laura Boi as part of her doctoral thesis, with the support of Dr. Kay-Yi Wang and Clémence Denis (INCI, *Institut des Neurosciences Cellulaires et Intégratives*, France). Detailed contributions are stated below.

Contributions to the project by Laura Boi:

- Design and execution of behavioral experiment
- Slice preparation and ex-vivo calcium imaging
- Quantification and statistical analysis
- Preparation of final figures and data interpretation of all results shown in this thesis

Contributions to the project by Dr. Kai-Yi Wang:

- Perfusion of mouse brains

Contributions to the project by Clémence Denis:

- Ex-vivo calcium imaging: teaching and support
- Data processing

8.1. Animals and husbandry

CD1 male and female mice (5-6 weeks old) were kept group-housed under standard conditions with food and water ad libitum on a 12-h light/dark cycle for two weeks before the start of the experiment. All experiments were conducted in accordance with European Union rules and approbation from the French Ministry of Research.

8.2. Social fear acquisition

The social fear acquisition protocol was performed as previously described (see 2.1.) with minor adaptations:

- In accordance with the animal license approbated at the local institution, mice were kept group-housed until the day of the social fear acquisition.
- The conditioning chamber consisted of a transparent perspex box with a stainless-steel grid floor, measuring 25 x 25 x 25. Behavior was monitored by using the ANY-maze software.

8.3. Perfusion, slice preparation and dye loading

All the following steps were conducted as described in (Baudon et al. 2022). 10 min after social fear acquisition, mice were anesthetized with an *ip* injection of ketamine (400mg/kg) and xylazine (80mg/kg). Intracardiac perfusion was then performed by ice-cold NMDG-based artificial cerebrospinal fluid (aCSF) solution (Table 6), oxygenated with carbogen (95% O_2 / 5% CO_2), condition kept for the whole procedure of perfusion, dissection, and slice preparation. After decapitation, the brain was removed and prepared to be mounted in the vibratome, to obtain 350 µm-thick horizontal or frontal slices containing the region of interest, i.e. LS. The whole procedure (perfusion, dissection, and slicing) was conducted in the same ice-cold oxygenated NMDG-based aCSF solution.

Six slices containing the LS were transferred into a chamber filled with carbogen-oxygenated aCSF solution and let them recover at RT for 1 h. Then, slices were incubated for 20 min at 37 °C in 10 ml of carbogen-oxygenated aCSF containing 10µl of SR101 (1µM, Sulforhodamine 101, Merck). After the incubation period, slices were gently moved to a 3 ml carbogen-oxygenated aCSF solution and 6 µl of OGB1-AM (Oregon Green 488 BAPTA-1, AM, Thermo Fisher Scientific) solubilized into PF-127 and Cremophor (Table 6) was loaded directly onto the region of interest to ensure of reaching an optimal dye concentration and kept it in incubation at 37 °C for 1 h. All slices were maintained in the same orientation so that both SR101 and OGB1-AM were loaded on the same side. After the incubation period, slices were washed at RT for 1 h in a recovery chamber filled with carbogen-oxygenated aCSF solution, before any recording was performed.

8.4. Calcium imaging and identification of astrocytes

To perform astrocyte calcium imaging a confocal microscope (Zeiss Axio Examiner) was used with a 40x water immersion objective. The brain slice was placed into an aCSF filled recording chamber connected to a peristaltic pump to ensure a continuous flow of oxygenated aCSF (~ 2ml/min) and hold in place with a harp. The region of interest was identified using a 4x objective and visualized with the uEye cockpit software. To identify SR101/OGB1-labeled astrocytes, the MetaFluor software was used and the following parameters were applied to illuminate the cells: 20ms

at 575nm for SR101 and 80ms at 475ms for OGB1 (2Hz, 500ms interval between acquisitions with a spinning disk pinhole diameter and rotation speed of 70µm and 15.000rpm respectively). The picture was acquired using a 40x water-immersion objective and after 5 min of registration TGOT 1 nM (OXTR agonist) was bath applied for 20s, and the kept recording for another 10 min.

8.5. Quantification and statistical analysis

Astrocytic calcium levels were assessed using the ImageJ software. A region of interest (ROI) including the cell body of SR101/OGB1-labeled astrocytes was hand-drawn and the fluorescence intensity for each ROI was measured for both SR101 and OGB1 channel. The result data were saved in an Excel file for further data analysis, which was performed using a custom-written Python-based script (available in the following resource section https://github.com/AngelBaudon/Canal.git). Since changes in fluorescence signals corresponded to variations of intracellular calcium levels, calcium peaks were detected whenever the fluorescence exceeded a certain threshold (for more details see (Baudon et al. 2022). The number of calcium transient (frequency) and the amplitude (area under the curve, AUC) of calcium peaks was quantified before (baseline, first 5min of the recording) and after TGOT (an OXT agonist) application (final 10min of the recording). Astrocytes were considered "responsive" to TGOT when the frequency or the AUC increased by 20% after TGOT exposure. However, considering that all data were normalized based on the duration of the recording and that TGOT application period was longer than the baseline (10min vs 5 min), astrocytes with only one peak in the whole recording were not considered "responsive".

9. Buffer and solutions

All the components used for the preparation of buffer and solution are listed in table 6 below.

Table 6: List of buffers and solutions with their respective applications

Buffer	Composition	Application
10 x PBS 0.1 M (1 l)	80 g NaCl, 2 g KCl, 14.4 g Na_2HPO_4, 2.4 g KH_2PO_4, dH_2O; pH 7.4	L-AAA dilution
1x PBS 0.01 M (1 l)	100 ml 10x PBS, dH_2O; pH 7.4	Perfusion, IHC
4% PFA in 1x PBS (2 l)	80 g para-Formaldehyd (PFA), 1x PBS; pH 7.4	Perfusion
Cryoprotection solution	150 ml Glycerol, 150 ml Ethylenglycol, 200 ml 1x PBS	IHC
4x Laemmli Buffer (LB)	2,4 ml 1M TRIS (pH 6.8), 0.8 g SDS, 4 ml Glycerol, 0.01% Bromphenol Blue, 1ml β-Mercaptoethanol, 2.8 ml dH_2O; pH 6.8	Western Blot
10x Electrophoresis Buffer (1 l)	30.3 g TRIS, 144.1 g Glycin, 10g SDS, dH_2O	Western Blot
10x Transfer Buffer (2 l)	288 g Glycin, 60.4 g TRIS, dH_2O; pH 8.3	Western Blot
10x TBS (1 l)	61 g TRIS, 80 g NaCl, dH_2O; pH 7.6	Western Blot
1x TBS-T (10 l)	1 l 10x TBS, 10 ml TWEEN, 9 l dH_2O	Western Blot
NMDG-based solution	90.7773 g NMGD, 0.9319 g KCl, 0.8625 g NaH_2PO_4, 12.6015 g $NaHCO_3$, 23.8310 g HEPES, 22.5250 g D-Glucose, 4.4030 g L-Ascorbic acid, 0.7612 g Thiourea, 1.6506 g Sodium Pyruvate, 8.1595 g N-acetyl-L-Cysteine, 2.3646 g Kynurenic acid, 12.324 g $MgSO_4$, 0.3675 g $CaCl_2$, 5 l dH_2O; pH 7.3-7.4	Calcium imaging (Perfusion and slice preparation)
aCSF solution	7.2416 g NaCl, 0.1864 g KCl, 0.1725 g NaH_2PO_4, 2.1843 g $NaHCO_3$, 2.7030 g D-Glucose, 0.493 g $MgSO_4$, 0.294 g $CaCl_2$, 1 l dH_2O; pH 7.3-7.4	Calcium imaging
SR 101 (Sulforhodamine 101)	10 µl SR101 (Merck) in 20 ml of aCSF	Calcium imaging
OGB1-AM (Oregon Green 488 BAPTA-1, AM)	2 µl PF-127 (20% in DMSO), 8 µl of Cremophor EL (0.5% in DMSO) in the OGB1-AM vial (Thermo Fisher Scientific, cat#06807)	Calcium imaging
TGOT (1 nM)	20 µl TGOT in 20 ml of aCSF	Calcium imaging

10. Statistical analysis and figures

For statistical analysis SPSS (Version 26.0, IBM Corp., USA) was used except for calcium imaging when GraphPad was used. Data were visualized using GraphPad Prism (Version 8, Graph Pad Software, San Diego, USA).

Particularly, for data analysis involving one factor and two groups, the independent t-Test was used or Mann-Whitney if the data were not normally distributed (factor SFC, factor sex, factor treatment, or factor brain region). When comparing more than two groups, the analysis of variance (ANOVA) was conducted, using one-way ANOVA for comparing more than two groups, with one factor (factor sex, or factor brain region), or mixed model ANOVA when assessing two factors over two or more time points (factor treatment x SFC x time, in SFC extinction and recall). Kruskall-Wallis or Geisser-Greenhouse correction were applied when sphericity was violated.

For the calcium imaging experiment GraphPad Prism was used for both statistical analysis and depiction of the pictures. Paired or unpaired t-test was conducted (if the data were not normally distributed Wilcoxon or Mann-Whitney was applied). Values of the *post hoc* are reported in the body text, while other values, group compositions, and statistical tests are detailed in separated tables for each experiment. Statistical significance was accepted at $p \leq 0.05$, while a trend was recognized at $p \leq 0.07$. Data are represented as the mean $\pm$ standard error of the mean (SEM).

All illustrations were generated using BioRender.com, while figures were created with Affinity Designer (https://affinity.serif.com/en-us/designer/), unless otherwise stated.

11. Experimental design

For a better understanding, the following section provide a short explanation of the experiments of this thesis.

11.1. Characterization of GFAP$^+$ and OXTR$^+$ astrocytes within the LS in male, female and lactating mice

Understanding the spatial distribution of astrocytes and OXTR$^+$ astrocyte in relation to neuronal population in the LS can provide insights into the functional organization of this brain region. To achieve this, a colocalization analysis was conducted to examine the distribution of GFAP- and S100β-expressing (GFAP/S100β $^+$) astrocytes and OXTR$^+$ astrocytes and neurons across the rostral-caudal and dorsal-ventral axis in the LS. Perfused brains from 3 adult male, virgin female and lactating mice were coronally cryosectioned at 20 µm, targeting the LSr (Bregma +1.1 — + 0.50 mm) and the LSc (Bregma +0.50 — - 0.10 mm). For each subdivision (rostral and caudal) three slices were collected, and images were taken from both the dorsal and ventral parts of each slice (Figure 9). Images were acquired at 20x magnification using a confocal laser scanning microscope (CLSM, Zeiss LSM 980 Airyscan, Germany). Co-localization was manually analyzed as follows: cells expressing GFAP and S1000β marker were identified as astrocytes, NeuN-expressing (NeuN$^+$) cells were identified as neurons, while nuclei with more than three OXTR mRNA dots were counted as OXTR$^+$.

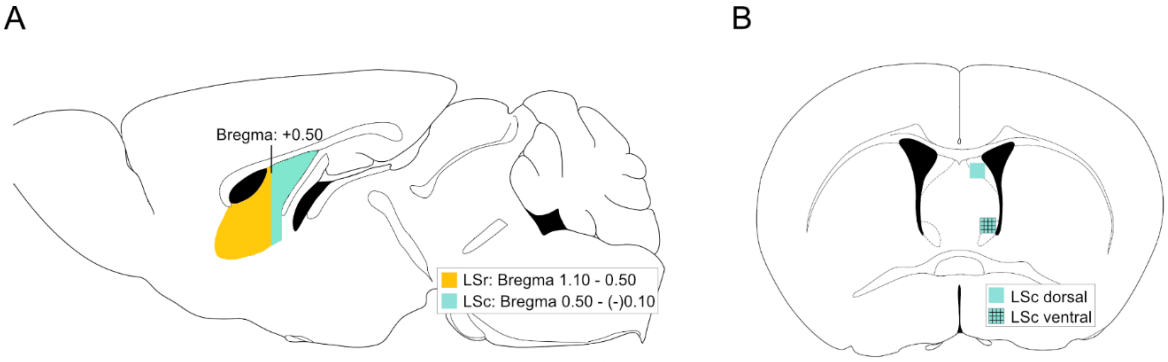

Figure 9. Experimental design to evaluate astrocyte and astrocytes expressing oxytocin receptor (OXTR) mRNA distribution along the lateral septum (LS) in male, female and lactating mice. *A) Illustration of the whole sampled area, with yellow representing the rostral part of the LS (LSr), and green representing the caudal part of the LS (LSc). Three slices for each part of the LS were collected. B) Image from the dorsal and ventral part was acquired of each single slice.*

11.2. Effects of social fear acquisition and extinction on astrocytes

Considering the emerging role of astrocyte in socio-emotional behaviors and learning processes, I aimed to analyze the astrocyte responses to the social fear acquisition and extinction phases of SFC paradigm in male mice. Brains from different cohorts of male mice were collected at either 90 min (Figure 10a) or 24 hrs (Figure 10b) after social fear acquisition, or 90 min after social fear extinction

(Figure 10c). For all experiments, changes in astrocyte morphology and astrocytic protein expression were analyzed in both the HIP and LS.

Additionally, I investigated whether social fear acquisition induced differential changes in astrocyte morphology in virgin female and lactating mice (Figure 10d). To assess morphology, brains were collected 90 min after exposure to social fear acquisition.

Figure 10. Experimental timeline to evaluate the effects of the Social Fear Conditioning (SFC) paradigm on astrocytes in male, female and lactating mice. *A) Experiment timeline to determine the effects of social fear acquisition on astrocytes in male mice. Brains were collected 90 min after social fear acquisition for molecular analysis. B) Experiment timeline to evaluate effects of social fear acquisition on astrocytes in male mice. Brains were collected 24 hrs after social fear acquisition for molecular analysis. C) Experiment timeline to evaluate effects of social fear extinction on astrocytes in male mice. Brains were collected 90 min after social fear extinction for molecular analysis. For all experiments (A, B, C), changes in astrocytic morphology and protein levels were analyzed in the hippocampus and the lateral septum (LS). D) Experiment timeline to evaluate effects of social fear acquisition on astrocytes in virgin female and lactating mice. Brains were collected 90 min after social fear acquisition for morphological analysis in the LS.*

11.3. Contribution of LS astrocytes to socio-emotional behaviors

Due to the emerging involvement of astrocytes in emotional behaviors, I aimed to investigate the involvement of astrocyte within the LS in regulating socio-emotional behaviors. To achieve this, a gliotoxin (L-AAA) was administered 3 days prior behavioral testing. Specifically, male mice underwent surgery for the bilateral implantation of a guide cannula targeting the LSc. After 7 days of recovery and daily handling, they were locally infused with either L-AAA (10 µg/µl or 25µg/µl; 0.2 µl/hemisphere) or Veh (PBS, 0.2 µl/hemisphere). Three days after the infusion, to allow for proper L-AAA-induced astrocytic structure depletion, mice were then tested for anxiety- and depressive-like behaviors using SPT, EPM and FST (Figure 11a). Subsequently, brains were collected to assess astrocyte impairment by measuring GFAP fluorescence.

To further investigate the involvement of astrocytes in SFC-induced social behaviors, L-AAA-induced astrocytic structure depletion was tested in the SFC paradigm in male and female mice. Seven days after bilateral cannula implantation, animals received either L-AAA (10 µg/µl or 25µg/µl; 0.2 µl/hemisphere) or Veh (PBS, 0.2 µl/hemisphere) into the LSc. Three days after the infusion, animals were exposed to the SFC paradigm (Figure 11b). Social investigation and vigilance behavior were monitored during social fear extinction training and recall phases. Afterwards, animals were euthanized, and their brains were infused with ink to verify the infusion site.

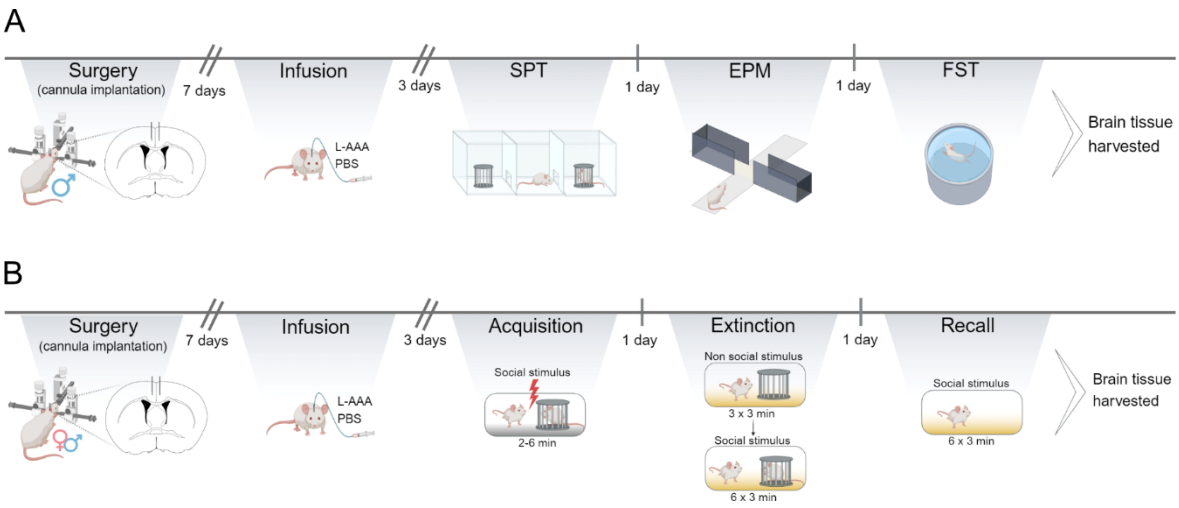

Figure 11. Experimental timeline to evaluate L-AAA-induced astrocytic dysfunction on socio-emotional behaviors. *A) Male mice recovered from surgery for 7 days before being infused with either L-AAA or PBS as vehicle. Three days after the infusion, animals were tested for anxiety- and depressive-like behaviors for three consecutive days: social preference test (SPT), elevated plus maze test (EPM) and forced swim test (FST). At the end brains were collected to be processed for further molecular analysis. B) Experimental timeline to evaluate L-AAA-induced astrocytic dysfunction on Social Fear Conditioning (SFC) paradigm in male and female mice. Animals recovered from surgery for 7 days before being infused with either L-AAA or PBS as vehicle. Three days after the infusion, animals were exposed to the SFC paradigm (acquisition, extinction, and recall). At the end of the experiment, postmortem, mice were infused with ink to verify the infusion site.*

11.4. Effects of social fear acquisition on astrocytic Ca^{2+} activity in the LS in male and female mice

To assess the impact of synthetic OXT on astrocytic activity in the LS following SFC, I measured astrocytic Ca^{2+} activity *ex vivo* in the LS of male and female mice after social fear acquisition (Figure 12a). Brains were harvested 10 min after social fear acquisition, and slices containing the LS were prepared for Ca^{2+} imaging. Using a confocal microscope (Zeiss Axio Examiner), Ca^{2+} transients in LS astrocytes were visualized (Figure 12b). Measurements of basal astrocytic Ca^{2+} activity were recorded for 5 min, followed by a 20s application of TGOT and an additional 10 min of recording (Figure 12c). The number of Ca^{2+} transient (frequency) and their amplitude (AUC) were quantified as indicator of Ca^{2+} activity in LS astrocytes. Astrocytes were considered "responsive" to TGOT if either the frequency or the AUC of Ca^{2+} peaks increased by 20% following TGOT exposure (Baudon et al. 2022) (see section 8.5. for details).

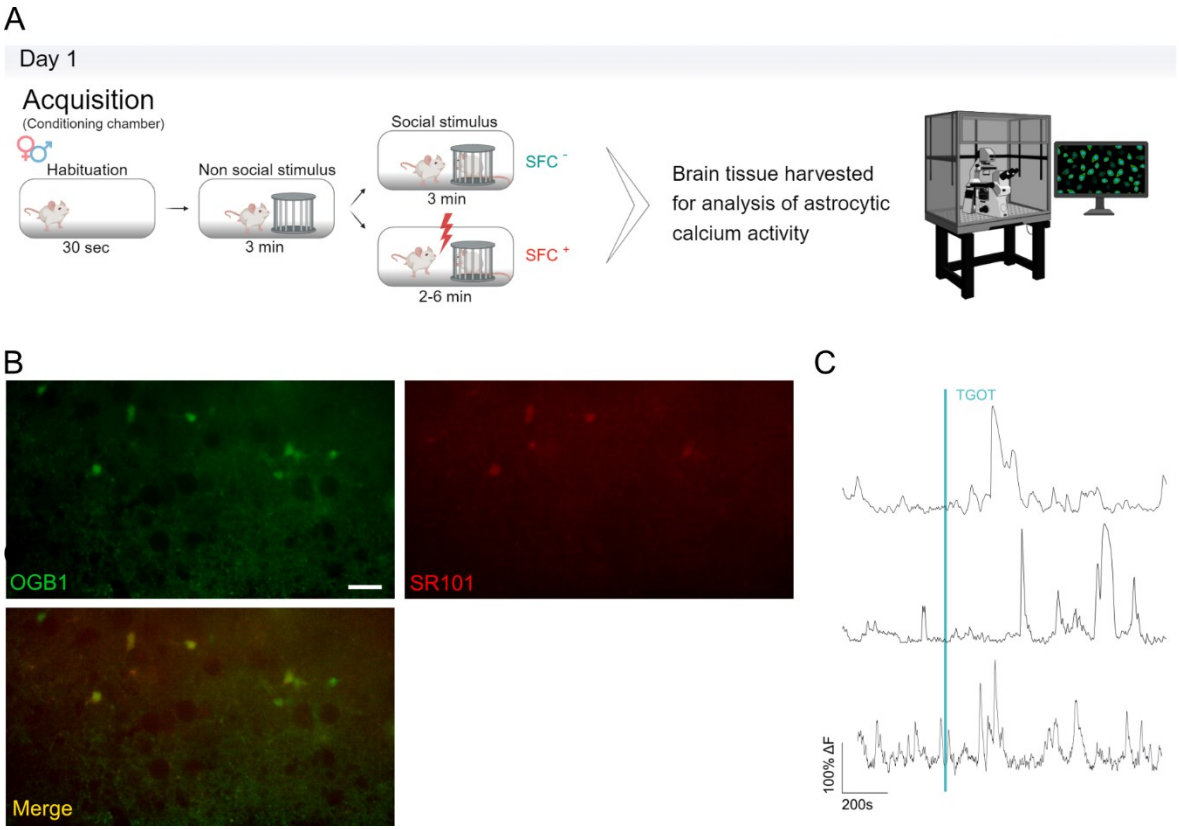

Figure 12. Experimental design of social fear acquisition effects on astrocytic Ca^{2+} activity in the LS. *A) Experimental timeline of calcium imaging experiment following social fear conditioning. B) Stacked picture of OGB1 (Ca^{2+}marker) staining (left), SR101, astrocytic marker (right) and the merge of both markers (below). Scale bar = 50 µm. C) Illustration showing traces of OGB1 fluorescence over time on OGB1-loaded astrocytes. The turquoise bar represents the application of TGOT (1 nM, 20s duration). The recording preceding the turquoise bar display basal astrocytic Ca^{2+} activity, while recording after the turquoise bar show astrocytic Ca^{2+} activity in response to TGOT.*

11.5. OXT effects on LS astrocyte morphology and the involvement of astrocytic OXTR signaling in the SFC paradigm

To further investigate OXT effects on astrocyte function, I focused on analyzing OXT influence on astrocyte morphology in the LSc of male mice (Figure 13a). Mice underwent to cannula implantation in the LSc and after recovery period of 7 days and daily handling, they received an infusion of either OXT (5 ng/0.2 µl/hemisphere) or Veh (PBS, 0.2 µl/hemisphere) infusions into the LSc (Figure 13a). Brains were then collected to assess changes in astrocyte morphology (see section 7.1. for details).

Additionally, considering the prosocial effects of OXT during social fear extinction, I aimed to determine whether these effects were mediated via astrocytic OXTR signaling in the LS. To this end, I downregulated the expression of astrocytic OXTR mRNA by locally infusing a viral vector combined with short harpin (shRNA), expressed under the GFAP promoter (AAV6-GFAP-*Oxtr*-mCherry-shRNA) in both male and female mice. Mice received bilateral microinfusions of either AAV6-GFAP::shRNA or a vector control (280 nl / hemisphere) into the LSc. Three weeks post-transfection, mice were exposed to the SFC paradigm (Figure 13b). To evaluate the effects of astrocytic OXTR knockdown on social behavior during the SFC paradigm, social investigation and vigilance behavior were monitored throughout the social fear extinction training and recall phases. Following these behavioral tests, brains were collected to measure the OXTR mRNA levels in the LSc (see section 6.3 for details).

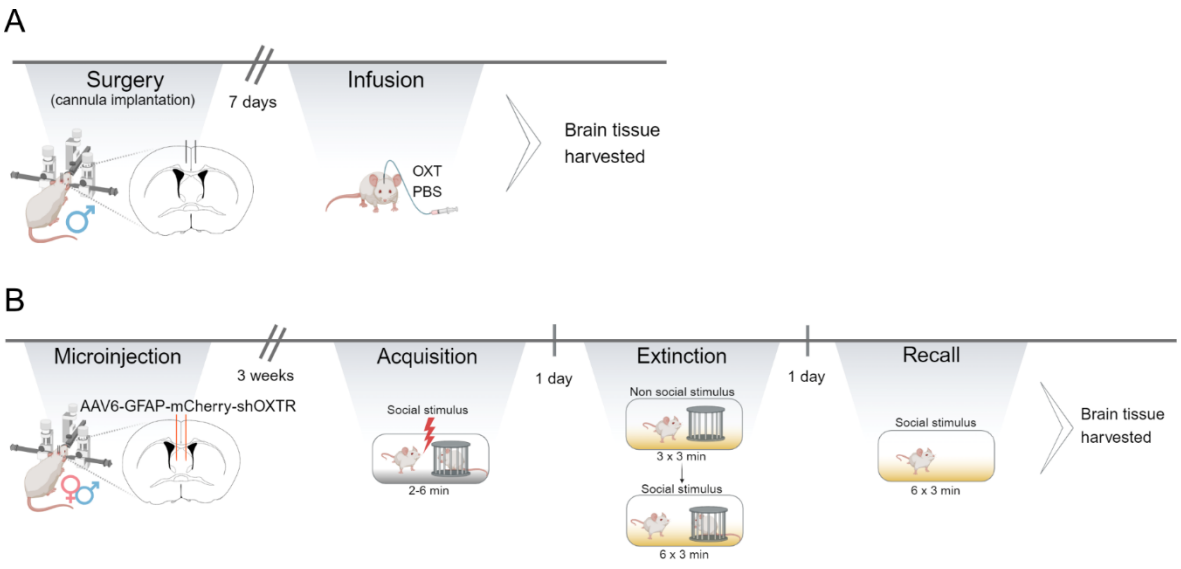

Figure 13. Experimental design to assess OXT effects on LS astrocytes and astrocytic OXT signaling in the Social Fear Conditioning (SFC) paradigm*. A) To assess OXT effects on astrocyte morphology male mice underwent to bilateral cannula implantation in the LSc. After 7 days of recovery, mice received either OXT (5 ng/0.2 µl/hemisphere) or PBS (vehicle, 0.2 µl/hemisphere) in the LSc via cannula infusion. 10 min after the infusion, brains were collected to OXT effects on LSc astrocytic morphology in male mice. B) Effect of astrocytic Oxtr knockdown on SFC paradigm in both male and female mice. Mice received either AAV6-GFAP-Oxtr-mCherry-shRNA or a vector control (280 nl / hemisphere) microinfusion in the LSc. 3 weeks post-transfection, animals were exposed to the SFC paradigm (acquisition, extinction, and recall). Brains were collected afterwards to analyze Oxtr mRNA levels.*

1. Characterization of LS astrocytes in male, virgin female and lactating mice

Although astrocyte expression in the LS of male and female mice has been recently reported (Althammer et al. 2022c), further investigation of the distribution and characterization along the LS is needed. Considering the neurochemical and functional heterogeneity described along this brain region (Wirtshafter and Wilson 2021), a detailed description of astrocyte distribution along the rostral-caudal and dorsal-ventral axes of the LS would be essential beneficial for a better understanding of their functionality.

A peculiar distribution pattern of astrocytes was found in the LS of male, virgin female and lactating mice. To investigate whether astrocyte expression varies along the LS, I performed a detailed analysis targeting and counting $GFAP^+/S100\beta^+$ cells along both the rostral-caudal and dorsal-ventral axes in the LS. Additionally, $NeuN^+$ cells were counted in the same condition to gain insights into the astrocyte-neuronal ratio across different LS subdivisions (see sections 7.3. and 11.1.).

1.1. Distribution of $GFAP^+$ astrocytes and OXTR $mRNA^+$ astrocytes expression along the LS in male mice

In male mice (Figure 14), analysis along the rostral-caudal axis revealed that the number of $GFAP^+$ cells is significantly higher in the LSc compared to the LSr ($p = 0.039$, Figure 14B). Furthermore, in the dorsal-ventral axis, $GFAP^+$ cells were more abundant in the LSd compared to the LSv in the LSr ($p = 0.037$, Figure 14D), while a trend toward increased $GFAP^+$ cells was observed in the LSc ($p = 0.054$; Figure H), it did not reach statistical significance. Regarding the analysis of astrocyte-neuron ratio, I found that astrocytes constitute a smaller proportion of the total cellular population compared to neurons ($NeuN^+$ cells) similarly across the LS (Figure 14E, I).

Similarly, the number of astrocytes expressing OXTR mRNA displayed a region-specific distribution, with a higher percentage of the OXTR $mRNA^+$ astrocytes in the LSc compared to the LSr ($p < 0.001$, Figure 14C). However, the percentage of OXTR $mRNA^+$ astrocytes remained low and consistent between the LSd and LSv in both LSr (Figure 14F) and LSc (Figure 14J). Interestingly, the analysis of the OXTR mRNA astrocyte-neuron ratio revealed that astrocytes expressing OXTR mRNA constitute a smaller population compared to neurons expressing OXTR mRNA, although this ratio was higher in the LSc compared to the LSr (5.7% vs 0.2%; Figure 14K and 14G).

Overall, these results indicate a region-specific distribution of astrocytes and astrocytes that express OXTR mRNA within the LS of male mice, with higher astrocytic presence in the caudal and dorsal

subdivisions of the LS. This differential distribution could suggest adapting functional roles for astrocytes across the different regions of the LS.

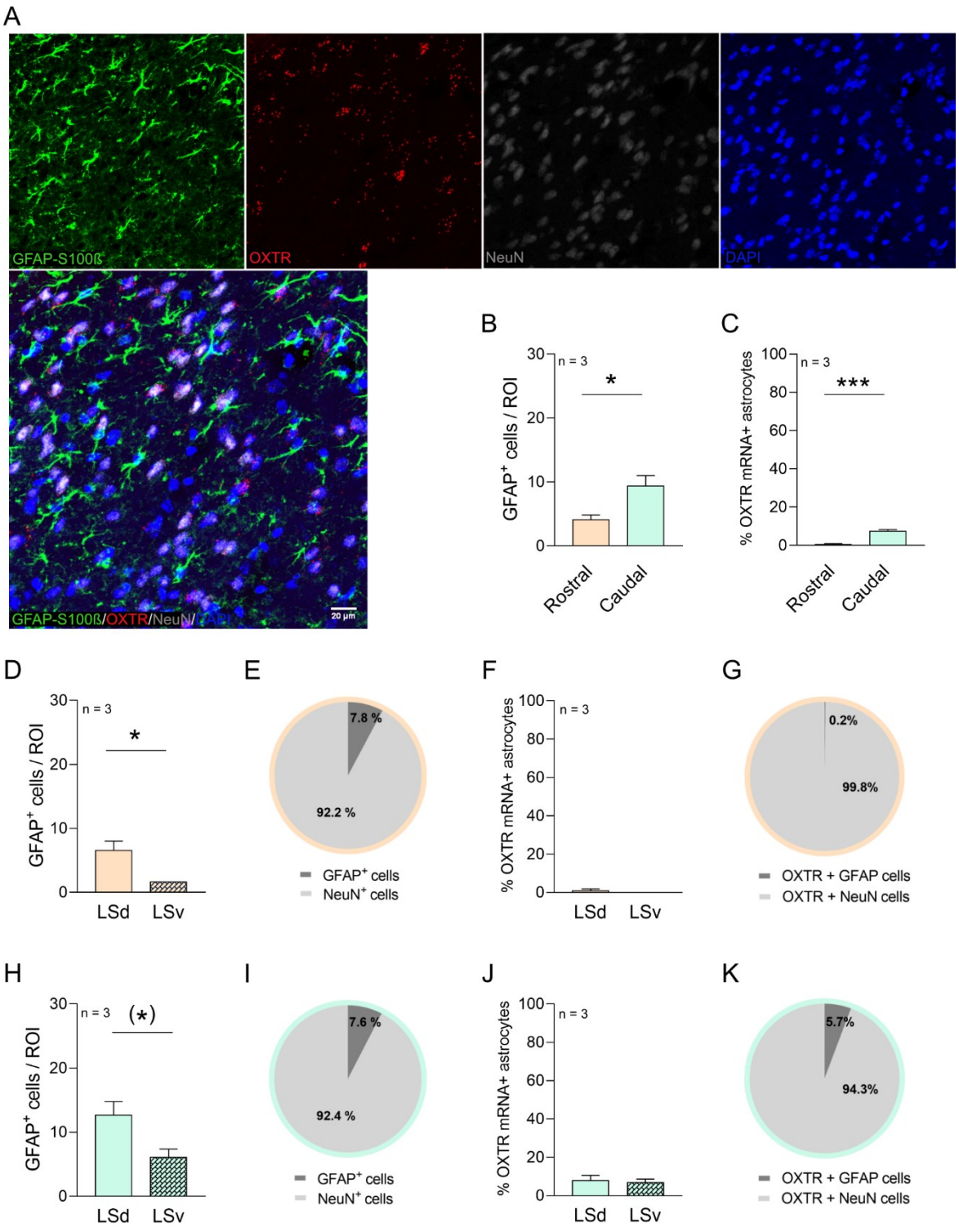

Figure 14. Expression of glial fibrillary acidic proteins expressing (GFAP⁺) cells and oxytocin receptor expressing (OXTR⁺) cells along the LS in male mice. *A) Representative image from the LS showing in situ hybridization of mRNA targeting OXTR (red) and immunohistochemistry targeting GFAP/S100ß (green), NeuN (grey) and a DAPI nuclear counterstain (blue). Scale bar 20 µm. B) Number of GFAP⁺ cells in the rostral LS (LSr) and caudal LS (LSc). C) Percentage of OXTR⁺ astrocytes in the LSr and LSc. D) Number of GFAP⁺ cells in the dorsal LSr and ventral LSr. E) Percentage of GFAP⁺ cells compared to NeuN+ in the LSr. F). Percentage of OXTR⁺ astrocytes in the dorsal LSr and ventral LSr. G) Percentage of OXTR⁺ astrocytes compared to OXTR⁺ neurons in the LSr. H) Number of GFAP⁺ cells in the dorsal LSc and ventral LSc. E) Percentage of GFAP⁺ cells compared to NeuN+ in the LSc. F). Percentage of OXTR⁺ astrocytes in the*

*dorsal LSc and ventral LSc. G) Percentage of OXTR$^+$ astrocytes compared to OXTR+ neurons in the LSc. n = animal number. Data represents means ± SEM. *** p < 0.001, * p < 0.05, (*) p < 0.07. For detailed statistics analysis see Table7.*

Table 7: Statistics of the astrocyte distribution and OXTR mRNA expression along the LS in male mice (Figure 14). Factor region represents LSr vs LSc; factor subregion represents LSd vs LSv.

GFAP$^+$ cells in males	Independent T-Test, Mann-Whitney-U Test	Figure B, D, H
Region	t_4 = -3.027	p = 0.039
Subregion - LSr	*U* = 0.000	p = 0.037
Subregion - LSc	t_4 = 2.708	p = 0.054
OXTR mRNA$^+$	Independent T-Test, Mann-Whitney-U Test	Figure C, F, J
Region	t_4 = -7.773	p = 0.001
Subregion - LSr	*U* = 3	p = 0.317
Subregion - LSc	t4 = 0.321	p = 0.764

1.2. Distribution of GFAP$^+$ astrocytes and OXTR$^+$ astrocytes expression along the LS in virgin female mice

Similar to the findings in males, analysis along the rostral-caudal axis in virgin female mice (Figure 15) revealed that the number of GFAP$^+$ cells is higher in the LSc compared to the LSr (p = 0.019; Figure 15A). Furthermore, in the dorsal-ventral axis, GFAP$^+$ cells were more abundant in the LSd compared to the LSv within the LSr (p = 0.037, Figure 15E). However, in the LSc, the distribution of GFAP$^+$ was more homogenous between the dorsal and ventral part (Figure 15I). Additionally, analysis of the astrocyte-neuron ratio revealed a smaller astrocytic population compared to neuronal population of about 18% in the LSc (Figure15F) and of 12% in the LSr (Figure 15J). Interestingly, when comparing GFAP$^+$ cells in the LSc, virgin females exhibited a higher expression in number of astrocytes compared to males (p = 0.018, Figure 15B).

In contrast to males, the presence of OXTR mRNA$^+$ astrocytes in virgin females showed a more uniform distribution along both the rostral-caudal (Figure 15C) and dorsal-ventral axes (Figure 15G and 15K). Consistent with the findings of the general astrocyte-neuron ratio, OXTR mRNA$^+$ astrocytes constituted a smaller population compared to OXTR mRNA$^+$ neurons overall. However, this proportion was higher in the LSc compared to the LSr (20% vs 13%, Figure 15L and 15H). Notably, the comparison of OXTR mRNA$^+$ astrocytes between males and virgin female revealed that, similarly to the GFAP$^+$ cells, virgin females had a higher expression of OXTR mRNA$^+$ astrocytes in the LSc compared to males (p = 0.001, Figure 15D).

Overall, these results indicate a region-specific distribution of astrocytes within the LS of female mice, with higher astrocytic presence in the LSc. However, unlike males, the expression of OXTR mRNA$^+$ astrocytes was more uniform homogenous across the LS. The observed sex differences in

both astrocyte distribution and OXTR mRNA$^+$ astrocyte expression, with higher levels in females, suggest potential functional differences between sexes in this region.

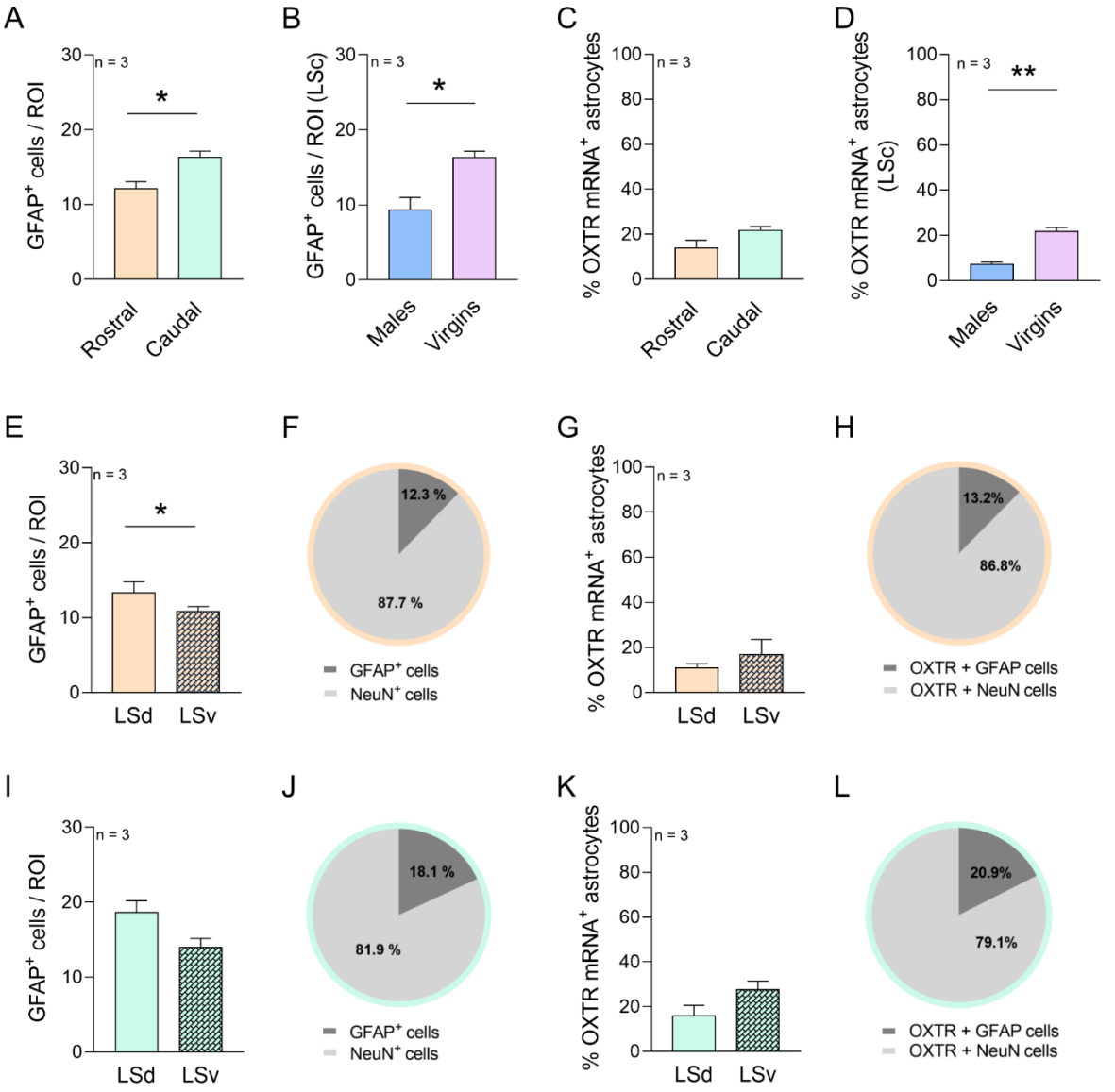

Figure 15. Expression of glial fibrillary acidic proteins expressing (GFAP$^+$) cells and oxytocin receptor expressing (OXTR$^+$) cells along the LS in female mice. *A) Number of GFAP$^+$ cells in the rostral LS (LSr) and caudal LS (LSc). B) Number of GFAP$^+$ cells in the LSc in male and virgin female mice. C) Percentage of OXTR$^+$ astrocytes in the LSr and LSc. D) Number of OXTR$^+$ astrocytes cells in the LSc in male and virgin female mice. E) Number of GFAP$^+$ cells in the dorsal LSr and ventral LSr. F) Percentage of GFAP$^+$ cells compared to NeuN+ in the LSr. G) Percentage of OXTR+ astrocytes in the dorsal LSr and ventral LSr. H) Percentage of OXTR$^+$ astrocytes compared to OXTR$^+$ neurons in the LSr. I) Number of GFAP$^+$ cells in the dorsal LSc and ventral LSc. J) Percentage of GFAP+ cells compared to NeuN+ in the LSc. K). Percentage of OXTR+ astrocytes in the dorsal LSc and ventral LSc. L) Percentage of OXTR+ astrocytes compared to OXTR+ neurons in the LSc. n = animal number. Data represents means ± SEM. ** $p < 0.01$, * $p < 0.05$. For detailed statistics see Table 8.*

Table 8: Statistics of the astrocyte distribution and OXTR mRNA expression along the LS in female virgin mice (Figure 15). Factor region represents LSr vs LSc; factor subregion represents LSd vs LSv; factor status represents virgin vs lactating females.

$GFAP^+$ cells	Independent T-Test	Figure A, E, I, B
Region	$t_4 = -3.816$	$p = 0.019$
Subregion - LSr	$t_4 = 3.463$	$p = 0.026$
Subregion - LSc	$t_4 = 0.502$	$p = 0.642$
Sex (LSc)	$t_4 = 3.868$	$p = 0.018$
OXTR $mRNA^+$ cells	Independent T-Test	Figure C, G, K, D
Region	$t_4 = -2.126$	$p = 0.101$
Subregion - LSr	$t_4 = -0.928$	$p = 0.406$
Subregion - LSc	$t_4 = -1.975$	$p = 0.119$
Sex (LSc)	$t_4 = 8.348$	$p = 0.001$

1.3. Distribution of $GFAP^+$ astrocytes and $OXTR^+$ astrocytes expression along the LS in lactating mice

Compared to virgin females, the analysis along the rostral-caudal axis in lactating mice (Figure 16), revealed that the number of $GFAP^+$ cells is quite uniform between the LSr and LSc (Figure 16A). However, in the dorsal-ventral axis, $GFAP^+$ cells were more abundant in the LSd compared to the LSv within the LSr ($p = 0.009$, Figure 16E). This pattern was not found in the LSc (Figure 16I). Additionally, when analyzing the astrocyte-neuron ratio, it was observed as male and virgin females, that the astrocytic population was smaller compared to neuronal population. Nevertheless, the proportion of astrocytes in the LSc reached 20% (Figure 16F), which is higher than the 11% observed in the LSr (Figure 16J). Furthermore, when comparing $GFAP^+$ cells in the LSc, virgin females and lactating mice exhibited a similar number of $GFAP^+$ astrocytes compared to males (Figure 16B).

In contrast to virgin females, but similar to males, there was a higher number of OXTR $mRNA^+$ astrocytes in the LSc compared to the LSr (Figure 16C), whereas a rather uniform distribution was found along the dorsal-ventral axis (Figure 16G and 16K). Consistent with the astrocyte-neuron ratio findings, OXTR $mRNA^+$ astrocytes constituted a smaller population compared to OXTR $mRNA^+$ neurons overall with similar proportion between LSr and LSc (10% vs 12%, Figure 16H and 16L). Finally, there was no difference in the number of OXTR $mRNA^+$ astrocytes between virgin female and lactating mice in the LSc (Figure 16D).

Overall, these results indicate that lactating mice exhibit a distinct pattern of astrocytes distribution within the LS compared to virgin females, indicating that the physiological state of lactation is accompanied by a modulate astrocytic population and probably their functional properties.

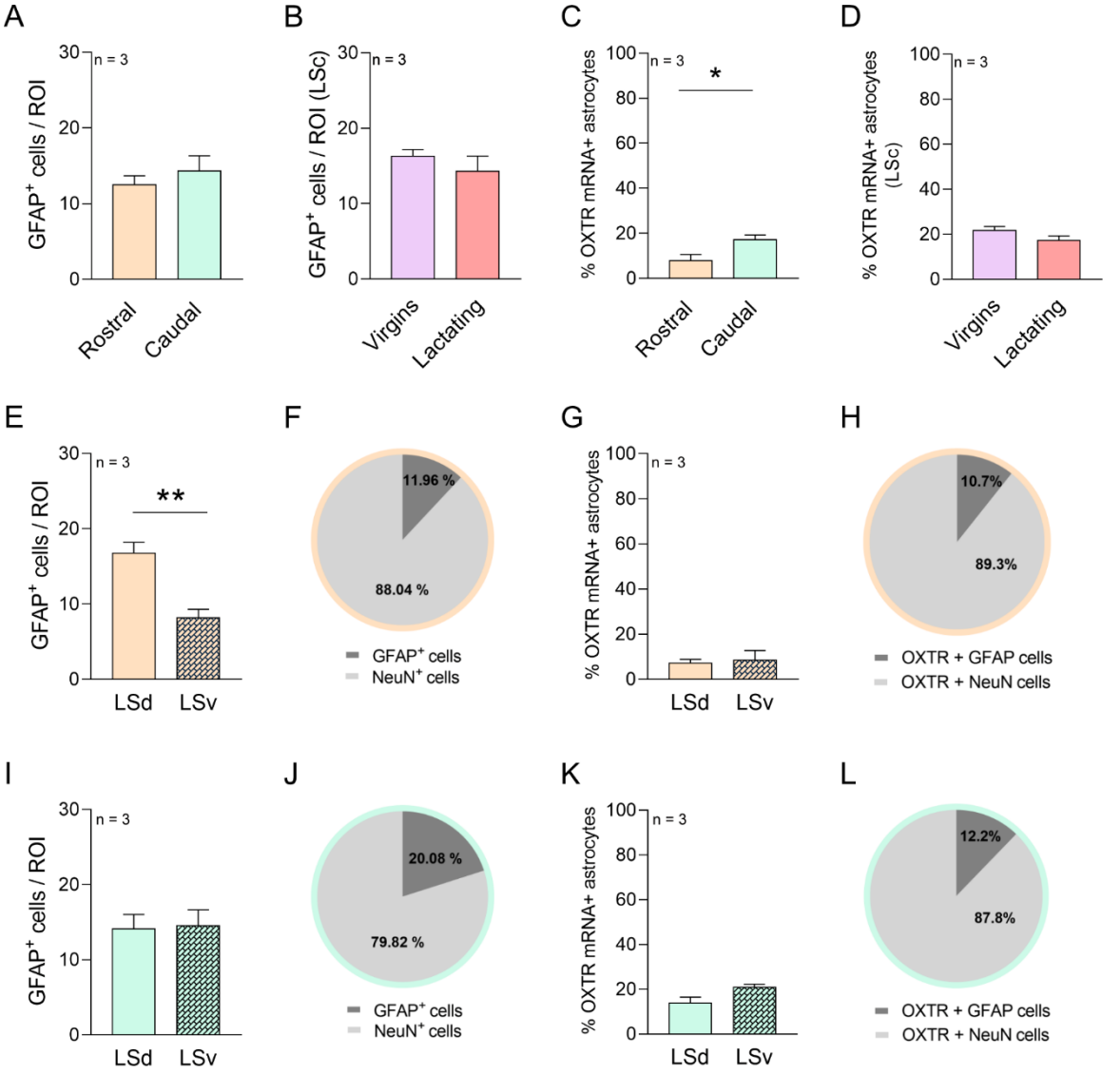

Figure 16. Expression of glial fibrillary acidic proteins expressing (GFAP⁺) cells and oxytocin receptor expressing (OXTR⁺) cells along the LS in lactating mice. *A) Number of GFAP⁺ cells in the rostral LS (LSr) and caudal LS (LSc). B) Number of GFAP⁺ cells in the LSc in virgin females and lactating mice. C) Percentage of OXTR⁺ astrocytes in the LSr and LSc. D) Number of OXTR⁺ astrocytes cells in the LSc in virgin females and lactating mice. E) Number of GFAP⁺ cells in the dorsal LSr and ventral LSr. F) Percentage of GFAP⁺ cells compared to NeuN+ in the LSr. G) Percentage of OXTR+ astrocytes in the dorsal LSr and ventral LSr. H) Percentage of OXTR⁺ astrocytes compared to OXTR⁺ neurons in the LSr. I) Number of GFAP⁺ cells in the dorsal LSc and ventral LSc. J) Percentage of GFAP+ cells compared to NeuN+ in the LSc. K). Percentage of OXTR+ astrocytes in the dorsal LSc and ventral LSc. L) Percentage of OXTR+ astrocytes compared to OXTR+ neurons in the LSc. n = animal number. Data represents means ± SEM. ** $p < 0.01$, * $p < 0.05$. For detailed statistics see Table 9.*

Table 9: Statistics of the astrocyte distribution and OXTR mRNA expression along the LS in lactating mice (Figure 16). Factor region represents LSr vs LSc; factor subregion represents LSd vs LSv; factor status represents virgin vs lactating female mice.

$GFAP^+$ cells	Independent T-Test	Figure A, E, I, B
Region	$t_4 = -0.793$	$p = 0.472$
Subregion - LSr	$t_4 = 4.723$	$p = 0.009$
Subregion - LSc	$t_4 = -0.155$	$p = 0.885$
Status	$t_4 = 0.927$	$p = 0.403$
$OXTR\ mRNA^+$ cells	Independent T-Test	Figure C, G, K, D
Region	$t_4 = -2.883$	$p = 0.045$
Subregion - LSr	$t_4 = -0.292$	$p = 0.785$
Subregion - LSc	$t_4 = -2.407$	$p = 0.074$
Status (LSc)	$t_4 = 1.848$	$p = 0.138$

2. Effects of social fear acquisition and extinction on astrocytes in male mice

Given the emerging role of astrocytes in regulating socio-emotional behaviors and learning processes, I explored the response of astrocytes to social fear acquisition and extinction in the HIP and LS in male mice, two brain regions critically involved in these processes (Menon et al. 2022).

2.1. Hippocampal astrocytic response to social fear acquisition and extinction in male mice

To examine the effects of social fear acquisition and extinction on astrocyte morphology, activation and protein expression, I applied immunofluorescence to assess changes in astrocyte structure and to analyze cFos as marker of cellular activation. Additionally, I used immunoblotting to evaluate the expression of key astrocytic proteins (see section 6.2. and 6.4. in Material and methods for details).

Hippocampal astrocyte response 90 min after SFC. In the HIP, morphological analysis revealed that 90 min after social fear acquisition (Figure 18), astrocytes of SFC^+ male mice showed a similar branching in the number and length of primary processes compared to SFC^- (Figure 18B and 17C). However, there was a trend toward an increased domain area ($p = 0.065$, Figure 18C), suggesting a potential response to the social fear acquisition. Examination of cFos, as an indicator of activated cells, revealed an increase in the percentage of $cFos^+$ astrocytes compared to naïve animals ($p < 0.001$, Figure 18E). Interestingly, SFC^+ animals revealed increased cFos activation (Figure 18F), similar to SFC^- animals. However, there was no difference in cFos activation between SFC^- and SFC^+, suggesting that hippocampal astrocytes are activated in response to social stimuli, regardless of the social fear acquisition process.

Furthermore, the protein expression analysis showed no differences in the levels of key astrocytic proteins (Cx30, Cx43, pCx43, GFAP, EAAT1 and EAAT2) between SFC^- and SFC^+ (Figure 18G). Overall, these findings suggest that hippocampal astrocytes acutely respond to social fear acquisition by altering their structure and activation state without altering the expression levels of proteins associated with their primary functions within 90 min. This is likely a mechanism involved in the modulation of the local neuronal network.

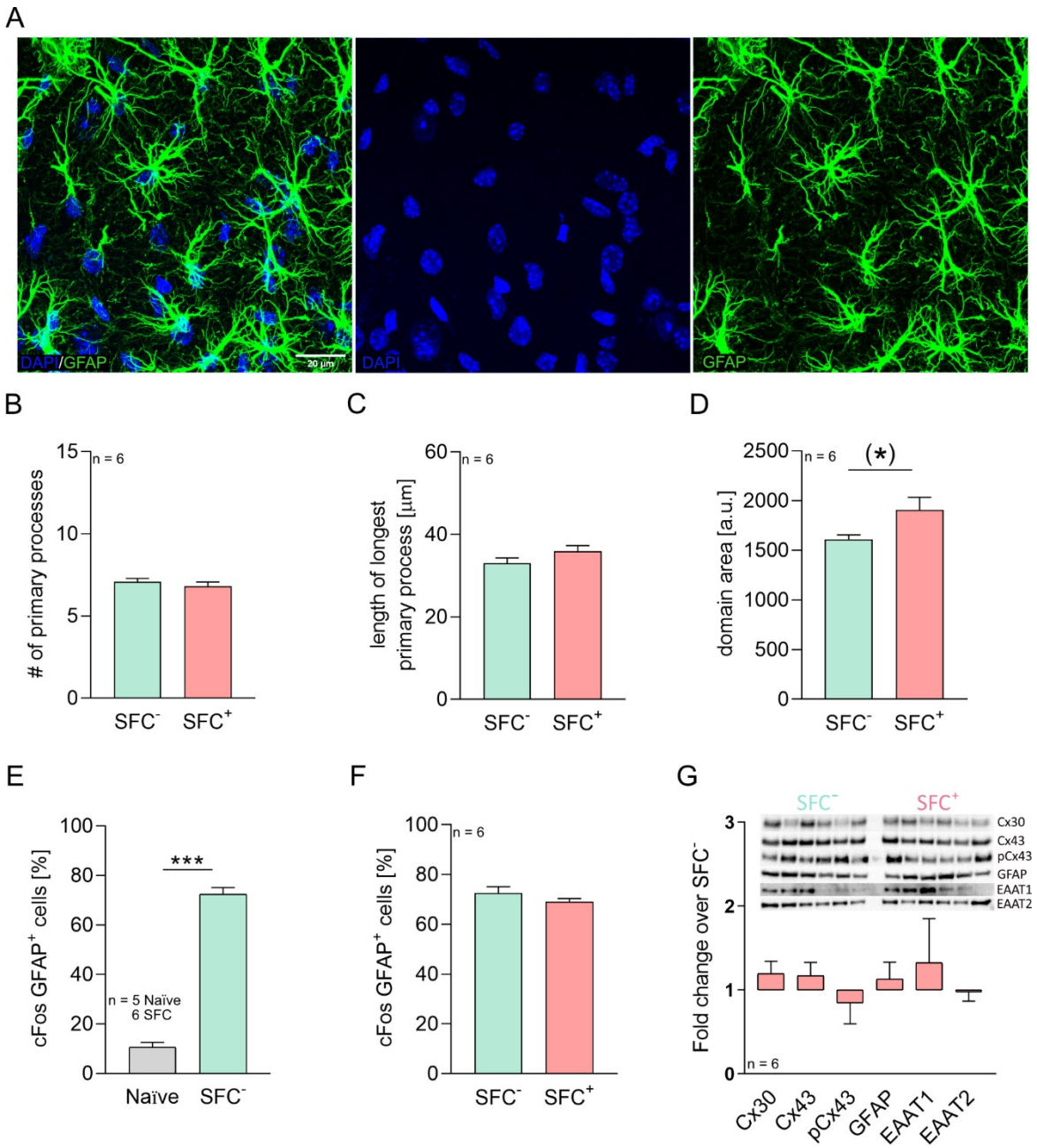

Figure 17. Effects of exposure to social fear conditioning (SFC) on hippocampal astrocytes 90 min after social fear acquisition in male mice. *A) Representative immunohistochemical image from the hippocampus (HIP) showing astrocytes stained for glial fibrillary acidic protein expressing (GFAP, green) and nuclei stained with DAPI (blue). Scale bar = 20 µm. B-D) Quantification of astrocytes morphology, including the number of primary processes (B), length of the longest primary process (C), and domain area (D). E-F) Percentage of $cFos^+$ astrocytes comparing naïve vs SFC^-(E), and SFC^-vs SFC^+(F). G) Protein expression analysis of astrocytic markers (Cx30, Cx43, pCx43, GFAP, EAAT1, EAAT2) comparing $SFC^-$and SFC^+, with representative western blots shown for each protein. n = animal number. Data represents means ± SEM. *** $p < 0.001$, (*) $p < 0.07$. For detailed statistics analysis see Table 10.*

Table 10: Statistics of the effects of SFC exposure on astrocytic response 90 min after social fear acquisition (Figure 18). Factor represents SFC- vs SFC+ effects or Naïve VS SFC$^-$.

Hippocampus	Independent T-Test	Figure B-G
Number of primary processes	$t_{10} = 0.729$	$p = 0.483$
Length of longest process	$t_{10} = -1.412$	$p = 0.188$
Domain area	$t_{10} = -2.071$	$p = 0.065$
cFos (Naïve VS SFC$^-$)	$t_9 = 17.702$	$p < 0.001$
cFos	$t_{10} = 1.147$	$p = 0.278$
Cx30	$t_{10} = -0.930$	$p = 0.374$
Cx43	$t_{10} = -0.918$	$p = 0.380$
pCx43	$t_{10} = 0.560$	$p = 0.588$
GFAP	$t_{10} = -0.534$	$p = 0.605$
EAAT1	$t_{10} = -0.515$	$p = 0.618$
EAAT2	$t_{10} = 0.149$	$p = 0.885$

Hippocampal astrocyte response 24 hrs after social fear acquisition. To examine the lasting effects of social fear conditioning, the astrocyte response was analyzed 24 hrs after social fear acquisition. Morphological analysis in the HIP revealed that astrocytes from SFC$^+$ male mice did not undergo to morphological changes 24 hrs after social fear acquisition compared to SFC$^-$ animals (Figure 19). Indeed, both SFC$^-$ and SFC$^+$ astrocytes showed similar branching and coverage in terms of number of primary processes (Figure 19A), the length of the longest process (Figure 19B) and domain area (Figure 19C). Interestingly, the quantification of cFos activation indicated a lower percentage of cFos$^+$ astrocytes in SFC$^+$ compared to SFC$^-$ animals ($p = 0.008$, Figure 18D), suggesting differential activation patterns in response to social fear.

Furthermore, protein expression analysis demonstrated an increase in the phosphorylated isoform of connexin43 (pCx43) in SFC$^+$ compared to SFC$^-$ ($p = 0.037$, Figure 18E). However, there were no differences in the expression levels of other astrocytic markers analyzed, including Cx30, Cx43, GFAP, EAAT1, EAAAT2.

Overall, these findings suggest that hippocampal astrocyte respond to social fear conditioning by a long-lasting alteration in their activation state and of specific protein expression, such as pCx43, but without substantial alterations in their cellular morphology or the expression levels of other astrocytic proteins associated with astrocyte function.

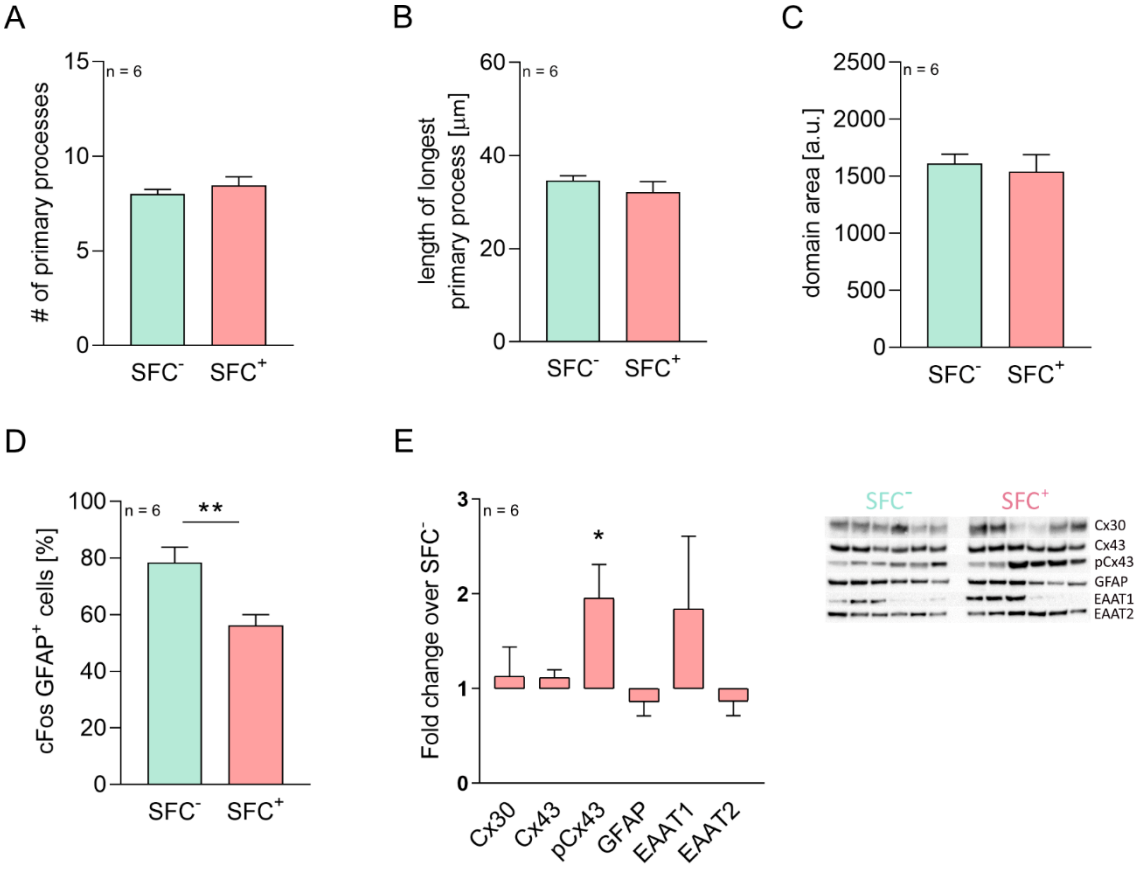

Figure 18. Effects of exposure to social fear conditioning (SFC) on hippocampal astrocytes 24 hrs after social fear acquisition in male mice. *A-C) Quantification of astrocytes morphology, including the number of primary processes (A), length of the longest primary process (B), and domain area (C). D) Percentage of cFos$^+$ astrocytes comparing SFC$^-$ vs SFC$^+$. E) Protein expression analysis of astrocytic markers (Cx30, Cx43, pCx43, GFAP, EAAT1, EAAT2) comparing SFC$^-$ and SFC$^+$, with representative western blots shown for each protein. n = animal number. Data represents means ± SEM. ** p < 0.01, * p = 0.05. For detailed statistics analysis see Table 11.*

Table 11: Statistics of the effects of SFC exposure on astrocytic response 24 hrs after social fear acquisition (Figure 18). Factor represents SFC$^-$ vs SFC$^+$ effects.

Hippocampus	Independent T-Test, Mann-Whitney-*U* Test	Figure A-E
Number of primary processes	$t_{10} = -0.841$	p = 0.420
Length of longest process	$t_{10} = 0.924$	p = 0.377
Domain area	$t_{10} = 0.396$	p = 0.700
cFos	$t_{10} = 3.266$	p = 0.008
Cx30	$t_{10} = -0.363$	p = 0.724
Cx43	$t_{10} = -0.716$	p = 0.491
pCx43	$t_{10} = -2.402$	p = 0.037
GFAP	$t_{10} = 0.691$	p = 0.505
EAAT1	$U = 15$	p = 0.631
EAAT2	$t_{10} = 0.560$	p = 0.588

Hippocampal astrocyte response 90 min after social fear extinction. Given the activation of astrocyte 90 min following social fear acquisition, I investigate whether they respond to the process called social fear extinction training. However, morphological analysis in the HIP revealed that astrocytes did not undergo morphological changes 90 min after social fear extinction (Figure 19). Both SFC^- and SFC^+ astrocytes showed similar branching and coverage in terms of number of primary processes (Figure 19A), the length of the longest process (Figure 19B) and domain area (Figure 19C). Interestingly, the quantification of cFos immunoactivity indicated a high activation of $cFos^+$ astrocytes in both SFC^- and SFC^+ animals, although no differences were found between the two groups (Figure 19D), suggesting similar astrocytic response to repeated exposure to social stimuli.

Interestingly, protein expression analysis revealed an increased in the Cx30 ($p = 0.026$, Figure 19E) and GFAP ($p = 0.015$, Figure 19E) in SFC^+ compared to SFC^-, suggesting that astrocytic structure and intercellular communication may be remodeled in response to social fear extinction. No significant differences were observed in the expression levels of other astrocytic markers analyzed, including Cx43, GFAP, EAAT1, EAAAT2.

Overall, these findings suggest that hippocampal astrocytes respond to the exposure to social extinction with altered expression of specific protein expression, such as Cx30 and GFAP, without showing morphological changes.

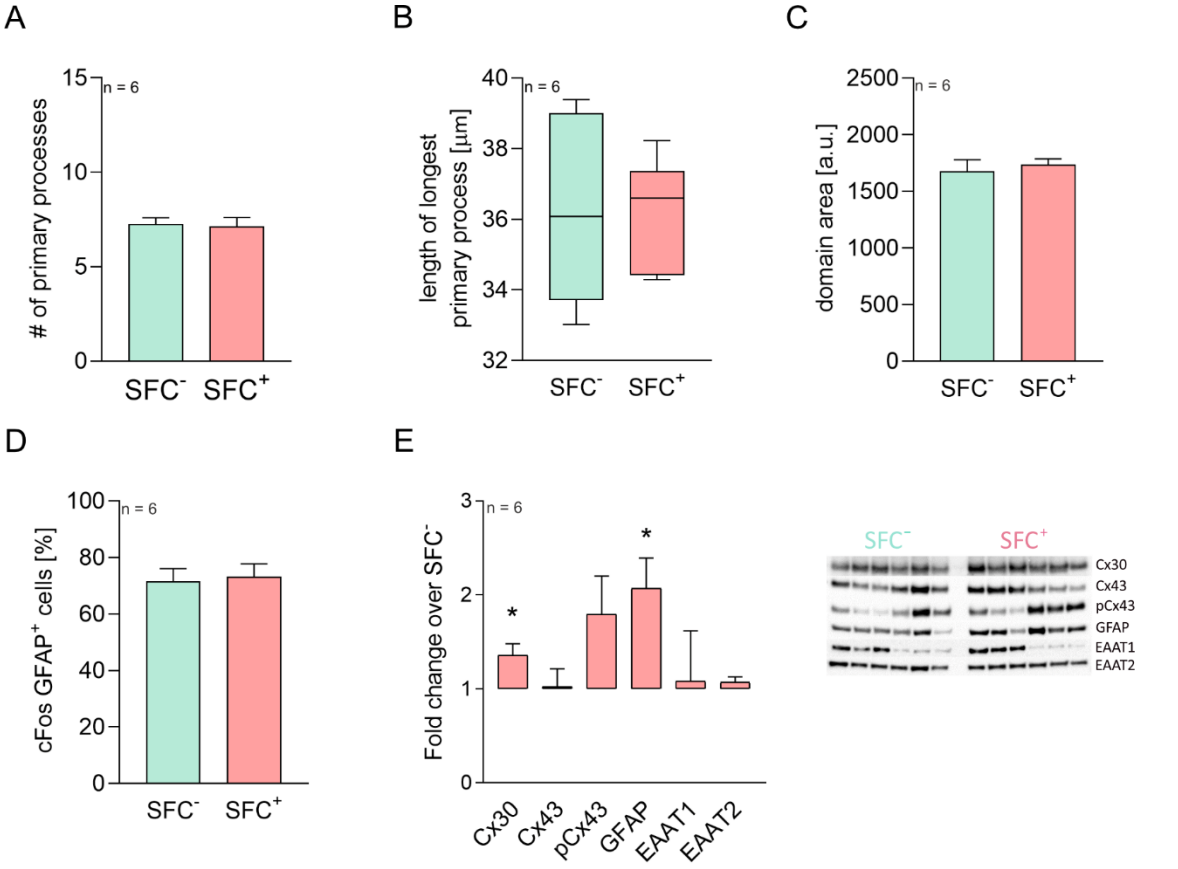

Figure 19. Effects of exposure to social fear conditioning (SFC) on hippocampal astrocytes 90 min after social fear extinction in male mice. *A-C) Quantification of astrocytes morphology, including the number of primary processes (A), length of the longest primary process (B), and domain area (C). D) Percentage of cFos⁺ astrocytes comparing SFC⁻ vs SFC⁺. E) Protein expression analysis of astrocytic markers (Cx30, Cx43, pCx43, GFAP, EAAT1, EAAT2) comparing SFC⁻ and SFC⁺, with representative western blots shown for each protein. n = animal number. Data represents means ± SEM. * p = 0.05. For detailed statistics analysis see Table 12.*

Table 12: Statistics of the effects of SFC exposure on astrocytic response 90 min after social fear extinction (Figure 19). Factor represents SFC⁻ vs SFC⁺ effects.

Hippocampus	Independent T-Test, Mann-Whitney-*U* Test	Figure A-E
Number of primary processes	$t_{10} = 0.189$	p = 0.854
Length of longest process	$U = 17$	p = 0.837
Domain area	$t_{10} = -0.471$	p = 0.648
cFos	$t_{10} = -0.256$	p = 0.803
Cx30	$t_{10} = -2.661$	p = 0.026
Cx43	$t_{10} = -0.085$	p = 0.934
pCx43	$t_{10} = -1.427$	p = 0.187
GFAP	$t_{10} = -2.998$	p = 0.015
EAAT1	$t_{10} = -0.132$	p = 0.898
EAAT2	$t_{10} = -0.627$	p = 0.546

2.2. Astrocytic response within the subdivisions of the LS to social fear acquisition and extinction in male mice

Given the high heterogeneity of the LS and the previously observed region-specific distribution of astrocytes within its subdivisions (see section 1 in Results), I investigated whether astrocytes participate to the processes associated with the acquisition and extinction of social fear across the LS in male mice, to better understand the functional role of astrocyte in relation to specific LS subdivisions.

2.2.1. Astrocytic response to social fear acquisition after 90 min

Astrocytic response to social fear acquisition after 90 min in the dorsal LSr (Figure 20). In the dorsal LSr, morphological analysis revealed that 90 min following social fear acquisition, astrocytes in both SFC^+ and SFC^- groups showed comparable branching patterns and coverage, as shown in the number of primary processes (Figure 20B), the length of longest primary process (Figure 20C) and domain area (Figure 20D). Additionally, cFos immunoactivity analysis showed no differences in the percentage of $cFos^+$ astrocytes between naïve animals and SFC^-, or between SFC^- and SFC^+ (Figure 20F). These results suggest that astrocytes in the dorsal LSr do not exhibit any response to social fear acquisition.

Astrocytic response to social fear acquisition after 90 min in the ventral LSr (Figure 21). In the ventral LSr, morphological analysis conducted 90 min following social fear acquisition revealed that astrocytes in both SFC^+ and SFC^- groups exhibited similar branching patterns, as indicated by the number of primary processes (Figure 21B) and the length of longest primary process (Figure 21C). However, astrocytic coverage was slightly increased in SFC^+ animals ($p = 0.051$, Figure 21D) compared to the SFC^- group. Notably, cFos immunoactivity analysis showed a significant increase in the percentage of $cFos^+$ astrocytes in SFC^- compared to naïve animals ($p = 0.004$, Figure 21E), but no significant differences were observed between SFC^- and SFC^+ groups (Figure 21F). These findings suggest that astrocytes in the ventral LSr have a distinct response to social fear acquisition.

Astrocytic response to social fear acquisition after 90 min in the dorsal LSc (Figure 22). In the dorsal LSc, morphological analysis conducted 90 min after social fear acquisition indicated that astrocytes in SFC^+ exhibited increased branching and coverage pattern as shown by the number of primary processes ($p = 0.055$, Figure 22B), the length of longest primary process ($p = 0.005$, Figure 22C) and the domain area ($p = 0.009$, Figure 22D). Notably, cFos immunoactivity analysis showed a significant increase in the percentage of $cFos^+$ astrocytes in SFC^- compared to naïve animals ($p = 0.030$, Figure 22E), but no significant differences were observed between SFC^- and SFC^+ groups (Figure 22F). These findings suggest that astrocytes in the dorsal LSc, have a greater response to social fear acquisition.

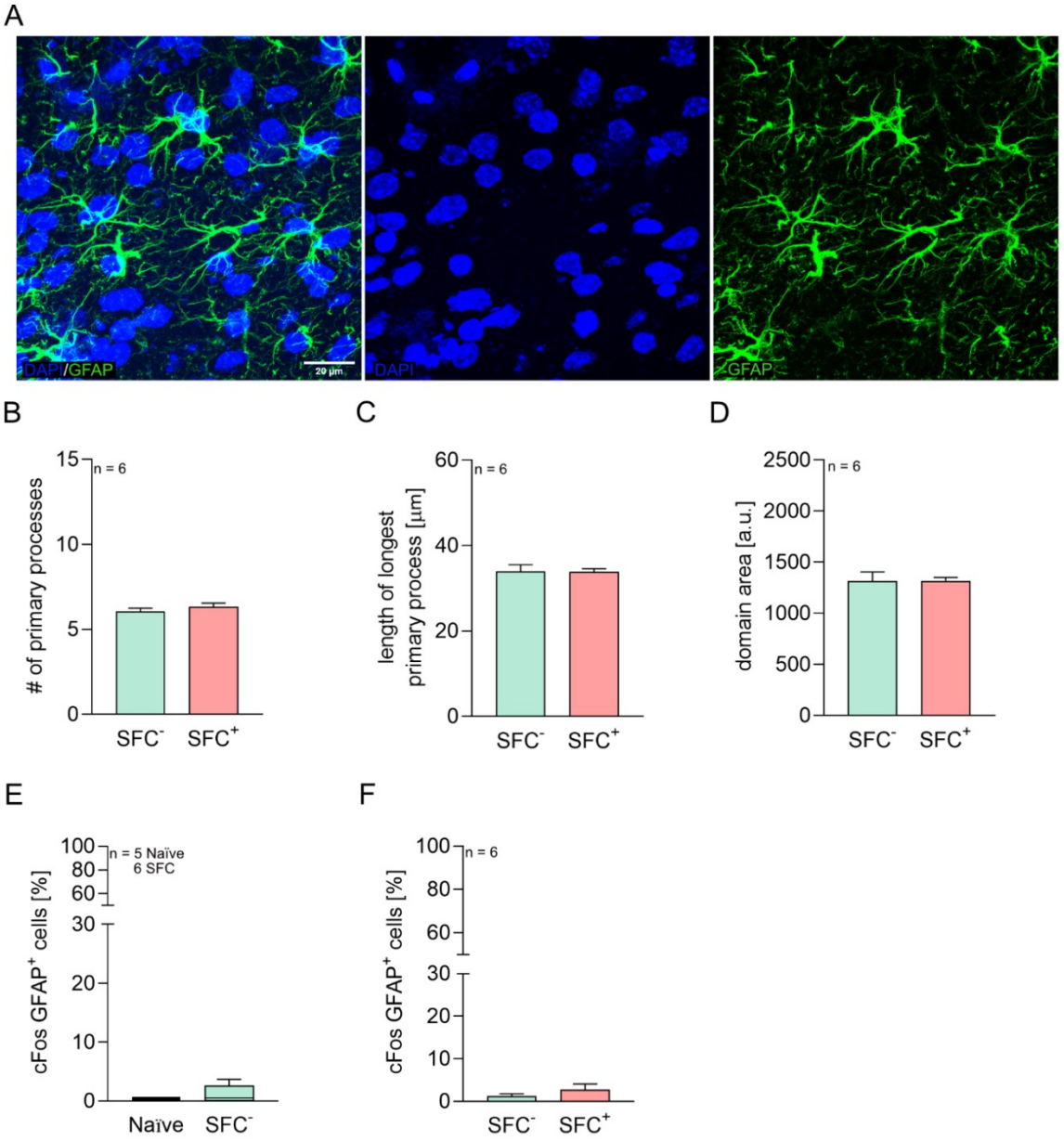

Figure 20. Effects of exposure to social fear conditioning (SFC) on astrocytes in the dorsal part of the rostral lateral septum (LSr) 90 min after social fear acquisition in male mice. *A) Representative immunohistochemical image from the dorsal LSr showing astrocytes stained for glial fibrillary acidic protein expressing (GFAP, green) and nuclei stained with DAPI (blue). Scale bar = 20 µm. B-D) Quantification of astrocytes morphology, including the number of primary processes (B), length of the longest primary process (C), and domain area (D). E-F) Percentage of cFos⁺ astrocytes comparing naïve vs SFC⁻(E), and SFC⁻vs SFC⁺(F). n = animal number. Data represents means ± SEM. For detailed statistics analysis see Table 13.*

Table 13: Statistics of the effects of SFC exposure on hippocampal astrocytic response 90 min after social fear acquisition (Figure 20). Factor represents SFC- vs SFC+ effects or Naïve VS SFC⁻.

Rostral dorsal	Independent T-Test, Mann-Whitney Test	Figure B-F
Number of primary processes	$t_{10} = -0.823$	p = 0.429
Length of longest process	$t_{10} = 0.057$	p = 0.956
Domain area	$t_{10} = 0.011$	p = 0.991
cFos (Naïve vs SFC⁻)	$U = 7.5$	p = 0.082
cFos	$t_{10} = -0.909$	p = 0.385

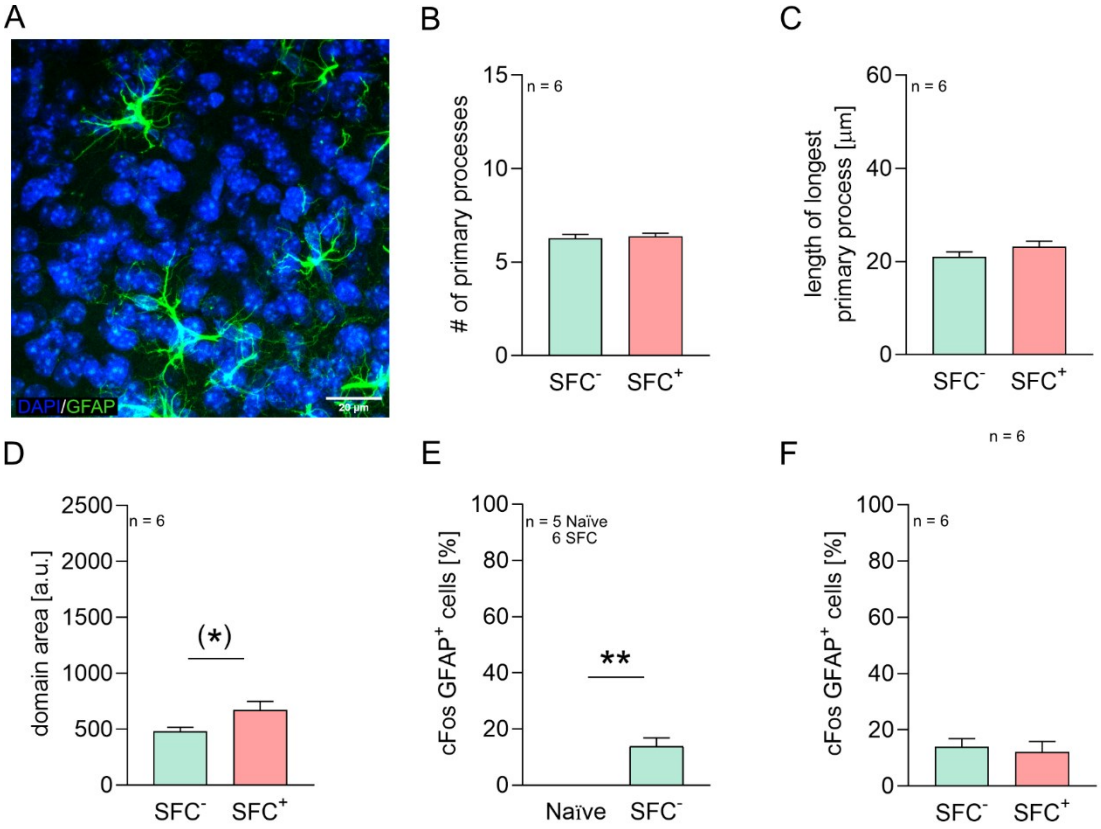

Figure 21. Effects of exposure to social fear conditioning (SFC) on astrocytes in the ventral part of the rostral lateral septum (LSr) 90 min after social fear acquisition in male mice. *A) Representative immunohistochemical image from the ventral LSr showing astrocytes stained for glial fibrillary acidic protein expressing (GFAP, green) and nuclei stained with DAPI (blue). Scale bar = 20 µm. B-D) Quantification of astrocytes morphology, including the number of primary processes (B), length of the longest primary process (C), and domain area (D). E-F) Percentage of cFos⁺ astrocytes comparing naïve vs SFC⁻(E), and SFC⁻vs SFC⁺(F). n = animal number. Data represents means ± SEM. ** p < 0.01, (*) p < 0.07. For detailed statistics analysis see Table 14.*

Table 14: Statistics of the effects of SFC exposure on hippocampal astrocytic response 90 min after social fear acquisition (Figure 21). Factor represents SFC- vs SFC+ effects or Naïve VS SFC⁻.

Rostral ventral	Independent T-Test, Mann-Whitney Test	Figure B-F
Number of primary processes	$t_{10} = -0.381$	p = 0.711
Length of longest process	$t_{10} = -1.315$	p = 0.218
Domain area	$t_{10} = -2.216$	p = 0.051
cFos (Naïve VS SFC⁻)	$U = 0$	p = 0.004
cFos	$t_{10} = 0.369$	p = 0.720

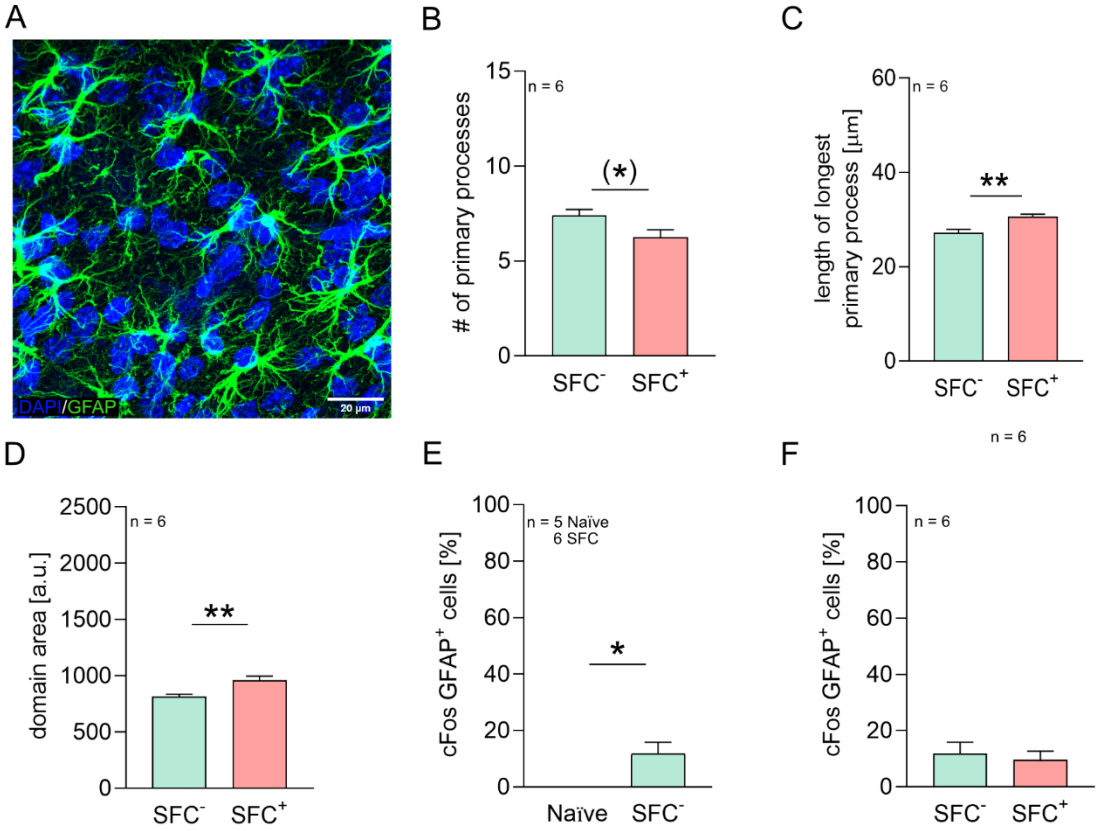

Figure 22. Effects of exposure to social fear conditioning (SFC) on astrocytes in the dorsal part of the caudal lateral septum (LSc) 90 min after social fear acquisition in male mice. *A) Representative immunohistochemical image from the dorsal LSc showing astrocytes stained for glial fibrillary acidic protein expressing (GFAP, green) and nuclei stained with DAPI (blue). Scale bar = 20 µm. B-D) Quantification of astrocytes morphology, including the number of primary processes (B), length of the longest primary process (C), and domain area (D). E-F) Percentage of cFos⁺ astrocytes comparing naïve vs SFC⁻(E), and SFC⁻vs SFC⁺(F). n = animal number. Data represents means ± SEM. ** p < 0.01, * p = 0.05 (*) p < 0.07. For detailed statistics analysis see Table 15.*

Table 15: Statistics of the effects of SFC exposure on hippocampal astrocytic response 90 min after social fear acquisition (Figure 22). Factor represents SFC- vs SFC+ effects or Naïve VS SFC⁻.

Caudal dorsal	Independent T-Test, Mann-Whitney Test	Figure B-F
Number of primary processes	$t_{10} = 2.175$	p = 0.055
Length of longest process	$t_{10} = -3.641$	p = 0.005
Domain area	$t_{10} = -3.233$	p = 0.009
cFos (Naïve VS SFC⁻)	$t_{9} = 2.567$	p = 0.030
cFos	$t_{10} = 0.424$	p = 0.680

Astrocytic response to social fear acquisition after 90 min in the ventral LSc (Figure 23). In the ventral LSc, morphological analysis conducted 90 min following social fear acquisition indicated that astrocytes in SFC⁺ exhibited increased coverage compared to SFC⁻ as shown by the length of the longest primary process (p = 0.034, Figure 23C) and the domain area (p = 0.048, Figure 23D), although no differences were observed in the number of primary processes (Figure 23B). Similar to the dorsal LSc, cFos immunoactivity analysis showed a significant increase in the percentage of

cFos$^+$ astrocytes in SFC$^-$ compared to naïve animals (p = 0.034, Figure 23E), but no significant differences were observed between SFC$^-$ and SFC$^+$ groups (Figure 23F). These findings suggest that, similar to the dorsal LSc, astrocytes in the ventral LSc, have a greater response to social fear acquisition.

Overall, these results show that the ventral part of the LS and in general the LSc seems to participate to the mechanisms associated with the acquisition of social fear in male mice.

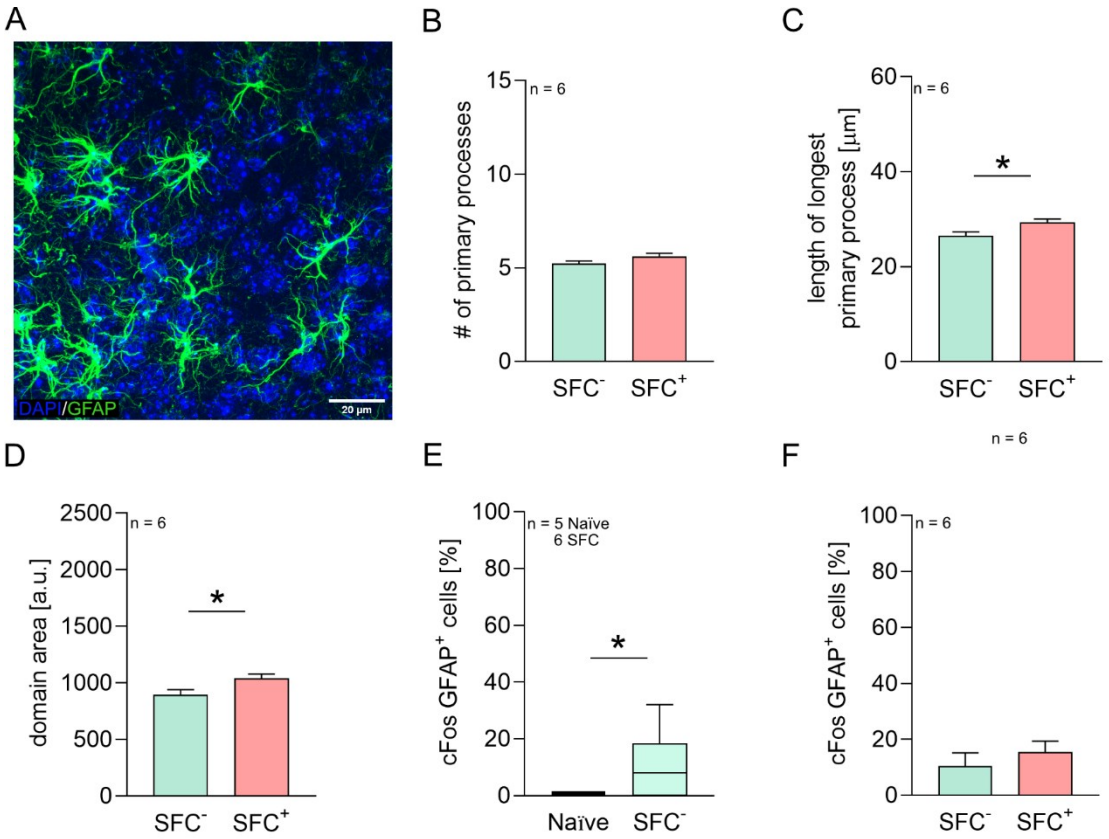

Figure 23. Effects of exposure to social fear conditioning (SFC) on astrocytes in the ventral part of the caudal lateral septum (LSc) 90 min after social fear acquisition in male mice. *A) Representative immunohistochemical image from the ventral LSc showing astrocytes stained for glial fibrillary acidic protein expressing (GFAP, green) and nuclei stained with DAPI (blue). Scale bar = 20 µm. B-D) Quantification of astrocytes morphology, including the number of primary processes (B), length of the longest primary process (C), and domain area (D). E-F) Percentage of cFos$^+$ astrocytes comparing naïve vs SFC$^-$(E), and SFC$^-$vs SFC$^+$(F). n = animal number. Data represents means ± SEM. * p < 0.05. For detailed statistics analysis see Table 16.*

Table 16: Statistics of the effects of SFC exposure on astrocytic response in the LSc ventral 90 min after social fear acquisition (Figure 23). Factor represents SFC- vs SFC+ effects or Naïve VS SFC$^-$.

Caudal ventral	Independent T-Test, Mann-Whitney Test	Figure B-F
Number of primary processes	$t_{10} = -1.378$	p = 0.198
Length of longest process	$t_{10} = -2.462$	p = 0.034
Domain area	$t_{10} = -2.251$	p = 0.048
cFos (Naïve VS SFC$^-$)	$U = 5$	p = 0.034
cFos	$t_{10} = -0.810$	p = 0.437

2.2.2. Astrocytic response to social fear acquisition after 24 hrs across the LS

To examine whether astrocyte adapt to the processes associated with social fear acquisition 24 hrs after conditioning (before social fear extinction), a morphological analysis was conducted across LS subdivisions of male mice (Figure 24). Parameters such as number of primary processes, length of the longest process, and the domain area were assessed in the dorsal LSr (Figure 24A-C), ventral LSr (Figure 24D-F), dorsal LSc (Figure 24H-J) and ventral LSc (Figure 24K-M). However, no differences were found between SFC$^-$ and SFC$^+$ groups across any region. Additionally, cFos immunoactivity in astrocytes was analyzed across the mentioned subdivision of the LS, although no differences were detected between SFC$^-$ and SFC$^+$ (Figure 24G, N). These results suggest that astrocytes adapt to the mechanisms related to social fear acquisition 90 min after social fear acquisition as shown in the previously paragraph, without observing long lasting effects one day after.

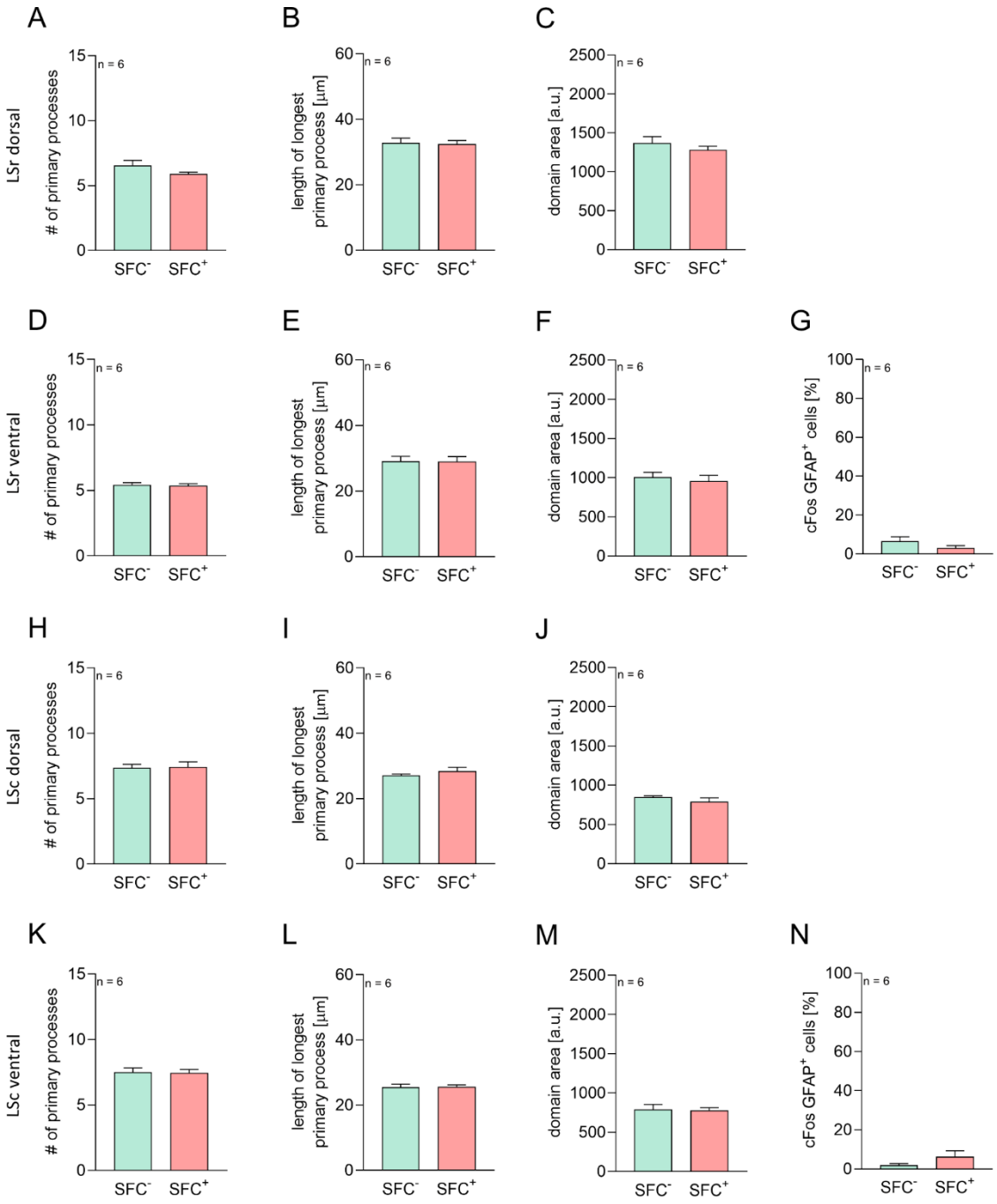

Figure 24. Effects of social fear conditioning (SFC) exposure on astrocytes across the LS 24 hrs after social fear acquisition in male mice. *A-C) Quantification of astrocytes morphology in the dorsal part of the rostral lateral septum (LSr), including the number of primary processes (A), length of the longest primary process (B), and domain area (C). D-F) Quantification of astrocytes morphology in the ventral part of the LSr, including the number of primary processes (D), length of the longest primary process (E), and domain area (F). G) Percentage of cFos⁺ astrocytes in the ventral LSr comparing SFC⁻vs SFC⁺. H-J) Quantification of astrocytes morphology in the dorsal part of the caudal lateral septum (LSc), including the number of primary processes (H), length of the longest primary process (I), and domain area (J). K-M) Quantification of astrocytes morphology in the ventral part of the LSc, including the number of primary processes (K), length of the longest primary process (L), and domain area (M). N) Percentage of cFos⁺ astrocytes in the ventral LSc, comparing SFC⁻vs SFC⁺. n = animal number. Data represents means ± SEM. For detailed statistics analysis see Table 17.*

Table 17: Statistics of the effects of SFC exposure on astrocytic response in the LS 24 hrs after social fear acquisition (Figure 24). Factor represents SFC- vs SFC+ effects.

Rostral dorsal	Independent T-Test	Figure A-C
Number of primary processes	$t_{10} = 1.516$	$p = 0.160$
Length of longest process	$t_{10} = 0.182$	$p = 0.859$
Domain area	$t_{10} = 0.870$	$p = 0.405$
Rostral ventral	Independent T-Test	Figure D-G
Number of primary processes	$t_{10} = 0.316$	$p = 0.759$
Length of longest process	$t_{10} = 0.019$	$p = 0.985$
Domain area	$t_{10} = 0.520$	$p = 0.614$
cFos	$t_{10} = 1.259$	$p = 0.237$
Caudal dorsal	Independent T-Test, Mann-Whitney Test	Figure H-J
Number of primary processes	$t_{10} = -0.150$	$p = 0.884$
Length of longest process	$U = 15$	$p = 0.631$
Domain area	$t_{10} = 0.999$	$p = 0.341$
Caudal ventral	Independent T-Test	Figure K-N
Number of primary processes	$t_{10} = 0.145$	$p = 0.888$
Length of longest process	$t_{10} = -0.111$	$p = 0.914$
Domain area	$t_{10} = 0.173$	$p = 0.866$
cFos	$t_{10} = -1.267$	$p = 0.234$

2.2.3. Astrocytic response to social fear extinction after 90 min

Given the established role of the LS in social fear extinction (Menon et al. 2018), I explored whether astrocytes participate to mechanisms behind the learning processes characteristic of the extinction phase of the fear. Morphological and cFos analysis were performed in the dorsal LSr (Figure 25A-D), ventral LSr (Figure 25E-H), dorsal LSc (Figure I-L) and ventral LSc (Figure M-P). However, no significant differences were observed in any of the LS subdivisions, indicating that their potential role in modulating neuronal mechanisms of social fear extinction could not be detected by the methods used in this analysis.

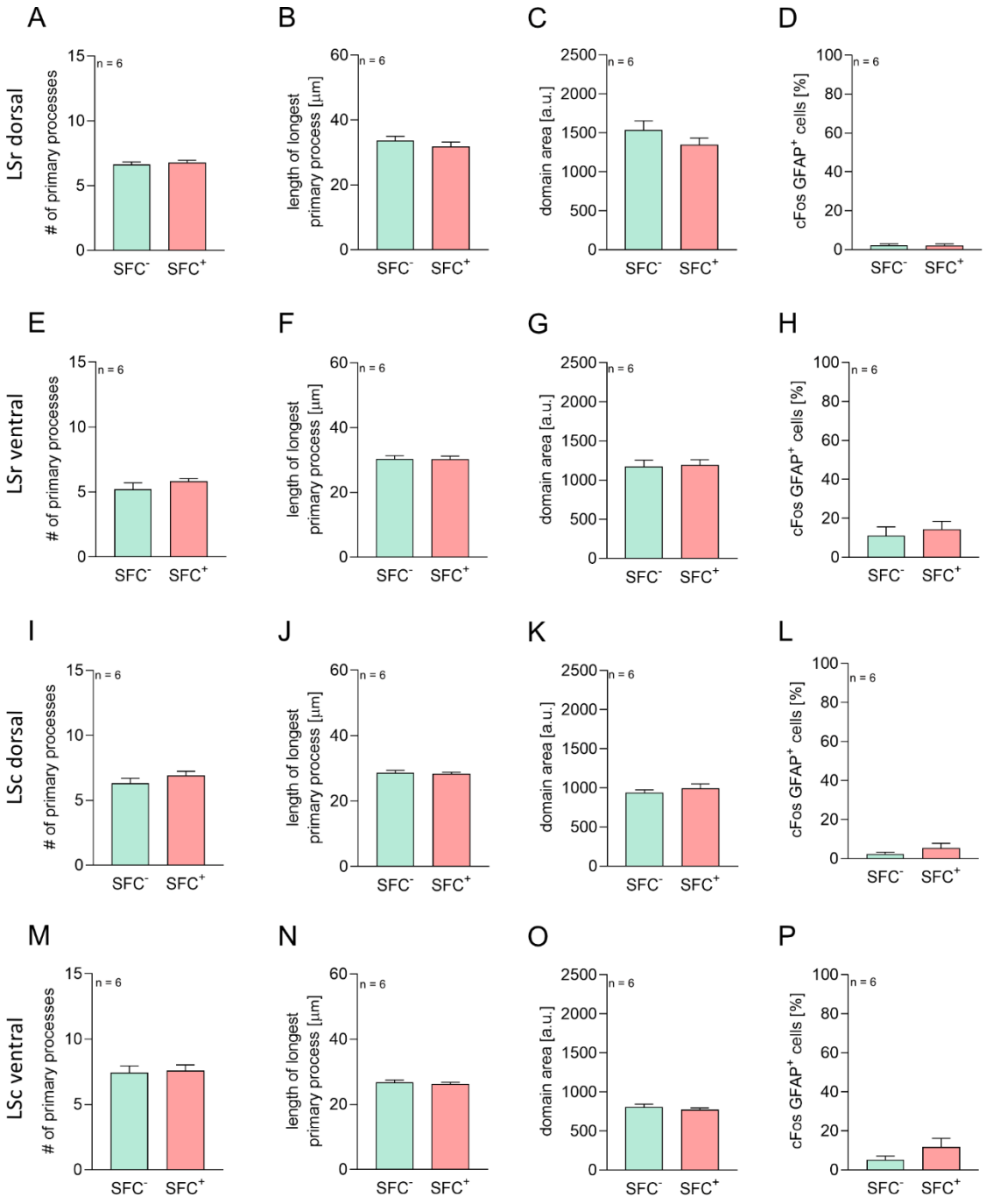

Figure 25. Effects of exposure to social fear conditioning (SFC) on astrocytes across the LS 90 min after social fear extinction in male mice. *A-C) Quantification of astrocytes morphology in the dorsal part of the rostral lateral septum (LSr), including the number of primary processes (A), length of the longest primary process (B), and domain area (C). D) Percentage of cFos⁺ astrocytes in the dorsal LSr comparing SFC⁻vs SFC⁺. E-G) Quantification of astrocytes morphology in the ventral part of the LSr, including the number of primary processes (E), length of the longest primary process (F), and domain area (G). H) Percentage of cFos⁺ astrocytes in the ventral LSr comparing SFC⁻vs SFC⁺. I-K) Quantification of astrocytes morphology in the dorsal part of the caudal lateral septum (LSc), including the number of primary processes (I), length of the longest primary process (J), and domain area (K). L) Percentage of cFos⁺ astrocytes in the dorsal LSc, comparing SFC⁻vs SFC⁺. M-O) Quantification of astrocytes morphology in the ventral part of the LSc, including the number of primary processes (M), length of the longest primary process (N), and domain area (O). P) Percentage of cFos⁺ astrocytes in the ventral LSc, comparing SFC⁻vs SFC⁺. n = animal number. Data represents means ± SEM. For detailed statistics analysis see Table 18.*

Table 18: Statistics of the effects of SFC exposure on astrocytic response in the LS 90 min after social fear extinction (Figure 25). Factor represents SFC- vs SFC+ effects.

Rostral dorsal	Independent T-Test	Figure A-D
Number of primary processes	$t_{10} = -0.511$	$p = 0.623$
Length of longest process	$t_{10} = 0.808$	$p = 0.442$
Domain area	$t_{10} = 1.290$	$p = 0.233$
cFos	$t_{10} = 0.062$	$p = 0.952$
Rostral ventral	Independent T-Test	Figure E-H
Number of primary processes	$t_{10} = -1.259$	$p = 0.244$
Length of longest process	$t_{10} = 0.105$	$p = 0.919$
Domain area	$t_{10} = -0.190$	$p = 0.854$
cFos	$t_{10} = -0.530$	$p = 0.607$
Caudal dorsal	Independent T-Test, Mann-Whitney Test	Figure I-L
Number of primary processes	$t_{10} = -1.171$	$p = 0.269$
Length of longest process	$t_{10} = 0.336$	$p = 0.744$
Domain area	$t_{10} = -0.815$	$p = 0.434$
cFos	$U = 13.5$	$p = 0.442$
Caudal ventral	Independent T-Test	Figure M-P
Number of primary processes	$t_{10} = -0.234$	$p = 0.820$
Length of longest process	$t_{10} = 0.503$	$p = 0.626$
Domain area	$t_{10} = 0.734$	$p = 0.480$
cFos	$t_{10} = -1.308$	$p = 0.220$

2.2.4. Astrocytic response to social fear acquisition and extinction in the caudal septum

To gain more insights in relation to astrocytic function following acquisition and extinction of social fear, analysis of the levels expression of specific astrocytic proteins was performed in the caudal part of the septum (see section 6.2. in Material and methods for details). Protein expression analysis revealed a decreased in the Cx43 ($p = 0.036$) and EAAT2 ($p = 0.004$), with a trend decrease in the GFAP ($p = 0.070$) in SFC^+ compared to SFC^- 90 min after social fear acquisition (Figure 26A); with no changes in other astrocytic protein. 24 hrs after social fear acquisition a trend with a decrease in the pCx43 ($p = 0.056$) level expression was observed in SFC^+ compared to SFC^- (Figure 26B). In line with morphological analysis, no differences were observed in the expression levels of other astrocytic markers analyzed 90 min after social fear extinction (Figure 26C). These findings suggest that alterations in astrocytic protein expression may be linked to adaptive mechanisms following social fear acquisition but do not persist following extinction, highlighting once again the dynamic role of astrocytes in socio-emotional regulation.

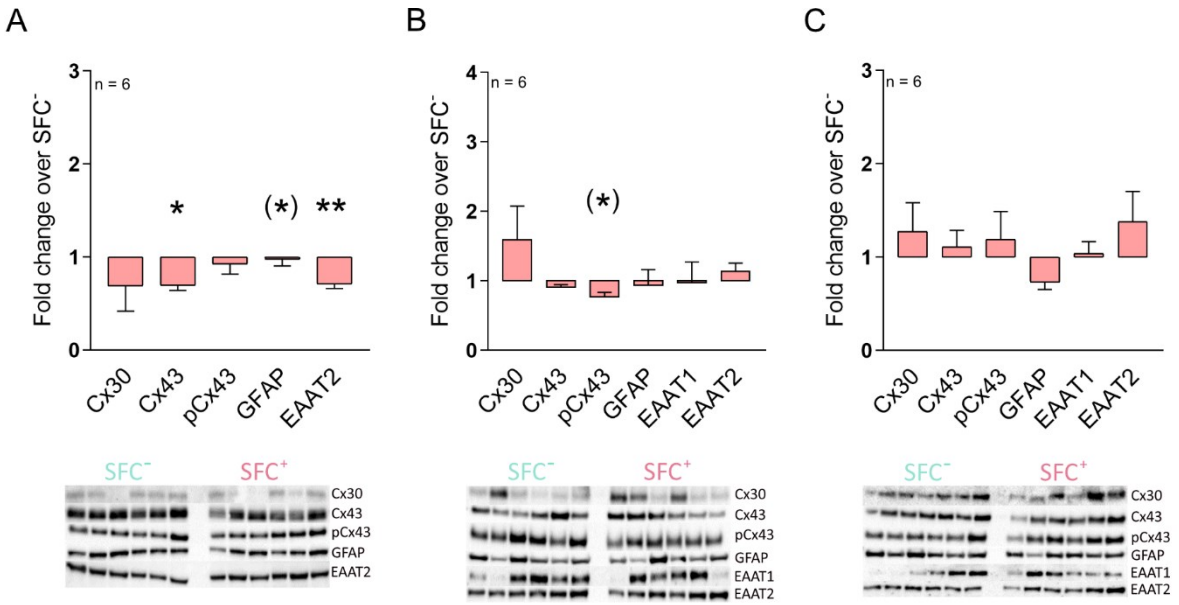

Figure 26. Effects of social fear acquisition and extinction on astrocytic protein expression in the caudal septum. *A-C) Protein expression analysis of astrocytic markers (Cx30, Cx43, pCx43, GFAP, EAAT1, EAAT2) comparing SFC⁻ and SFC⁺, with representative western blots shown for each protein 90 min after social fear acquisition A), 24 hrs after social fear acquisition B) and 90 min after social fear extinction C). n = animal number. Data represents means ± SEM. ** p < 0.01, * p 0.05 (*) p < 0.07. For detailed statistics analysis see Table 19.*

Table 19: Statistics of the effects of SFC exposure on astrocytic proteins expression in the caudal septum (Figure 26). Factor represents SFC- vs SFC+ effects.

90 min after Acquisition	Independent T-Test, Mann-Whitney Test	Figure A
Cx30	$U = 8$	p = 0.347
Cx43	$t_8 = 2.516$	p = 0.036
pCx43	$t_8 = -0.917$	p = 0.386
GFAP	$t_9 = -2.052$	p = 0.070
EAAT2	$t_9 = 3.904$	p = 0.004
24 hrs after Acquisition	**Independent T-Test, Mann-Whitney Test**	**Figure B**
Cx30	$U = 8$	p = 0.201
Cx43	$U = 15$	p = 0.631
pCx43	$t_{10} = 2.163$	p = 0.056
GFAP	$t_{10} = 0.200$	p = 0.845
EAAT1	$t_{10} = 0.053$	p = 0.959
EAAT2	$U = 15$	p = 0.631
90 min after Extinction	**Independent T-Test, Mann-Whitney Test**	**Figure C**
Cx30	$U = 16$	p = 0.749
Cx43	$t_{10} = -0.543$	p = 0.599
pCx43	$t_{10} = -0.373$	p = 0.717
GFAP	$t_{10} = 1.488$	p = 0.168
EAAT1	$t_{10} = -0.213$	p = 0.835
EAAT2	$t_{10} = -1.169$	p = 0.270

2.3. Astrocytic response to social fear acquisition in the LSc of female and lactating mice

Given the astrocyte response observed predominantly in the LSc following social fear acquisition in male mice, I investigated whether a similar response was found in female mice as well. Branching and coverage of astrocytes was analyzed in the dorsal and ventral LSc as morphological analysis 90 min after social fear acquisition (Figure 27). Morphological analysis in both dorsal and ventral LSc in virgin female mice revealed no differences between SFC^- and SFC^+, in any of the parameters considered including number of primary processes (Figure 27B, F), length of the longest primary process (Figure 27C, G) or domain area (Figure 27D, H), suggesting caudal LS astrocytes did not exhibit morphological changes in virgin female mice compared to males. Additionally, analysis of the cFos activation in the ventral LSc showed no changes between SFC^- and SFC^+ (Figure 27I).

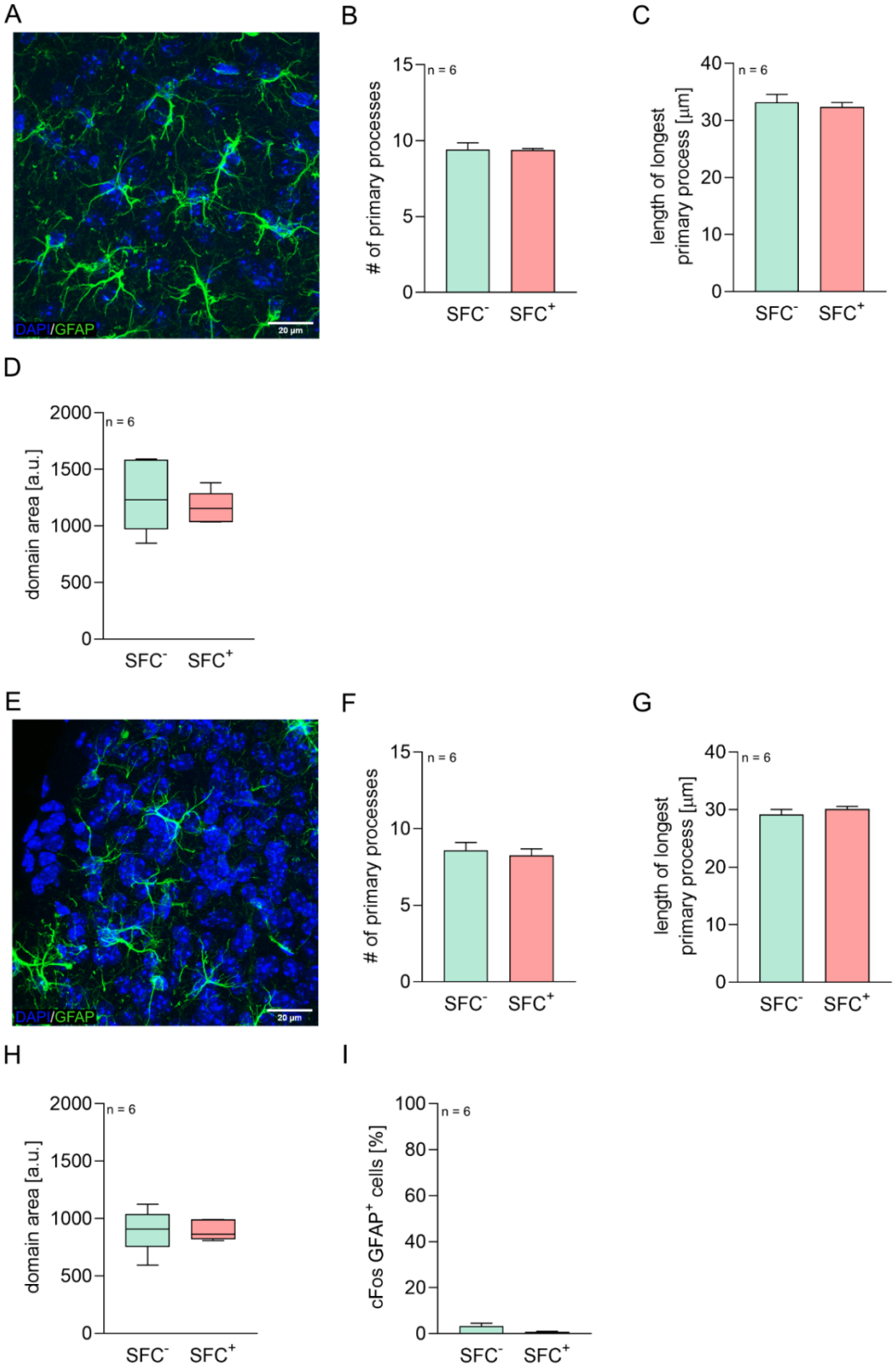

Figure 27. Effects of exposure to SFC on astrocyte morphology within the LSc in virgin female mice 90 min after social fear acquisition. *A) Representative immunohistochemical image from the dorsal LSc showing astrocytes stained for glial fibrillary acidic protein expressing (GFAP, green) and nuclei stained with DAPI (blue). Scale bar = 20 µm. B-D) Quantification of astrocytes morphology, including the number of primary processes (B), length of the longest primary process (C), and domain area (D). E) Representative immunohistochemical image from the ventral LSc showing astrocytes stained for glial fibrillary acidic protein expressing (GFAP, green) and nuclei stained with DAPI (blue). Scale bar = 20 µm. F-H) Quantification of astrocytes morphology, including the number of primary processes (F), length of the longest primary process (G), and domain area (H). I) Percentage of cFos$^+$ astrocytes comparing SFC$^-$vs SFC$^+$. n = animal number. Data represents means ± SEM. For detailed statistics analysis see Table 20.*

Table 20: Statistics of the effects of SFC exposure on astrocytic morphology 90 min after social fear acquisition (Figure 27). Factor represents SFC^- vs SFC^+ effects.

Caudal dorsal LS	Independent T-Test, Mann-Whitney Test	Figure B-D
Number of primary processes	$t_9 = 0.063$	$p = 0.951$
Length of longest process	$t_{10} = 0.470$	$p = 0.649$
Domain area	$U = 17$	$p = 0.873$
Caudal ventral LS	**Independent T-Test, Mann-Whitney Test**	**Figure F-I**
cFos	$t_{10} = 1.724$	$p = 0.115$
Number of primary processes	$t_{10} = 0.469$	$p = 0.649$
Length of longest process	$t_{10} = -0.946$	$p = 0.366$
Domain area	$U = 17$	$p = 0.873$

Additionally, considering the facilitation of the extinction phase observed in lactating mice (Menon et al. 2018), I investigated whether the state of lactation affects astrocytic responsiveness. Morphological analysis in the dorsal LSc in lactating mice revealed no differences between SFC^- and SFC^+, in any of the parameters considered including number of primary processes (Figure 28B), length of the longest primary process (Figure 28C) or domain area (Figure 28D). However, in the ventral LSc an increase in the number of the primary processes was observed in SFC^+ compared to SFC^- ($p = 0.012$; Figure 28G), but no other differences were detected in the other parameters analyzed including the length of the primary processes (Figure 28H), and the domain area (Figure 28I). Additionally, cFos analysis showed no differences in the activation of $cFos^+$ astrocytes between SFC^- and SFC^+ in neither the dorsal LSc (Figure 28E) or ventral LSc (Figure 28J). These findings suggest no morphological changes in the dorsal LSc of lactating mice following social fear acquisition, while in the ventral LSc, astrocytes seem to adapt to the mechanisms associated with social fear acquisition by enriching the branching of the processes to improve the neuronal support and neural connectivity. This suggests that, unlike in virgin females, the state of lactation affects astrocytic responsiveness, despite expressing a similar number of astrocytic cells (see section 1 in Results).

Overall, these findings show that astrocytes within the LS, particularly in the caudal part, they exhibit a response to those processes following social fear acquisition in male mice. Although in virgin female mice no morphological changes were observed following social fear acquisition, the higher number of astrocytic cells found in females compared to males would probably compensate for the adapting processes related to social fear acquisition. Interestingly, lactating mice, which have a similar number of astrocytic cells to virgin females, showed astrocytic structural changes in the LSc, suggesting that lactation may influence astrocytic responsiveness.

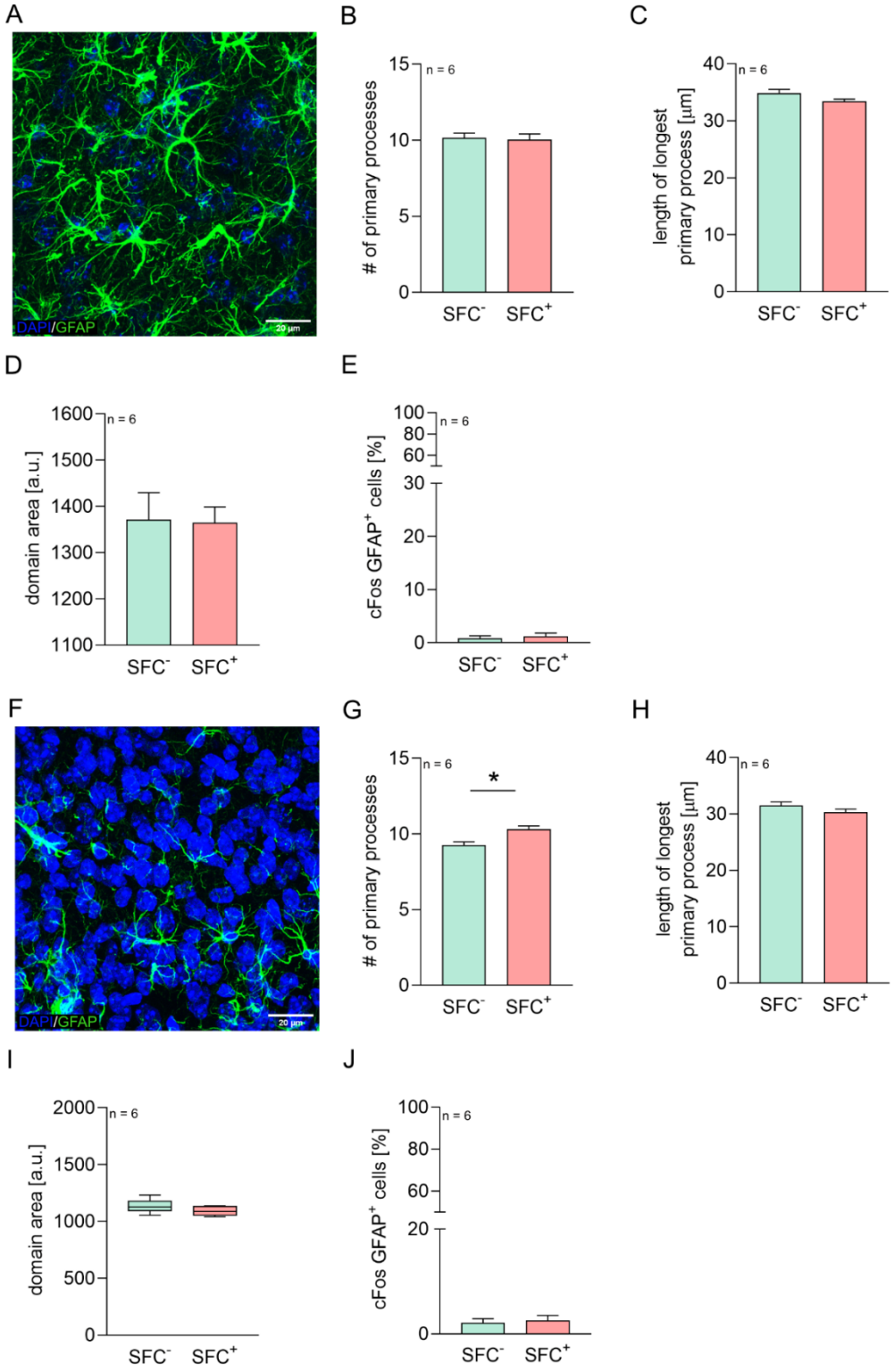

Figure 28. Effects of exposure to SFC on astrocyte morphology within the LSc in lactating mice 90 min after social fear acquisition. *A) Representative immunohistochemical image from the dorsal LSc showing astrocytes stained for glial fibrillary acidic protein expressing (GFAP, green) and nuclei stained with DAPI (blue). Scale bar = 20 µm. B-D) Quantification of astrocytes morphology, including the number of primary processes (B), length of the longest primary process (C), and domain area (D). E) Percentage of cFos+ astrocytes comparing SFC-vs SFC-. F) Representative immunohistochemical image from the ventral LSc showing astrocytes stained for glial fibrillary acidic protein expressing (GFAP, green) and nuclei stained with DAPI (blue). Scale bar = 20 µm. G-I) Quantification of astrocytes morphology, including the number of primary processes (G), length of the longest primary process (H), and domain area (I). J) Percentage of cFos+ astrocytes comparing SFC-vs SFC-. n = animal number. Data represents means ± SEM. * $p < 0.05$. For detailed statistics analysis see Table 21.*

.

Table 21: Statistics of the effects of SFC exposure on astrocytic response 90 min after social fear acquisition in lactating mice (Figure 28). Factor represents SFC^- vs SFC^+ effects.

Caudal dorsal LS	Independent T-Test	Figure B-E
cFos	$t_{10} = -0.375$	$p = 0.716$
Number of primary processes	$t_{10} = 0.221$	$p = 0.830$
Length of longest process	$t_{10} = 0.662$	$p = 0.137$
Domain area	$t_{10} = 0.097$	$p = 0.925$
Caudal ventral LS	**Independent T-Test, Mann-Whitney Test**	**Figure G-J**
cFos	$t_{10} = -0.322$	$p = 0.754$
Number of primary processes	$t_{10} = -3.064$	$p = 0.012$
Length of longest process	$t_{10} = 1.297$	$p = 0.224$
Domain area	$U = 9$	$p = 0.273$

3. Contribution of LS astrocytes to socio-emotional behaviors

Given the emerging role of astrocytes observed in depressive and anxiety-like behaviors, as well as the morphological adaptation and activity patterns of astrocytes within the LS described above especially at 90 min after social fear acquisition, I investigated whether impairment of astrocytic functions within the LSc would affect socio-emotional behaviors in male mice. To induce astrocytic dysfunction, I bilaterally applied L-AAA, a glutamine synthetase inhibitor (see section 4.1. in Material and Methods), into the LSc 3 days prior to behavioral testing in the SPT, EPM and FST, as well the SFC paradigm.

3.1. Effects of LS astrocytic dysfunction on anxiety and depressive-related behaviors in male mice

Based on previous studies (Banasr and Duman 2008; David et al. 2019), two doses of L-AAA were tested (10 µg/µl and 25 µg/µl) to successfully induce astrocytic structure depletion, indicated by a reduction of GFAP expression. Immunohistochemical analysis of GFAP fluorescence in the LSc (Figure 29 B-D) revealed a reduction in GFAP in mice treated with 10 µg/µl-LAAA ($p = 0.02$; Figure 29C, E) compared to the Veh-treated group (Figure 29B, E). Additionally, a more pronounced reduction in GFAP was observed in the group treated with 25 µg/µl L-AAA- ($p < 0.001$ versus Veh-treated group; Figure 29D, E). Despite this astrocytic dysfunction, no significant difference was found between the Veh-treated and the L-AAA-treated groups in either social preference (Figure 29F) or novel social stimulus preference (Figure 29G) in the SPT. The following day, animals were tested in the EPM to assess anxiety-related behaviors. No changes were observed between treatment groups in the latency to first entry into open arms (Figure 29H), the number of entries in open arms (Figure 29I), or the percentage of time spent in open arms (Figure 29J), indicating that astrocytic dysfunction in the LSc did not affect anxiety-like behaviors. Lastly, to assess passive stress coping behavior, the FST was conducted the day after. Immobility time and climbing time were measured as indicators of passive stress coping behaviors (see section 2.4, in Material and Methods). However, no behavioral differences were detected between the Veh-treated group and the two L-AAA-treated groups, either in the immobility or climbing time, suggesting that astrocyte depletion did not affect depressive-like behaviors either.

Overall, these findings demonstrate that L-AAA treatment successfully reduced GFAP in the LSc, particularly at higher concentrations (25 µg/µl). Despite the treatment-induced reduction of astrocytic coverage in the neural networks of the LSc, no changes were observed in social, novelty-seeking, anxiety- or depressive-like behaviors, suggesting astrocytes in LSc do not directly regulate these specific behaviors.

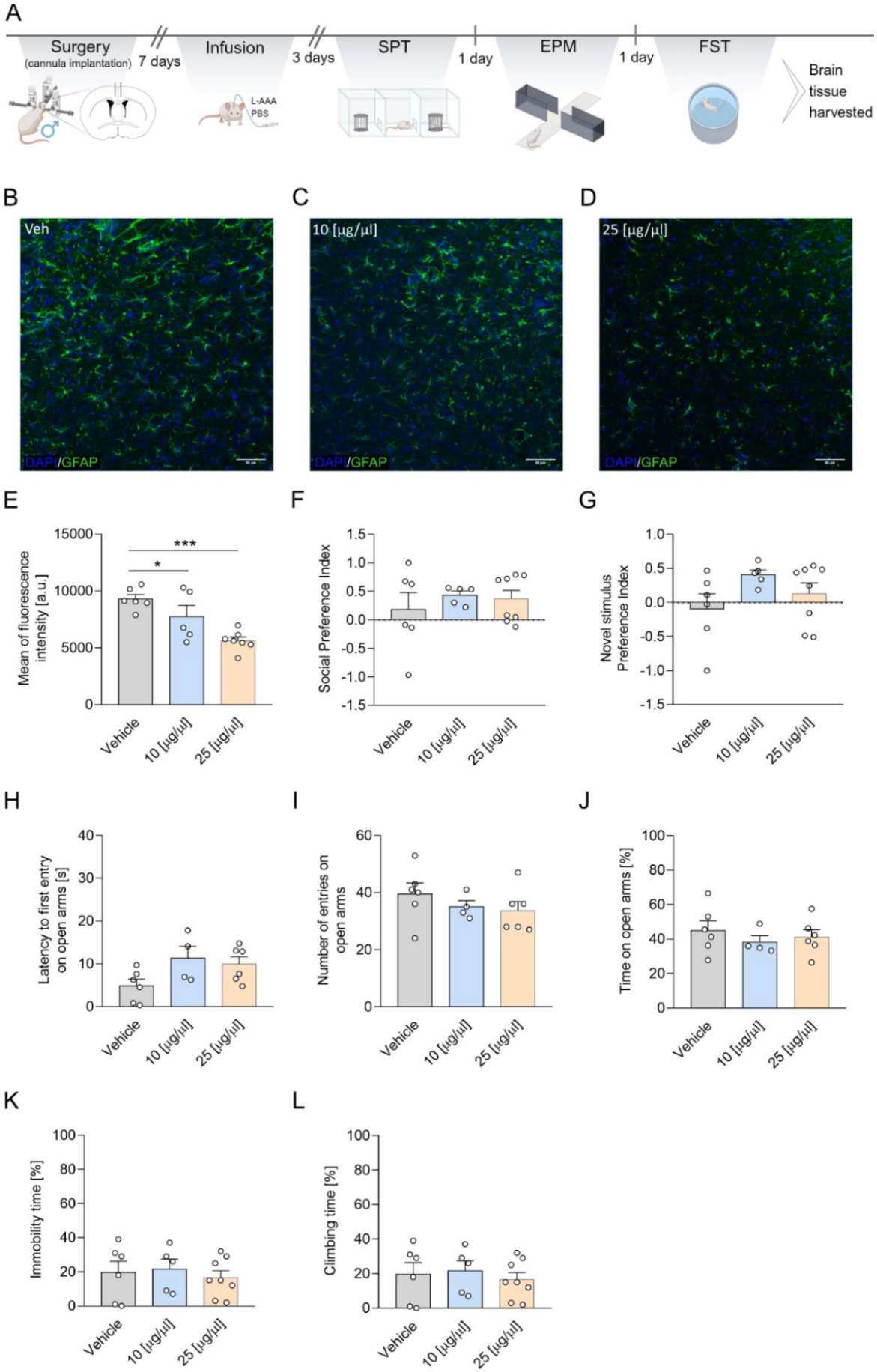
A
Surgery
(cannula implantation)
7 days
Infusion
3 days
SPT
1 day
EPM
1 day
FST
Brain
tissue
harvested
L-AAA
PBS
B
Veh
DAPI/GFAP
C
10 [µg/µl]
DAPI/GFAP
D
25 [µg/µl]
DAPI/GFAP
E
Mean of fluorescence intensity [a.u.]
***
*
Vehicle
10 [µg/µl]
25 [µg/µl]
F
Social Preference Index
G
Novel stimulus Preference Index
H
Latency to first entry on open arms [s]
I
Number of entries on open arms
J
Time on open arms [%]
K
Immobility time [%]
L
Climbing time [%]

Figure 29. Effects of L-AAA-induced astrocytic dysfunction in the caudal lateral septum (LSc) in male mice. *A) Illustration of the experimental timeline. B) Representative image from the LSc showing immunohistochemical staining for glial fibrillary acidic protein expressing (GFAP, green) and nuclei stained with DAPI (blue) from Vehicle-treated group (B), 10 µg/µl (C) and 25 µg/µl (D) L-AAA-treated group. Scale bar = 20 µm. E) Quantification of mean fluorescence of GFAP in Vehicle, 10 µg/µl and 25 µg/µl L-AAA treated group. F-G) show Social Preference Index (F) and Novel stimulus Preference Index (G) from the Social Preference Test in Veh-, 10 µg/µl and 25 µg/µl L-AAA-treated animals. H, I, J) show quantification of the latency to the first entry into open arms (H), the number of entries (J), and the percentage of time spent in open arms (J) in the Elevated Plus Maze in Veh, 10 µg/µl and 25 µg/µl L-AAA-treated groups. K, L) show the immobility time (K) and climbing time (L) during the Forced Swim Test between Veh, 10 µg/µl and 25 µg/µl L-AAA-treated group. Data represents means ± SEM. * $p \leq 0.05$, *** $p < 0.001$. For detailed statistics analysis see Table 22.*

Table 22: Statistics of behavioral effects of L-AAA-induced astrocyte dysfunction within the caudal part of the lateral septum (LSc) on Social Preference Test (SPT), Elevated Plus Maze (EPM) and Forced Swim Test (FST) in male mice (Figure 29). Factor represents Veh vs 10 µg/ µg L-AAA vs 25 µg/ µg L-AAA effects.

	One way ANOVA	Figure E-L
Mean fluorescence intensity	$F_{2,15} = 11.509$	$p < 0.001$
Social Preference Index	$F_{2,16} = 0.397$	$p = 0.679$
Novel stimulus Preference Index	$F_{2,16} = 1.869$	$p = 0.186$
Latency to first entry on open arms	$F_{2,13} = 3.194$	$p = 0.074$
Number of entries on open arms	$F_{2,13} = 0.887$	$p = 0.435$
Time on open arms	$F_{2,13} = 0.464$	$p = 0.639$
Immobility time	$F_{2,16} = 0.212$	$p = 0.811$
Climbing time	$F_{2,16} = 1.172$	$p = 0.335$

3.2. Effects of LS astrocytic structure depletion on social fear acquisition and extinction in male and female mice

Considering the morphological changes in astrocytes observed following social fear acquisition (see section 2.2.), I investigated the effects of L-AAA-induced astrocytic structural depletion in the LSc on social fear acquisition and extinction learning in male and female mice. To further investigate the effects of L-AAA-induced astrocytic coverage depletion on social fear, the higher dose of L-AAA (25 µg/µl) was used.

In male mice, L-AAA-induced astrocytic structural depletion did not influence the number of foot shocks necessary to induce social avoidance during social fear conditioning (Figure 30B). On the following day and prior to extinction training both L-AAA and Veh-treated groups displayed similar investigation time toward non-social stimulus during the first two presentations (ns1 and ns2). However, in the third non-social stimulus (ns3), SFC^+/L-AAA animals showed higher investigation time compared to the SFC^+/Veh group (* $p = 0.035$, Figure 30C) reflecting lower anxiety-like behavior. During social fear extinction training, all SFC^+ animals independent of treatment exhibited social fear, as evidenced by reduced investigation time during exposure to the first 3 social stimuli

(Figure 30D). However, during the fourth social stimulus exposure (s4), SFC^+/L-AAA mice showed a trend toward higher investigation time compared to SFC^+/Veh ((*) < 0.07), suggesting reduced social fear in the L-AAA group. This reduced social fear is also evidenced by lower investigation time in SFC^+/L-AAA compared to the SFC^-/L-AAA group during early social stimuli exposure (s1 and s2 $p < 0.001$, s3 $p = 0.003$, s4 $p = 0.021$, s5 $p = 0.023$), until investigation levels converged during the final social stimulus. In contrast, SFC^+/Veh animals displayed consistently lower investigation time compared to the SFC^-/Veh across all stimuli (s1 -s4 $p < 0.001$, s5 $p = 0.001$, s6 $p = 0.016$), suggesting sustained social fear.

During social fear recall, SFC^+/Veh animals showed reduced investigation time compared to SFC^-/Veh during the first four social stimuli exposure (s1 $p < 0.001$, s2 $p = 0.001$, s3 $p = 0.034$, s4 $p = 0.034$), until investigation levels converged from the third stimulus until the sixth (Figure 30E). This indicates successful extinction of social fear in the vehicle-treated group, where repeated social stimulus presentations led to diminished social fear response. Interestingly, SFC^+/L-AAA animals did not exhibit differences in investigation time compared to the SFC^-/L-AAA, suggesting successful acquisition of social fear. Moreover, when comparing SFC^+ between the two treatment groups, L-AAA-treated animals showed higher social investigation during the first social stimulus exposure (s1 $p = 0.029$) with a trend toward a similar difference in the second stimulus (s2 $p = 0.069$). These findings suggest that while SFC^+/L-AAA animals successfully acquired social fear, the memory and retention of social fear were weaker compared to the vehicle-treated group.

In terms of vigilance behavior, both L-AAA and Veh-treated groups displayed similar vigilance time towards the non-social stimulus during the first two exposures (ns1 and ns2). However, in the third non-social stimulus (ns3), SFC^+/L-AAA animals showed lower vigilance time compared to the SFC^+/Veh group (* $p = 0.031$, Figure 30F). During exposure to social stimuli (Figure 30G), in SFC^+/Veh animals showed a more pronounced fear response than SFC^+/L-AAA, as indicated by higher vigilance time across social stimuli s2 to s6 (s2 -s3 $p = 0.07$, s4 $p = 0.012$, s5 $p = 0.030$, s6 $p = 0.009$). Furthermore, SFC^+/Veh animals showed increased vigilance time compared to SFC^-/Veh- during all social stimuli (s1-s5 $p < 0.001$, s6 $p = 0.001$), reflecting a sustained social fear response already observed in the investigation time analysis. In contrast, SFC^+/L-AAA animals showed higher vigilance behavior than SFC^-/L-AAA mainly during the first three social stimuli (s1-s2 $p < 0.001$, s3 $p = 0.017$), with a trend toward higher vigilance behavior in the fourth and fifth social stimuli (s4 $p = 0.070$, s5 $p = 0.065$), suggesting a reduced fear response following repeated social stimulus exposure.

During recall, SFC^+/Veh displayed fear response during the first five social stimuli, as indicated by higher vigilance behaviors compared to the SFC^-/Veh (s1 $p < 0.001$, s2 $p = 0.001$, s3 $p = 0.002$, s4 $p = 0.007$, s5 $p = 0.028$). Vigilance behavior reached comparable time during the final social exposure,

indicating a diminished social fear response. In contrast, SFC^+/L-AAA animals exhibited similar vigilance behavior to the SFC^-/L-AAA group throughout all social stimuli, suggesting a reduced social fear response. This is further sustained by lower vigilance behavior observed in SFC^+/L-AAA compared to SFC^+/Veh during the first four social stimuli (s1 $p = 0.011$, s2 $p = 0.007$, s3 $p = 0.003$, s4 $p = 0.037$).

Overall, these findings suggest that L-AAA-induced astrocytic structural depletion in the LSc impairs the consolidation and retention of social fear memory in male mice, leading to faster extinction of social fear and reduced fear responses compared to the vehicle-treated group. This suggests an important role for LSc astrocytes in the regulation of social fear learning and memory in male mice.

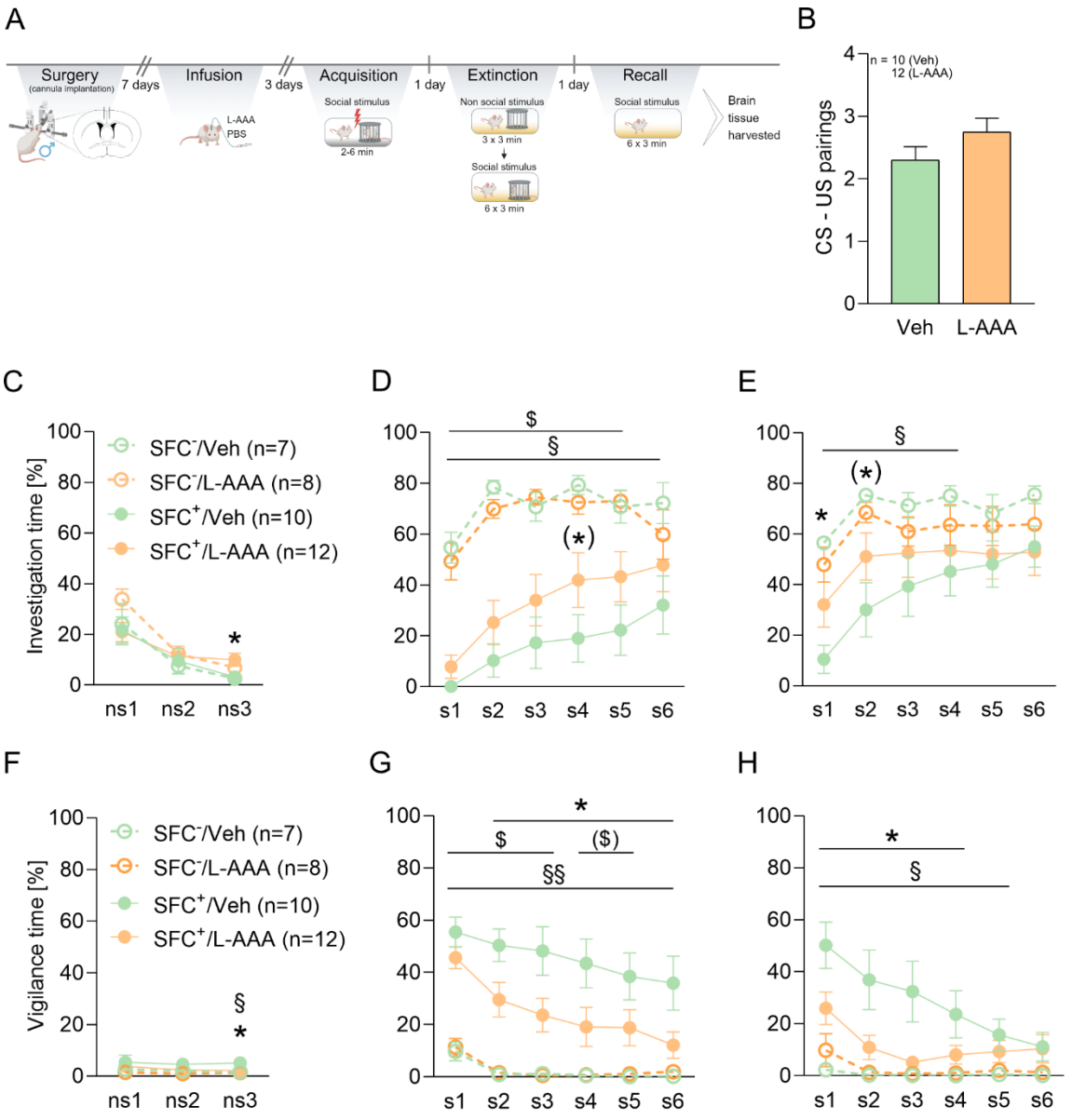

Figure 30. Effects of L-AAA-induced astrocytic structural depletion during social fear extinction and recall in male mice. *A) Illustration of the experimental timeline. B) Number of CS-US pairings presented to conditioned mice (SFC⁺) during acquisition of social fear. C-D) Percentage of investigation time during social fear extinction of non-social stimulus (C) and social stimuli (D). E) Percentage of investigation time of social stimuli during social fear extinction recall. F-G) Percentage of vigilance time during social fear extinction of non-social stimulus (F) and social stimuli (G). H) Percentage of vigilance time of social stimuli during social fear extinction recall. Data represents ± SEM. * p ≤ 0.05 SFC⁺/L-AAA vs SFC⁺/Veh, (*) p < 0.07 SFC⁺/L-AAA vs SFC⁺/Veh, ($) p < 0.07 SFC⁺/L-AAA vs SFC⁻/L-AAA, $ p ≤ 0.05 SFC⁺/L-AAA vs SFC⁻/L-AAA, § p ≤ 0.05 SFC⁺/Veh vs SFC⁻/Veh, §§§ p < 0.01 SFC⁺/Veh vs SFC⁻/Veh. For detailed statistics analysis see Table 23-24.*

Table 23: Statistical analysis of the effects of L-AAA-induced astrocyte dysfunction within the caudal part of the lateral septum (LSc) on investigation time during social fear extinction and recall in male mice (Figure 30). Factor Time represents stimulus presentation during SFC; factor Conditioning represents SFC^- vs SFC^+ effects; factor Treatment represents the effects of L-AAA vs Veh administration.

Acquisition	Independent T-Test	Figure B
CS-US pairings	$t_{20} = -1.461$	$p = 0.160$
Extinction ns1-3	Mixed Model ANOVA	Figure C
	(Time) $F_{2,32} = 60.048$	$p < 0.001$
	(Conditioning) $F_{1,32} = 0.398$	$p = 0.533$
	(Treatment) $F_{1,32} = 1.517$	$p = 0.227$
Investigation time	(Time x Conditioning) $F_{2,32} = 3.225$	$p = 0.046$
	(Time x Treatment) $F_{2,32} = 0.101$	$p = 0.904$
	(Conditioning x Treatment) $F_{1,32} = 0.427$	$p = 0.518$
	(Time x Conditioning x Treatment) $F_{2,32} = 1.177$	$p = 0.315$
Extinction s1-6	Mixed Model ANOVA	Figure D
	(Time) $F_{2.47,81.5} = 13.792$	$p < 0.001$
	(Conditioning) $F_{1,33} = 36.999$	$p < 0.001$
	(Treatment) $F_{1,33} = 0.698$	$p = 0.410$
Investigation time	(Time x Conditioning) $F_{2.47,81.5} = 3.857$	$p = 0.018$
	(Time x Treatment) $F_{2.47,81.5} = 0.751$	$p = 0.501$
	(Conditioning x Treatment) $F_{1,33} = 2.157$	$p = 0.151$
	(Time x Conditioning x Treatment) $F_{2.47,81.5} = 0.486$	$p = 0.491$
Recall s1-6	Mixed Model ANOVA	Figure E
	(Time) $F_{3.79,125} = 15.183$	$p < 0.001$
	(Conditioning) $F_{1,33} = 7.940$	$p = 0.008$
	(Treatment) $F_{1,33} = 0.017$	$p = 0.898$
Investigation time	(Time x Conditioning) $F_{3.79,125} = 2.367$	$p = 0.059$
	(Time x Treatment) $F_{3.79,125} = 1.309$	$p = 0.271$
	(Conditioning x Treatment) $F_{1} = 1.596$	$p = 0.215$
	(Time x Conditioning x Treatment) $F_{3.79,125} = 0.959$	$p = 0.430$

Table 24: Statistical analysis of the effects of L-AAA-induced astrocyte dysfunction within the caudal part of the lateral septum (LSc) on vigilance time during social fear extinction and recall in male mice (Figure 30). Factor Time represents stimulus presentation during SFC; factor Conditioning represents SFC^- vs SFC^+ effects; factor Treatment represents the effects of L-AAA vs Veh administration.

Extinction ns 1-3	Mixed Model ANOVA	Figure F
	(Time) $F_{1.35,44.3} = 0.673$	$p = 0.459$
	(Conditioning) $F_{1,33} = 3.157$	$p = 0.085$
	(Treatment) $F_{1,33} = 1.448$	$p = 0.237$
Vigilance time	(Time x Conditioning) $F_{1.35,44.3} = 0.071$	$p = 0.860$
	(Time x Treatment) $F_{1.35,44.3} = 0.001$	$p = 0.992$
	(Conditioning x Treatment) $F_{1,33} = 0.402$	$p = 0.530$
	(Time x Conditioning x Treatment) $F_{1.35,44.3} = 0.223$	$p = 0.711$
Extinction s 1-6	Mixed Model ANOVA	Figure G
	(Time) $F_{2.73,90.0} = 10.680$	$p < 0.001$
	(Conditioning) $F_{1,33} = 38.392$	$p < 0.001$
	(Treatment) $F_{1,33} = 3.491$	$p = 0.071$
Vigilance time	(Time x Conditioning) $F_{2.73,80.0} = 2.833$	$p = 0.048$
	(Time x Treatment) $F_{2.73,80.0} = 0.640$	$p = 0.577$
	(Conditioning x Treatment) $F_{1,33} = 4.058$	$p = 0.052$
	(Time x Conditioning x Treatment) $F_{2.73,80.0} = 0.457$	$p = 0.695$
Recall ns 1-6	Mixed Model ANOVA	Figure H
	(Time) $F_{2.85,94.0} = 12.075$	$p < 0.001$
	(Conditioning) $F_{1,33} = 12.638$	$p = 0.001$
	(Treatment) $F_{1,33} = 1.982$	$p = 0.169$
Vigilance time	(Time x Conditioning) $F_{2.85,94.0} = 5.715$	$p = 0.001$
	(Time x Treatment) $F_{2.85,94.0} = 2.429$	$p = 0.073$
	(Conditioning x Treatment) $F_{1,33} = 3.329$	$p = 0.077$
	(Time x Conditioning x Treatment) $F_{2.85,94.0} = 3.052$	$p = 0.035$

3.3. Effects of L-AAA-induced astrocytic dysfunction within the LSc in female mice

In female mice, L-AAA treatment impaired the acquisition of social fear, as evidenced by the increased number of foot shocks required to induce social avoidance during social fear acquisition (* p = 0.003, Figure 31B). On the following day, prior extinction training, both L-AAA and Veh-treated groups displayed similar investigation time toward non-social stimulus during all three presentations (ns1, ns2, ns3), indicating that L-AAA did not affect responses to non-social stimuli (Figure 31C). When exposed to social stimuli (Figure 31D), both all SFC^+ animals exhibited social fear responses, as evidenced by reduced social investigation at the beginning of social exposure (Figure 30D). SFC^+/Veh had significantly lower investigation time than SFC^-/Veh during the first two social stimuli (s1 p = 0.002, s2 p = 0.015), with a trend toward reduced social investigation in the third stimulus (s3 p = 0.066), before reaching similar levels to the unconditioned group (SFC^-/Veh). This indicates that repeated exposure of social stimuli led, as expected, to a reduction in social fear. Similarly, SFC^+/L-AAA showed reduced social investigation during the first three social exposures (s1 p < 0.001, s2 p = 0.002, s3 p = 0.006), until reaching comparable investigation time to the SFC^-/L-AAA group in later exposures. This suggests that, despite the delayed acquisition, SFC^+/L-AAA mice were able to learn and extinguish social fear in a manner similar to the SFC^+/Veh group, as shown by the lack of differences in investigation time between the SFC^+/Veh and SFC^+/L-AAA groups.

During social fear recall (Figure 31E), SFC^+/Veh animals showed similar investigation time to the SFC^- animals, indicating successful extinction of social fear. SFC^+/L-AAA animals showed a trend toward lower investigation time compared to SFC^-/L-AAA animals during the first social exposure (s1 p = 0.058), although from the second until the last exposure, no differences were observed between the two groups. This indicates that, similar to the Veh-treated group, L-AAA-treated animals were able to successfully extinguish the social fear. This consideration is sustained by an extinction curve that remains similar between SFC^+/Veh and SFC^+/L-AAA, with no differences.

Regarding vigilance behavior, no differences were detected across Veh- and L-AAA-treated groups during non-social exposure (Figure 31F). During social extinction training (Figure 31G), SFC^+/L-AAA and SFC^+/Veh groups showed no differences in vigilance behavior. SFC^+/Veh exhibited higher vigilance time than SFC^-/Veh during the first two social exposures (s1 p = 0.002, s2 p = 018), with a trend toward higher vigilance behavior in the third stimulus (s3 p = 0.061). Similarly, SFC^+/L-AAA showed higher vigilance time compared to the SFC^-/L-AAA in the first three social stimuli (s1 p < 0.001, s2 p = 0.003, s3 p = 013), indicating social fear response. During social fear recall (Figure 31H), SFC^+/Veh showed no differences in social fear responses compared to the unconditioned controls, suggesting successful extinction. In contrast, SFC^+/L-AAA animals displayed some

residual vigilance during the first social exposure (s1 p = 0.021), reaching levels comparable to the unconditioned L-AAA group from the second stimulus on.

Overall, these findings suggest that, in contrast to males, L-AAA-induced astrocytic dysfunction in female mice leads to a delayed acquisition of social fear, but does not alter the process of social fear extinction, as seen in males.

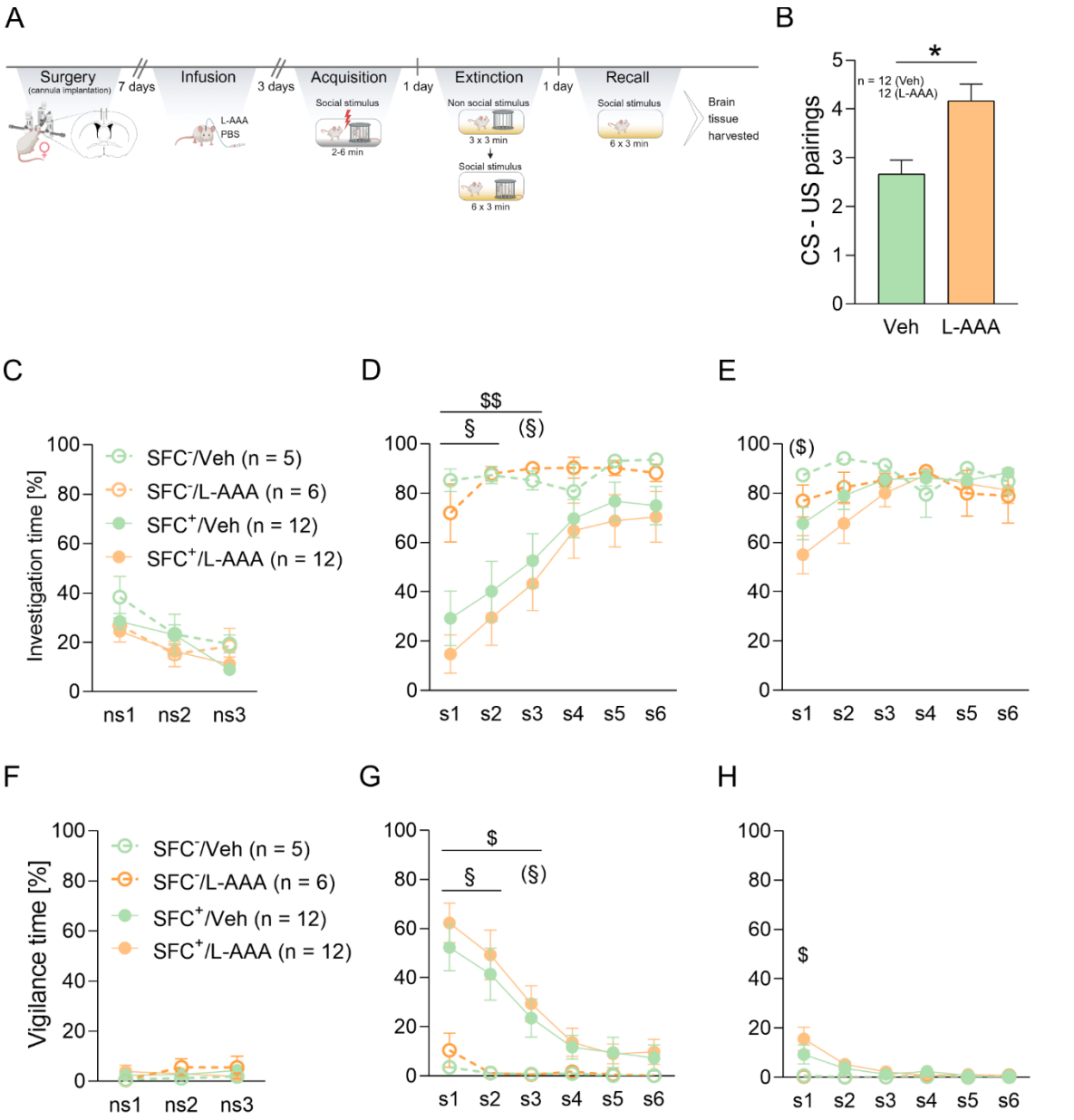

Figure 31. Effects of L-AAA-induced structural depletion during social fear extinction and recall in female mice. *A) Illustration of the experimental timeline. B) Number of CS-US pairings presented to conditioned mice (SFC⁺) during acquisition of social fear. C-D) Percentage of investigation time during social fear extinction of non-social stimulus (C) and social stimuli (D). E) Percentage of investigation time of social stimuli during social fear extinction recall. F-G) Percentage of vigilance time during social fear extinction of non-social stimulus (F) and social stimuli (G). H) Percentage of vigilance time of social stimuli during social fear extinction recall. Data represents ± SEM. ($) p < 0.07 SFC⁺/L-AAA vs SFC⁻/L-AAA, $ p ≤ 0.05 SFC⁺/L-AAA vs SFC⁻/L-AAA, $$ p < 0.01 SFC⁺/L-AAA vs SFC⁻/L-AAA, (§) p < 0.07 SFC⁺/Veh vs SFC⁻/Veh § p ≤ 0.05 SFC⁺/Veh vs SFC⁻/Veh, §§§ p < 0.01 SFC⁺/Veh vs SFC⁻/Veh. For detailed statistics analysis see Table 25-26.*

Table 25: Statistical analysis of the effects of L-AAA-induced astrocyte dysfunction within the caudal part of the lateral septum (LSc) on investigation time during social fear extinction and recall in female mice (Figure 31). Factor Time represents stimulus presentation during SFC; factor Conditioning represents SFC^- vs SFC^+ effects; factor Treatment represents the effects of L-AAA vs Veh administration.

Acquisition	Independent T-Test	Figure B
CS-US pairings	$t_{22} = -3.358$	$p = 0.003$
Extinction ns 1-3	Mixed Model ANOVA	Figure C
Investigation time	(Time) $F_{2,62} = 26.152$	$p < 0.001$
	(Conditioning) $F_{1,31} = 1.575$	$p = 0.219$
	(Treatment) $F_{1,31} = 1.547$	$p = 0.223$
	(Time x Conditioning) $F_{2,62} = 2.537$	$p = 0.087$
	(Time x Treatment) $F_{2,62} = 2.460$	$p = 0.094$
	(Conditioning x Treatment) $F_{1,31} = 0.262$	$p = 0.613$
	(Time x Conditioning x Treatment) $F_{2,62} = 0.270$	$p = 0.764$
Extinction s 1-6	Mixed Model ANOVA	Figure D
Investigation time	(Time) $F_{2.13,66.0} = 12.473$	$p < 0.001$
	(Conditioning) $F_{1,31} = 14.643$	$p < 0.001$
	(Treatment) $F_{1,31} = 0.296$	$p = 0.590$
	(Time x Conditioning) $F_{2.13,66.0} = 6.329$	$p = 0.003$
	(Time x Treatment) $F_{2.13,66.0} = 0.550$	$p = 0.590$
	(Conditioning x Treatment) $F_{1,31} = 0.182$	$p = 0.672$
	(Time x Conditioning x Treatment) $F_{2.13,66.0} = 0.218$	$p = 0.818$
Recall ns 1-6	Mixed Model ANOVA	Figure E
Investigation time	(Time) $F_{3.11,96.3} = 5.577$	$p = 0.001$
	(Conditioning) $F_{1,31} = 1.739$	$p = 0.197$
	(Treatment) $F_{1,31} = 1.713$	$p = 0.200$
	(Time x Conditioning) $F_{3.11,96.3} = 4.738$	$p = 0.004$
	(Time x Treatment) $F_{3.11,96.3} = 1.882$	$p = 0.136$
	(Conditioning x Treatment) $F_{1,31} = 0.001$	$p = 0.976$
	(Time x Conditioning x Treatment) $F_{3.11,96.3} = 0.371$	$p = 0.781$

Table 26: Statistical analysis of the effects of L-AAA-induced astrocyte dysfunction within the caudal part of the lateral septum (LSc) on vigilance time during social fear extinction and recall in female mice (Figure 31). Factor Time represents stimulus presentation during SFC; factor Conditioning represents SFC^- vs SFC^+ effects; factor Treatment represents the effects of L-AAA vs Veh administration.

Extinction ns 1-3	Mixed Model ANOVA	Figure F
Vigilance time	(Time) $F_{1.27,39.5} = 1.017$	$p = 0.339$
	(Conditioning) $F_{1,31} = 0.068$	$p = 0.795$
	(Treatment) $F_{1,31} = 0.549$	$p = 0.464$
	(Time x Conditioning) $F_{1.27,39.5} = 1.261$	$p = 0.280$
	(Time x Treatment) $F_{1.27,39.5} = 0.380$	$p = 0.592$
	(Conditioning x Treatment) $F_{1,31} = 0.733$	$p = 0.399$
	(Time x Conditioning x Treatment) $F_{1.27,39.5} = 1.477$	$p = 0.237$
Extinction s 1-6	**Mixed Model ANOVA**	**Figure G**
Vigilance time	(Time) $F_{1.80,55.5} = 16.165$	$p < 0.001$
	(Conditioning) $F_{1,31} = 17.049$	$p < 0.001$
	(Treatment) $F_{1,31} = 0.240$	$p = 0.628$
	(Time x Conditioning) $F_{1.80,55.5} = 10.842$	$p < 0.001$
	(Time x Treatment) $F_{1.80,55.5} = 0.289$	$p = 0.726$
	(Conditioning x Treatment) $F_{1,31} = 0.075$	$p = 0.786$
	(Time x Conditioning x Treatment) $F_{1.80,55,5} = 0.082$	$p = 0.903$
Recall ns 1-6	**Mixed Model ANOVA**	**Figure H**
Vigilance time	(Time) $F_{1.62,50.3} = 5.946$	$p = 0.008$
	(Conditioning) $F_{1,31} = 4.945$	$p = 0.034$
	(Treatment) $F_{1,31} = 0.247$	$p = 0.623$
	(Time x Conditioning) $F_{1.62,50.3} = 5.510$	$p = 0.011$
	(Time x Treatment) $F_{1.62,50.3} = 0.400$	$p = 0.630$
	(Conditioning x Treatment) $F_{1,31} = 0.192$	$p = 0.664$
	(Time x Conditioning x Treatment) $F_{1.62,50.3} = 0.600$	$p = 0.519$

4. Effects of social fear acquisition on astrocytic Ca^{2+} activity in the LS in male and female mice

Due to the activity-dependent of astrocyte morphology already found in previous studies (Theodosis et al. 2008; Arizono et al. 2021; Denizot et al. 2022) and the morphological changes revealed following SFC (see section 2 in Results), I investigated to which extent social fear acquisition impacts astrocytic Ca^{2+} activity within the LS. The experiments were performed in collaboration with Dr. Alexander Charlet at the University of Strasbourg (France). Understanding the effects of social fear processes on calcium signaling in astrocytes can provide insights into the role of astrocytes in the regulation of fear processing and intercellular communication.

4.1. Baseline astrocytic Ca^{2+} activity within the LS *ex vivo* in male and female mice after social fear acquisition

To explore astrocytic Ca^{2+} activity following social fear acquisition in the LSc, brains were harvested 10 min after social acquisition for *ex vivo* calcium imaging in both male and female mice (see section 8. in Material and Methods for details). The number of Ca^{2+} transients (frequency) and the AUC of Ca^{2+} peaks were quantified during the first 5 min of recording as indicators of baseline Ca^{2+} activity.

In male mice, calcium imaging revealed that both the frequency ($p = 0.043$; Figure 31B) and the AUC ($p = 0.017$; Figure 31B) of Ca^{2+} transients in the LSc were higher in SFC^+ compared to SFC^- mice under baseline conditions, i.e. without further manipulation. However, when analyzing the recordings separately for the dorsal and ventral regions of the LSc, distinct patterns emerged. In the dorsal LSc, only the frequency of Ca^{2+} transients ($p = 0.034$; Figure 31C) was elevated in SFC^+, while in the ventral LSc both the frequency ($p = 0.001$; Figure 31D) and AUC ($p < 0.0001$; Figure 31D) of Ca^{2+} transients were higher in SFC^+ compared to SFC- mice. In line with morphological analysis, these findings suggest that astrocyte in the LSc, particularly in the ventral part, exhibit heightened responsiveness in male mice following social fear acquisition.

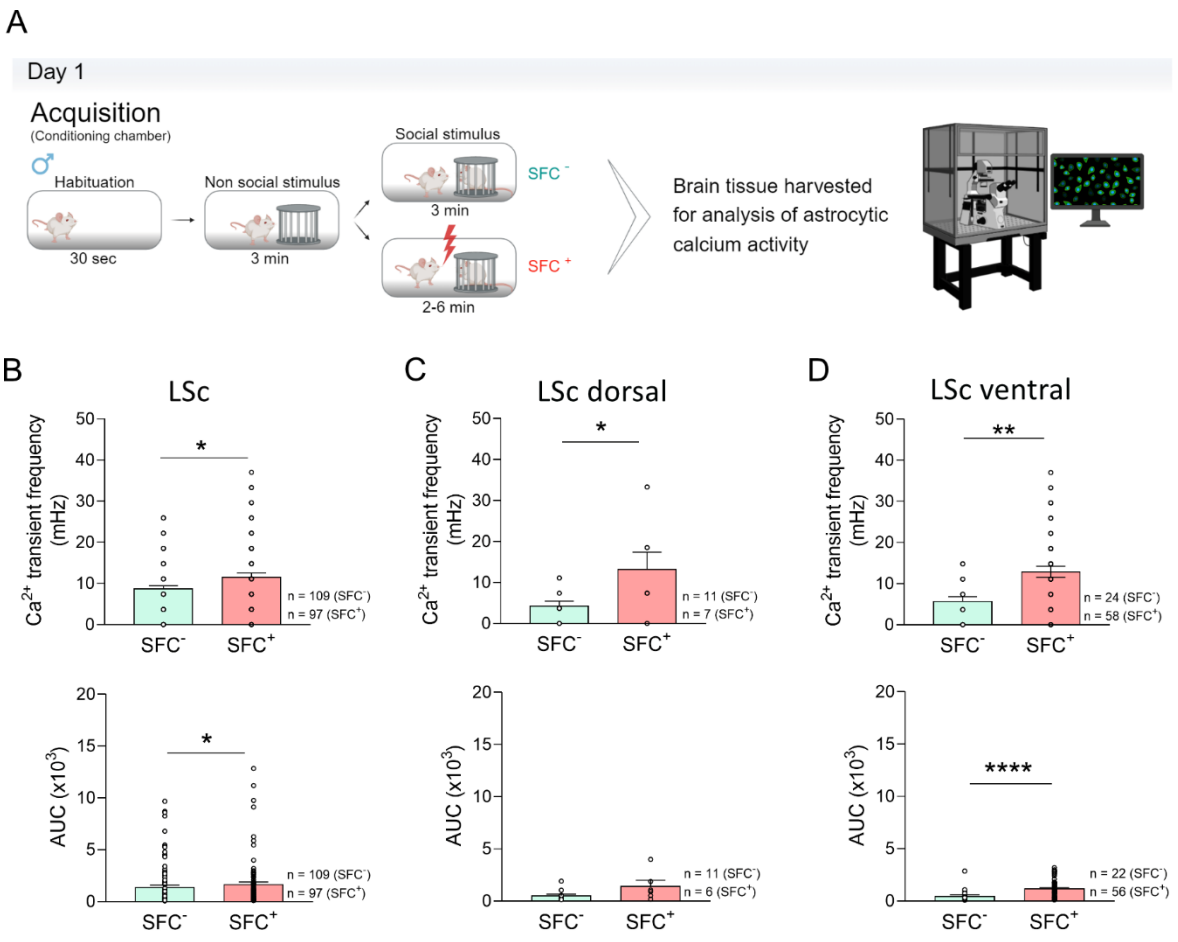

Figure 32. Social fear acquisition increased astrocytic calcium acitivty in the caudal part of the lateral septum (LSc) of male mice. *A) Illustration of the experimental design. Brains were harvested 10 min after social fear acquisiiton for ex vivo calcium imaging in male mice. Ca^{2+} transients frequency (up) and AUC (down) in the LSc (B), the dorsal LSc (C) and the ventral LSc (D) of SFC^- and SFC^+ animals. n = number of cells recorded. In each experiment 3-4 mice were used. Data represents means ± SEM. * p < 0.05, ** p < 0.01. For detailed statistics analysis see Table 27.*

Table 27: Statistics of the baseline astrocytic calcium activity in the caudal lateral septum (LSc) after social fear acquisition in male mice (Figure 32). Factor represents SFC- vs SFC+ effects.

LSc	Mann-Whitney U Test	Figure B
Calcium transient frequency	$U = 4435$	p = 0.043
AUC	$U = 4187$	p = 0.017
LSc dorsal	Mann-Whitney U Test	Figure C
Calcium transient frequency	$U = 18$	p = 0.034
AUC	$U = 15$	p = 0.078
LSc ventral	Mann-Whitney U Test	Figure D
Calcium transient frequency	$U = 399.5$	p = 0.001
AUC	$U = 273$	p < 0.0001

In female mice, similar to the results observed in males, a higher baseline frequency ($p = 0.006$; Figure 33B) and AUC ($p < 0.001$; Figure 33B) of Ca^{2+} transients were observed in SFC^{+} compared to SFC^{-} mice across the LSc (Figure 33B). However, in contrast to males, no differences in the frequency or AUC of Ca^{2+} transients were found, when the recordings were separated into the dorsal and ventral regions of the LSc, (Figure 33C-D). These findings align with the morphological analysis, where, in contrast to male mice, no differences in astrocytic morphology were observed between conditioned and unconditioned mice in females, indicating potential sex-specific astrocytic responses to social fear acquisition.

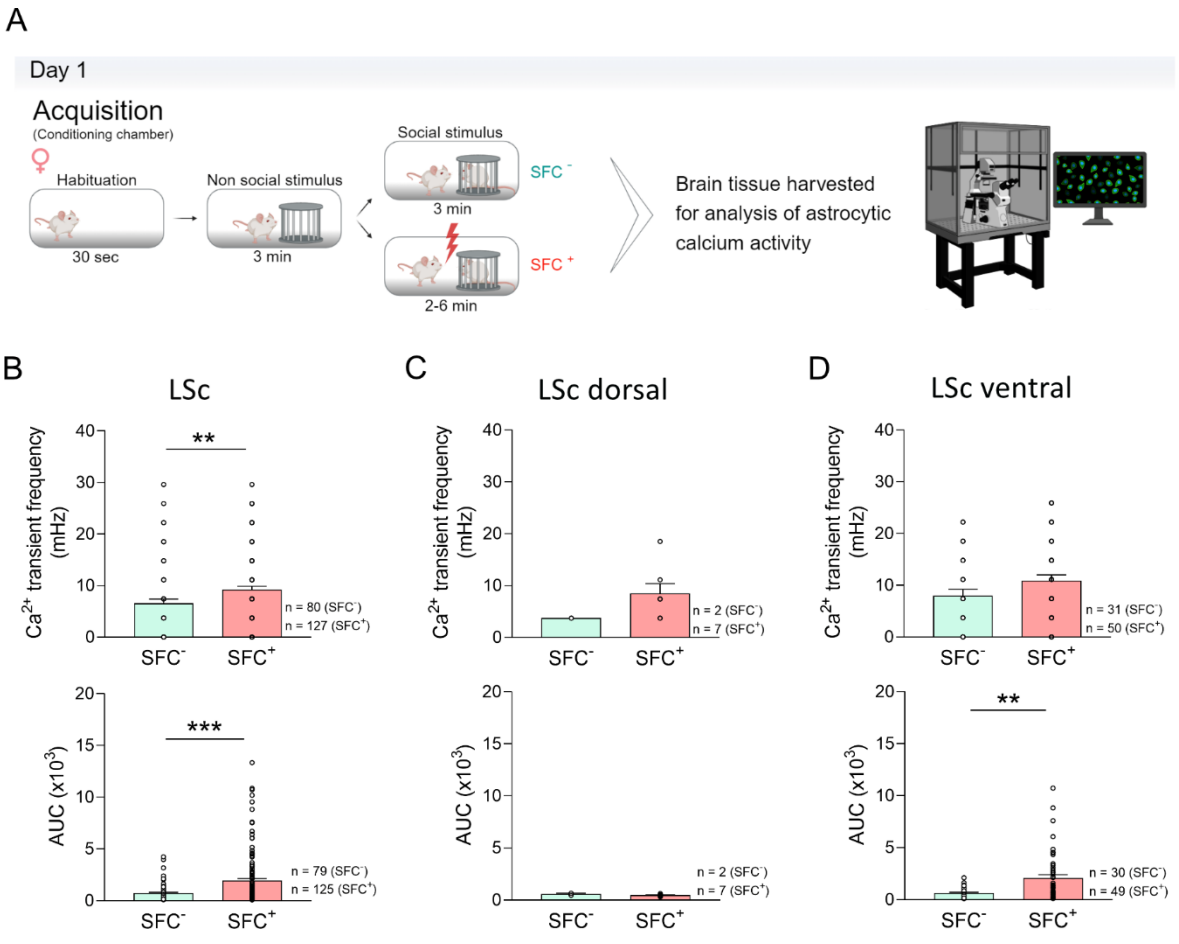

Figure 33. Social fear acquisition increased astrocytic calcium acitivty in the caudal part of the lateral septum (LSc) of female mice. *A) Illustration of the experimental design. Brains were harvested 10 min after social fear acquisiiton for ex vivo calcium imaging in female mice. Ca^{2+} transients frequency (up) and AUC (down) in the LSc (B), the dorsal LSc (C) and the ventral LSc (D) of SFC^{-} and SFC^{+} animals. n = number of cells recorded. In each experiment 3-4 mice were used. Data represents means ± SEM. ** $p < 0.01$, *** $p < 0.001$. For detailed statistics analysis see Table 28.*

Table 28: Statistics of the baseline astrocytic calcium activity in the caudal lateral septum (LSc) after social fear acquisition in female mice (Figure 33). Factor represents SFC- vs SFC+ effects.

LSc	Mann-Whitney U Test	Figure B
Calcium transient frequency	$U = 3960$	$p = 0.006$
AUC	$U = 3574$	$p < 0.001$
LSc dorsal	Mann-Whitney U Test	Figure C
Calcium transient frequency	$U = 2$	$p = 0.278$
AUC	$U = 3$	$p = 0.333$
LSc ventral	Mann-Whitney U Test	Figure D
Calcium transient frequency	$U = 625.5$	$p = 0.142$
AUC	$U = 432$	$p = 0.001$

4.2. Sex difference of the baseline calcium astrocytic activity in the LSc

Based on the observed differences in astrocytic Ca^{2+} activity in the LSc of male and female mice, I further investigated potential sex differences in astrocytic Ca^{2+} dynamics of SFC^{+} and SFC^{-} animals (Figure 34). When comparing male and female SFC^{-} mice, males exhibited a higher baseline Ca^{2+} transient frequency (Figure 34A, $p = 0.020$) and AUC ($p = 0.023$; Figure 34B) compared to females. However, in SFC^{+} mice, no sex-differences were detected in either the baseline Ca^{2+} transient frequency or AUC (Figure 34C-D). This suggest that under baseline conditions, male mice display increased astrocytic Ca^{2+} activity compared to females, but this sex-differences are dissolved following social fear conditioning suggesting a potential ceiling effect in females.

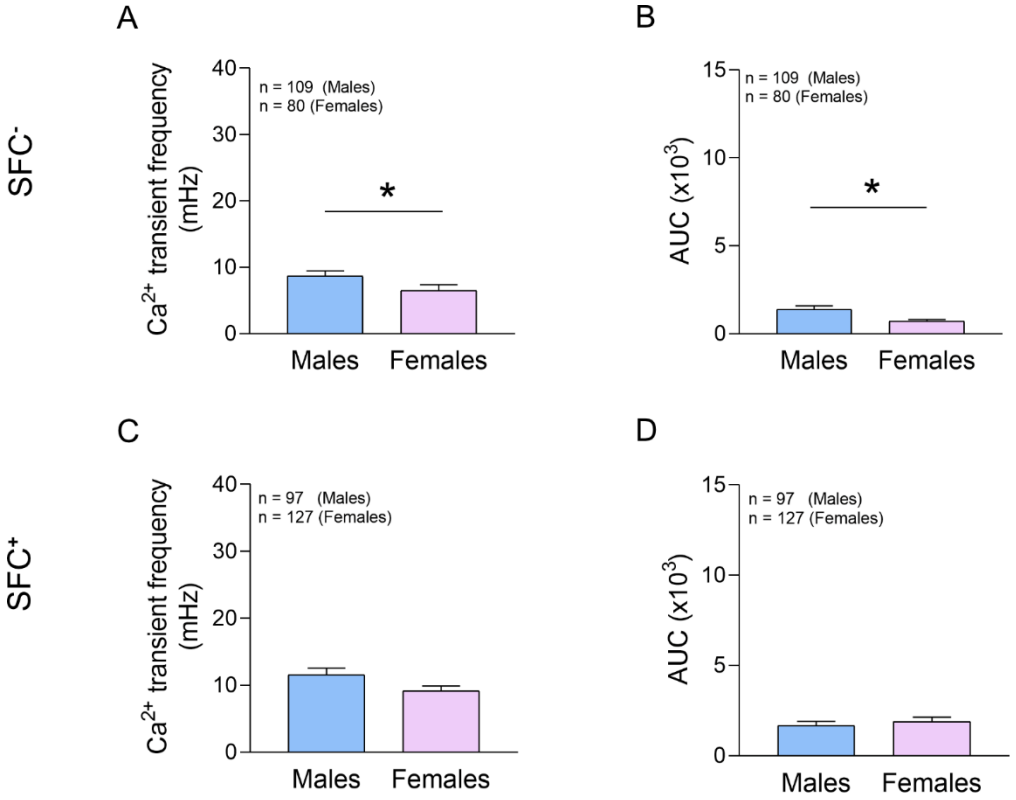

Figure 34. Baseline astrocytic Ca^{2+}activity is higher in unconditioned male mice compared to SFC- female mice. *A-B) Sex differences of Ca^{2+} transient frequency (A) and amplitude (AUC) (B) in unconditioned mice. C-D) Sex differences of Ca^{2+} transient frequency (A) and amplitude (AUC) (B) in conditioned mice. n = number of cells. Data represents means ± SEM. * $p \leq 0.05$. For detailed statistics analysis see Table 29.*

Table 29: Statistics of the baseline astrocytic calcium activity in the caudal lateral septum (LSc) after social fear acquisition between male and female mice (Figure 34). Factor represents Males vs Females effects.

SFC$^-$	Mann-Whitney U Test	Figure A-B
Calcium transient frequency	$U = 3516$	p = 0.020
AUC	$U = 3439$	p = 0.023
SFC$^+$	Mann-Whitney U Test	Figure C-D
Calcium transient frequency	$U = 5377$	p = 0.099
AUC	$U = 5606$	p = 0.352

4.3. Astrocytic Ca^{2+} activity in response to TGOT in male and female mice after social fear acquisition

Due to the morphological changes revealed following SFC in male mice (see section 2 in Results) and the expression of OXTR in astrocytes in the LSc in both sexes (see section 1 in Results), I explored the impact of social fear acquisition on astrocytic calcium activity in response to TGOT application in both male and female mice (see section 8.5 in Material and Methods for details).

In male mice, TGOT application raised Ca^{2+} transient frequency and AUC in both SFC^- (** $p < 0.01$, Figure 35C; ** $p < 0.01$, Figure 35D) and SFC^+ (#### $p < 0.0001$, Figure 35C; #### $p < 0.0001$, Figure 35D) conditions. However, the astrocytic Ca^{2+} response to TGOT did not differ between SFC^- and SFC^+ animals. Additionally, when comparing the percentage of TGOT responding cells, no differences were observed between SFC^- and SFC^+ groups.

Interestingly, when considering the overall astrocytic population in the LSc, which includes both TGOT-responsive and non-responding cells (Figure 35F-G), there was a notable decrease in Ca^{2+} transient frequency and AUC following TGOT application in the LSc of SFC^- mice (*** $p = 0.0001$, Figure 35F; *** $p = 0.018$, Figure 35G). In contrast, in SFC^+ animals, only the Ca^{2+} transient frequency was reduced after TGOT (## $p = 0.005$, Figure 35F), with no change in the AUC. Moreover, comparing TGOT responses between SFC^- and SFC^+ revealed in both a higher Ca^{2+} transient frequency ($$ $p = 0.009$, Figure 35F) and AUC ($$ $p = 0.005$, Figure 35G) in SFC^+ compared to SFC^- animals. These findings suggest that the activity patterns of astrocytes in the LSc of male mice are affected by social fear acquisition and that the heightened response in conditioned animals following TGOT application might reflect an adaptation in astrocytic function related to social fear processes.

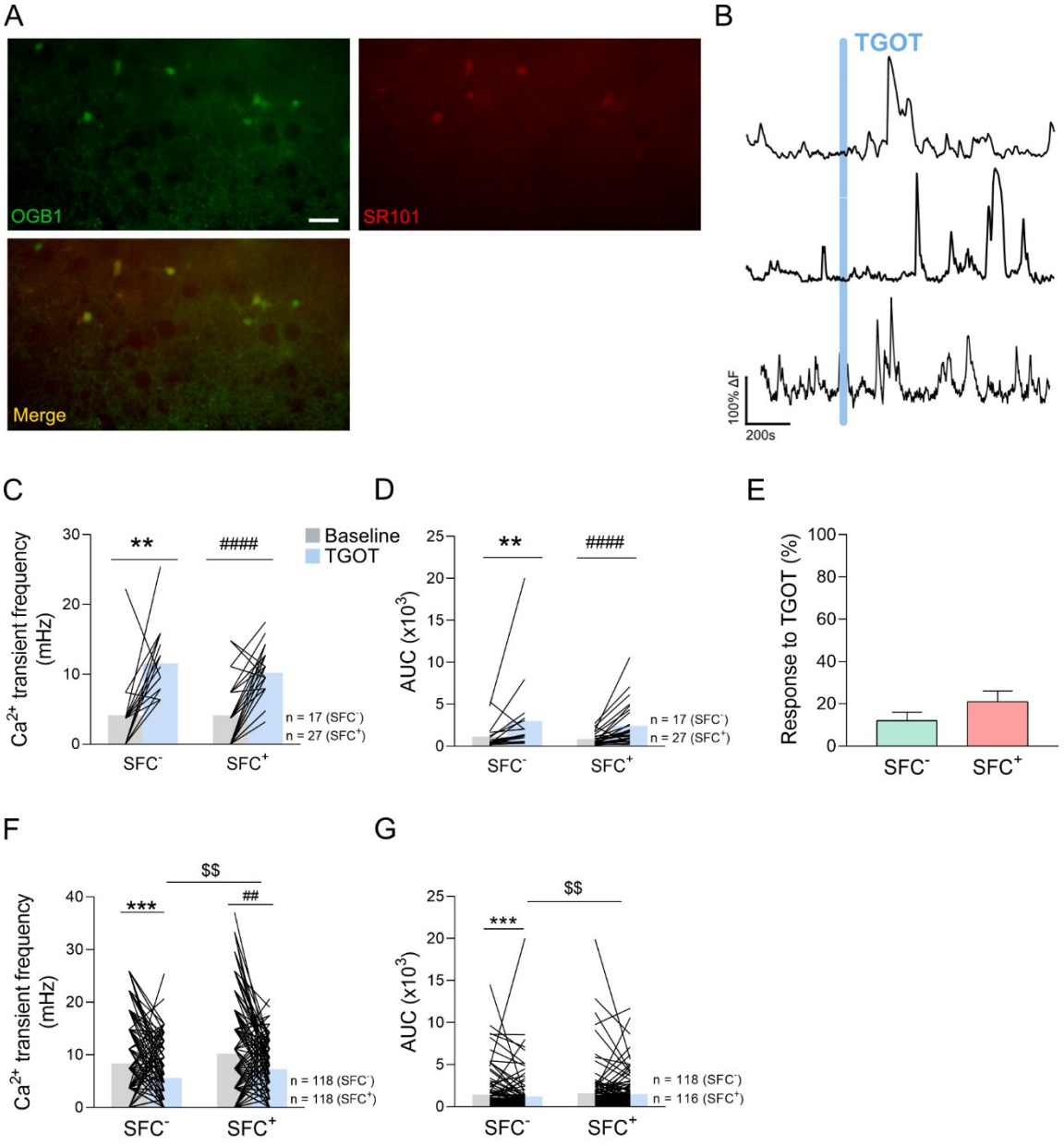

Figure 35. Social fear acquisition increased astrocytic calcium activityin female mice following TGOT application. *B) Illustration of ΔF traces following application of TGOT (0.4 μM) in conditioned mice. Responding astrocytes Ca^{2+} transients frequency (C), AUC (D) and proportion of responding astrocytes (E). F) Ca^{2+} transients frequency and G) AUC in all astrocytic population (responding and non-responding cells). n = number of cells. Data represents means ± SEM. ** p < 0.01 Baseline vs TGOT (SFC-), *** p < 0.001 Baseline vs TGOT (SFC-), ## p < 0.01 Baseline vs TGOT (SFC+), #### p < 0.0001 Baseline vs TGOT (SFC+), $$ p < 0.01 SFC- vs SFC- (TGOT). For detailed statistics analysis see Table 30.*

Table 30: Statistics of the astrocytic calcium activity in the response to TGOT in the caudal lateral septum (LSc) after social fear acquisition in male mice (Figure 35). Factor represents Baseline vs TGOT or SFC- vs SFC+ of TGOT response.

TGOT responding cells

Baseline vs TGOT (SFC^-)	Wilcoxon Test	Figure B-C
Calcium transient frequency	W = 125	p = 0.001
AUC	W = 123	p = 0.002
Baseline vs TGOT (SFC^+)	Wilcoxon Test	Figure B-C
Calcium transient frequency	W = 346	p < 0.0001
AUC	W = 338	p < 0.0001
SFC^- vs SFC^+	Independent T-Test, Mann-Whitney U Test	Figure B-C-D
Calcium transient frequency	t_{41} = 0.457	p = 0.649
AUC	*U* = 197	p = 0.788
Response to TGOT	*U = 534*	p = 0.133

Global response (all cells, responding and non-responding TGOT cells)

Baseline vs TGOT (SFC-)	Wilcoxon Test	Figure F-G
Calcium transient frequency	W = 118	p = 0.0001
AUC	W = 118	p = 0.018
Baseline vs TGOT (SFC+)	Wilcoxon Test	Figure F-G
Calcium transient frequency	W = 118	p = 0.005
AUC	W = 116	p = 0.776
SFC- vs SFC+	Mann-Whitney U Test	Figure F-G
Calcium transient frequency	U = 5621	p = 0.009
AUC	U = 5415	p = 0.005

Similarly to male mice, in females TGOT application increased both the Ca^{2+} transient frequency and AUC of Ca^{2+} activity in the LSc in both SFC^- (*** p = 0.0002, Figure 36A; *** p = 0.0005, Figure 36B) and SFC^+ mice (#### p < 0.0001, Figure 36A; #### p < 0.0001, Figure 36B). Notably, SFC^+ showed higher Ca^{2+} transient frequency ($$ p = 0.003, Figure 36A) and AUC ($$ p = 0.005, Figure 36B) compared to SFC^- animals following TGOT application. Furthermore, there was a trend toward increased astrocytic responsiveness in SFC^+ ((*), p = 0.051, Figure 36C) compared to SFC-, suggesting that social fear acquisition enhances astrocytic responsiveness to TGOT.

Interestingly, when considering the global astrocytic population in the LSc, a decreased in Ca^{2+} transient frequency and AUC was observed following TGOT application in SFC^- (* p = 0.012, Figure 36D; * p = 0.049, Figure 36E) compared to baseline conditions. In contrast, SFC^+ showed no changes in either Ca^{2+} transient frequency or AUC, after TGOT application. However, comparing TGOT responses between SFC^- and SFC^+ groups, revealed an increased in both Ca^{2+} transient frequency ($$$$ p < 0.0001, Figure 36D) and AUC ($$$$ p < 0.0001¸ Figure 36E) in SFC^+ animals.

Overall, these results indicate the social fear acquisition enhances the astrocytic calcium activity in response to TGOT application independent of sex. Specifically, SFC+ mice demonstrated significantly higher Ca^{2+} transient frequency and AUC in both TGOT-responsive and all astrocytes compared to SFC- animals. This heightened activity in SFC+ suggest that astrocytes could modulate oxytocin-related signaling pathways involved in social fear regulation.

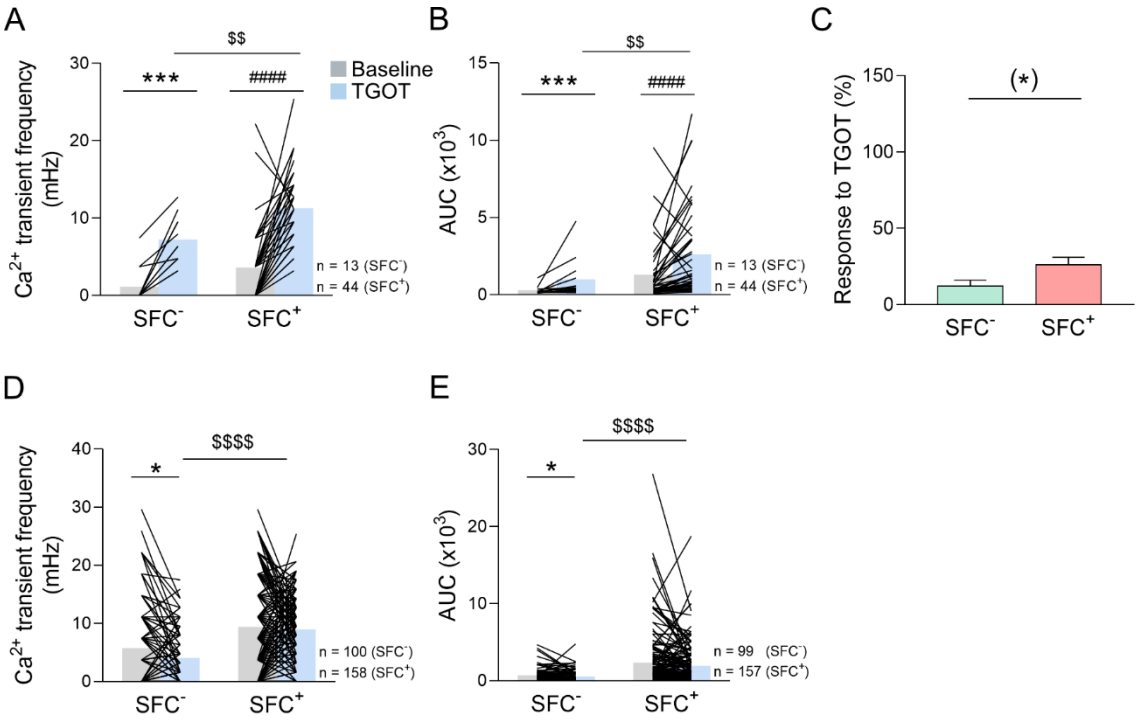

Figure 36. Social fear acquisition increased astrocytic calcium activity following TGOT application in female mice. *Responding astrocytes Ca^{2+} transients frequency (A), AUC (B) and proportion of responding astrocytes (C). D) Ca^{2+} transients frequency and E) AUC in all astrocytic population (responding and non-responding cells). n = number of cells. Data represents means ± SEM. * $p \leq 0.05$ Baseline vs TGOT (SFC-), *** $p < 0.001$ Baseline vs TGOT (SFC-), #### $p < 0.0001$ Baseline vs TGOT (SFC+), $$ $p < 0.01$ SFC- vs SFC- (TGOT), $$$$ $p < 0.0001$ SFC- vs SFC- (TGOT). For detailed statistics analysis see Table 31.*

Table 31: Statistics of the astrocytic calcium activity in the response to TGOT in the caudal lateral septum (LSc) after social fear acquisition in female mice (Figure 36). Factor represents Baseline vs TGOT or SFC- vs SFC+ of TGOT response.

TGOT responding cells

Baseline vs TGOT (SFC^-)	Wilcoxon Test	Figure B-C
Calcium transient frequency	W = 13	p = 0.0002
AUC	W = 13	p = 0.0005
Baseline vs TGOT (SFC^+)	Wilcoxon Test	Figure B-C
Calcium transient frequency	W = 44	p < 0.0001
AUC	W = 44	p < 0.0001
SFC^- vs SFC^+	Independent T-Test, Mann-Whitney U Test	Figure B-C-D
Calcium transient frequency	t_{54} = 3.065	p = 0.003
AUC	*U* = 125	p = 0.005
Response to TGOT	*U* = 563	p = 0.051

Global response (responding and non-responding TGOT cells)

Baseline vs TGOT (SFC^-)	Wilcoxon Test	Figure E-F
Calcium transient frequency	W = 100	p = 0.012
AUC	W = 99	p = 0.049
Baseline vs TGOT (SFC^+)	Wilcoxon Test	Figure E-F
Calcium transient frequency	W = 158	p = 0.902
AUC	W = 157	p = 0.392
SFC^- vs SFC^+	Mann-Whitney U Test	Figure B-C-D
Calcium transient frequency	*U* = 4067	p < 0.0001
AUC	*U* = 4067	p < 0.0001

When the effects of TGOT application on astrocytic Ca^{2+} activity was compared between male and female mice (Figure 37), significant sex differences in SFC^- were found. Female mice exhibited a reduced TGOT response compared to males, with lower Ca^{2+} transient frequency (** p = 0.007, Figure 37A) and AUC (* p = 0.019, Figure 37B). In contrast, no differences were observed in either Ca^{2+} transient frequency (Figure 37C) or AUC (Figure 37D) between sexes in SFC^+ animals, indicating that social fear conditioning led to a comparable astrocytic Ca^{2+} activity response in both sexes following TGOT application.

Overall, these results suggest a baseline sex-difference in astrocytic calcium response to TGOT, with males exhibiting higher activity in unconditioned states. Interestingly, this sex difference disappears after social fear conditioning, implying that the reduced response observed in female mice under baseline conditions may be due to a ceiling effect.

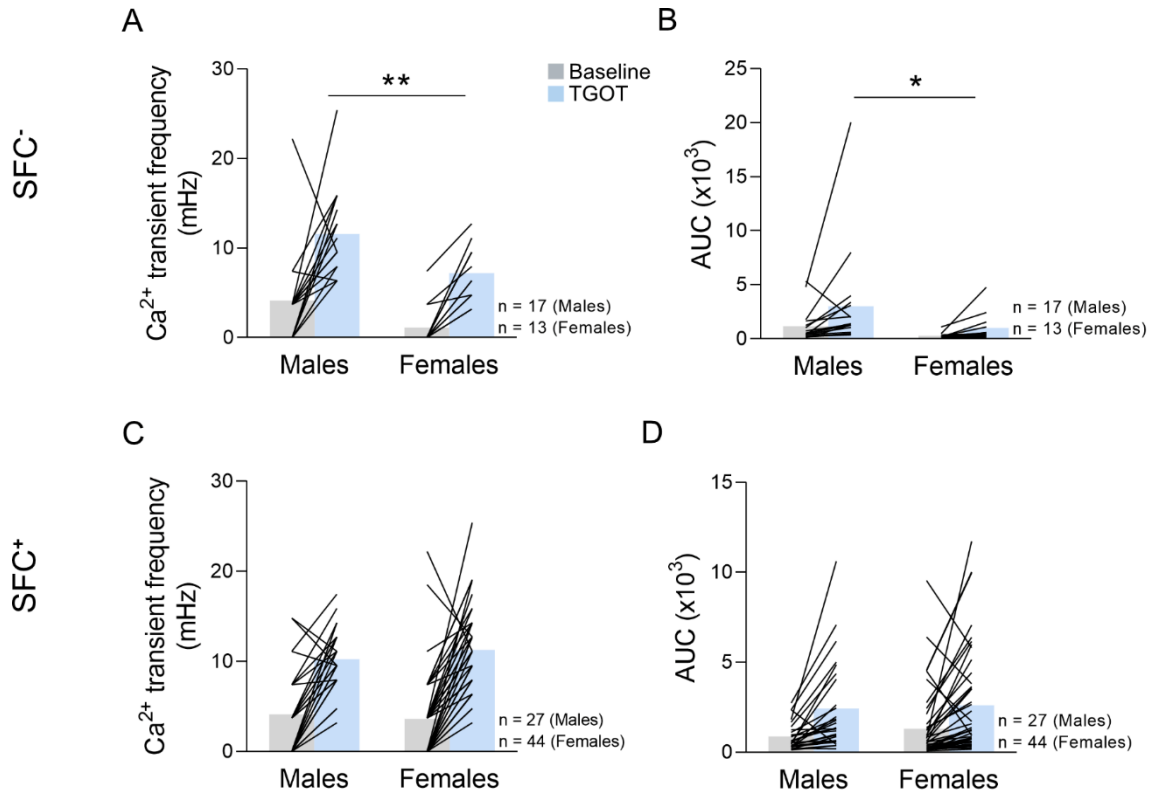

Figure 37. Effects of TGOT on astrocytic calcium activity in male and female mice following social fear conditioning. *A-B) Responding astrocytes Ca^{2+} transients frequency (A), AUC (B) between male and female mice in SFC- animals. C-D) Responding astrocytes Ca^{2+} transients frequency (C), AUC (D) between male and female mice in SFC+ animals. n = number of cells. Data represents means ± SEM. * $p \leq 0.05$ Baseline vs TGOT (SFC-), ** $p < 0.01$. For detailed statistics analysis see Table 31.*

Table 32: Statistics of the TGOT response astrocytic calcium activity in the caudal lateral septum (LSc) after social fear acquisition between male and female mice (Figure 37). Factor represents Males vs Females effects.

SFC^-	Mann-Whitney U Test	Figure C
Calcium transient frequency	$U = 48.5$	$p = 0.007$
AUC	$U = 55$	$p = 0.019$
SFC^+	Mann-Whitney U Test	Figure C
Calcium transient frequency	$U = 530$	$p = 0.449$
AUC	$U = 551$	$p = 0.616$

Consistent with the findings in TGOT-responding cells, an analysis of astrocytic Ca^{2+} activity in response to TGOT across all astrocytes (Figure 38) revealed a trend towards a decreased activity in female mice compared to males in SFC^-. This reduction was observed both in Ca^{2+} transient frequency ($p = 0.052$; Figure 38A) and AUC ($p = 0.059$; Figure 38B). Interestingly, in SFC^+ animals an increase of Ca^{2+} transient frequency was observed in females compared to males ($p = 0.036$; Figure 38C), although no difference in AUC (Figure 38D) was detected between male and female mice. This aligns with the previous results, suggesting that social fear conditioning enhances astrocytic

Ca^{2+} activity across all astrocytes in response to TGOT, with female showing even higher activity levels compared to males. This furthers reinforce a ceiling effect in female mice under baseline conditions, which is mitigated following social fear conditioning, leading to heightened astrocytic response in females.

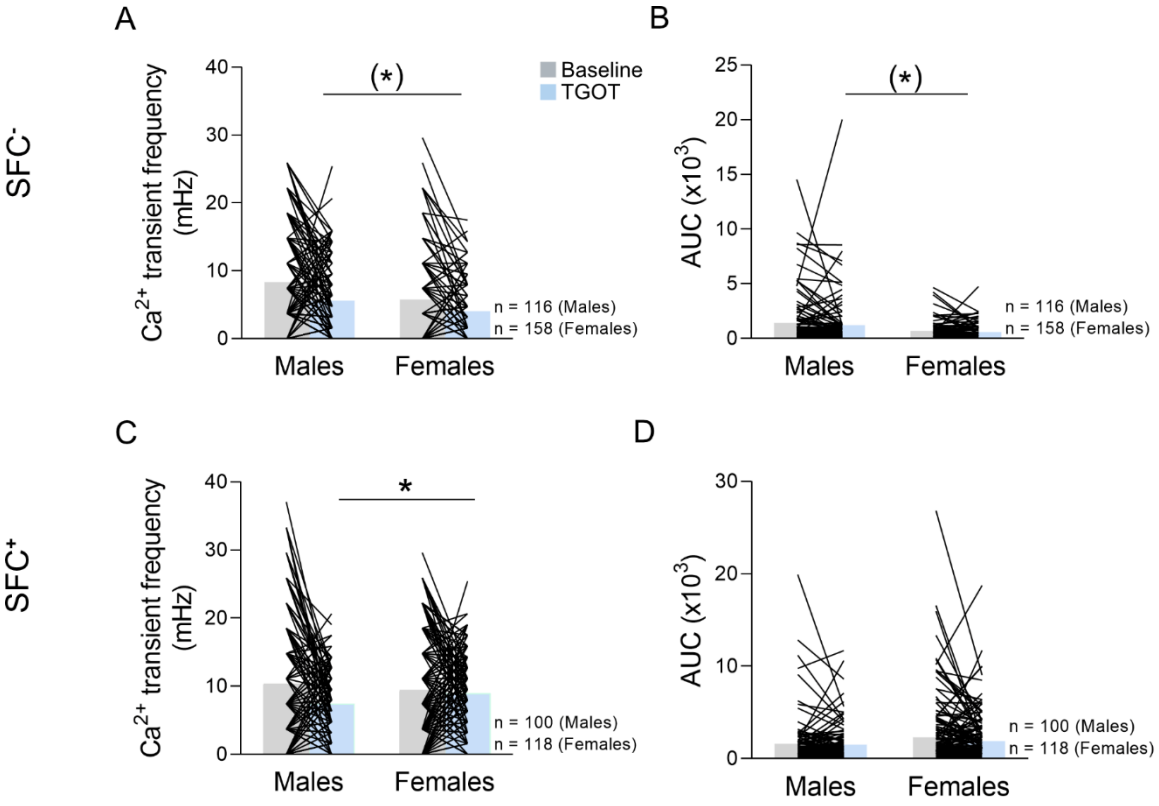

Figure 38. Effects of TGOT on astrocytic calcium activity in all astrocytes in male and female mice following social fear conditioning. *A-B) Responding astrocytes Ca^{2+} transients frequency (A), AUC (B) between male and female mice in SFC- animals. C-D) Responding astrocytes Ca^{2+} transients frequency (C), AUC (D) between male and female mice in SFC+ animals. n = number of cells. Data represents means ± SEM. (*) $p < 0.07$ Baseline vs TGOT (SFC-), * $p < 0.05$. For detailed statistics analysis see Table 32.*

Table 32: Statistics of the global response astrocytic calcium activity in the caudal lateral septum (LSc) after social fear acquisition between male and female mice (Figure 38). Factor represents Males vs Females effects.

SFC$^-$	Mann-Whitney U Test	Figure D
Calcium transient frequency	$U = 5021$	p = 0.052
AUC	$U = 5026$	p = 0.059
SFC$^+$	Mann-Whitney U Test	Figure D
Calcium transient frequency	$U = 7811$	p = 0.036
AUC	$U = 8435$	p = 0.260

5. OXT effects on astrocytic morphology and function in the LS

Based on the previous findings from literature showing OXT effects on astrocyte morphology in the PVN (Theodosis et al. 1986b) and AMY (Wahis et al. 2021) and considering the expression of OXTR found in astrocytes within the LS in both male and female (for details see section 1 in Results), I first investigated OXT effects on astrocytic morphology in the LSc and then explored the involvement of astrocytic OXT signaling in the social fear conditioning paradigm by downregulating the expression of astrocytic OXTR in the LSc in both males and female mice.

5.1. OXT effects on LS astrocytic morphology in male mice

To investigate OXT effects on LSc astrocyte structure, OXT (5 ng/ 0.2 µl/ hemisphere) or Veh (PBS, 0.2 µl/ hemisphere) was infused bilaterally into the LSc of male mice with a third group serving as a sham control. Analysis of the mean fluorescence intensity of astrocytes labeled as GFAP revealed no differences between the sham, Veh or OXT group (Figure 39B). Additionally, when analyzing astrocyte morphology, no differences were detected in the number of primary processes (Figure 39F), in the length of longest primary process (Figure 39G) or in the domain area (Figure 39H), indicating that synthetic OXT did not alter astrocyte structure in the LSc of male mice.

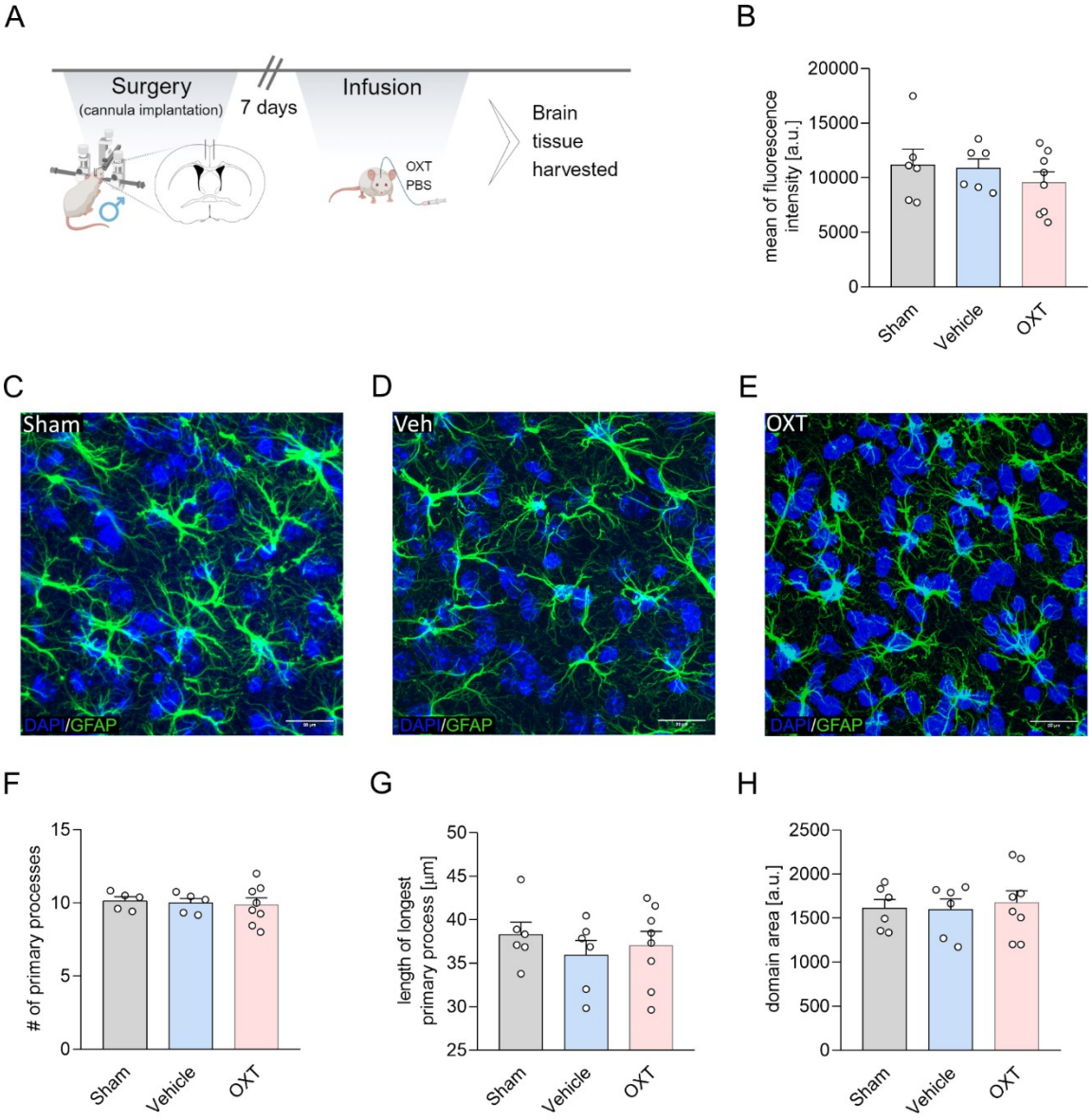

Figure 39. OXT did not alter astrocyte morphology in the caudal lateral septum (LSc) of male mice. *A) Illustration of the experimental timeline. B) E) Quantification of mean fluorescence of GFAP in Sham, Veh or OXT (5 ng/ 0.2 µl/hemisphere) treated group. C-E) Representative image from the LSc showing immunohistochemical staining for glial fibrillary acidic protein expressing (GFAP, green) and nuclei stained with DAPI (blue) from Sham (C), Veh (D) and OXT group (E). F-H) Quantification of astrocytes morphology, including the number of primary processes (F), length of the longest primary process (G), and domain area (H). n = animal number. Data represents means ± SEM. For detailed statistics analysis see Table 33.*

Table 33: Statistics of oxytocin (OXT) effects on astrocyte morphology within the caudal part of the lateral septum (LSc) (Figure 39). Factor represents Sham Vs Veh vs OXT effects.

	One way ANOVA	Figure C-F-G-H
Mean fluorescence intensity	$F_{2,19} = 0.645$	$p = 0.537$
Number of primary processes	$F_{2,17} = 0.110$	$p = 0.897$
Length of longest process	$F_{2,19} = 0.464$	$p = 0.637$
Domain area	$F_{2,19} = 0.120$	$p = 0.887$

5.2. Effects of OXTR knockdown on LS astrocytes on social fear behavior in male and female mice

Although morphological analysis did not reveal any changes in astrocyte structure following OXT infusion, calcium imaging experiment demonstrated astrocytic response to TGOT in both SFC^- and SFC^+ animals. This indicates that astrocytic OXT signaling is involved in socio-emotional behavior. To explore this further, I investigated the behavioral effects of astrocytic *Oxtr* mRNA knockdown in the LSc (see section 3.2. in Material and Methods for details) during the social fear conditioning paradigm in both male and female mice. Particularly, mice were injected with either shRNA or scrRNA, and 3 weeks post-surgery, social behavioral was analyzed during social fear extinction and recall.

Relative *Oxtr* mRNA expression in the caudal septum was measured to assess the efficiency of the knockdown in the shRNA groups. However, no reduction was observable in the shRNA group compared to the scr group in male mice (see section 5. in Discussion).

In male mice, astrocytic *Oxtr* mRNA knockdown did not influence the acquisition of social fear, as equal number of foot shocks were required to induce social avoidance during social fear acquisition in SFC^+/scr compared to SFC^+/*Oxtr* (Figure 40B). On the next day, prior extinction training, both scrambled (scr) control and *Oxtr* shRNA groups displayed similar investigation time towards the 3 non-social stimuli (ns1, ns2, ns3), indicating that astrocytic *Oxtr* shRNA did not influence anxiety-related behaviro (Figure 40C). When exposed to the first social stimulus (Figure 40D), both SFC^+/scr animals and SFC^+/*Oxtr* shRNA mice exhibited social fear responses, reflected by reduced social investigation. SFC^+/scr showed reduced social investigation during the first five social exposures (s1-2 $p < 0.001$, s3 $p = 0.006$, s4 $p = 0.007$), reaching comparable investigation time to the SFC^-/scr group during the exposure to the sixth social stimulus (s6 $p = 0.053$). Interestingly, SFC^+/*Oxtr* shRNA exhibited a reduced investigation time than SFC^-/*Oxtr* shRNA during the first four social stimuli (s1-3 $p < 0.001$, s4 $p = 0.006$), reaching comparable levels to the SFC^- group during the last two social exposure. This suggest that *Oxtr* knockdown accelerated the extinction curve, which is also sustained by increased social investigation in SFC^+/*Oxtr* shRNA observed in the fifth social stimulus compared to the SFC^+/scr group ($p = 0.028$).

During social fear recall (Figure 40E), SFC^+/scr animals showed similar investigation time to the unconditioned controls, indicating successful extinction of social fear. However, SFC^+/*Oxtr* shRNA animals exhibited lower investigation time compared to SFC^-/*Oxtr* shRNA animals during the first fifth social exposures (s1 $p = 0.011$, s2 $p = 0.032$, s3 $p = 0.068$, s4 $p = 0.040$, s5 $p = 0.011$), before reaching comparable levels by the final exposure. This indicates that both scr and *Oxtr* shRNA groups

successfully extinguished social fear, as indicated by similar extinction curve between SFC^+/scr and SFC^+/ *Oxtr* shRNA.

In terms of vigilance behavior, both scr and *Oxtr* shRNA treated groups displayed similar vigilance time towards the non-social stimulus during the exposures (Figure 40F, ns1, ns2, n3). During social stimuli exposure (Figure 40G), SFC^+/scr animals showed increased vigilance time compared to SFC^-/scr during the first four exposures (s1 $p < 0.001$, s2 $p = 0.014$, s3 $p = 0.032$, s4 $p = 0.024$), reflecting a sustained social fear response. Similarly, SFC^+/*Oxtr* shRNA animals showed higher vigilance behavior than SFC^-/*Oxtr* shRNA during the first four social exposures (s1-s2 $p < 0.001$, s3 $p = 0.002$, s4 $p = 0.049$). No differences between SFC^+/scr and SFC^+/*Oxtr* shRNA groups were observed.

During recall, SFC^+/scr displayed heightened fear response only during the first social stimulus (s1 $p = 0.030$), with no differences for the remaining exposures, indicating complete extinction of social fear. Similarly, SFC^+/*Oxtr* shRNA animals exhibited higher vigilance behavior compared to the SFC^-/*Oxtr* shRNA only during the first social stimulus (s1, $p = 0.009$), showing no fear responses thereafter.

Overall, these findings suggest that astrocytic *Oxtr* mRNA knockdown in the LSc of male mice does not affect the acquisition of social fear but accelerates the extinction of social fear. However, the vigilance behavior was not influenced by the Oxtr reduction.

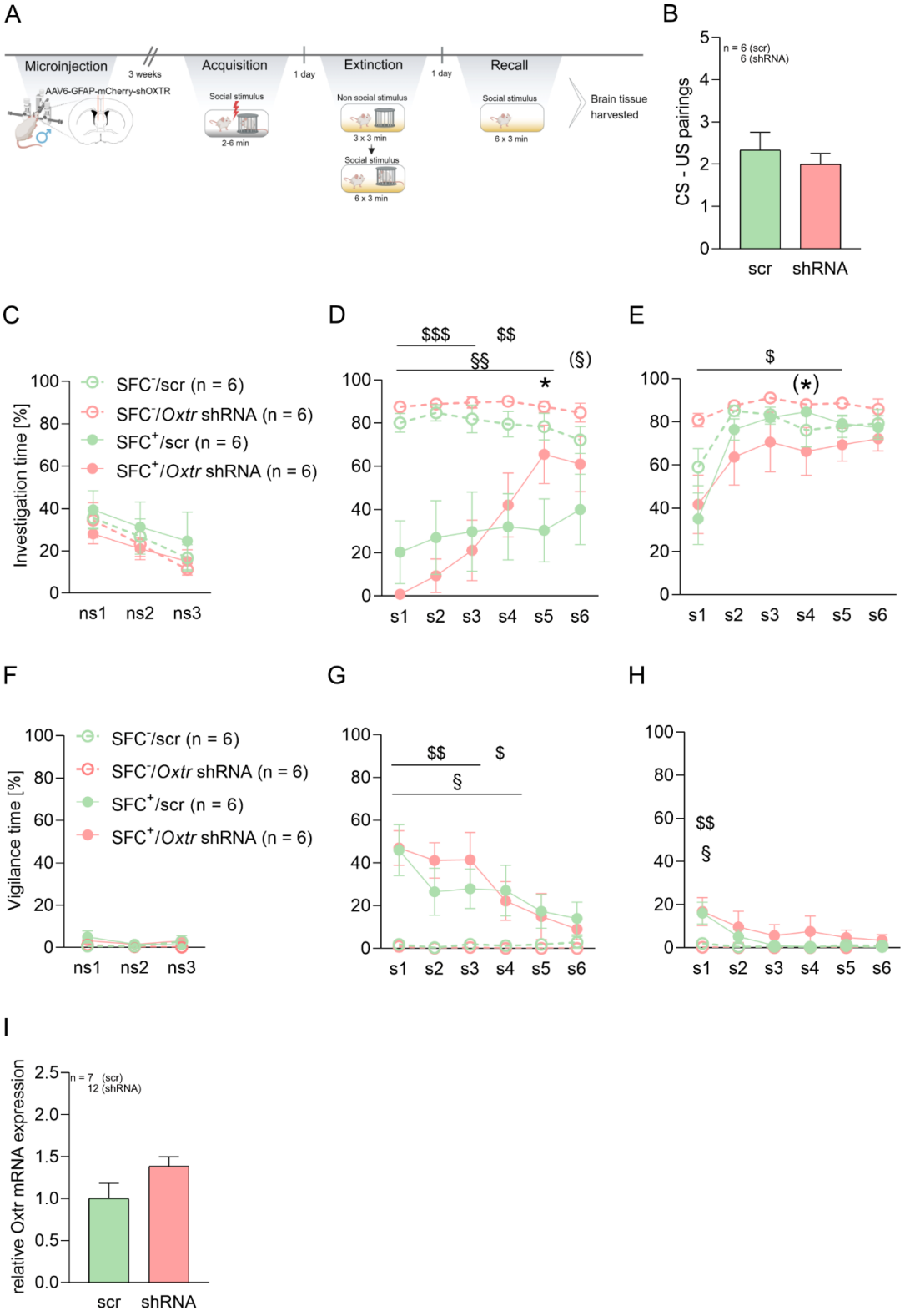

Figure 40. Effects of Oxtr mRNA knockdown in the caudal lateral septum (LSc) on social fear conditioning and extinction in male mice. *A) Illustration of the experimental timeline. B) Number of CS-US pairings presented to conditioned mice (SFC⁺) during acquisition of social fear. C-D) Percentage of investigation time during social fear extinction of non-social stimulus (C) and social stimuli (D). E) Percentage of investigation time of social stimuli during social fear extinction recall. F-G) Percentage of vigilance time during social fear extinction of non-social stimulus (F) and social stimuli (G). H) Percentage of vigilance time of social stimuli during social fear extinction recall. Data represents ± SEM. * $p \leq 0.05$ SFC⁺/Oxtr shRNA vs SFC⁺/scr, (*) $p < 0.07$ SFC⁺/Oxtr shRNA vs SFC⁺/scr, (§) $p < 0.07$ SFC⁺/scr vs SFC⁻/scr, § $p \leq 0.05$ SFC⁺/scr vs SFC⁻/scr, §§ $p < 0.01$ SFC⁺/scr vs SFC⁻/scr, $ $p \leq 0.05$ SFC⁺/Oxtr shRNA vs SFC⁻/Oxtr shRNA, $$ $p < 0.01$ SFC⁺/Oxtr shRNA vs SFC⁻/Oxtr shRNA, $$$ $p < 0.001$ SFC⁺/Oxtr shRNA vs SFC⁻/Oxtr shRNA For detailed statistics analysis see Table 34-35.*

Table 34: Statistical analysis of the effects of Oxtr mRNA knockdown in the caudal lateral septum (LSc) on investigation time in male mice (Figure 40). Factor Time represents stimulus presentation during SFC; factor Conditioning represents SFC^- vs SFC^+ effects; factor Treatment represents *Oxtr* shRNA vs scr effects.

Acquisition	Independent T-Test	Figure B
CS-US pairings	$t_{10} = 0.674$	$p = 0.515$
Oxtr mRNA	Independent T-Test	Figure I
Relative Oxtr mRNA	$t_{17} = -1.904$	$p = 0.074$
Extinction ns 1-3	Mixed Model ANOVA	Figure C
Investigation time	(Time) $F_{2,40} = 8.301$	$p < 0.001$
	(Conditioning) $F_{1,20} = 0.106$	$p = 0.748$
	(Treatment) $F_{1,20} = 1.317$	$p = 0.265$
	(Time x Conditioning) $F_{2,40} = 0.372$	$p = 0.692$
	(Time x Treatment) $F_{2,40} = 0.011$	$p = 0.989$
	(Conditioning x Treatment) $F_{1,20} = 0.106$	$p = 0.748$
	(Time x Conditioning x Treatment) $F_{2,40} = 0.067$	$p = 0.935$
Extinction s 1-6	Mixed Model ANOVA	Figure D
Investigation time	(Time) $F_{1.87,37.4} = 3.878$	$p = 0.032$
	(Conditioning) $F_{1,20} = 42.540$	$p < 0.001$
	(Treatment) $F_{1,20} = 0.561$	$p = 0.462$
	(Time x Conditioning) $F_{1.87,37.4} = 6.253$	$p = 0.005$
	(Time x Treatment) $F_{1.87,37.4} = 2.799$	$p = 0.077$
	(Conditioning x Treatment) $F_{1,20} = 0.107$	$p = 0.747$
	(Time x Conditioning x Treatment) $F_{1.87,37.4} = 1.902$	$p = 0.166$
Recall ns 1-6	Mixed Model ANOVA	Figure E
Investigation time	(Time) $F_{2.37,44.9} = 15.385$	$p < 0.001$
	(Conditioning) $F_{1,19} = 5.742$	$p = 0.027$
	(Treatment) $F_{1,19} = 0.009$	$p = 0.926$
	(Time x Conditioning) $F_{2.37,44.9} = 3.408$	$p = 0.035$
	(Time x Treatment) $F_{2.37,44.9} = 1.724$	$p = 0.185$
	(Conditioning x Treatment) $F_{1,19} = 3.016$	$p = 0.099$
	(Time x Conditioning x Treatment) $F_{2.37,44.9} = 0.460$	$p = 0.666$

Table 35: Statistical analysis of the effects of Oxtr mRNA knockdown in the caudal lateral septum (LSc) on investigation time in male mice (Figure 40). Factor Time represents stimulus presentation during SFC; factor Conditioning represents SFC^- vs SFC^+ effects; factor Treatment represents *Oxtr* shRNA vs scr effects.

Extinction ns 1-3	Mixed Model ANOVA	Figure F
	(Time) $F_{2,40} = 1.595$	$p = 0.216$
	(Conditioning) $F_{1,20} = 2.386$	$p = 0.138$
	(Treatment) $F_{1,20} = 0.144$	$p = 0.708$
Vigilance time	(Time x Conditioning) $F_{2,40} = 1.253$	$p = 0.297$
	(Time x Treatment) $F_{2,40} = 0.041$	$p = 0.960$
	(Conditioning x Treatment) $F_{1,20} = 0.127$	$p = 0.726$
	(Time x Conditioning x Treatment) $F_{2,40} = 2.035$	$p = 0.144$
Extinction s 1-6	Mixed Model ANOVA	Figure G
	(Time) $F_{2.55,51.1} = 7.268$	$p < 0.001$
	(Conditioning) $F_{1,20} = 25.222$	$p < 0.001$
	(Treatment) $F_{1,20} = 0.016$	$p = 0.900$
Vigilance time	(Time x Conditioning) $F_{2.55,51.1} = 7.282$	$p < 0.001$
	(Time x Treatment) $F_{2.55,51.1} = 0.983$	$p = 0.398$
	(Conditioning x Treatment) $F_{1,20} = 0.158$	$p = 0.696$
	(Time x Conditioning x Treatment) $F_{2.55,51.1} = 0.781$	$p = 0.492$
Recall ns 1-6	Mixed Model ANOVA	Figure H
	(Time) $F_{2.16,41.1} = 9.320$	$p < 0.001$
	(Conditioning) $F_{1,19} = 4.081$	$p = 0.058$
	(Treatment) $F_{1,19} = 0.342$	$p = 0.566$
Vigilance time	(Time x Conditioning) $F_{2.16,41.1} = 8.116$	$p < 0.001$
	(Time x Treatment) $F_{2.16,41.1} = 0.456$	$p = 0.652$
	(Conditioning x Treatment) $F_{1,19} = 0.683$	$p = 0.419$
	(Time x Conditioning x Treatment) $F_{2.16,41.1} = 0.200$	$p = 0.836$

Unlike in males, reduction of relative *Oxtr* mRNA expression in the caudal septum of female mice revealed successful knockdown in the shRNA group compared to the scr group (Figure 41I, $p = 0.023$).

Similar to male mice, astrocytic *Oxtr* mRNA knockdown in female mice did not affect the acquisition of social fear, as indicated by equal number of foot shocks required to induce social avoidance during social fear acquisition (Figure 41B). During extinction training, both scr and *Oxtr* shRNA groups displayed similar investigation time toward the non-social stimulus during all three presentations (ns1, ns2, ns3), indicating that astrocytic *Oxtr* shRNA did not influence responses to non-social stimuli (Figure 41C). Upon exposure to social stimuli (Figure 41D), both SFC^+/scr animals and SFC^+/*Oxtr* shRNA mice exhibited social fear responses, as evidenced by reduced social investigation at the beginning of social exposure. SFC^+/scr showed reduced social investigation throughout all six social exposures (s1-4 $p < 0.001$, s5 $p = 0.006$, s6 $p = 0.040$). In contrast, SFC^+/*Oxtr* shRNA mice displayed reduced investigation time compared to SFC^-/*Oxtr* shRNA only during the first three social stimuli (s1-3 $p < 0.001$) reaching similar levels during the last three social exposures. This suggest that Oxtr knockdown accelerated the extinction curve, which is also supported by the increased social investigation observed in SFC^+/*Oxtr* shRNA animals compared to the SFC^+/scr group observed during the fourth and fifth social exposure (s4 $p = 0.065$, s5 $p = 0.030$), reaching comparable investigation time in the last exposure.

During social fear recall (Figure 41E), SFC^+/scr animals showed lower investigation time to the unconditioned controls in the first two social exposures (s1 $p < 0.001$, s2 $p = 0.007$) before reaching similar levels in the later social stimuli, indicating successful social fear extinction. In contrast, SFC^+/*Oxtr* shRNA animals exhibited a trend toward lower investigation time than SFC^-/*Oxtr* shRNA animals during only the first social stimulus (s1 $p = 0.065$) before reaching comparable levels in the following exposures. Additionally, SFC^+/ *Oxtr* shRNA showed higher investigation during the first social stimulus (s1 $p = 0.042$) compared to SFC^+/scr, shRNA, with a trend in the second social exposure (s2 $p = 0.060$). This suggest that both groups successfully extinguished social fear, although SFC^+/ *Oxtr* shRNA animals may have extinguished social fear faster than SFC^+/scr mice.

Regarding vigilance behavior, both scr and *Oxtr* shRNA groups displayed similar vigilance time toward the non-social stimulus during the exposures (Figure 41F, ns1, ns2, n3). During exposure to social stimuli (Figure 41G), SFC^+/scr animals showed increased vigilance time compared to SFC^-/scr during the entire extinction phase (s1-s4 $p < 0.001$, s5 $p = 0.001$, s6 $p = 0.012$), reflecting a sustained social fear response. In contrast, SFC^+/*Oxtr* shRNA animals showed higher vigilance behavior than SFC^-/*Oxtr* shRNA only during the first 3 social exposures (s1-s2 $p < 0.001$, s3 $p = 0.003$), aligning with the faster extinction curve observed in social investigation behavior. Furthermore, SFC^+/scr displayed higher vigilance behavior compared to SFC^+/*Oxtr* shRNA during

the first, fourth and fifth social stimuli (s1 $p = 0.020$, s4 $p = 0.012$, s5 $p = 0.016$), with both groups showing comparable vigilance behavior by the last exposure.

During recall phase, SFC^+/scr exhibited heightened fear response only during the first thre social stimuli (s1 $p < 0.001$, s2 $p = 0.008$, s3 $p = 0.028$), with no differences for the remaining exposures, indicating complete extinction of social fear. In contrast, SFC^+/*Oxtr* shRNA animals exhibited vigilance behavior comparable to SFC^-/*Oxtr* shRNA animals throughout all six social stimuli, indicating a reduced fear response relative to SFC^+/scr group. Increased vigilance behavior in SFC^+/scr compared to SFC^+/*Oxtr* shRNA was detected during the first two social stimuli (s1 $p = 0.005$, s2 $p = 0.034$), with similar levels for the remaining exposures.

Overall, these findings suggest that astrocytic *Oxtr* mRNA knockdown in the LSc of female mice does not affect the acquisition of social fear but accelerates the extinction of social fear and reduces overall the fear responses.

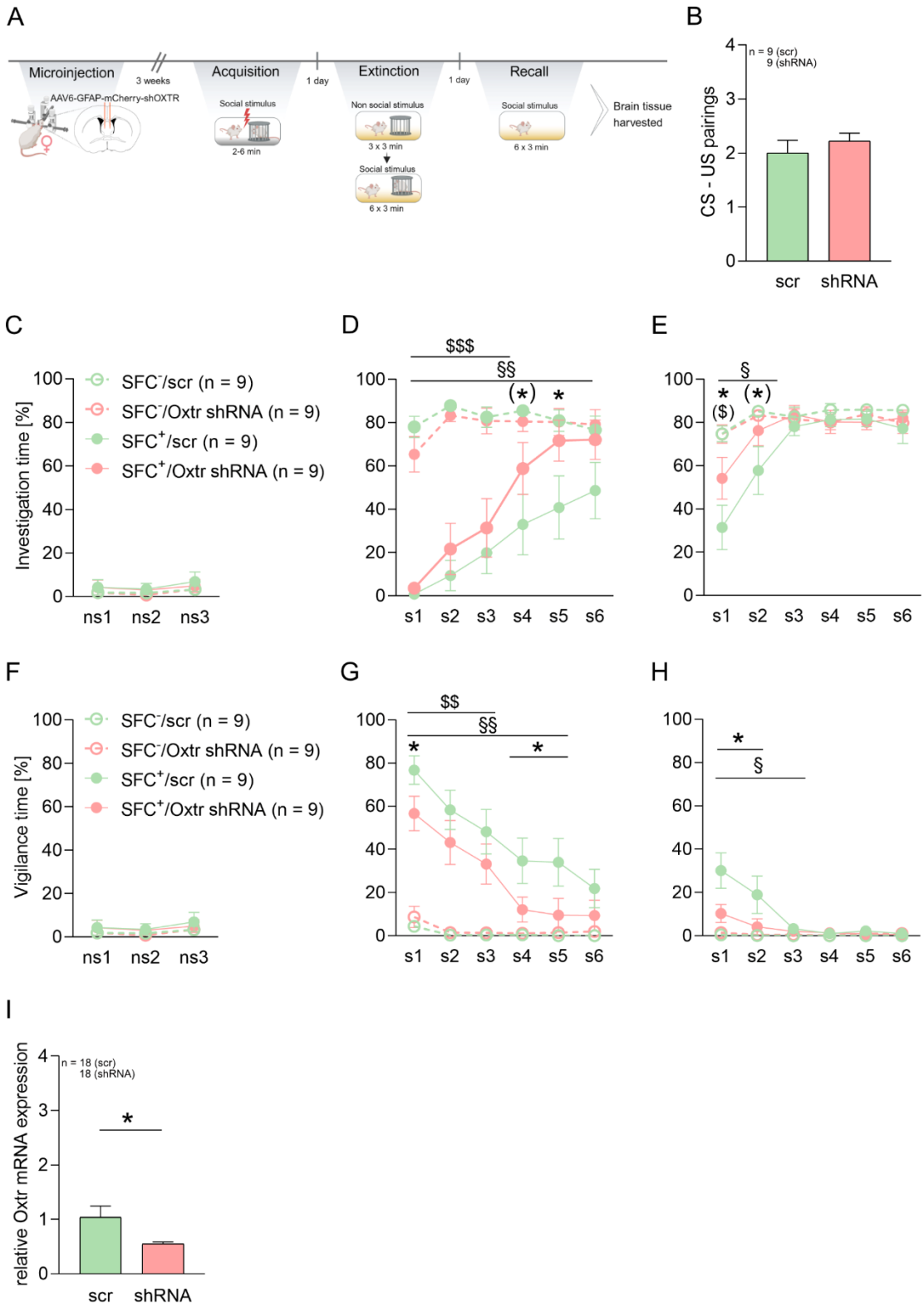

Figure 41. Effects of Oxtr mRNA knockdown in the caudal lateral septum (LSc) on social fear conditioning and extinction in female mice. *A) Illustration of the experimental timeline. B) Number of CS-US pairings presented to conditioned mice (SFC⁺) during acquisition of social fear. C-D) Percentage of investigation time during social fear extinction of non-social stimulus (C) and social stimuli (D). E) Percentage of investigation time of social stimuli during social fear extinction recall. F-G) Percentage of vigilance time during social fear extinction of non-social stimulus (F) and social stimuli (G). H) Percentage of vigilance time of social stimuli during social fear extinction recall. Data represents ± SEM. * p ≤ 0.05 SFC⁺/Oxtr shRNA vs SFC⁺/scr, (*) p < 0.07 SFC⁺/Oxtr shRNA vs SFC⁺/scr, (§) p < 0.07 SFC⁺/scr vs SFC⁻/scr, § p ≤ 0.05 SFC⁺/scr vs SFC⁻/scr, §§ p < 0.01 SFC⁺/scr vs SFC⁻/scr, $ p ≤ 0.05 SFC⁺/Oxtr shRNA vs SFC⁻/Oxtr shRNA, $$ p < 0.01 SFC⁺/Oxtr shRNA vs SFC⁻/Oxtr shRNA, $$$ p < 0.001 SFC⁺/Oxtr shRNA vs SFC⁻/Oxtr shRNA For detailed statistics analysis see Table 36-37.*

Table 36: Statistical analysis of the effects of Oxtr mRNA knockdown in the caudal lateral septum (LSc) on investigation time in female mice (Figure 41). Factor Time represents stimulus presentation during SFC; factor Conditioning represents SFC^- vs SFC^+ effects; factor Treatment represents *Oxtr* shRNA vs scr effects.

Acquisition	Independent T-Test	Figure X
CS-US pairings	$t_{10} = -0.800$	$p = 0.435$
Oxtr mRNA	**Independent T-Test**	**Figure X**
Relative Oxtr mRNA	$t_{34} = 2.377$	$p = 0.023$
Extinction ns 1-3	**Mixed Model ANOVA**	**Figure X**
	(Time) $F_{2,64} = 24.022$	$p < 0.001$
	(Conditioning) $F_{1,32} = 0.006$	$p = 0.939$
	(Treatment) $F_{1,32} = 2.809$	$p = 0.103$
Investigation time	(Time x Conditioning) $F_{2,64} = 0.174$	$p = 0.841$
	(Time x Treatment) $F_{2,640} = 2.671$	$p = 0.077$
	(Conditioning x Treatment) $F_{1,32} = 0.844$	$p = 0.365$
	(Time x Conditioning x Treatment) $F_{2,40} = 2.359$	$p = 0.103$
Extinction s 1-6	**Mixed Model ANOVA**	**Figure X**
	(Time) $F_{2.81,89.9} = 18.052$	$p < 0.001$
	(Conditioning) $F_{1,32} = 49.754$	$p < 0.001$
	(Treatment) $F_{1,32} = 1.173$	$p = 0.287$
Investigation time	(Time x Conditioning) $F_{2.81,89.9} = 14.842$	$p < 0.001$
	(Time x Treatment) $F_{2.81,89.9} = 1.542$	$p = 0.211$
	(Conditioning x Treatment) $F_{1,32} = 2.746$	$p = 0.107$
	(Time x Conditioning x Treatment) $F_{2.81,89.9} = 0.449$	$p = 0.706$
Recall ns 1-6	**Mixed Model ANOVA**	**Figure X**
	(Time) $F_{2.48,79.3} = 17.904$	$p < 0.001$
	(Conditioning) $F_{1,32} = 7.959$	$p = 0.008$
	(Treatment) $F_{1,32} = 0.578$	$p = 0.453$
Investigation time	(Time x Conditioning) $F_{2.48,79.3} = 7.836$	$p < 0.001$
	(Time x Treatment) $F_{2.37,44.9} = 1.803$	$p = 0.163$
	(Conditioning x Treatment) $F_{1,32} = 2.409$	$p = 0.130$
	(Time x Conditioning x Treatment) $F_{2.48,79.3} = 1.034$	$p = 0.373$

Table 37: Statistical analysis of the effects of Oxtr mRNA knockdown in the caudal lateral septum (LSc) on investigation time in male mice (Figure 41). Factor Time represents stimulus presentation during SFC; factor Conditioning represents SFC^- vs SFC^+ effects; factor Treatment represents *Oxtr* shRNA vs scr effects.

Extinction ns 1-3	Mixed Model ANOVA	Figure X
	(Time) $F_{1.36,43.6} = 2.325$	$p = 0.126$
	(Conditioning) $F_{1,32} = 1.191$	$p = 0.283$
	(Treatment) $F_{1,32} = 0.067$	$p = 0.797$
Vigilance time	(Time x Conditioning) $F_{1.36,43.6} = 1.198$	$p = 0.912$
	(Time x Treatment) $F_{1.36,43.6} = 2.726$	$p = 0.849$
	(Conditioning x Treatment) $F_{1,32} = 0.016$	$p = 0.901$
	(Time x Conditioning x Treatment) $F_{1.36,43.6} = 5.947$	$p = 0.144$
Extinction s 1-6	Mixed Model ANOVA	Figure X
	(Time) $F_{2.43,77.9} = 28.092$	$p < 0.001$
	(Conditioning) $F_{1,32} = 25.222$	$p < 0.001$
	(Treatment) $F_{1,32} = 0.016$	$p = 0.123$
Vigilance time	(Time x Conditioning) $F_{2.43,77.9} = 19.794$	$p < 0.001$
	(Time x Treatment) $F_{2.43,77.9} = 0.359$	$p = 0.740$
	(Conditioning x Treatment) $F_{1,32} = 0.158$	$p = 0.064$
	(Time x Conditioning x Treatment) $F_{2.43,77.9} = 0.386$	$p = 0.722$
Recall ns 1-6	Mixed Model ANOVA	Figure X
	(Time) $F_{1.60,51.5} = 11.037$	$p < 0.001$
	(Conditioning) $F_{1,32} = 12.948$	$p = 0.001$
	(Treatment) $F_{1,32} = 2.907$	$p = 0.098$
Vigilance time	(Time x Conditioning) $F_{1.60,51.5} = 9.998$	$p < 0.001$
	(Time x Treatment) $F_{1.60,51.5} = 3.175$	$p = 0.060$
	(Conditioning x Treatment) $F_{1,32} = 4.412$	$p = 0.044$
	(Time x Conditioning x Treatment) $F_{1.60,51.5} = 3.268$	$p = 0.056$

Traditionally considered as passive support cells, astrocytes have now recognized as key components in modulating synaptic plasticity and regulating emotional behaviors. In recent years, increasing evidence has highlighted their significant role in anxiety- and depressive-like behaviors, particularly with the involvement of astrocytic OXT signaling. While the role of OXT in regulating social behavior within the LS has been widely characterized, the specific contribution of astrocytes in this context is not discovered. Given the limited treatment options for SAD, there is a pressing need for deeper investigation into this field. In this thesis I demonstrated the astrocytic involvement in the learning processes of social fear acquisition and its influence on social behaviors. Furthermore, a potential role of astrocytic OXT signaling has emerged in modulating social behaviors during the extinction phase. To address potential sex differences, males and females have been analyzed.

In the present study I found sex- and spatial-dependent differences in the distribution of astrocytes as well in the OXTR mRNA, with the highest density in females and the LSc. In response to social fear acquisition and extinction astrocytes of male mice responded to social fear acquisition in both the HIP and LSc, suggesting an astrocytic role in remodeling synaptic signaling during the learning process. When male and female mice were tested for social behavior during SFC, following astrocytic structural depletion in the LSc induced by L-AAA, male mice properly acquired social fear, but exhibited reduced social fear behavior during social fear extinction and recall. In contrast, females showed impaired acquisition of social fear, but exhibited equal social fear extinction behavior compared to controls. These results suggest that astrocytes contribute differently to regulating social behaviors in male and female mice. To further investigate astrocytic activity after social fear conditioning, I measured astrocytic Ca^{2+} activity *ex vivo* in both sexes. I found that social fear acquisition increased baseline astrocytic Ca^{2+} activity in both sexes, with males showing higher baseline activity. When I measured the effect of OXT signaling on astrocytic activity, using the OXTR agonist TGOT, I found that social fear acquisition even enhanced Ca^{2+} activity in response to treatment. Here, females displayed a higher Ca^{2+} response compared to males. These data suggest a potential “ceiling effect” in female mice under baseline conditions, which is then triggered by social fear conditioning, leading to elevated activity compared to males. Lastly, I found that downregulating astrocytic OXTR led to faster extinction of social fear in both male and female mice, as evidenced by reduced fear responses during the extinction phase. This underscores the importance of astrocytic OXT signaling in regulating social behaviors during the extinction process.

1. Characterization of LS astrocytes and OXTR$^+$ astrocytes in male, virgin female and lactating mice

To highlight the neurochemical and functional heterogeneity of the LS (Wirtshafter and Wilson 2021; Menon et al. 2022), I performed a detailed analysis of astrocyte distribution and OXTR mRNA$^+$ astrocytes across the rostral-caudal and dorsal-ventral axes of the LS in male, female and lactating mice. My findings revealed distinct patterns in astrocyte distribution, with higher number of astrocytes in the dorsal LS of male, virgin female, and lactating mice (Figure 14-16). Along the rostral-caudal axis, I detected more astrocytes in the LSc compared to the LSr, in both sexes (Figure 14-16), while lactating mice showed a more homogenous distribution (Figure 15). Additionally, the astrocyte-to-neuron ratio observed in this thesis suggests region-specific astrocytic functions, with a higher proportion of astrocytes in the caudal LS, consistent with prior studies linking higher glial density to increased neuronal activity in brain regions like the cortex, cerebellum, and brainstem (Bartheld et al. 2016; Verkhratsky and Nedergaard 2018; Falcone 2022). The correlation between neuronal activity and glial density suggests that in the LSc astrocytes are recruited to support heightened neuronal demand, aiding energy metabolism and synaptic function. I also identified notable sex differences in astrocyte distribution, with virgin female mice showing higher astrocyte density in the LSc compared to males (Figure 14), a finding consistent with previous research (Althammer et al. 2022b). This difference suggests potential sex-specific roles for astrocytes within the LS. Sex hormones, particularly estrogen, have been shown to modulate astrocyte proliferation and function (Fuente-Martin et al. 2013; Mong and Blutstein 2006; Crespo-Castrillo and Arevalo 2020), such as increasing the expression of glutamine synthetase, a glia-specific gene involved in the glutamate-glutamine cycle (Mong and Blutstein 2006). The higher astrocyte density in virgin females suggests a greater involvement of this brain region in regulating social behaviors, functions typically associated with the LS (Menon et al. 2022). Lactating mice, however, showed a more uniform astrocyte distribution, implying that physiological states like lactation can influence astrocytic function to meet the demands of maternal behaviors. During periods of elevated OXT activity, such as lactation, astrocytes play a critical role in astrocytes help regulate synaptic transmission, plasticity, and the neurochemical environment (Moos et al. 1989; Wang and Hatton 2009; Papouin et al. 2017; Wang et al. 2019).

The observed heterogeneity in astrocyte distribution along the rostral-caudal and dorsal-ventral axes of the LS in both males and females, as well as in lactating mice, underscores the spatial and functional variability of astrocytes in this brain region (Wirtshafter and Wilson 2021; Menon et al. 2022). This mirrors the complex circuitry of the LS, which is implicated in a wide range of diverse and sometimes opposing functions and behaviors (Rizzi-Wise and Wang 2021; Sheehan et al. 2004; Oliveira et al. 2021; Leroy et al. 2018; Wirtshafter and Wilson 2021). This variability suggests a

specialized role of astrocytes in regulating various functions associated with LS. Furthermore, differences in overall astrocyte populations between males and females may reflect sex-specific energy and neuronal demands, potentially leading to distinct behavioral outcomes. To fully understand astrocyte diversity in the LS, further research is necessary to explore the specialization of astrocytes in relation to neuronal populations. The morphological heterogeneity and functional specificity of astrocytes across different brain regions, particularly their responses to neuronal activity, make them a particularly challenging yet critical area for future investigation.

The detailed analysis conducted in this thesis revealed that astrocytes expressing OXTR mRNA are present throughout the LS in male, female and lactating mice. Notably, I observed a distribution pattern similar to astrocyte density for OXTR mRNA along the rostral-caudal axis, with a higher density of OXTR mRNA+ astrocytes in the LSc compared to the LSr (Figure 14-16). However, no differences were found along the dorsal-ventral axis across any groups. Furthermore, although astrocytes expressing OXTR mRNA represent a small proportion compared to neurons, this ratio was notably higher in the LSc than in the LSr (20% vs 13% respectively, Figure 14). These results align with Dr. Theresa Suß's findings showing higher OXTR binding expression in the LSc of both sexes through autoradiography, although here there was no cell discrimination (unpublished). This aligns with the understanding that elevated neuronal activity can drive increased protein turnover, potentially explaining the greater astrocyte density in the LSc and dorsal LS compared to the ventral region. I also identified notable sex differences in astrocyte distribution, with virgin female mice showing higher astrocyte density in the LSc compared to males (Figure 14), a finding consistent with previous research (Althammer et al. 2022c). The sex-differences in OXTR expression in both neurons and astrocytes across various brain regions have been already documented (Smith et al. 2017; Althammer et al. 2022c), with females typically showing higher levels of OXT and OXTR expression compared to males (Carter 2007). These differences are influenced by estrogen and fluctuate with the estrous cycle, peaking during ovulation (Froemke and Carcea 2017; Jurek and Neumann 2018). Although the estrous cycle was not controlled for in this study due to the small sample size, future research should explore OXTR expression across different estrous stages. Interestingly, no significant difference was found between virgin and lactating females in terms of OXTR mRNA$^+$ astrocyte expression, which remained elevated in the LSc compared to males. However, lactation is known to be a state of heightened OXT. Studies have demonstrated increased OXTergic fibers in the LS during lactation (Menon et al. 2018), which implies that astrocytes in lactating mice, particularly those expressing OXTR in the LSc, may play a crucial role in supporting maternal behaviors. This aligns with evidence that during periods of heightened OXT activity, such as lactation, astrocytes help regulate synaptic transmission, plasticity, and the neurochemical environment (Wang and Hatton 2009; Papouin et al. 2017). This region-specific expression of OXTR mRNA$^+$ astrocyte suggests a specialized role for astrocytes in the LSc, particularly in relation to OXT

signaling. Previous studies have shown that the dorsal and intermediate parts of the LS receive projections from the PVN and SON (Liao et al. 2020), and an increased number of OXTergic fibers in the LS of lactating mice supports the idea that increased OXT activity correlates with higher astrocyte density and OXTR mRNA$^+$ astrocytes, particularly during lactation. Astrocytes in lactating mice might be more responsive to OXT signaling, aiding in the regulation of key maternal behaviors such as pup retrieval, bonding, and aggression reduction. This mediation of social behavior during lactation could be supported by the increased astrocyte density and higher astrocytic OXTR expression in the LSc, a region associated with regulating social behaviors. Although astrocytic OXTR mRNA levels in lactating females were comparable to virgin females, it is possible that the functional role of OXTR in astrocytes becomes more prominent during lactation due to the elevated OXT activity needed for maternal care. However, one limitation to take into consideration in the interpretation of these findings, is the use of in situ hybridization to target the mRNA of the OXTR, which was necessary due to the lack of an OXTR antibody. Indeed, the OXTR mRNA expression observed does not reflect the functional levels of the OXTR protein, as post-transcriptional mechanisms could affect mRNA translation into protein (Cohen et al. 2013; Jiménez et al. 2022).

In summary, the higher density of astrocytes in the LSc, particularly in virgin females, may reflect sex-specific differences in astrocyte distribution, potentially corresponding to functional variations in LS-regulated behaviors. The elevated expression of OXTR mRNA in astrocytes in the LSc of virgin females suggests a more prominent role for astrocytes in OXT signaling pathways, potentially influencing social and emotional behaviors modulated by OXT. The similar distribution patterns of both astrocytes and OXTR mRNA+ astrocytes point to a possible role in mediating OXT-related behaviors in the LS, including maternal behaviors, aggression, and suppression of social fear during lactation (Lukas et al. 2013; Zoicas et al. 2014; Menon et al. 2018; Oliveira et al. 2021). These findings underscore the need to investigate the role that astrocytes may play in mediating these OXT-dependent processes in a region-specific and sex-dependent manner.

2. Astrocyte response to social fear acquisition and extinction in male mice

Given the emerging role of astrocytes in regulating socio-emotional behaviors and learning processes (Kofuji and Araque 2021a; Bernardinelli et al. 2014), I explored how these glial cells respond to social fear acquisition and extinction in the HIP and LS of male mice, two brain regions critically involved in regulating emotional processing (Taylor and Liberzon 2007; Markham et al. 2010; Wirtshafter and Wilson 2021; Menon et al. 2022). Interestingly, in the HIP, no changes were observed in astrocytic number or process length 90 minutes after social fear acquisition (Figure 17). However, a trend toward increased domain area was noted in SFC$^+$ animals compared to the SFC$^-$

group (Figure 17D). Additionally, no alterations were detected in the expression of key astrocytic proteins in the caudal septum at this time point, such as Cx30, Cx43, GFAP, and glutamate transporters (EAAT1, EAAT2), which closely associated with cytoskeletal dynamics and astrocytic gap junction communication respectively (Giaume et al. 1991; Nagy et al. 2001; Hol and Pekny 2015; Verkhratsky and Nedergaard 2018). The slight increase in astrocytic coverage, despite stable protein levels, suggests that astrocytes may detect neuronal changes following social fear acquisition, even without undergoing immediate or complete morphological reorganization. An increase in cFos expression, a marker of cellular activation (Matsuda et al. 1996; Cruz-Mendoza et al. 2022; Herrera and Robertson 1996), was observed in SFC^- animals 90 minutes after social fear acquisition compared to naïve controls, indicating astrocytic responsiveness to behavioral stimuli beyond social fear itself. While stress and cognitive assessments have been shown to induce cFos in astrocytes (Adamsky and Goshen 2018; Cruz-Mendoza et al. 2022; Fan et al. 2018), the lack of significant cFos differences between SFC^- and SFC^+ suggests that astrocytic activation is influenced by general environmental stimuli within the SFC paradigm.

Notably, 24 hours post-social fear acquisition (Figure 18), phosphorylation of Cx43 (pCx43) was increased in the HIP of SFC^+ animals suggesting alterations in astrocytic gap junction communication as part of a functional adaptation to restore homeostasis. Normally, astrocytes exhibit high gap junction communication with minimal hemichannel activity (Chever et al. 2014). However, phosphorylation of Cx43 can activate hemichannels, leading to the release of gliotransmitters like glutamate and ATP (Zhang et al. 2023; Fukuyama et al. 2020). Therefore, this increase in pCx43 may reflect an astrocytic response to enhance synaptic transmission following social trauma. Indeed, connexins, particularly Cx43, play a crucial role in astrocytic communication, influencing ion exchange (Orellana et al. 2013), astrocytic activation (Ren et al. 2018) and gliotransmitter release (Meunier et al. 2017). Dysfunctions in Cx30 and Cx43 have been linked to impaired neuronal activity and depressive-like behaviors (Huang et al. 2019). Similarly, chronic unpredictable stress was found to decrease Cx43 expression (Sun et al. 2012).

Interestingly, a reduction in $cFos^+$ astrocytes was noted in SFC^+ animals 24 hours post-acquisition, possibly indicating a time-dependent downregulation of astrocyte activity after the initial fear response. This aligns with studies showing long-term changes in cFos expression linked to diminished neural network activity (Clarkson et al. 2010), suggesting a dynamic astrocytic role in regulating neural circuits post-social fear exposure. Further investigation into the neuronal aspect of this process would provide a more comprehensive understanding of the LS neural network.

In conclusion, the involvement of astrocytes in synaptic transmission, neurotransmitter clearance, and structural integrity positions them at the forefront of research into emotion and memory. In line with previous studies demonstrating the role of hippocampal astrocytes in memory enhancement

(Kol et al. 2020; Adamsky et al. 2018; Adamsky and Goshen 2018), this thesis offers evidence for future investigations into the role of hippocampal astrocytes in synaptic communication following social fear acquisition. Nonetheless, further exploration is essential to comprehensively elucidate their contributions to these intricate processes.

In contrast to the HIP, the LS exhibited region-specific astrocytic responses to social fear acquisition (Figure 20-23), with the LSc (Figure 22-23) of SFC^+ animals showing more pronounced structural changes than the LSr (Figure 20-21). Specifically, both the dorsal and ventral LSc of SFC+ mice displayed increased astrocytic coverage, while only the ventral LSr showed a slight increase. This suggests that astrocytes in the LSc may play a more active role in modulating emotional processing and memory consolidation associated with social fear acquisition. The astrocytic coverage of synapses is crucial for regulating synaptic transmission and plasticity, contributing to overall brain signaling (Lavialle et al. 2011; Bernardinelli et al. 2014; Aguado et al. 2002). This highlights the dynamic astrocyte-neuron communication, which is influenced by changes in astrocytic morphology and vice versa (Aguado et al. 2002; Verkhratsky and Nedergaard 2018). Particularly, PAPs express glutamate transporters that regulate excitatory transmission and can sense changes in neuronal activity, allowing them to modify their actin filaments to regulate spine density (Lavialle et al. 2011; Bernardinelli et al. 2014; Verkhratsky and Nedergaard 2018). Thus, the increase in astrocyte coverage observed in the LSc of SFC^+ animals following social fear acquisition may indicate a restructuring of synapses aimed at enhancing the synaptic transmission of neuronal circuits involved in the regulation of social behaviors. As in the HIP, SFC^- animals in the LS exhibited increased $cFos^+$ astrocytes compared to naïve controls, but no differences were found between SFC^- and SFC^+, suggesting that astrocytic activation in this region is not specific to social fear acquisition but may also reflect responses to general environmental stimuli. Interestingly, protein analysis revealed significant reductions in Cx43 and EAAT2 levels in SFC^+ animals compared to controls, alongside a trend toward decreased GFAP expression (Figure 26). As previously mentioned, Cxs are essential for astrocyte-astrocyte communication, which is enhanced by the opening of channels formed by these proteins, such as Cx43, which is associated with glutamate release and synaptic transmission (Orellana et al. 2013; Meunier et al. 2017; Ren et al. 2018). The observed reduction in Cx43 levels in animals subjected to social fear acquisition found in this thesis, suggests an impairment in astrocytic function, which is consistent with previous studies that have linked Cx43 deficiency to anxiety-related behaviors (Huang et al. 2019; Sun et al. 2012). Furthermore, the hypothesis of a decrease in astrocytic function is supported by the observed reduction in EAAT2 levels. EAAT2, along with EAAT1, is responsible for uptaking approximately 90% of the glutamate in the brain (Anderson and Swanson 2000; Eulenburg and Gomeza 2010), and its expression, located in the astrocytic processes, is positively correlated with synaptic activity of glutamatergic neurons (Poitry-Yamate et al. 2002; Swanson et al. 1997). Changes in the expression of these proteins can

significantly impact neuronal communication. Unlike EAAT1 (Watase et al. 1998), research has shown that the reduction or knockout of EAAT2 leads to neuronal degeneration and death (Todd and Hardingham 2020; Tanaka et al. 1997). While the LS is predominantly composed of GABAergic neurons, a small population of glutamatergic neurons exists in its most ventral region (Lin et al. 2003), which receives glutamatergic projections from the ventral hippocampus (Trent and Menard 2010). Therefore, the reduction of EAAT2 in the ventral part of the septum in SFC^{+} mice could lead to an increased availability of glutamate, resulting in heightened excitation of GABAergic fibers and a consequent decrease in septal activity. This may suggest that the underlying mechanisms involved in the acquisition of social fear and its behavioral phenotype may be related to an increase in GABAergic neurons in the LS. Furthermore, the downregulation of Cx43 and EAAT2 may signal a reduction in astrocytic communication via gap junctions and impaired glutamate clearance, resulting in less effective regulation of neural activity and the balance between excitatory and inhibitory signals in septal circuits. Previous research has indicated that blocking Cx43 channel activity within the BLA can prevent the acquisition of fear memories (Stehberg et al. 2012), suggesting that gliotransmitters and astrocyte-astrocyte communication play a significant role in modulating fear learning circuits (Orellana and Stehberg 2014). Furthermore, the observed trend toward a decrease in GFAP protein levels in the caudal septum may seem to contradict the increase in astrocytic coverage observed in the morphological analysis. However, this divergence may be attributed to the methodological approaches used. Indeed, while morphological analysis focused specifically on subdivisions of the LSc, protein level analysis involved isolating the entire caudal septum, which may have masked subtle differences in protein expression specific to the LSc. The decrease in Cx43 and EAAT2 indicates an impairment of astrocytic functions, particularly regarding astrocyte-astrocyte communication, which appears contradictory to the evidence of increased astrocytic branching and coverage in the LSc, observed following social fear conditioning (Figure 22-23). This discrepancy underscores the distinct roles that astrocytes may play during social fear processing. The structural reorganization observed in the LSc suggests that astrocytes dynamically adjust to modulate synaptic networks, while the downregulation of proteins like Cx43 and EAAT2 may reflect a functional adaptation that compromises gap junction communication and glutamate clearance. This could lead to less effective regulation of the excitatory-inhibitory balance within LS neural circuits, ultimately enhancing neuronal circuits associated with social fear behaviors.

Taken together, these changes do not necessarily contradict the observed morphological adaptations. Instead, they underscore the complexity of astrocytes capable of regulating synaptic transmission by regulating extracellular environment following specific stimuli (Volterra and Meldolesi 2005; Halassa and Haydon 2010) and whose functions may involve in both structural and functional regulation of neural signaling. The structural reorganization in the LSc indicates that astrocytes actively reshape synaptic networks during emotional processing, while the downregulation of key

astrocytic proteins like Cx43 and EAAT2 suggests an impaired ability to maintain coordinated astrocytic signaling and effective neurotransmission. Given that connexins, particularly Cx43, are implicated in regulating cytoskeletal processes (Ghézali et al. 2018) and that astrocytes clear approximately 90% of available glutamate in the synaptic cleft via EAAT1 and EAAT2 (Anderson and Swanson 2000; Eulenburg and Gomeza 2010), alterations in the expression of these proteins can significantly impact neuronal communication and, consequently, the overall neural network. This dual role of astrocytes in both structural reorganization and functional modulation likely represents a concerted effort to adapt to the neural demands imposed by social fear acquisition, balancing network stability with the need for synaptic plasticity.

In contrast to HIP, 24 hours after social fear acquisition no significant changes in astrocytic structure or differences in cFos activation of SFC^+ mice were detected in any LS subdivisions (Figure 24). This indicates that astrocytic responses in the LS are more immediate, suggesting their involvement in the early stages of emotional processing. This supports and mediates neural network changes during the initial phase of social fear, preparing neuronal circuits for further behavioral assessments. However, these changes do not persist over time, as evidenced by the lack of morphological changes observed 24 hours post-acquisition. Instead, other mechanisms may take over as the emotional memory is consolidated.

Another interesting aspect I investigated was the astrocytic response to processes related to the emotional processing of social fear extinction. Again, astrocytes exhibited region-specific responses between the HIP and LS. While astrocytes in the LS did not show any structural or protein level changes 90 minutes after social fear extinction (Figure 25), in the HIP, astrocytes revealed no structural changes, but protein expression demonstrated increased levels of Cx30 and GFAP in the caudal septum of SFC^+ animals after extinction (Figure 19). Notably, recent findings indicate that the upregulation of Cx30 in hippocampal astrocytes enhances the astrocytic network but reduces neuronal excitability and glutamate concentration, leading to impairments in synaptic plasticity and learning processes (Hardy et al. 2023). Therefore, the upregulation of Cx30 observed after social fear extinction may suggest that astrocytes undergo adaptations in their network to support the learning processes associated with the extinction of social fear. Furthermore, the observed increase in GFAP levels in the caudal septum does not correlate with the absence of structural changes identified in the morphological analysis. This discrepancy may be attributed to the methodological approach. For instance, GFAP is commonly used as a marker of astrocytic structural integrity in morphological studies, but it primarily stains the major somatic branches of astrocytes (Connor and Berkowitz 1985). This limitation renders it insufficient to capture a complete picture of astrocytic morphology under physiological conditions (Reichenbach et al. 2010). Thus, while GFAP may indicate certain functional or adaptive changes in astrocytes, it does not necessarily reflect alterations in the overall structural dynamics of the astrocytic network during processes like social fear extinction

(Reichenbach et al. 2010). These findings highlight a potential involvement of hippocampal astrocytes in regulating the learning processes associated with the extinction of social fear. However, further studies are necessary to better investigate this aspect and to better understand astrocyte contribution to emotional processing and memory extinction involved in social fear behaviors, paving the way for potential therapeutic interventions.

Collectively, these results highlight the active participation of astrocytes in the neural network and emphasize the complexity of their involvement in social fear processes, characterized by region- and time-specific activation. The differential response observed in the HIP and LS at different stages of emotional processing indicates a specialized role for astrocytes in distinct brain regions, a characteristic supported by previous studies (Ostroff et al. 2014; Martin-Fernandez et al. 2017; Adamsky and Goshen 2018). Additionally, an aspect to investigate in future studies is the involvement of astrocytes in long-term memory processes, especially considering recent findings that activation of hippocampal astrocytes impaired memory retrieval one month later (Kol et al. 2020). Finally, further research is necessary to explore intercellular communication to better understand how astrocytes coordinate network activity during emotional processing associated with social fear.

2.1. Astrocyte response to social fear acquisition in female and lactating mice

Once the potential role of astrocytes in modulating and supporting network adaptation following social fear acquisition in male mice was established, I investigated whether these changes occur in LS astrocytes of virgin female and lactating mice. Interestingly, in contrast to male mice, no structural changes were observed in the LSc of virgin female mice (Figure 27). This absence of structural changes in virgin females following social fear acquisition suggests that typical responses observed in male mice could be masked in females by baseline differences in astrocyte density or functionality. The heightened baseline expression of astrocytes in females might provide a buffering capacity that compensates for the rapid adaptation needs observed in males. This phenomenon emphasizes the complexity of astrocytic roles across different physiological states and indicates that female astrocytes may be intrinsically different in their functional response compared to their male counterparts. Recent studies have highlighted sex differences in astrocytic responses to chronic stress, showing increased GFAP immunoreactivity in the PFC and PAG of male animals, while females exhibited decreased GFAP levels in the AMY and CA1 region of the hippocampus (Zhang et al. 2024). In the context of emotional processing, these differential responses may significantly influence how fear is experienced and managed in females, potentially reflecting adaptive mechanisms that have evolved to support social behaviors. For instance, the heightened astrocytic

activity observed in males could suggest a heightened response to stressors, potentially enhancing fear processing and expression. In contrast, the reduced astrocytic activity in key emotional centers in females might facilitate a different approach to emotional regulation, possibly promoting resilience and adaptive social interactions.

In lactating mice, an increase in the domain area of ventral LSc astrocytes was observed after social fear acquisition (Figure 28), suggesting that the physiological state associated with lactation may induce an astrocytic response that differs from that of males. The heightened OXT system present during lactation is particularly relevant, as previous studies have demonstrated OXT effects on astrocytic structure and coverage, especially in regions such as the SON and PVN (Theodosis et al. 1986b; Theodosis et al. 2008; Oliet et al. 2008). This hormonal milieu enhance astrocyte-neuronal communication (Gómora-Arrati et al. 2010; Li et al. 2021), potentially regulating adaptive responses to social fear acquisition, as observed in this study. Interestingly, while OXT signaling within the LS was found to prevent social fear responses in SFC^{+} of lactating mice, the astrocytic involvement in these protective effects remains unknown. The observed uniform distribution of astrocytic OXTR mRNA across the LSc of lactating mice, combined with the increase in astrocytic coverage, may indicate a potential role of astrocytes in the LS in mediating mechanisms associated with social behaviors. Future studies should investigate how astrocytes respond to OXT signaling during lactation, focusing on astrocyte-neuronal communication. Additionally, exploring the roles of astrocytes in shaping social behaviors and emotional responses could provide valuable insights into the neural mechanisms underlying these processes and their implications for social anxiety disorders.

3. Contribution of LSc astrocytes to socio-emotional behaviors

In the past, astrocytes were considered passive support cells but nowadays, their crucial role in synaptic maintenance and neuronal communication (Kofuji and Araque 2021a; Lawal et al. 2022; Shigetomi and Koizumi 2023), as well as in regulating emotional and cognitive processes (Kofuji and Araque 2021a; Shigetomi and Koizumi 2023), has been recognized. Building on the findings from this study, which indicate an astrocytic response with possible impairment of astrocytic function in the LSc after social fear acquisition, I investigated whether disrupting the astrocytic glutamate-glutamine cycle within the LSc using a could influence socio-emotional behaviors. Astrocytic dysfunction was induced by injecting L-AAA, a glutamine synthetase inhibitor into the LSc, impairing the conversion of glutamate into glutamine. This intervention diminished the functional activity of astrocytes, as evidenced by structural changes (McBean 1994; Brown and Kretzschmar 1998), including a reduction in GFAP immunoreactivity (Banasr and Duman 2008; David et al. 2019). The glutamate-glutamine cycle is crucial for maintaining balanced excitatory

neurotransmission, with astrocytes converting glutamate into glutamine via glutamine synthetase (Bak et al. 2006). Given astrocytic essential role in mediating and modulating synaptic plasticity and transmission, a decrease in astrocytic coverage likely impairs neuronal communication and network function. Interestingly, while disrupting glutamate signaling in the LSc did not affect anxiety- and depressive-like behaviors, it did have a significant impact on social behaviors, particularly during social fear extinction and recall.

To assess the impact of astrocytic dysfunction on socio-emotional behaviors, sociability was tested using the SPT, anxiety using the EPM, and depressive-like behaviors using the FST in two doses of L-AAA (Figure 29).

The successful induction of astrocytic dysfunction was confirmed by a greater reduction in GFAP expression at the higher L-AAA dose (25 µg/µl) compared to the vehicle and lower dose (10 µg/µl), which aligns with previous studies (Banasr and Duman 2008; David et al. 2019). However, no significant changes in sociability, novelty-seeking, or anxiety- and depressive-like behaviors were observed in L-AAA-treated male mice compared to the control group (Figure 29). This suggests that astrocytes in the LSc do not directly regulate these specific socio-emotional processes. This finding contrasts with studies showing a depressive-like phenotype following L-AAA application in the prefrontal cortex (PFC), prelimbic cortex, and CA3 of male rats and mice (Banasr and Duman 2008; David et al. 2019; Zhou et al. 2019). However, while the PFC and prelimbic cortex are regions strongly associated with anxiety- and depressive-like behaviors (Codeluppi et al. 2023; Pizzagalli and Roberts 2022; Hare and Duman 2020), the LS is known to be involved in modulating social behaviors and fear processing (Menon et al. 2018; Oliveira et al. 2021; Wirtshafter and Wilson 2021; Menon and Neumann 2023; Grossmann et al. 2024). This suggests that astrocytes within the LS may be more engaged in regulating social fear processes. Supporting this hypothesis, recent findings show that astrocytes adapt differently depending on the mechanism analyzed. For example, while chemogenetic activation of astrocytes in CeA reduced fear expression in a fear-conditioning paradigm in mice (Martin-Fernandez et al. 2017), activation in the hippocampal CA1 region enhanced contextual fear memory (Adamsky and Goshen 2018; Mederos et al. 2019). This indicates that astrocytes have region-specific roles in fear regulation and memory processes and may similarly play a role in modulating social fear within the LS.

3.1. Contribution of LSc astrocytes to socio fear behaviors in male and female mice

To further investigate the role of astrocytes in social fear, I analyzed the effects of L-AAA-induced astrocytic structural depletion in the LSc during SFC paradigm in male and female mice. In male mice, despite the absence of behavioral changes in the sociability and anxiety-related tests,

astrocytic structural depletion in the LSc had a significant impact on social fear behavior (Figure 30). Interestingly, while astrocytic dysfunction did not impair the acquisition of social fear in male mice, it did influence the social behavior during the extinction and recall phases. Specifically, SFC^+ animals treated with L-AAA, exhibiting an astrocytic structural depletion, displayed higher social investigation and reduced vigilance behavior during later exposures to social stimuli compared to Veh/SFC^+ animals. The disruption of the glutamate-glutamine cycle induced by L-AAA led to impaired astrocytic function, as indicated by the depletion of astrocytic structure. Impairments in astrocytic functionality have been linked to disruptions in synaptic transmission and network maintenance (Pannasch et al. 2011; Hardy et al. 2023). This suggests that inhibiting astrocytic ability to convert glutamate into glutamine in the LSc may disrupt synaptic transmission, which might weaken the consolidation of social fear memories and accelerates extinction, alongside reducing vigilance toward social threats during extinction and recall phases. This effect may arise from two factors: i) due to their functional impairment, astrocytes fail to provide the neuronal support required for maintaining synaptic transmission and plasticity, and ii) increased glutamate availability could prolong excitatory transmission, negatively affecting neuronal health in the long term. Interestingly, astrocytic functional adaptation to processes associated with social fear was shown earlier in this thesis by the reduction in Cx43 and EAAT2 protein levels observed in SFC^+ animals after social fear acquisition. Given their role in modulating synaptic transmission (Orellana et al. 2013), alterations in connexin activity and therefore in astrocytic network may affect glutamatergic transmission, which has been linked to anxiety-related disorders (Nasir et al. 2020; Cortese and Phan 2005). Increased glutamate levels have been correlated with the severity of social anxiety symptoms (Phan et al. 2005), highlighting astrocytic regulatory role in glutamatergic transmission, especially through calcium signaling (Kang et al. 2013; Meunier et al. 2017) and connexin hemichannel activity (Stout et al. 2002). Astrocytic plastic morphology and cytoskeletal structures allow them to regulate the diffusion of signaling molecules and metabolites, which are essential in regulating synaptic transmission (Reichenbach et al. 2010; Heller and Rusakov 2015; Zeug et al. 2018). Since impairments in astrocytes are associated with disrupted synaptic transmission (Hardy et al. 2023), L-AAA-induced astrocytic structural depletion, and subsequent dysfunction, likely results in impaired synaptic transmission during social fear processing. This impairment may lead to alterations in social fear memory, as evidenced by decreased vigilance in SFC^+ animals, a critical response to environmental threats (Williams et al. 2020; Steinman et al. 2019). These findings suggest that LSc astrocytes play a prominent role in regulating fear responses, particularly in the consolidation of fear memories and synaptic plasticity, roles that have been demonstrated in other studies (Stehberg et al. 2012; Ostroff et al. 2014; Orellana and Stehberg 2014).

As mentioned above, impairment of the glutamate-glutamine cycle could disrupt not only astrocyte-neuron communication but also the regulation of synaptic transmission itself. The failure to clear

glutamate from the synaptic cleft compromises astrocytic regulatory mechanisms in neural circuits, while the accumulation of glutamate leads to excitotoxicity through the overactivation of NMDA and AMPA receptors (Mark et al. 2001; Verkhratsky 2007). This process triggers excessive calcium influx and a cascade of destructive events, including oxidative stress and damage to cellular structures (Mark et al. 2001; Verkhratsky 2007). During social fear acquisition, such dysfunction could increase neuronal vulnerability, disrupt circuits, and prevent astrocytes from supporting proper synaptic transmission, resulting in abnormal fear responses to social stimuli. The essential role of glutamate in synaptic plasticity processes, such as LTP, are well known. Excessive glutamate could theoretically enhance memory consolidation (Riedel and Reymann 1996; Lüscher and Malenka 2012; Gonçalves-Ribeiro et al. 2019), suggesting that L-AAA-treated animals may form more persistent fear memories, complicating extinction. However, since SFC^+ animals treated with L-AAA displayed reduced fear and vigilance during extinction, it suggests that excessive glutamate during extinction may either: (i) accelerate the consolidation of extinction-related memory processes, which are distinct from those involved in fear memory acquisition, or (ii) promote LTD, a process that weakens previously established synaptic connections (Riedel and Reymann 1996; Lüscher and Malenka 2012) or both processes may occur in parallel. or possibly both processes may occur simultaneously. Indeed, the differing synaptic mechanisms underlying fear conditioning and extinction, where conditioning is linked to LTP and extinction is associated with LTD, synaptic depotentiation, or LTP of inhibitory transmission (Maren 2005; Nabavi et al. 2014; Maren 2015), may also take place in the LSc. Therefore, this may suggest that, in the context of social fear, excessive glutamate did not impair fear acquisition but rather it might have facilitated social fear extinction of, leading to quicker extinction in male mice. Even though no significant morphological or protein-level changes were found after social fear extinction, this study shows that LSc astrocytes are actively involved in regulating the extinction of social fear, a learning process where LS have been found to be involved (Toth et al. 2012; Menon et al. 2018), although nothing was known about astrocytes.

Interestingly, my investigating into astrocyte structural depletion in social fear behavior in female mice (Figure 31) revealed sex differences in the involvement of astrocytes in regulating processes associated with social fear. Unlike males, astrocytic structural depletion induced by L-AAA impaired social fear acquisition in females, as evidenced by the greater number of foot shocks needed to elicit social avoidance behavior. This suggests that impaired clearance of glutamate in females may lead to overactivation of glutamate receptors, promoting LTP processes and making it more challenging to establish fear associations during the acquisition phase. However, in contrast to males, L-AAA did not affect extinction learning or vigilance responses in female SFC^+ mice, as indicated by their consistent investigation times and vigilance behaviors during both extinction and recall. The apparent absence of astrocytic involvement in regulating memory processes associated with the extinction of

social fear in females may be compensated by the higher number of astrocytic cells observed in the LSc of female mice compared to males. This increased astrocyte density might help offset the structural depletion induced by L-AAA, leading to comparable levels of social fear extinction similar to those seen in the vehicle group. Additionally, other compensatory mechanisms and neural circuits, such as in the AMY or HIP, could play crucial roles in restoring synaptic homeostasis and regulating fear learning, thereby compensating for the synaptic transmission dysfunction that may occur following L-AAA treatment. Moreover, the influence of sex hormones, particularly estrogen, must also be considered (McCarthy and Arnold 2011). Estrogen modulates both glutamatergic neurotransmission and astrocytic activity (Mong and Blutstein 2006), potentially influencing LTP and LTD processes during social fear acquisition and extinction. The neuroprotective effects of estrogens might also mitigate the excitotoxic effects of glutamate, explaining the different responses to glutamate dysregulation observed in females compared to males. This could clarify why males experience faster synaptic weakening, while females demonstrate only slight impairments during acquisition without significant behavioral effects in the extinction phase. Thus, estrogen likely plays a key role in shaping these differences by influencing astrocytic function and synaptic transmission (Fuente-Martin et al. 2013; Mong and Blutstein 2006; Crespo-Castrillo and Arevalo 2020)

In summary, these data reveal sex-specific differences in the regulation of fear processes, consistent with my earlier findings of increased astrocytic coverage following social fear acquisition in males but not in females. In males, LSc astrocytes appear to have a more pronounced role in social fear processing, while in females, the regulation of fear learning and extinction relies on other compensatory mechanisms. Additionally, the higher density of astrocytes in females may compensate for the depletion induced by L-AAA, effectively masking the morphological changes that were not observed following social fear acquisition.

4. Effects of social fear acquisition on astrocytic Ca^{2+} activity in the LS of male and female mice

Beyond their established role in the tripartite synapse, astrocytic Ca^{2+} signaling has garnered attention for its influence on neuronal network synchronization (Verkhratsky and Nedergaard 2018). This emerging hypothesis is supported by evidence showing that astrocytic Ca^{2+} activity modulates extracellular glutamate levels, ultimately reducing overall neuronal excitability (Poskanzer and Yuste 2011). Given the activity-dependent nature of astrocyte morphology observed in previous studies (Theodosis et al. 2008; Arizono et al. 2021; Denizot et al. 2022) and based on my prior research demonstrating the regulatory role of astrocytes in social fear processes, including acquisition and extinction, I investigated the extent to which social fear acquisition impacts astrocytic Ca^{2+}

activity within the LSc in male and female mice ex vivo. This research was conducted in collaboration with Dr. Alexander Charlet at the University of Strasbourg (France).

One key finding from this study is the differential baseline astrocytic Ca^{2+} activity observed in SFC^{+} male and female mice (Figure 32-33). Males exhibited higher baseline Ca^{2+} activity, characterized by both increased frequency and amplitude of Ca^{2+} transients, compared to females (Figure 34). This heightened baseline activity in males suggests greater intrinsic astrocytic function, which could enhance synaptic modulation and neurotransmitter clearance, potentially leading to reduced overall neural excitability (Poskanzer and Yuste 2011). Following social fear acquisition, both male and female SFC^{+} mice showed elevated Ca^{2+} activity compared to their SFC^{-} counterparts, aligning with the morphological results in males that indicate astrocytic adaptation to social fear processes. The ability of astrocytic structures to propagate Ca^{2+} signals through gap junctions facilitates intercellular communication within the astrocytic network, supporting synaptic modulation (Pasti et al. 1997; Suadicani et al. 2004; Scemes and Spray 2012; Khakh and McCarthy 2015; Lia et al. 2021). Ca^{2+} signals represent a significant aspect of intercellular communication within the astrocytic network and the interplay between astrocytes and other cells, including neurons (Khakh and McCarthy 2015; Verkhratsky and Nedergaard 2018; Eitelmann et al. 2023). Interestingly, while no structural changes were observed in astrocytes of females following social fear conditioning as shown previously in thesis, they did exhibit increased Ca^{2+} activity (Figure 33). This finding suggests that in female mice, the greater number of astrocytes in the LS may compensate for the lack of structural remodeling, allowing for the maintenance of efficient synaptic transmission and neural network regulation without visible structural changes. Furthermore, the absence of sex differences in Ca^{2+} activity post-social fear acquisition indicates that compensatory mechanisms in females may activate in response to trauma, resulting in elevated astrocytic activity. This phenomenon may represent a "ceiling effect," whereby astrocytic activity reaches its maximum capacity during social fear conditioning, effectively regulating social fear circuits. Hormonal factors, such as estrogen, likely play a role in this effect, as estrogen is known to modulate calcium signaling in both neurons and astrocytes (Zhang et al. 2010; Kuo et al. 2010; Chaban et al. 2004). Indeed, estrogens have been shown to influence social behaviors, including social preference, aggression, and learning and memory for social stimuli (Ervin et al. 2015), as well as fundamental social behaviors like social approach and avoidance in both male and female mice (Choleris et al. 2009; Choleris et al. 2012). Moreover, estrogen enhances astrocytic Ca^{2+} responses and promotes the release of neurotrophic factors (Zhang et al. 2010), potentially explaining the ceiling effect observed in astrocytic activity following social fear conditioning in females. Additionally, the ceiling effect in Ca^{2+} activity after social fear acquisition may elucidate why the impairment of astrocytic function induced by L-AAA did not affect social fear behavior. A recent study identified estrogen receptors (ER), particularly ERβ, in the LSr of male mice, suggesting their involvement in regulating social anxiety behaviors (Hasunuma et al. 2024). Although this study

focused on males, females exhibit higher ERβ expression in the LS (Milner et al. 2010; Zuloaga et al. 2014), implying that estrogen could play an even more pronounced role in female astrocytic activity and social behavior.

Furthermore, given that the LS is a complex brain region with multiple neuropeptide receptors that are known to mediate social behaviors, including OXT, AVP and CRF (Oliveira et al. 2021; Borie et al. 2021; Menon et al. 2022; León Reyes et al. 2023), it is plausible that these neuropeptides also modulate calcium activity in astrocytes. Therefore, I aimed to investigate the effects of astrocytic OXTR following SFC, as the OXT system is known for its profound pro-social and anxiolytic effects, as well as its ability to reduce SFC-induced social fear (Zoicas et al. 2014; Menon et al. 2018; Menon et al. 2022). Although the expression of OXTR in astrocytes of the LS in both sexes has been previously described in thesis, the functional role of astrocytic OXTR in this brain region remains largely unexplored. To address this gap, I examined the astrocytic response via calcium imaging to TGOT, a selective OXTR agonist, and how this response varied between SFC^- and SFC^+ in both male and female mice. In line with previous studies demonstrating OXT-induced intracellular Ca^{2+} increases (Di Scala-Guenot et al. 1994; Wang and Hatton 2007; Wahis et al. 2021), TGOT significantly elevated astrocytic Ca^{2+} activity in both male and female mice (Figure 35-36). Notably, this effect was more pronounced in SFC^+ animals, suggesting that social fear acquisition sensitizes astrocytes to OXT signaling. These results imply that astrocytes may mediate the neuromodulatory effects of OXT in the LSc, particularly in the regulation of fear and anxiety circuits.

Interestingly, sex differences were observed in the astrocytic response to TGOT (Figure 37). In SFC^- males, astrocytic Ca^{2+} activity was higher than in females, despite females exhibiting greater OXTR expression. However, following SFC, the sex differences diminished, with both sexes demonstrating similar astrocytic responses. This finding aligns with the baseline Ca^{2+} activity results, reinforcing the notion that social fear acquisition enhances female astrocytic responsiveness to OXT, potentially due to a ceiling effect. Female mice may require heightened astrocytic activity to adapt to social fear processing, while male astrocytes display consistently elevated activity across conditions. The enhanced global astrocytic Ca^{2+} response to TGOT in females following social fear acquisition (Figure 38) supports the hypothesis that OXT signaling recruits and activates neighboring astrocytes, as previously observed (Wahis et al. 2021). This greater response may stem from the higher density of astrocytes in the LSc of females compared to males, facilitating a more extensive network of astrocytic communication.

Taken together, these findings underscore the importance of astrocytic Ca^{2+} signaling in modulating social fear and OXT-related pathways. Social fear acquisition leads to an increase in astrocytic Ca^{2+} activity in both male and female mice, with females exhibiting a more pronounced response compared to their baseline levels. The heightened Ca^{2+} activity observed in response to TGOT, a

selective OXT receptor agonist, indicates that astrocytes play a mediating role in the effects of OXT on social behavior, particularly by influencing synaptic plasticity and transmission in the LS. Interestingly, the baseline Ca^{2+} activity in females suggests a potential "ceiling effect." This means that female astrocytes may already have elevated activity under normal conditions, which limits the potential for further increases. Consequently, when exposed to social fear conditioning, the overall astrocytic activity in females can show a significant spike compared to males, who exhibit higher baseline activity but less variability across different conditions. In contrast, male astrocytic responses remain consistent without the same level of adaptation.

Given that the increase in astrocytic Ca^{2+} levels is triggered by GPCR activation, regardless of the specific G protein subtype involved (Durkee et al. 2019), future research should focus on examining the effects of OXT agonists such as atosiban or carbetocin, which selectively activate different G protein subtypes (Busnelli and Chini 2018). The rationale for using TGOT in bath applications, rather than OXT, lies in TGOT's specificity for OXTR, whereas OXT can also activate AVP receptors (Chini et al. 2017). Considering that AVP is expressed in the LS (Menon et al. 2022) and that astrocytes also express AVP receptors (Verkhratsky and Nedergaard 2018), the influence of OXT on these receptors cannot be disregarded. To overcome this issue, further investigations could involve optogenetic stimulation of OXT neurons to induce endogenous OXT release within the LS, thereby allowing for a more direct analysis of astrocytic Ca^{2+} activity. Additionally, it would be valuable to explore neuronal excitability in response to astrocytic Ca^{2+} activity. This study currently isolates astrocytic Ca^{2+} responses from neuronal stimulation using tetrodotoxin and assessing the interaction between these two components could provide deeper insights into the functional role of astrocytes in regulating neuronal networks during social fear processes.

5. OXT effects on astrocytic morphology and function in the LS

Finally, I aimed to identify the specific effects of OXT on astrocytes morphology within the LS and the role of astrocytic OXT signaling in regulating social behaviors.

In males, while the functionality of OXTR function has been previously described in this thesis, direct infusion of OXT into the LSc did not result in observable structural changes in astrocytes (Figure 39). This finding contrasts with previous research indicating that OXT can alter the astrocytic cytoskeleton, particularly in regions such as the PVN and SON, where it promotes retraction of astrocytic processes (Langle et al. 2003; Theodosis et al. 1986a; Theodosis et al. 1986b). Similarly, Meinung et al. (*in revision*) reported an increased spatial relationship between astrocytes and neurons in OXT-treated hippocampal slices, potentially facilitating new synapse formation, as seen in the

HYP (Hatton et al. 1984). Although no changes in astrocyte morphology were observed in this study, calcium imaging revealed functional astrocytic OXTR in the LSc of male mice, suggesting that astrocytes in this region are responsive to OXT despite the lack of visible structural remodeling. One possible explanation for the absence of cytoskeletal changes could be the region-specific differences in their responsiveness to OXT, as well as variations in the doses of OXT used or the timing of structural reorganization. Structural alterations may necessitate sustained OXT signaling or longer observation periods than those utilized in this experiment (10 minutes post-infusion). Furthermore, the relatively lower expression of OXTR in the LSc of males compared to females might account for the absence of observable effects on astrocytic morphology. Investigating the effects of OXT infusion on astrocytes in female and lactating mice would be particularly valuable, given that OXT has been shown to influence astrocytic morphology in the PVN and SON, especially during periods of heightened OXT activity such as lactation (Theodosis et al. 1986a; Theodosis et al. 1986b). In these regions, OXT is known to induce the retraction of astrocytic processes and enhance neuronal-somata contacts, thereby reshaping synapses (Langle et al. 2003; Theodosis et al. 1986a; Theodosis et al. 1986b).

Given the functional OXTR activity demonstrated by Ca^{2+} imaging in both male and female mice, and the increased responsiveness after social fear acquisition, I further explored astrocytic OXT signaling by downregulating OXTR mRNA expression in LSc astrocytes to examine its role in social fear behaviors in both sexes (Figure 40-41). The OXTR was knocked down in astrocytes of male and female mice using the AAV6-GFAP-Oxtr-mCherry-shRNA construct. The results indicated a more successful knockdown of Oxtr mRNA in females, likely attributable to their higher baseline OXTR expression levels. In contrast, the already low baseline expression of OXTR in the LSc of males may have limited the effectiveness of the knockdown in this sex. Interestingly, astrocytic OXTR knockdown did not impact social fear acquisition in either males or females, indicating that astrocytic OXT signaling may not play a direct role in the initial consolidation of social fear memory. In line with this, both Oxtr shRNA-treated males and females exhibited reduced investigation time during the initial exposure to social stimuli in the extinction phase, akin to their respective controls, suggesting successful acquisition of social trauma memory in both sexes.

During the extinction phase, both male and female SFC^{+}/Oxtr shRNA animals displayed an accelerated extinction curve compared to their controls (SFC^{+}/scrRNA). This reduction in social fear was accompanied by a trend toward increased social approach and decreased vigilance behaviors in the later phases of extinction among SFC+/Oxtr shRNA animals. Notably, during the recall phase, female SFC+/Oxtr shRNA animals showed longer investigation times compared to SFC^{-}/Oxtr shRNA animals, indicating that astrocytic OXTR knockdown in females had a more pronounced effect in facilitating social fear extinction and reducing vigilance responses.

The more significant impact of OXTR knockdown on social behavior in female mice compared to males may stem from the more effective knockdown of OXTR mRNA expression in females. Reduced astrocytic OXT signaling appeared to facilitate a faster extinction of social fear by diminishing astrocytes' ability to support synaptic plasticity in fear-related circuits. Given that astrocytes are crucial for synaptic transmission and memory consolidation, the knockdown of OXTR in these cells could lead to decreased synaptic support and impaired plasticity, thereby promoting the extinction of social fear. However, these findings challenge the well-established view of OXT as a prosocial neuropeptide during the extinction process, where OXT in the LS has been associated with reduced fear and enhanced social behaviors (Zoicas et al. 2014; Menon et al. 2018). Although OXT is typically recognized for its prosocial effects, some studies indicate that it can increase social anxiety under specific conditions (Steinman et al. 2019). This dual role of OXT in both anxiolytic and anxiogenic processes complicates the interpretation of its effects on astrocytic signaling.

Moreover, sex differences in OXT signaling must be considered. Males and females express OXTR at different levels (Dumais and Veenema 2016), and OXTR signaling may vary between sexes. For instance, OXTR agonists infused in the VTA decreased social place preference in females but increased it in males whereas OXTR signaling might vary between sexes. For example, OXTR agonists infused in the VTA decreased social place preference in females but increased it in males (Borland et al. 2019; Steinman et al. 2019). These sex-specific effects may explain why female mice exhibited a more substantial prosocial effect following astrocytic OXTR knockdown, showing increased social investigation and faster extinction of social fear compared to males. Astrocytes are vital for regulating synaptic transmission and modulating higher cognitive functions and behaviors across species, especially in vertebrates, where they maintain CNS homeostasis. While previous studies have shown that astrocytic OXT signaling mediates anxiolytic effects in the CeA and PVN (Wahis et al. 2021), our findings suggest that reduced astrocytic OXT signaling in the LS facilitates a prosocial approach toward conspecifics, underscoring the complexity of OXT role in social behavior. These results reinforce the notion that OXT has both anxiolytic (Knobloch et al. 2012; Blume et al. 2008; Domes et al. 2007; van den Burg et al. 2015) and anxiogenic (Eckstein et al. 2014; Martinon et al. 2019; Nasanbuyan et al. 2018) effects, though the precise mechanism underlying these effects in both neurons and astrocytes remain unclear.

In conclusion, this study demonstrates that astrocytic OXT signaling plays a significant role in regulating social behaviors during the extinction of social fear. The reduction of astrocytic OXTR signaling facilitated faster extinction, suggesting a diminished capacity for astrocytes to maintain synaptic plasticity, particularly in circuits associated with social fear. These findings highlight the complexity of OXT signaling in astrocytes and suggest that the balance between anxiolytic and anxiogenic effects may differ based on sex, brain region, and behavioral context. Future research

should continue to explore how astrocytes modulate synaptic plasticity and behavior in response to OXT and other neuropeptides, especially within fear and anxiety-related circuits.

6. Conclusion and future perspectives

The present study provides novel insights into the involvement of astrocytes in socio-emotional behaviors, focusing on their role in social fear acquisition and extinction, particularly in the context of OXT signaling within the LS. Traditionally viewed as passive support cells, astrocytes have now emerged as active regulators of synaptic plasticity, neurotransmission, and emotional processing. This research demonstrates their pivotal role in modulating fear-related behaviors through sex-specific mechanisms, highlighting the functional heterogeneity of astrocytes in the LS across different brain regions.

The key findings suggest that astrocytes contribute differently to social fear acquisition and extinction in male and female mice. In males, astrocytes exhibit structural changes and increased Ca^{2+} signaling in response to social fear acquisition, particularly in the LSc and HIP. The observed astrocytic reorganization in males likely reflects their involvement in synaptic plasticity and memory consolidation. In females, despite a lack of detectable structural changes, astrocytes demonstrate elevated baseline Ca^{2+} activity, suggesting a "ceiling effect" where heightened astrocytic activity is induced by social fear acquisition. This effect is particularly pronounced during the extinction phase, indicating sex-specific astrocytic adaptation to social fear.

Additionally, the study underscores the importance of OXT signaling in astrocytes, particularly $OXTR^{+}$ astrocytes in the LSc, in modulating social behavior. The expression of OXTR in astrocytes is higher in females than in males, and OXTR knockdown experiments revealed that reducing astrocytic OXT signaling accelerates social fear extinction, with females exhibiting more pronounced effects. This suggests that astrocytic OXT signaling may play a more significant role in regulating social fear processing in females, potentially influenced by hormonal factors such as estrogen.

The results also reveal that astrocytic dysfunction, particularly impairments in the glutamate-glutamine cycle, impacts social fear extinction and recall. Disrupting astrocytic glutamate signaling in male mice leads to faster extinction of social fear, potentially due to weakened astrocytic support for synaptic plasticity. However, this effect was not observed in females, suggesting that different compensatory mechanisms, recruiting brain regions such as HIP or AMY, may regulate fear extinction in females.

These findings open several avenues for future research, particularly in understanding the role of astrocytes in emotional regulation and social behavior. Below are key areas for further investigation:

1. Sex-Specific Mechanisms in Astrocytic Function

The sex differences observed in astrocytic responses to social fear acquisition and extinction, particularly in relation to Ca^{2+} activity and OXT signaling, warrant further investigation. Future studies should investigate the molecular mechanisms underlying these sex differences, with a focus on how sex hormones like estrogen influence astrocytic function. Understanding these hormonal effects on astrocytes, particularly in different stages of the estrous cycle, will reveal insights on the sex-specific regulation of social behaviors and emotional processing.

Further research could also explore the influence of sex hormones on the astrocytic-neuronal interaction during emotional processing, which may help explain the different responses seen in males and females during social fear extinction.

2. Astrocytes in Long-Term Memory and Fear Processing

While this study focused on short-term responses to social fear acquisition and extinction, future investigations should examine how astrocytes contribute to long-term memory consolidation and retrieval in the context of social fear and whether these effects differ by sex.

The role of astrocytes in fear-related circuits, particularly in the context of synaptic plasticity and network maintenance, still remains unknown. Specifically, how astrocytic dysfunction might influence the persistence of fear memories and how targeting astrocytic functions might enhance therapies for conditions like SAD.

3. Oxytocin's Dual Role in Social and Emotional Regulation

In this study I demonstrated that reduced astrocytic OXTR signaling facilitated social fear extinction behavior, highlighting the dual role of oxytocin (OXT) in exerting both anxiolytic and anxiogenic effects. These findings underscore the need for further research to unravel the complex interactions between OXT signaling in astrocytes and its broader influence on anxiety and emotional regulation.

Future studies should aim to clarify the precise mechanisms by which OXT signaling influences astrocytic functions including synaptic plasticity, neurotransmitter release, and neuronal excitability, particularly in circuits related to fear, anxiety, and social behaviors. Understanding the balance between OXT's anxiolytic and anxiogenic effects will be crucial for developing therapeutic interventions targeting OXT pathways in emotional disorders.

4. Astrocyte-Neuron Communication and Network Regulation

The present study highlights the importance of astrocytic Ca^{2+} signaling and glutamate-glutamine cycling in regulating synaptic transmission and emotional processing. However, the full extent of astrocyte-neuron communication, particularly through gap junctions and connexins, remains to be explored. In particular, how astrocytes coordinate network activities in fear learning and extinction circuits, with particular attention to the role of connexins such as Cx43 and Cx30 in astrocytic communication and synaptic plasticity.

Hereby, the specific pathway of how astrocytes regulate the balance between excitatory and inhibitory signaling in neural circuits, particularly in the LS, HIP, and AMY, is crucial to understanding how astrocytic dysfunction contributes to emotional disorders.

The findings of this study suggest that astrocytic dysfunction, particularly in the glutamate-glutamine cycle, can impair social fear extinction and recall. Given the growing recognition of astrocytes as key regulators of emotional processing, targeting astrocytic functions may offer novel therapeutic approaches for treating anxiety disorders, depression, and other emotional disorders.

- Carl-Philipp Meinung, **Laura Boi**, Sareh Pandamooz, David Mazaud, Grégory Ghézali, Nathalie Rouach, Inga D. Neumann, in revision in *Molecular Psychiatry*. "OXTR-mediated signaling in astrocytes contributes to anxiolysis".

- **Laura Boi**, Rohit Menon, Barbara Dei Benedetto, 2024 "Astrocyte morphological adaptations in a mouse model of social anxiety disorders". https://doi.org/10.20944/preprints202409.1333.v1

Here, I would like to express my heartfelt gratitude to all the people who, in one way or another, have been part of this journey. This PhD and thesis would not have been possible without your support. I will always be grateful for your presence in my life, and I will never forget you.

First and foremost, I would like to thank my supervisor, Prof. Dr. Inga D. Neumann, for the invaluable opportunity to work in her lab. Over these past four years, I have grown both scientifically and personally, and I owe much of that to her. Scientifically, she has provided numerous opportunities to enhance my scientific skills, from attending conferences and organizing events, to conducting experiments abroad, and entrusting me with responsibilities. Her constant encouragement and challenges pushed me beyond my limits and helped me evolve into a mature PhD student. On a personal level, she has been a source of endless energy, inspiring me to seek new motivations and ways to persevere. When I arrived, I was uncertain of my path, and Inga, I am deeply grateful to you for illuminating the way.

I would also like to thank my mentor, Dr. Barbara Di Benedetto, for the countless scientific discussions and her uncountable support from the very beginning of my PhD. She helped me navigate the challenges of this journey, pushing me to keep going. Thank you, Barbara, for always believing in me, even when I didn't believe in myself. I could not have wished for a better mentor.

A special thank you to Prof. Dr. Oliver Bosch for all his support throughout these four years. His helpful and encouraging attitude has greatly aided me in so many aspects of my PhD, even before I officially started. Thank you, Oliver, for always being available and ready to assist with everything. Sincerely, this PhD would not have gone as smoothly without you.

I would also like to express my gratitude to Prof. Dr. Valery Grinevich for being my mentor and for his scientific support.

A big thank you to Dr. Alexander Charlet for giving me the opportunity to conduct part of my experiments in his lab in Strasbourg. I thoroughly enjoyed my time there, and I also want to thank Clémence and Kai for both your scientific support and the wonderful time we shared.

I also want to thank to Dr. Rohit Menon for his continuous support throughout my PhD. I enjoyed our scientific discussions, and I deeply appreciated your encouragement in helping me push through challenges. Your support, both scientifically and personally, was invaluable in reaching this milestone.

I would also like to thank my colleagues, Dr. Katharina Gryksa-Zotz, Dr. Theresa Schäfer, Dr. Melanie Royer, and Dr. Carl Meinung, for their constant help and support throughout the PhD. I couldn't have done it without your scientific collaboration.

I am grateful to Dr. Anna Bludau, Dr. Virginie Rappeneau, and Dr. Fernando Castillo-Diaz for always being available for scientific discussions. A special thank you to Dr. Luisa Demarchi, Dr. Tobias Pohl, Dr. Cindy Grossman, Alice Sanson, Dr. Eugenia Vivi, and Dr. Nadia Falhani for their support at the beginning and throughout my entire PhD. I am also thankful to our technicians, Andrea, Rodrigue, and Martina. Thank you, Rodrigue, for always bringing positivity and your smile to the

lab, and Martina, for your contagious energy. A big thank you to Tanja and Eva, our wonderful secretaries, who helped me navigate the endless bureaucracy from the very beginning. I appreciate everything you've done.

To my amazing officemates, Kathi, Lilith, Melanie R., Ivaldo, Elena, Stefanie, Melanie K. Patrick, and Nina, thank you for just being wonderful. I couldn't have asked for better office companions, especially since you had to deal with my constant "Italian" manners. Thank you for always being patient and kind.

I would also like to thank my students, Julia Gärtig, Johannes Muenderlein, Dilara Bekdas, Judith Nerb and Carina Koelbl for the great work you have done. Julia, you are a truly wonderful person, and I will never forget you.

A special thank you to the PhD students of the GRK 2174, Eugenia, Luisa, Theresa, Nadia, Anna, Leopold, Atefeh, Iseline, and Philipp, for being such an amazing group. I thoroughly enjoyed all the time we spent together.

A sincere thank you to all the members of the Neumann and Egger labs for the nice time spent together. Thanks, Haji, Michael, Esteban, Manon, Nicolas, and Mohammed, for being a breath of fresh air in the cloudy days typical of Regensburg.

A heartfelt thank you to my "German family" here in Regensburg: Theresa, Max, little Niklas, Kathi, Tobi, little Elias, and Lilith. Thank you for welcoming me into your family as one of your own. I can't express what you all have meant to me during these years. Theresa and Kathi, thank you for always being there in every situation, for challenging me, supporting me, motivating me, and being my german big sisters. I will always love you.

A huge thank you to my Italian-Argentinian-Japanese-German friends, Luisa, Alice, Luca, Eugenia, Fernando, Pablo, Haji, and Isa, for being amazing during these four years. We shared so a wonderful time together. You were always by my side and I couldn´t have done it without you.

Finally, I also want to thank Christian, Nicolas L., Laura S., Laure, Vini, Marianella, Kassandra, Alan, Kathi, Munni, Emma, Clara and Stefano. You have all been part of my journey in one way or another, making it brighter, more fun, and better in every way. I am grateful to have met you and to have shared some of my best memories with you.

Grazie di cuore a Luisa e Alice per esserci state sempre, in ogni momento, sia buio che luminoso, nei miei momenti difficili e in quelli felici. Qualunque distanza ci separerà, ci ritroveremo sempre. Vi voglio bene.

Un grazie speciale ai miei amici sardi-tedeschi Ale, Giò, Luca, Sofia, la piccola Alba, Alessio e Lisa per avermi accolto e per aver creato un'amicizia indissolubile. Con voi ho respirato aria di Sardegna, di casa dolce casa. Ale, sei stata la mia àncora, quella che mi ha tenuta salda nel mezzo della tempesta.

Grazie ai miei amici Sonia, Alice, Madda, Silvia, Ilaria e Daniele che rappresentano quel filo invisibile che mi riporta sempre alle mie origini e ai ricordi unici della mia infanzia e adolescenza. Grazie per essere semplicemente voi.

Un grazie a Enzo, Sofia, Marina e Sabrina per avermi sempre accolta e fatta sentire una di voi. Marina e Sofia, siete la mia luce e vi voglio un bene dell'anima.

Un ringraziamento speciale va a mia madrina e padrino, Delfina e Giulio, per essere stati sempre presenti e avermi sostenuto in ogni passo sin dalla nascita. La vostra presenza nella mia vita è inestimabile.

Grazie a tutti gli altri familiari e amici che sono sempre stati nei miei pensieri, motivandomi a non mollare.

Infine, un grazie che viene dal profondo del cuore va alla mia famiglia. Ho sempre detto che non esistono distanze abbastanza lontane da separare le persone che si amano. Potremo essere lontani, ma non ci perdiamo mai. Io, soprattutto, non mi perdo, perché siete voi i miei punti cardinali. Grazie papà, per essere il mio est, quel porto sicuro in cui trovo sempre serenità, affetto, protezione e pace interiore, dove posso sempre sentirmi sempre bambina. Grazie mamma, per essere il mio ovest, dove ogni sfida diventa avventura e rischio, e dove istinto e razionalità si alternano in una continua danza di estroversione. Grazie Giulio, per essere il mio nord, dove nel freddo riesco sempre a sentire una calda fiamma e dove i limiti diventano fattibili, superabili e portano sempre con se un pizzico di avventura. E grazie a te, Fiamma, a Marcello e ai piccoli Diego e Mirko, per essere il mio sud: quel luogo caldo e accogliente in cui vorrei rifugiarmi ogni volta per dimenticare il resto del mondo, dove ogni pensiero negativo svanisce. Non ci sono parole per descrivere ciò che rappresentate per me e nella mia vita. Grazie per esserci sempre stati, per avermi sostenuto, capito e amato.

Grazie.

References

Acarturk, C.; Cuijpers, P.; van Straten, A.; Graaf, R. de (2009): Psychological treatment of social anxiety disorder: a meta-analysis. In *Psychological medicine* 39 (2), pp. 241–254. DOI: 10.1017/S0033291708003590.

Adamsky, Adar; Goshen, Inbal (2018): Astrocytes in Memory Function: Pioneering Findings and Future Directions. In *Neuroscience* 370, pp. 14–26. DOI: 10.1016/j.neuroscience.2017.05.033.

Adamsky, Adar; Kol, Adi; Kreisel, Tirzah; Doron, Adi; Ozeri-Engelhard, Nofar; Melcer, Talia et al. (2018): Astrocytic Activation Generates De Novo Neuronal Potentiation and Memory Enhancement. In *Cell* 174 (1), 59-71.e14. DOI: 10.1016/j.cell.2018.05.002.

Aguado, Fernando; Espinosa-Parrilla, Juan F.; Carmona, María A.; Soriano, Eduardo (2002): Neuronal activity regulates correlated network properties of spontaneous calcium transients in astrocytes in situ. In *The Journal of neuroscience: the official journal of the Society for Neuroscience* 22 (21), pp. 9430–9444. DOI: 10.1523/JNEUROSCI.22-21-09430.2002.

Albert, D. J.; Chew, G. L. (1980): The septal forebrain and the inhibitory modulation of attack and defense in the rat. A review. In *Behavioral and neural biology* 30 (4), pp. 357–388. DOI: 10.1016/S0163-1047(80)91247-9.

Allen, Nicola J.; Lyons, David A. (2018): Glia as architects of central nervous system formation and function. In *Science (New York, N.Y.)* 362 (6411), pp. 181–185. DOI: 10.1126/science.aat0473.

Alonso, Jordi; Liu, Zhaorui; Evans-Lacko, Sara; Sadikova, Ekaterina; Sampson, Nancy; Chatterji, Somnath et al. (2018): Treatment gap for anxiety disorders is global: Results of the World Mental Health Surveys in 21 countries. In *Depression and anxiety* 35 (3), pp. 195–208. DOI: 10.1002/da.22711.

Althammer, Ferdinand; Grinevich, Valery (2017): Diversity of oxytocin neurons: beyond magno- and parvocellular cell types? In *Journal of neuroendocrinology*. DOI: 10.1111/jne.12549.

Althammer, Ferdinand; Krause, Eric G.; Kloet, Anette D. de; Smith, Justin; Grinevich, Valery; Charlet, Alexandre; Stern, Javier E. (2022a): Identification and three-dimensional reconstruction of oxytocin receptor expressing astrocytes in the rat and mouse brain. In *STAR protocols* 3 (1), p. 101160. DOI: 10.1016/j.xpro.2022.101160.

Althammer, Ferdinand; Roy, Ranjan K.; Lefevre, Arthur; Najjar, Rami S.; Schoenig, Kai; Bartsch, Dusan et al. (2022b): Altered PVN-to-CA2 hippocampal oxytocin pathway and reduced number of oxytocin-receptor expressing astrocytes in heart failure rats. In *Journal of neuroendocrinology* 34 (7), e13166. DOI: 10.1111/jne.13166.

Althammer, Ferdinand; Wimmer, Moritz Claudius; Krabichler, Quirin; Küppers, Stephanie; Schimmer, Jonas; Fröhlich, Henning et al. (2022c): Analysis of the hypothalamic oxytocin

system and oxytocin receptor-expressing astrocytes in a mouse model of Prader-Willi syndrome. In *Journal of neuroendocrinology* 34 (12), e13217. DOI: 10.1111/jne.13217.

Anderson, C. M.; Swanson, R. A. (2000): Astrocyte glutamate transport: review of properties, regulation, and physiological functions. In *Glia* 32 (1), pp. 1–14. PMID: 10975906.

Araque, A.; Parpura, V.; Sanzgiri, R. P.; Haydon, P. G. (1999): Tripartite synapses: glia, the unacknowledged partner. In *Trends in neurosciences* 22 (5), pp. 208–215. DOI: 10.1016/S0166-2236(98)01349-6.

Araque, Alfonso; Carmignoto, Giorgio; Haydon, Philip G.; Oliet, Stéphane H. R.; Robitaille, Richard; Volterra, Andrea (2014): Gliotransmitters travel in time and space. In *Neuron* 81 (4), pp. 728–739. DOI: 10.1016/j.neuron.2014.02.007.

Arizono, Misa; Bancelin, Stéphane; Bethge, Philipp; Chéreau, Ronan; Idziak, Agata; Inavalli, V.V.G. Krishna et al. (2021): Nanoscale imaging of the functional anatomy of the brain. In *Neuroforum* 0 (0), Article 000010151520210004. DOI: 10.1515/nf-2021-0004.

Asher, Maya; Asnaani, Anu; Aderka, Idan M. (2017): Gender differences in social anxiety disorder: A review. In *Clinical psychology review* 56, pp. 1–12. DOI: 10.1016/j.cpr.2017.05.004.

Bak, Lasse K.; Schousboe, Arne; Waagepetersen, Helle S. (2006): The glutamate/GABA-glutamine cycle: aspects of transport, neurotransmitter homeostasis and ammonia transfer. In *Journal of neurochemistry* 98 (3), pp. 641–653. DOI: 10.1111/j.1471-4159.2006.03913.x.

Baldwin, Katherine T.; Murai, Keith K.; Khakh, Baljit S. (2024): Astrocyte morphology. In *Trends in cell biology* 34 (7), pp. 547–565. DOI: 10.1016/j.tcb.2023.09.006.

Bale, T. L.; Davis, A. M.; Auger, A. P.; Dorsa, D. M.; McCarthy, M. M. (2001): CNS region-specific oxytocin receptor expression: importance in regulation of anxiety and sex behavior. In *The Journal of neuroscience: the official journal of the Society for Neuroscience* 21 (7), pp. 2546–2552. DOI: 10.1523/JNEUROSCI.21-07-02546.2001.

Bale, Tracy L.; Epperson, C. Neill (2015): Sex differences and stress across the lifespan. In *Nature neuroscience* 18 (10), pp. 1413–1420. DOI: 10.1038/nn.4112.

Ballabh, Praveen; Braun, Alex; Nedergaard, Maiken (2004): The blood-brain barrier: an overview: structure, regulation, and clinical implications. In *Neurobiology of disease* 16 (1), pp. 1–13. DOI: 10.1016/j.nbd.2003.12.016.

Balon, Richard; Starcevic, Vladan (2020): Role of Benzodiazepines in Anxiety Disorders. In *Advances in experimental medicine and biology* 1191, pp. 367–388. DOI: 10.1007/978-981-32-9705-0_20.

Banasr, Mounira; Duman, Ronald S. (2008): Glial loss in the prefrontal cortex is sufficient to induce depressive-like behaviors. In *Biological psychiatry* 64 (10), pp. 863–870. DOI: 10.1016/j.biopsych.2008.06.008.

Bandelow, Borwin (2020): Current and Novel Psychopharmacological Drugs for Anxiety Disorders. In *Advances in experimental medicine and biology* 1191, pp. 347–365. DOI: 10.1007/978-981-32-9705-0_19.

Bartheld, Christopher S. von; Bahney, Jami; Herculano-Houzel, Suzana (2016): The search for true numbers of neurons and glial cells in the human brain: A review of 150 years of cell counting. In *The Journal of comparative neurology* 524 (18), pp. 3865–3895. DOI: 10.1002/cne.24040.

Bartz, Jennifer A.; Zaki, Jamil; Ochsner, Kevin N.; Bolger, Niall; Kolevzon, Alexander; Ludwig, Natasha; Lydon, John E. (2010): Effects of oxytocin on recollections of maternal care and closeness. In *Proceedings of the National Academy of Sciences of the United States of America* 107 (50), pp. 21371–21375. DOI: 10.1073/pnas.1012669107.

Baudon, Angel; Clauss-Creusot, Etienne; Darbon, Pascal; Patwell, Ryan; Grinevich, Valery; Charlet, Alexandre (2022): Calcium imaging and BAPTA loading of amygdala astrocytes in mouse brain slices. In *STAR protocols* 3 (1), p. 101159. DOI: 10.1016/j.xpro.2022.101159.

Bazargani, Narges; Attwell, David (2016): Astrocyte calcium signaling: the third wave. In *Nature neuroscience* 19 (2), pp. 182–189. DOI: 10.1038/nn.4201.

Beatty, W. W.; Beatty, P. A. (1970): Hormonal determinants of sex differences in avoidance behavior and reactivity to electric shock in the rat. In *Journal of comparative and physiological psychology* 73 (3), pp. 446–455. DOI: 10.1037/h0030216.

Belzung, Catherine; Lemoine, Maël (2011): Criteria of validity for animal models of psychiatric disorders: focus on anxiety disorders and depression. In *Biology of mood & anxiety disorders* 1 (1), p. 9. DOI: 10.1186/2045-5380-1-9.

Bender, Christian Luis; Calfa, Gastón Diego; Molina, Víctor Alejandro (2017): Effects of Emotional Stress on Astrocytes and Their Implications in Stress-Related Disorders. In Pascual Ángel Gargiulo, Humberto Luis Mesones-Arroyo (Eds.): Psychiatry and Neuroscience Update - Vol. II. Cham: Springer International Publishing, pp. 119–133. DOI: 10.1007/978-3-319-53126-7_10.

Bernardinelli, Yann; Muller, Dominique; Nikonenko, Irina (2014): Astrocyte-synapse structural plasticity. In *Neural plasticity* 2014, p. 232105. DOI: 10.1155/2014/232105.

Besnard, Antoine; Gao, Yuan; TaeWoo Kim, Michael; Twarkowski, Hannah; Reed, Alexander Keith; Langberg, Tomer et al. (2019): Dorsolateral septum somatostatin interneurons gate mobility to calibrate context-specific behavioral fear responses. In *Nature neuroscience* 22 (3), pp. 436–446. DOI: 10.1038/s41593-018-0330-y.

Besnard, Antoine; Miller, Samara M.; Sahay, Amar (2020): Distinct Dorsal and Ventral Hippocampal CA3 Outputs Govern Contextual Fear Discrimination. In *Cell reports* 30 (7), 2360-2373.e5. DOI: 10.1016/j.celrep.2020.01.055.

Biagianti, Bruno; Foti, Giuseppe; Di Liberto, Asia; Bressi, Cinzia; Brambilla, Paolo (2023): CBT-informed psychological interventions for adult patients with anxiety and depression symptoms:

A narrative review of digital treatment options. In *Journal of affective disorders* 325, pp. 682–694. DOI: 10.1016/j.jad.2023.01.057.

Blume, Annegret; Bosch, Oliver J.; Miklos, Sandra; Torner, Luz; Wales, Lynn; Waldherr, Martin; Neumann, Inga D. (2008): Oxytocin reduces anxiety via ERK1/2 activation: local effect within the rat hypothalamic paraventricular nucleus. In *The European journal of neuroscience* 27 (8), pp. 1947–1956. DOI: 10.1111/j.1460-9568.2008.06184.x.

Borie, Amélie M.; Dromard, Yann; Guillon, Gilles; Olma, Aleksandra; Manning, Maurice; Muscatelli, Françoise et al. (2021): Correction of vasopressin deficit in the lateral septum ameliorates social deficits of mouse autism model. In *The Journal of clinical investigation* 131 (2). DOI: 10.1172/JCI144450.

Borland, Johnathan M.; Rilling, James K.; Frantz, Kyle J.; Albers, H. Elliott (2019): Sex-dependent regulation of social reward by oxytocin: an inverted U hypothesis. In *Neuropsychopharmacol* 44 (1), pp. 97–110. DOI: 10.1038/s41386-018-0129-2.

Bourne, A. R.; Mohan, G.; Stone, M. F.; Pham, M. Q.; Schultz, C. R.; Meyerhoff, J. L.; Lumley, L. A. (2013): Olfactory cues increase avoidance behavior and induce Fos expression in the amygdala, hippocampus and prefrontal cortex of socially defeated mice. In *Behavioural brain research* 256, pp. 188–196. DOI: 10.1016/j.bbr.2013.08.020.

Bracha, H. Stefan (2004): Freeze, flight, fight, fright, faint: adaptationist perspectives on the acute stress response spectrum. In *CNS spectrums* 9 (9), pp. 679–685. DOI: 10.1017/s1092852900001954.

Brown, D. R.; Kretzschmar, H. A. (1998): The glio-toxic mechanism of alpha-aminoadipic acid on cultured astrocytes. In *Journal of neurocytology* 27 (2), pp. 109–118. DOI: 10.1023/A:1006947322342.

Busch, Fredric N. (2024): Psychodynamic Approaches to Social Anxiety Disorder. In Christos Charis, Georgia Panayiotou (Eds.): Anxiety Disorders and Related Conditions. Cham: Springer Nature Switzerland, pp. 141–153. DOI: 10.1007/978-3-031-56798-8

Busnelli, Marta; Chini, Bice (2018): Molecular Basis of Oxytocin Receptor Signalling in the Brain: What We Know and What We Need to Know. In *Current topics in behavioral neurosciences* 35, pp. 3–29. DOI: 10.1007/7854_2017_6.

Calandreau, Ludovic; Jaffard, Robert; Desmedt, Aline (2007): Dissociated roles for the lateral and medial septum in elemental and contextual fear conditioning. In *Learning & memory (Cold Spring Harbor, N.Y.)* 14 (6), pp. 422–429. DOI: 10.1101/lm.531407.

Campion, D. R.; Olson, J. C.; Topel, D. G.; Christian, L. L.; Kuhlers, D. L. (1975): Mitochondrial traits of muscle from stress-susceptible pigs. In *Journal of animal science* 41 (5), pp. 1314–1317. DOI: 10.2527/jas1975.4151314x.

Cannon, Walter B. (Ed.) (1915): Bodily changes in pain, hunger, fear and rage: An account of recent researches into the function of emotional excitement. New York: D Appleton & Company. PMCID: PMC5138305.

Carter, c. (2007): Sex differences in oxytocin and vasopressin: Implications for autism spectrum disorders? In *Behavioural brain research* 176 (1), pp. 170–186. DOI: 10.1016/j.bbr.2006.08.025.

Chaban, Victor V.; Lakhter, Alexander J.; Micevych, Paul (2004): A membrane estrogen receptor mediates intracellular calcium release in astrocytes. In *Endocrinology* 145 (8), pp. 3788–3795. DOI: 10.1210/en.2004-0149.

Charles, A. C.; Merrill, J. E.; Dirksen, E. R.; Sanderson, M. J. (1991): Intercellular signaling in glial cells: calcium waves and oscillations in response to mechanical stimulation and glutamate. In *Neuron* 6 (6), pp. 983–992. DOI: 10.1016/0896-6273(91)90238-U.

Charmandari, Evangelia; Tsigos, Constantine; Chrousos, George (2005): Endocrinology of the stress response. In *Annual review of physiology* 67, pp. 259–284. DOI: 10.1146/annurev.physiol.67.040403.120816.

Chever, Oana; Lee, Chun-Yao; Rouach, Nathalie (2014): Astroglial connexin43 hemichannels tune basal excitatory synaptic transmission. In *The Journal of neuroscience : the official journal of the Society for Neuroscience* 34 (34), pp. 11228–11232. DOI: 10.1523/JNEUROSCI.0015-14.2014.

Chini, Bice; Verhage, Matthijs; Grinevich, Valery (2017): The Action Radius of Oxytocin Release in the Mammalian CNS: From Single Vesicles to Behavior. In *Trends in pharmacological sciences* 38 (11), pp. 982–991. DOI: 10.1016/j.tips.2017.08.005.

Cho, Maeng Je; Kim, Jang-Kyu; Jeon, Hong Jin; Suh, Tongwoo; Chung, In-Won; Hong, Jin Pyo et al. (2007): Lifetime and 12-month prevalence of DSM-IV psychiatric disorders among Korean adults. In *The Journal of nervous and mental disease* 195 (3), pp. 203–210. DOI: 10.1097/01.nmd.0000243826.40732.45.

Cho, Woo-Hyun; Noh, Kyungchul; Lee, Byung Hun; Barcelon, Ellane; Jun, Sang Beom; Park, Hye Yoon; Lee, Sung Joong (2022): Hippocampal astrocytes modulate anxiety-like behavior. In *Nature communications* 13 (1), p. 6536. DOI: 10.1038/s41467-022-34201-z.

Choleris, Elena; Clipperton-Allen, Amy E.; Phan, Anna; Kavaliers, Martin (2009): Neuroendocrinology of social information processing in rats and mice. In *Frontiers in neuroendocrinology* 30 (4), pp. 442–459. DOI: 10.1016/j.yfrne.2009.05.003.

Choleris, Elena; Clipperton-Allen, Amy E.; Phan, Anna; Valsecchi, Paola; Kavaliers, Martin (2012): Estrogenic involvement in social learning, social recognition and pathogen avoidance. In *Frontiers in neuroendocrinology* 33 (2), pp. 140–159. DOI: 10.1016/j.yfrne.2012.02.001.

Chrousos, G. P. (1998): Stressors, stress, and neuroendocrine integration of the adaptive response. The 1997 Hans Selye Memorial Lecture. In *Annals of the New York Academy of Sciences* 851, pp. 311–335. DOI: 10.1111/j.1749-6632.1998.tb09006.x.

Chrousos, G. P.; Gold, P. W. (1992): The concepts of stress and stress system disorders. Overview of physical and behavioral homeostasis. In *JAMA* 267 (9), pp. 1244–1252. PMID: 1538563.

Clarkson, Cheryl; Juíz, José M.; Merchán, Miguel A. (2010): Transient Down-Regulation of Sound-Induced c-Fos Protein Expression in the Inferior Colliculus after Ablation of the Auditory Cortex. In *Frontiers in neuroanatomy* 4, p. 141. DOI: 10.3389/fnana.2010.00141.

Codeluppi, S. A.; Xu, M.; Bansal, Y.; Lepack, A. E.; Duric, V.; Chow, M. et al. (2023): Prefrontal cortex astroglia modulate anhedonia-like behavior. In *Molecular psychiatry* 28 (11), pp. 4632–4641. DOI: 10.1038/s41380-023-02246-1.

Cohen, Laurie D.; Zuchman, Rina; Sorokina, Oksana; Müller, Anke; Dieterich, Daniela C.; Armstrong, J. Douglas et al. (2013): Metabolic turnover of synaptic proteins: kinetics, interdependencies and implications for synaptic maintenance. In *PloS one* 8 (5), e63191. DOI: 10.1371/journal.pone.0063191.

Collins, Kerry A.; Westra, Henny A.; Dozois, David J. A.; Burns, David D. (2004): Gaps in accessing treatment for anxiety and depression: challenges for the delivery of care. In *Clinical psychology review* 24 (5), pp. 583–616. DOI: 10.1016/j.cpr.2004.06.001.

Connor, J. R.; Berkowitz, E. M. (1985): A demonstration of glial filament distribution in astrocytes isolated from rat cerebral cortex. In *Neuroscience* 16 (1), pp. 33–44. DOI: 10.1016/0306-4522(85)90044-2.

Corcoran, Kevin A.; Desmond, Timothy J.; Frey, Kirk A.; Maren, Stephen (2005): Hippocampal inactivation disrupts the acquisition and contextual encoding of fear extinction. In *The Journal of neuroscience : the official journal of the Society for Neuroscience* 25 (39), pp. 8978–8987. DOI: 10.1523/JNEUROSCI.2246-05.2005.

Corcoran, Kevin A.; Maren, Stephen (2004): Factors regulating the effects of hippocampal inactivation on renewal of conditional fear after extinction. In *Learning & memory (Cold Spring Harbor, N.Y.)* 11 (5), pp. 598–603. DOI: 10.1101/lm.78704.

Cremers, Henk R.; Roelofs, Karin (2016): Social anxiety disorder: a critical overview of neurocognitive research. In *Wiley interdisciplinary reviews. Cognitive science* 7 (4), pp. 218–232. DOI: 10.1002/wcs.1390.

Crespo-Castrillo, Andrea; Arevalo, Maria-Angeles (2020): Microglial and Astrocytic Function in Physiological and Pathological Conditions: Estrogenic Modulation. In *International journal of molecular sciences* 21 (9). DOI: 10.3390/ijms21093219.

Cruz-Mendoza, Fernando; Jauregui-Huerta, Fernando; Aguilar-Delgadillo, Adriana; García-Estrada, Joaquín; Luquin, Sonia (2022): Immediate Early Gene c-fos in the Brain: Focus on Glial Cells. In *Brain sciences* 12 (6). DOI: 10.3390/brainsci12060687.

Cryan, John F.; Slattery, David A. (2007): Animal models of mood disorders: Recent developments. In *Current opinion in psychiatry* 20 (1), pp. 1–7. DOI: 10.1097/yco.0b013e3280117733.

Dale, H. H. (1909): The Action of Extracts of the Pituitary Body. In *The Biochemical journal* 4 (9), pp. 427–447. DOI: 10.1042/bj0040427.

Dalla, Christina; Shors, Tracey J. (2009): Sex differences in learning processes of classical and operant conditioning. In *Physiology & behavior* 97 (2), pp. 229–238. DOI: 10.1016/j.physbeh.2009.02.035.

Daneman, Richard (2012): The blood-brain barrier in health and disease. In *Annals of neurology* 72 (5), pp. 648–672. DOI: 10.1002/ana.23648.

Daneman, Richard; Prat, Alexandre (2015): The blood-brain barrier. In *Cold Spring Harbor perspectives in biology* 7 (1), a020412. DOI: 10.1101/cshperspect.a020412.

Dantzer, R.; Koob, G. F.; Bluthé, R. M.; Le Moal, M. (1988): Septal vasopressin modulates social memory in male rats. In *Brain research* 457 (1), pp. 143–147. DOI: 10.1016/0006-8993(88)90066-2.

David, J.; Gormley, S.; McIntosh, A. L.; Kebede, V.; Thuery, G.; Varidaki, A. et al. (2019): L-alpha-amino adipic acid provokes depression-like behaviour and a stress related increase in dendritic spine density in the pre-limbic cortex and hippocampus in rodents. In *Behavioural brain research* 362, pp. 90–102. DOI: 10.1016/j.bbr.2019.01.015.

Davidson, J. R.; Hughes, D. L.; George, L. K.; Blazer, D. G. (1993): The epidemiology of social phobia: findings from the Duke Epidemiological Catchment Area Study. In *Psychological medicine* 23 (3), pp. 709–718. DOI: 10.1017/s0033291700025484.

Denizot, Audrey; Arizono, Misa; Nägerl, U. Valentin; Berry, Hugues; Schutter, Erik de (2022): Control of Ca2+ signals by astrocyte nanoscale morphology at tripartite synapses. In *Glia* 70 (12), pp. 2378–2391. DOI: 10.1002/glia.24258.

Derouiche, A.; Frotscher, M. (1991): Astroglial processes around identified glutamatergic synapses contain glutamine synthetase: evidence for transmitter degradation. In *Brain research* 552 (2), pp. 346–350. DOI: 10.1016/0006-8993(91)90103-3.

Di Scala-Guenot, D.; Mouginot, D.; Strosser, M. T. (1994): Increase of intracellular calcium induced by oxytocin in hypothalamic cultured astrocytes. In *Glia* 11 (3), pp. 269–276. DOI: 10.1002/glia.440110308.

Diaz, Veronica; Lin, Dayu (2020): Neural circuits for coping with social defeat. In *Current opinion in neurobiology* 60, pp. 99–107. DOI: 10.1016/j.conb.2019.11.016.

Domes, Gregor; Heinrichs, Markus; Gläscher, Jan; Büchel, Christian; Braus, Dieter F.; Herpertz, Sabine C. (2007): Oxytocin attenuates amygdala responses to emotional faces regardless of valence. In *Biological psychiatry* 62 (10), pp. 1187–1190. DOI: 10.1016/j.biopsych.2007.03.025.

Donato, R.; Cannon, B. R.; Sorci, G.; Riuzzi, F.; Hsu, K.; Weber, D. J.; Geczy, C. L. (2013): Functions of S100 Proteins. In *Current molecular medicine* 13 (1), pp. 24–57.

Dumais, Kelly M.; Veenema, Alexa H. (2016): Vasopressin and oxytocin receptor systems in the brain: Sex differences and sex-specific regulation of social behavior. In *Frontiers in neuroendocrinology* 40, pp. 1–23. DOI: 10.1016/j.yfrne.2015.04.003.

Duque-Wilckens, Natalia; Torres, Lisette Y.; Yokoyama, Sae; Minie, Vanessa A.; Tran, Amy M.; Petkova, Stela P. et al. (2020): Extrahypothalamic oxytocin neurons drive stress-induced social vigilance and avoidance. In *Proceedings of the National Academy of Sciences of the United States of America* 117 (42), pp. 26406–26413. DOI: 10.1073/pnas.2011890117.

Durkee, Caitlin A.; Covelo, Ana; Lines, Justin; Kofuji, Paulo; Aguilar, Juan; Araque, Alfonso (2019): Gi/o protein-coupled receptors inhibit neurons but activate astrocytes and stimulate gliotransmission. In *Glia* 67 (6), pp. 1076–1093. DOI: 10.1002/glia.23589.

Duval, Elizabeth R.; Javanbakht, Arash; Liberzon, Israel (2015): Neural circuits in anxiety and stress disorders: a focused review. In *Therapeutics and Clinical Risk Management* 11, pp. 115–126. DOI: 10.2147/TCRM.S48528.

Eckstein, Monika; Scheele, Dirk; Weber, Kristina; Stoffel-Wagner, Birgit; Maier, Wolfgang; Hurlemann, René (2014): Oxytocin facilitates the sensation of social stress. In *Human brain mapping* 35 (9), pp. 4741–4750. DOI: 10.1002/hbm.22508.

Eilam, David; Izhar, Rony; Mort, Joel (2011): Threat detection: behavioral practices in animals and humans. In *Neuroscience and biobehavioral reviews* 35 (4), pp. 999–1006. DOI: 10.1016/j.neubiorev.2010.08.002.

Eitelmann, Sara; Everaerts, Katharina; Petersilie, Laura; Rose, Christine R.; Stephan, Jonathan (2023): Ca2+-dependent rapid uncoupling of astrocytes upon brief metabolic stress. In *Frontiers in cellular neuroscience* 17, p. 1151608. DOI: 10.3389/fncel.2023.1151608.

Ekman, Paul (1992): An argument for basic emotions. In *Cognition and Emotion* 6 (3-4), pp. 169–200. DOI: 10.1080/02699939208411068.

Eliava, Marina; Melchior, Meggane; Knobloch-Bollmann, H. Sophie; Wahis, Jérôme; Da Silva Gouveia, Miriam; Tang, Yan et al. (2016): A New Population of Parvocellular Oxytocin Neurons Controlling Magnocellular Neuron Activity and Inflammatory Pain Processing. In *Neuron* 89 (6), pp. 1291–1304. DOI: 10.1016/j.neuron.2016.01.041.

Engel, G. L.; Schmale, A. H. (1972): Conservation-withdrawal: a primary regulatory process for organismic homeostasis. In *Ciba Foundation symposium* 8, pp. 57–75. DOI: 10.1002/9780470719916.ch5.

Engel, Kirsten; Bandelow, Borwin; Gruber, Oliver; Wedekind, Dirk (2009): Neuroimaging in anxiety disorders. In *Journal of neural transmission (Vienna, Austria : 1996)* 116 (6), pp. 703–716. DOI: 10.1007/s00702-008-0077-9.

Engin, Elif (2022): GABAA receptor subtypes and benzodiazepine use, misuse, and abuse. In *Frontiers in psychiatry* 13, p. 1060949. DOI: 10.3389/fpsyt.2022.1060949.

Ervin, Kelsy S.J.; Lymer, Jennifer M.; Matta, Richard; Clipperton-Allen, Amy E.; Kavaliers, Martin; Choleris, Elena (2015): Estrogen involvement in social behavior in rodents: Rapid and long-term actions. In *Hormones and behavior* 74, pp. 53–76. DOI: 10.1016/j.yhbeh.2015.05.023.

Eulenburg, Volker; Gomeza, Jesús (2010): Neurotransmitter transporters expressed in glial cells as regulators of synapse function. In *Brain research reviews* 63 (1-2), pp. 103–112. DOI: 10.1016/j.brainresrev.2010.01.003.

Evans, Karleyton C.; Wright, Christopher I.; Wedig, Michelle M.; Gold, Andrea L.; Pollack, Mark H.; Rauch, Scott L. (2008): A functional MRI study of amygdala responses to angry schematic faces in social anxiety disorder. In *Depression and anxiety* 25 (6), pp. 496–505. DOI: 10.1002/da.20347.

Falcone, Carmen (2022): Evolution of astrocytes: From invertebrates to vertebrates. In *Frontiers in cell and developmental biology* 10, p. 931311. DOI: 10.3389/fcell.2022.931311.

Fan, Fangcheng; Li, Lei; Liu, Wenkai; Yang, Mengzhu; Ma, Xiaoli; Sun, Haiji (2018): Astrocytes and neurons in locus coeruleus mediate restraint water immersion stress-induced gastric mucosal damage through the ERK1/2 signaling pathway. In *Neuroscience letters* 675, pp. 95–102. DOI: 10.1016/j.neulet.2018.03.054.

Fanselow, M. S.; LeDoux, J. E. (1999): Why we think plasticity underlying Pavlovian fear conditioning occurs in the basolateral amygdala. In *Neuron* 23 (2), pp. 229–232. DOI: 10.1016/s0896-6273(00)80775-8.

Franklin, Keith B. J.; Paxinos, George (2019): Paxino's and Franklin's the Mouse Brain in Stereotaxic Coordinates. Compact 5th Edition. 5th ed. San Diego: Elsevier Science & Technology.

Franklin, Tamara B.; Silva, Bianca A.; Perova, Zinaida; Marrone, Livia; Masferrer, Maria E.; Zhan, Yang et al. (2017): Prefrontal cortical control of a brainstem social behavior circuit. In *Nature neuroscience* 20 (2), pp. 260–270. DOI: 10.1038/nn.4470.

Freud, Sigmund; Richards, Angela (1953-74): The standard edition of the complete psychological works of Sigmund Freud. Edited by James Strachey, Anna Freud, Carrie Lee Rothgeb. London: Hogarth Press.

Froemke, Robert C.; Carcea, Ioana (2017): Oxytocin and Brain Plasticity. In : Principles of Gender-Specific Medicine: Elsevier, pp. 161–182.DOI: 10.1016/B978-0-12-803506-1.00037-1

Fuente-Martin, E.; Garcia-Caceres, C.; Morselli, E.; Clegg, D. J.; Chowen, J. A.; Finan, B. et al. (2013): Estrogen, astrocytes and the neuroendocrine control of metabolism. In *Reviews in endocrine & metabolic disorders* 14 (4), pp. 331–338. DOI: 10.1007/s11154-013-9263-7.

Fujii, Yuki; Maekawa, Shohei; Morita, Mitsuhiro (2017): Astrocyte calcium waves propagate proximally by gap junction and distally by extracellular diffusion of ATP released from volume-

regulated anion channels. In *Scientific reports* 7 (1), p. 13115. DOI: 10.1038/s41598-017-13243-0.

Fukuyama, Kouji; Ueda, Yuto; Okada, Motohiro (2020): Effects of Carbamazepine, Lacosamide and Zonisamide on Gliotransmitter Release Associated with Activated Astroglial Hemichannels. In *Pharmaceuticals (Basel, Switzerland)* 13 (6). DOI: 10.3390/ph13060117.

Ghézali, Grégory; Calvo, Charles-Félix; Pillet, Laure-Elise; Llense, Flora; Ezan, Pascal; Pannasch, Ulrike et al. (2018): Connexin 30 controls astroglial polarization during postnatal brain development. In *Development (Cambridge, England)* 145 (4). DOI: 10.1242/dev.155275.

Giaume, C.; Fromaget, C.; el Aoumari, A.; Cordier, J.; Glowinski, J.; Gros, D. (1991): Gap junctions in cultured astrocytes: single-channel currents and characterization of channel-forming protein. In *Neuron* 6 (1), pp. 133–143. DOI: 10.1016/0896-6273(91)90128-m.

Giaume, C.; Venance, L. (1998): Intercellular calcium signaling and gap junctional communication in astrocytes. In *Glia* 24 (1), pp. 50–64. PMID: 9700489.

Goldin, Philippe R.; Ziv, Michal; Jazaieri, Hooria; Hahn, Kevin; Heimberg, Richard; Gross, James J. (2013): Impact of cognitive behavioral therapy for social anxiety disorder on the neural dynamics of cognitive reappraisal of negative self-beliefs: randomized clinical trial. In *JAMA psychiatry* 70 (10), pp. 1048–1056. DOI: 10.1001/jamapsychiatry.2013.234.

Goldstein, David S.; Kopin, Irwin J. (2007): Evolution of concepts of stress. In *Stress (Amsterdam, Netherlands)* 10 (2), pp. 109–120. DOI: 10.1080/10253890701288935.

Gómora-Arrati, Porfirio; González-Arenas, Aliesha; Balandrán-Ruiz, Marco Antonio; Mendoza-Magaña, María Luisa; González-Flores, Oscar; Camacho-Arroyo, Ignacio (2010): Changes in the content of GFAP in the rat brain during pregnancy and the beginning of lactation. In *Neuroscience letters* 484 (3), pp. 197–200. DOI: 10.1016/j.neulet.2010.08.052.

Gonçalves-Ribeiro, Joana; Pina, Carolina Campos; Sebastião, Ana Maria; Vaz, Sandra Henriques (2019): Glutamate Transporters in Hippocampal LTD/LTP: Not Just Prevention of Excitotoxicity. In *Frontiers in cellular neuroscience* 13, p. 357. DOI: 10.3389/fncel.2019.00357.

Gottschalk, Michael G.; Domschke, Katharina (2017): Genetics of generalized anxiety disorder and related traits. In *Dialogues in clinical neuroscience* 19 (2), pp. 159–168. DOI: 10.31887/DCNS.2017.19.2/kdomschke.

Gray, J. A.; McNaughton, N. (1996): The neuropsychology of anxiety: reprise. In *Nebraska Symposium on Motivation. Nebraska Symposium on Motivation* 43, pp. 61–134. PMID: 8912308.

Grillon, C.; Krimsky, M.; Charney, D. R.; Vytal, K.; Ernst, M.; Cornwell, B. (2013): Oxytocin increases anxiety to unpredictable threat. In *Molecular psychiatry* 18 (9), pp. 958–960. DOI: 10.1038/mp.2012.156.

Grinevich, Valery; Knobloch-Bollmann, H. Sophie; Eliava, Marina; Busnelli, Marta; Chini, Bice (2016): Assembling the Puzzle: Pathways of Oxytocin Signaling in the Brain. In *Biological psychiatry* 79 (3), pp. 155–164. DOI: 10.1016/j.biopsych.2015.04.013.

Grinevich, Valery; Neumann, Inga D. (2021): Brain oxytocin: how puzzle stones from animal studies translate into psychiatry. In *Molecular psychiatry* 26 (1), pp. 265–279. DOI: 10.1038/s41380-020-0802-9.

Grossmann, Cindy P.; Sommer, Christopher; Fahliogullari, Ilayda Birben; Neumann, Inga D.; Menon, Rohit (2024): Mating-induced release of oxytocin in the mouse lateral septum: Implications for social fear extinction. In *Psychoneuroendocrinology*, p. 107083. DOI: 10.1016/j.psyneuen.2024.107083.

Gryksa, Katharina; Neumann, Inga D. (2022): Consequences of pandemic-associated social restrictions: Role of social support and the oxytocin system. In *Psychoneuroendocrinology* 135, p. 105601. DOI: 10.1016/j.psyneuen.2021.105601.

Guzmán, Yomayra F.; Tronson, Natalie C.; Jovasevic, Vladimir; Sato, Keisuke; Guedea, Anita L.; Mizukami, Hiroaki et al. (2013): Fear-enhancing effects of septal oxytocin receptors. In *Nature neuroscience* 16 (9), pp. 1185–1187. DOI: 10.1038/nn.3465.

Hackney, Anthony C. (2006): Stress and the neuroendocrine system: the role of exercise as a stressor and modifier of stress. In *Expert review of endocrinology & metabolism* 1 (6), pp. 783–792. DOI: 10.1586/17446651.1.6.783.

Halassa, Michael M.; Fellin, Tommaso; Takano, Hajime; Dong, Jing-Hui; Haydon, Philip G. (2007): Synaptic islands defined by the territory of a single astrocyte. In *The Journal of neuroscience : the official journal of the Society for Neuroscience* 27 (24), pp. 6473–6477. DOI: 10.1523/JNEUROSCI.1419-07.2007.

Halassa, Michael M.; Haydon, Philip G. (2010): Integrated brain circuits: astrocytic networks modulate neuronal activity and behavior. In *Annual review of physiology* 72, pp. 335–355. DOI: 10.1146/annurev-physiol-021909-135843.

Harada, Kazuki; Kamiya, Taichi; Tsuboi, Takashi (2015): Gliotransmitter Release from Astrocytes: Functional, Developmental, and Pathological Implications in the Brain. In *Frontiers in neuroscience* 9, p. 499. DOI: 10.3389/fnins.2015.00499.

Hardy, Eléonore; Moulard, Julien; Walter, Augustin; Ezan, Pascal; Bemelmans, Alexis-Pierre; Mouthon, Franck et al. (2023): Upregulation of astroglial connexin 30 impairs hippocampal synaptic activity and recognition memory. In *PLoS biology* 21 (4), e3002075. DOI: 10.1371/journal.pbio.3002075.

Hare, Brendan D.; Duman, Ronald S. (2020): Prefrontal cortex circuits in depression and anxiety: contribution of discrete neuronal populations and target regions. In *Molecular psychiatry* 25 (11), pp. 2742–2758. DOI: 10.1038/s41380-020-0685-9.

Hasunuma, Kansuke; Murakawa, Tomoaki; Takenawa, Satoshi; Mitsui, Koshiro; Hatsukano, Tetsu; Sano, Kazuhiro et al. (2024): Estrogen Receptor β in the Lateral Septum Mediates Estrogen Regulation of Social Anxiety-like Behavior in Male Mice. In *Neuroscience* 537, pp. 126–140. DOI: 10.1016/j.neuroscience.2023.11.019.

Hatton, G. I.; Perlmutter, L. S.; Salm, A. K.; Tweedle, C. D. (1984): Dynamic neuronal-glial interactions in hypothalamus and pituitary: implications for control of hormone synthesis and release. In *Peptides* 5 Suppl 1, pp. 121–138. DOI: 10.1016/0196-9781(84)90271-7.

Heller, Janosch P.; Rusakov, Dmitri A. (2015): Morphological plasticity of astroglia: Understanding synaptic microenvironment. In *Glia* 63 (12), pp. 2133–2151. DOI: 10.1002/glia.22821.

Herrera, D. G.; Robertson, H. A. (1996): Activation of c-fos in the brain. In *Progress in neurobiology* 50 (2-3), pp. 83–107. DOI: 10.1016/S0301-0082(96)00021-4.

Hill, E. E.; Zack, E.; Battaglini, C.; Viru, M.; Viru, A.; Hackney, A. C. (2008): Exercise and circulating cortisol levels: the intensity threshold effect. In *Journal of endocrinological investigation* 31 (7), pp. 587–591. DOI: 10.1007/BF03345606.

Hofmann, Stefan G.; Gómez, Angelina F. (2017): Mindfulness-Based Interventions for Anxiety and Depression. In *The Psychiatric clinics of North America* 40 (4), pp. 739–749. DOI: 10.1016/j.psc.2017.08.008.

Hol, Elly M.; Pekny, Milos (2015): Glial fibrillary acidic protein (GFAP) and the astrocyte intermediate filament system in diseases of the central nervous system. In *Current opinion in cell biology* 32, pp. 121–130. DOI: 10.1016/j.ceb.2015.02.004.

Hol, T.; van den Berg, C. L.; van Ree, J. M.; Spruijt, B. M. (1999): Isolation during the play period in infancy decreases adult social interactions in rats. In *Behavioural brain research* 100 (1-2), pp. 91–97. DOI: 10.1016/s0166-4328(98)00116-8.

Holsboer, Florian; Ising, Marcus (2010): Stress hormone regulation: biological role and translation into therapy. In *Annual review of psychology* 61, 81-109, C1-11. DOI: 10.1146/annurev.psych.093008.100321.

Huang, Dongming; Li, Changliu; Zhang, Wen; Qin, Jiaoqin; Jiang, Wenyu; Hu, Caiyou (2019): Dysfunction of astrocytic connexins 30 and 43 in the medial prefrontal cortex and hippocampus mediates depressive-like behaviours. In *Behavioural brain research* 372, p. 111950. DOI: 10.1016/j.bbr.2019.111950.

Hunsaker, Michael R.; Tran, Giang T.; Kesner, Raymond P. (2009): A behavioral analysis of the role of CA3 and CA1 subcortical efferents during classical fear conditioning. In *Behavioral neuroscience* 123 (3), pp. 624–630. DOI: 10.1037/a0015455.

Iadecola, Costantino; Nedergaard, Maiken (2007): Glial regulation of the cerebral microvasculature. In *Nature neuroscience* 10 (11), pp. 1369–1376. DOI: 10.1038/nn2003.

Ipser, Jonathan C.; Kariuki, Catherine M.; Stein, Dan J. (2008): Pharmacotherapy for social anxiety disorder: a systematic review. In *Expert review of neurotherapeutics* 8 (2), pp. 235–257. DOI: 10.1586/14737175.8.2.235.

Jasnow, Aaron M.; Davis, Michael; Huhman, Kim L. (2004): Involvement of central amygdalar and bed nucleus of the stria terminalis corticotropin-releasing factor in behavioral responses to social defeat. In *Behavioral neuroscience* 118 (5), pp. 1052–1061. DOI: 10.1037/0735-7044.118.5.1052.

Jiménez, Alba; Lu, Dan; Kalocsay, Marian; Berberich, Matthew J.; Balbi, Petra; Jambhekar, Ashwini; Lahav, Galit (2022): Time-series transcriptomics and proteomics reveal alternative modes to decode p53 oscillations. In *Molecular systems biology* 18 (3), e10588. DOI: 10.15252/msb.202110588.

Joëls, M.; Karst, H.; Sarabdjitsingh, R. A. (2018): The stressed brain of humans and rodents. In *Acta physiologica (Oxford, England)* 223 (2), e13066. DOI: 10.1111/apha.13066.

John, Catherine S.; Smith, Karen L.; Van't Veer, Ashlee; Gompf, Heinrich S.; Carlezon, William A.; Cohen, Bruce M. et al. (2012): Blockade of astrocytic glutamate uptake in the prefrontal cortex induces anhedonia. In *Neuropsychopharmacology : official publication of the American College of Neuropsychopharmacology* 37 (11), pp. 2467–2475. DOI: 10.1038/npp.2012.105.

Jurek, Benjamin; Meyer, Magdalena (2020): Anxiolytic and Anxiogenic? How the Transcription Factor MEF2 Might Explain the Manifold Behavioral Effects of Oxytocin. In *Frontiers in endocrinology* 11, p. 186. DOI: 10.3389/fendo.2020.00186.

Jurek, Benjamin; Neumann, Inga D. (2018): The Oxytocin Receptor: From Intracellular Signaling to Behavior. In *Physiological reviews* 98 (3), pp. 1805–1908. DOI: 10.1152/physrev.00031.2017.

Jurek, Benjamin; Slattery, David A.; Maloumby, Rodrigue; Hillerer, Katharina; Koszinowski, Sophie; Neumann, Inga D.; van den Burg, Erwin H. (2012): Differential contribution of hypothalamic MAPK activity to anxiety-like behaviour in virgin and lactating rats. In *PloS one* 7 (5), e37060. DOI: 10.1371/journal.pone.0037060.

Kameritsch, Petra; Pogoda, Kristin; Pohl, Ulrich (2012): Channel-independent influence of connexin 43 on cell migration. In *Biochimica et biophysica acta* 1818 (8), pp. 1993–2001. DOI: 10.1016/j.bbamem.2011.11.016.

Kandel, Eric R.; Mack, Sarah (2013): Principles of neural science. 5. ed. New York N.Y.: McGraw-Hill medical.

Kandola, Aaron; Hendrikse, Joshua; Lucassen, Paul J.; Yücel, Murat (2016): Aerobic Exercise as a Tool to Improve Hippocampal Plasticity and Function in Humans: Practical Implications for Mental Health Treatment. In *Frontiers in human neuroscience* 10, p. 373. DOI: 10.3389/fnhum.2016.00373.

Kandola, Aaron; Stubbs, Brendon (2020): Exercise and Anxiety. In *Advances in experimental medicine and biology* 1228, pp. 345–352. DOI: 10.1007/978-981-15-1792-1_23.

Kaufman, J.; Plotsky, P. M.; Nemeroff, C. B.; Charney, D. S. (2000): Effects of early adverse experiences on brain structure and function: clinical implications. In *Biological psychiatry* 48 (8), pp. 778–790. DOI: 10.1016/S0006-3223(00)00998-7.

Kendler, K. S.; Myers, J. (2014): The boundaries of the internalizing and externalizing genetic spectra in men and women. In *Psychological medicine* 44 (3), pp. 647–655. DOI: 10.1017/S0033291713000585.

Kent, J. M.; Coplan, J. D.; Gorman, J. M. (1998): Clinical utility of the selective serotonin reuptake inhibitors in the spectrum of anxiety. In *Biological psychiatry* 44 (9), pp. 812–824. DOI: 10.1016/S0006-3223(98)00210-8.

Kessler, Ronald C.; Petukhova, Maria; Sampson, Nancy A.; Zaslavsky, Alan M.; Wittchen, Hans-Ullrich (2012): Twelve-month and lifetime prevalence and lifetime morbid risk of anxiety and mood disorders in the United States. In *International journal of methods in psychiatric research* 21 (3), pp. 169–184. DOI: 10.1002/mpr.1359.

Khakh, Baljit S.; McCarthy, Ken D. (2015): Astrocyte calcium signaling: from observations to functions and the challenges therein. In *Cold Spring Harbor perspectives in biology* 7 (4), a020404. DOI: 10.1101/cshperspect.a020404.

Kilkenny, Carol; Browne, William J.; Cuthill, Innes C.; Emerson, Michael; Altman, Douglas G. (2010): Improving bioscience research reporting: the ARRIVE guidelines for reporting animal research. In *PLoS biology* 8 (6), e1000412. DOI: 10.1371/journal.pbio.1000412.

Kim, Jeansok J.; Jung, Min Whan (2006): Neural circuits and mechanisms involved in Pavlovian fear conditioning: a critical review. In *Neuroscience and biobehavioral reviews* 30 (2), pp. 188–202. DOI: 10.1016/j.neubiorev.2005.06.005.

Kimmel, Ryan J.; Roy-Byrne, Peter P.; Cowley, Deborah S. (2015): Oxford University Press (1).

Kloet, E. Ron de; Joëls, Marian; Holsboer, Florian (2005): Stress and the brain: from adaptation to disease. In *Nature reviews. Neuroscience* 6 (6), pp. 463–475. DOI: 10.1038/nrn1683.

Knobloch, H. Sophie; Charlet, Alexandre; Hoffmann, Lena C.; Eliava, Marina; Khrulev, Sergey; Cetin, Ali H. et al. (2012): Evoked axonal oxytocin release in the central amygdala attenuates fear response. In *Neuron* 73 (3), pp. 553–566. DOI: 10.1016/j.neuron.2011.11.030.

Knobloch, H. Sophie; Grinevich, Valery (2014): Evolution of oxytocin pathways in the brain of vertebrates. In *Frontiers in behavioral neuroscience* 8, p. 31. DOI: 10.3389/fnbeh.2014.00031.

Kofuji, Paulo; Araque, Alfonso (2021a): Astrocytes and Behavior. In *Annual review of neuroscience* 44, pp. 49–67. DOI: 10.1146/annurev-neuro-101920-112225.

Kofuji, Paulo; Araque, Alfonso (2021b): G-Protein-Coupled Receptors in Astrocyte-Neuron Communication. In *Neuroscience* 456, pp. 71–84. DOI: 10.1016/j.neuroscience.2020.03.025.

Koizumi, Schuichi (2010): Synchronization of Ca2+ oscillations: involvement of ATP release in astrocytes. In *The FEBS journal* 277 (2), pp. 286–292. DOI: 10.1111/j.1742-4658.2009.07438.x.

Kol, Adi; Adamsky, Adar; Groysman, Maya; Kreisel, Tirzah; London, Michael; Goshen, Inbal (2020): Astrocytes contribute to remote memory formation by modulating hippocampal-cortical communication during learning. In *Nature neuroscience* 23 (10), pp. 1229–1239. DOI: 10.1038/s41593-020-0679-6.

Kozlowska, Kasia; Walker, Peter; McLean, Loyola; Carrive, Pascal (2015): Fear and the Defense Cascade: Clinical Implications and Management. In *Harvard review of psychiatry* 23 (4), pp. 263–287. DOI: 10.1097/HRP.0000000000000065.

Kuchibhotla, Kishore V.; Lattarulo, Carli R.; Hyman, Bradley T.; Bacskai, Brian J. (2009): Synchronous hyperactivity and intercellular calcium waves in astrocytes in Alzheimer mice. In *Science (New York, N.Y.)* 323 (5918), pp. 1211–1215. DOI: 10.1126/science.1169096.

Kundakovic, Marija; Tickerhoof, Maria (2024): Epigenetic mechanisms underlying sex differences in the brain and behavior. In *Trends in neurosciences* 47 (1), pp. 18–35. DOI: 10.1016/j.tins.2023.09.007.

Kuo, John; Hamid, Naheed; Bondar, Galyna; Prossnitz, Eric R.; Micevych, Paul (2010): Membrane estrogen receptors stimulate intracellular calcium release and progesterone synthesis in hypothalamic astrocytes. In *The Journal of neuroscience : the official journal of the Society for Neuroscience* 30 (39), pp. 12950–12957. DOI: 10.1523/JNEUROSCI.1158-10.2010.

Landgraf, Rainer; Neumann, Inga D. (2004): Vasopressin and oxytocin release within the brain: a dynamic concept of multiple and variable modes of neuropeptide communication. In *Frontiers in neuroendocrinology* 25 (3-4), pp. 150–176. DOI: 10.1016/j.yfrne.2004.05.001.

Langle, Sarah L.; Poulain, Dominique A.; Theodosis, Dionysia T. (2003): Induction of rapid, activity-dependent neuronal-glial remodelling in the adult rat hypothalamus in vitro. In *The European journal of neuroscience* 18 (1), pp. 206–214. DOI: 10.1046/j.1460-9568.2003.02741.x.

Lavialle, Monique; Aumann, Georg; Anlauf, Enrico; Pröls, Felicitas; Arpin, Monique; Derouiche, Amin (2011): Structural plasticity of perisynaptic astrocyte processes involves ezrin and metabotropic glutamate receptors. In *Proceedings of the National Academy of Sciences of the United States of America* 108 (31), pp. 12915–12919. DOI: 10.1073/pnas.1100957108.

Lawal, Oluwadamilola; Ulloa Severino, Francesco Paolo; Eroglu, Cagla (2022): The role of astrocyte structural plasticity in regulating neural circuit function and behavior. In *Glia* 70 (8), pp. 1467–1483. DOI: 10.1002/glia.24191.

Lebron-Milad, Kelimer; Abbs, Brandon; Milad, Mohammed R.; Linnman, Clas; Rougemount-Bücking, Ansgar; Zeidan, Mohammed A. et al. (2012): Sex differences in the neurobiology of fear conditioning and extinction: a preliminary fMRI study of shared sex differences with stress-arousal circuitry. In *Biology of mood & anxiety disorders* 2, p. 7. DOI: 10.1186/2045-5380-2-7.

Lecrubier, Y.; Wittchen, H. U.; Faravelli, C.; Bobes, J.; Patel, A.; Knapp, M. (2000): A European perspective on social anxiety disorder. In *European psychiatry : the journal of the Association of European Psychiatrists* 15 (1), pp. 5–16. DOI: 10.1016/s0924-9338(00)00216-9.

LeDoux, J. E. (1992): Brain mechanisms of emotion and emotional learning. In *Current opinion in neurobiology* 2 (2), pp. 191–197. DOI: 10.1016/0959-4388(92)90011-9.

LeDoux, J. E. (2000): Emotion circuits in the brain. In *Annual review of neuroscience* 23, pp. 155–184. DOI: 10.1146/annurev.neuro.23.1.155.

LeDoux, Joseph (2003): The emotional brain, fear, and the amygdala. In *Cellular and molecular neurobiology* 23 (4-5), pp. 727–738. DOI: 10.1023/a:1025048802629.

LeDoux, Joseph (2012): Rethinking the emotional brain. In *Neuron* 73 (4), pp. 653–676. DOI: 10.1016/j.neuron.2012.02.004.

Leichsenring, Falk; Leweke, Frank (2017): Social Anxiety Disorder. In *The New England journal of medicine* 376 (23), pp. 2255–2264. DOI: 10.1056/NEJMcp1614701.

León Reyes, Noelia Sofia de; Sierra Díaz, Paula; Nogueira, Ramon; Ruiz-Pino, Antonia; Nomura, Yuki; Solis, Christopher A. de et al. (2023): Corticotropin-releasing hormone signaling from prefrontal cortex to lateral septum suppresses interaction with familiar mice. In *Cell* 186 (19), 4152-4171.e31. DOI: 10.1016/j.cell.2023.08.010.

Leroy, Felix; Park, Jung; Asok, Arun; Brann, David H.; Meira, Torcato; Boyle, Lara M. et al. (2018): A circuit from hippocampal CA2 to lateral septum disinhibits social aggression. In *Nature* 564 (7735), pp. 213–218. DOI: 10.1038/s41586-018-0772-0.

Li, Dongyang; Li, Tong; Yu, Jiawei; Liu, Xiaoyu; Jia, Shuwei; Wang, Xiaoran et al. (2021): Astrocytic Modulation of Supraoptic Oxytocin Neuronal Activity in Rat Dams with Pup-Deprivation at Different Stages of Lactation. In *Neurochemical research* 46 (10), pp. 2601–2611. DOI: 10.1007/s11064-020-03129-5.

Lia, Annamaria; Henriques, Vanessa Jorge; Zonta, Micaela; Chiavegato, Angela; Carmignoto, Giorgio; Gómez-Gonzalo, Marta; Losi, Gabriele (2021): Calcium Signals in Astrocyte Microdomains, a Decade of Great Advances. In *Frontiers in cellular neuroscience* 15, p. 673433. DOI: 10.3389/fncel.2021.673433.

Liao, Po-Yu; Chiu, Yan-Min; Yu, Jo-Hsien; Chen, Shih-Kuo (2020): Mapping Central Projection of Oxytocin Neurons in Unmated Mice Using Cre and Alkaline Phosphatase Reporter. In *Frontiers in neuroanatomy* 14, p. 559402. DOI: 10.3389/fnana.2020.559402.

Lin, Winston; McKinney, Kyle; Liu, Liansheng; Lakhlani, Shruti; Jennes, Lothar (2003): Distribution of vesicular glutamate transporter-2 messenger ribonucleic Acid and protein in the septum-hypothalamus of the rat. In *Endocrinology* 144 (2), pp. 662–670. DOI: 10.1210/en.2002-220908.

Lippman Bell, Jocelyn J.; Lordkipanidze, Tamar; Cobb, Natalie; Dunaevsky, Anna (2010): Bergmann glial ensheathment of dendritic spines regulates synapse number without affecting spine motility. In *Neuron glia biology* 6 (3), pp. 193–200. DOI: 10.1017/S1740925X10000165.

Lister, R. G. (1987): The use of a plus-maze to measure anxiety in the mouse. In *Psychopharmacology* 92 (2), pp. 180–185. DOI: 10.1007/BF00177912.

Lorberbaum, Jeffrey P.; Kose, Samet; Johnson, Michael R.; Arana, George W.; Sullivan, Lindsay K.; Hamner, Mark B. et al. (2004): Neural correlates of speech anticipatory anxiety in generalized social phobia. In *Neuroreport* 15 (18), pp. 2701–2705. PMID: 15597038.

Lukas, Michael; Toth, Iulia; Reber, Stefan O.; Slattery, David A.; Veenema, Alexa H.; Neumann, Inga D. (2011): The neuropeptide oxytocin facilitates pro-social behavior and prevents social avoidance in rats and mice. In *Neuropsychopharmacology : official publication of the American College of Neuropsychopharmacology* 36 (11), pp. 2159–2168. DOI: 10.1038/npp.2011.95.

Lukas, Michael; Toth, Iulia; Veenema, Alexa H.; Neumann, Inga D. (2013): Oxytocin mediates rodent social memory within the lateral septum and the medial amygdala depending on the relevance of the social stimulus: male juvenile versus female adult conspecifics. In *Psychoneuroendocrinology* 38 (6), pp. 916–926. DOI: 10.1016/j.psyneuen.2012.09.018.

Luo, Pei X.; Zakharenkov, Hannah Cortez; Torres, Lisette Y.; Rios, Roberto A.; Gegenhuber, Bruno; Black, Alexis M. et al. (2022): Oxytocin receptor behavioral effects and cell types in the bed nucleus of the stria terminalis. In *Hormones and behavior* 143, p. 105203. DOI: 10.1016/j.yhbeh.2022.105203.

Lupien, Sonia J.; McEwen, Bruce S.; Gunnar, Megan R.; Heim, Christine (2009): Effects of stress throughout the lifespan on the brain, behaviour and cognition. In *Nature reviews. Neuroscience* 10 (6), pp. 434–445. DOI: 10.1038/nrn2639.

Lüscher, Christian; Malenka, Robert C. (2012): NMDA receptor-dependent long-term potentiation and long-term depression (LTP/LTD). In *Cold Spring Harbor perspectives in biology* 4 (6). DOI: 10.1101/cshperspect.a005710.

Ma, Y. (2015): Neuropsychological mechanism underlying antidepressant effect: a systematic meta-analysis. In *Molecular psychiatry* 20 (3), pp. 311–319. DOI: 10.1038/mp.2014.24.

MacDonald, Kai; Feifel, David (2014): Oxytocin's role in anxiety: a critical appraisal. In *Brain research* 1580, pp. 22–56. DOI: 10.1016/j.brainres.2014.01.025.

Maren, S. (2001): Neurobiology of Pavlovian fear conditioning. In *Annual review of neuroscience* 24, pp. 897–931. DOI: 10.1146/annurev.neuro.24.1.897.

Maren, Stephen (2005): Synaptic mechanisms of associative memory in the amygdala. In *Neuron* 47 (6), pp. 783–786. DOI: 10.1016/j.neuron.2005.08.009.

Maren, Stephen (2015): Out with the old and in with the new: Synaptic mechanisms of extinction in the amygdala. In *Brain research* 1621, pp. 231–238. DOI: 10.1016/j.brainres.2014.10.010.

Mark, L. P.; Prost, R. W.; Ulmer, J. L.; Smith, M. M.; Daniels, D. L.; Strottmann, J. M. et al. (2001): Pictorial review of glutamate excitotoxicity: fundamental concepts for neuroimaging. In *AJNR. American journal of neuroradiology* 22 (10), pp. 1813–1824. PMID: 11733308.

Markham, Chris M.; Taylor, Stacie L.; Huhman, Kim L. (2010): Role of amygdala and hippocampus in the neural circuit subserving conditioned defeat in Syrian hamsters. In *Learning & memory (Cold Spring Harbor, N.Y.)* 17 (2), pp. 109–116. DOI: 10.1101/lm.1633710.

Maroun, Mouna; Wagner, Shlomo (2016): Oxytocin and Memory of Emotional Stimuli: Some Dance to Remember, Some Dance to Forget. In *Biological psychiatry* 79 (3), pp. 203–212. DOI: 10.1016/j.biopsych.2015.07.016.

Martin, Elizabeth I.; Ressler, Kerry J.; Binder, Elisabeth; Nemeroff, Charles B. (2009): The neurobiology of anxiety disorders: brain imaging, genetics, and psychoneuroendocrinology. In *The Psychiatric clinics of North America* 32 (3), pp. 549–575. DOI: 10.1016/j.psc.2009.05.004.

Martin-Fernandez, Mario; Jamison, Stephanie; Robin, Laurie M.; Zhao, Zhe; Martin, Eduardo D.; Aguilar, Juan et al. (2017): Synapse-specific astrocyte gating of amygdala-related behavior. In *Nature neuroscience* 20 (11), pp. 1540–1548. DOI: 10.1038/nn.4649.

Martinon, Daisy; Lis, Paulina; Roman, Alexandra N.; Tornesi, Patricio; Applebey, Sarah V.; Buechner, Garrett et al. (2019): Oxytocin receptors in the dorsolateral bed nucleus of the stria terminalis (BNST) bias fear learning toward temporally predictable cued fear. In *Translational psychiatry* 9 (1), p. 140. DOI: 10.1038/s41398-019-0474-x.

Matsuda, S.; Peng, H.; Yoshimura, H.; Wen, T. C.; Fukuda, T.; Sakanaka, M. (1996): Persistent c-fos expression in the brains of mice with chronic social stress. In *Neuroscience research* 26 (2), pp. 157–170. PMID: 8953578.

Matsuuchi, Linda; Naus, Christian C. (2013): Gap junction proteins on the move: connexins, the cytoskeleton and migration. In *Biochimica et biophysica acta* 1828 (1), pp. 94–108. DOI: 10.1016/j.bbamem.2012.05.014.

McBean, G. J. (1994): Inhibition of the glutamate transporter and glial enzymes in rat striatum by the gliotoxin, alpha aminoadipate. In *British journal of pharmacology* 113 (2), pp. 536–540. DOI: 10.1111/j.1476-5381.1994.tb17022.x.

McCarthy, Margaret M.; Arnold, Arthur P. (2011): Reframing sexual differentiation of the brain. In *Nature neuroscience* 14 (6), pp. 677–683. DOI: 10.1038/nn.2834.

McCarthy, Margaret M.; Wright, Christopher L.; Schwarz, Jaclyn M. (2009): New tricks by an old dogma: mechanisms of the Organizational/Activational Hypothesis of steroid-mediated sexual differentiation of brain and behavior. In *Hormones and behavior* 55 (5), pp. 655–665. DOI: 10.1016/j.yhbeh.2009.02.012.

McEwen, Bruce S. (2004): Protection and damage from acute and chronic stress: allostasis and allostatic overload and relevance to the pathophysiology of psychiatric disorders. In *Annals of the New York Academy of Sciences* 1032, pp. 1–7. DOI: 10.1196/annals.1314.001.

McKinney, W. T.; Bunney, W. E. (1969): Animal model of depression. I. Review of evidence: implications for research. In *Archives of general psychiatry* 21 (2), pp. 240–248. DOI: 10.1001/archpsyc.1969.01740200112015.

McLean, Carmen P.; Asnaani, Anu; Litz, Brett T.; Hofmann, Stefan G. (2011): Gender differences in anxiety disorders: prevalence, course of illness, comorbidity and burden of illness. In *Journal of psychiatric research* 45 (8), pp. 1027–1035. DOI: 10.1016/j.jpsychires.2011.03.006.

Mederos, Sara; Hernández-Vivanco, Alicia; Ramírez-Franco, Jorge; Martín-Fernández, Mario; Navarrete, Marta; Yang, Aimei et al. (2019): Melanopsin for precise optogenetic activation of astrocyte-neuron networks. In *Glia* 67 (5), pp. 915–934. DOI: 10.1002/glia.23580.

Meier, Sandra M.; Deckert, Jürgen (2019): Genetics of Anxiety Disorders. In *Current psychiatry reports* 21 (3), p. 16. DOI: 10.1007/s11920-019-1002-7.

Meier, Sandra M.; Trontti, Kalevi; Purves, Kirstin L.; Als, Thomas Damm; Grove, Jakob; Laine, Mikaela et al. (2019): Genetic Variants Associated With Anxiety and Stress-Related Disorders: A Genome-Wide Association Study and Mouse-Model Study. In *JAMA psychiatry* 76 (9), pp. 924–932. DOI: 10.1001/jamapsychiatry.2019.1119.

Melin, P.; Kihlstroem, J. E. (1963): Influence of Oxytocin on Sexual Behavior in Male Rabbits. In *Endocrinology* 73, pp. 433–435. DOI: 10.1210/endo-73-4-433.

Menon, Rohit; Grund, Thomas; Zoicas, Iulia; Althammer, Ferdinand; Fiedler, Dominik; Biermeier, Verena et al. (2018): Oxytocin Signaling in the Lateral Septum Prevents Social Fear during Lactation. In *Current biology : CB* 28 (7), 1066-1078.e6. DOI: 10.1016/j.cub.2018.02.044.

Menon, Rohit; Neumann, Inga D. (2023): Detection, processing and reinforcement of social cues: regulation by the oxytocin system. In *Nature reviews. Neuroscience* 24 (12), pp. 761–777. DOI: 10.1038/s41583-023-00759-w.

Menon, Rohit; Süß, Theresa; Oliveira, Vinícius Elias de Moura; Neumann, Inga D.; Bludau, Anna (2022): Neurobiology of the lateral septum: regulation of social behavior. In *Trends in neurosciences* 45 (1), pp. 27–40. DOI: 10.1016/j.tins.2021.10.010.

Meunier, Claire; Wang, Nan; Yi, Chenju; Dallerac, Glenn; Ezan, Pascal; Koulakoff, Annette et al. (2017): Contribution of Astroglial Cx43 Hemichannels to the Modulation of Glutamatergic Currents by D-Serine in the Mouse Prefrontal Cortex. In *The Journal of neuroscience : the official journal of the Society for Neuroscience* 37 (37), pp. 9064–9075. DOI: 10.1523/JNEUROSCI.2204-16.2017.

Meyer-Lindenberg, Andreas; Domes, Gregor; Kirsch, Peter; Heinrichs, Markus (2011): Oxytocin and vasopressin in the human brain: social neuropeptides for translational medicine. In *Nature reviews. Neuroscience* 12 (9), pp. 524–538. DOI: 10.1038/nrn3044.

Milner, Teresa A.; Thompson, Louisa I.; Wang, Gang; Kievits, Justin A.; Martin, Eugene; Zhou, Ping et al. (2010): Distribution of estrogen receptor beta containing cells in the brains of

bacterial artificial chromosome transgenic mice. In *Brain research* 1351, pp. 74–96. DOI: 10.1016/j.brainres.2010.06.038.

Mong, J. A.; Blutstein, T. (2006): Estradiol modulation of astrocytic form and function: implications for hormonal control of synaptic communication. In *Neuroscience* 138 (3), pp. 967–975. DOI: 10.1016/j.neuroscience.2005.10.017.

Moos, F.; Poulain, D. A.; Rodriguez, F.; Guerné, Y.; Vincent, J. D.; Richard, P. (1989): Release of oxytocin within the supraoptic nucleus during the milk ejection reflex in rats. In *Experimental brain research* 76 (3), pp. 593–602. DOI: 10.1007/BF00248916.

Nabavi, Sadegh; Fox, Rocky; Proulx, Christophe D.; Lin, John Y.; Tsien, Roger Y.; Malinow, Roberto (2014): Engineering a memory with LTD and LTP. In *Nature* 511 (7509), pp. 348–352. DOI: 10.1038/nature13294.

Nagy, J. I.; Li, X.; Rempel, J.; Stelmack, G.; Patel, D.; Staines, W. A. et al. (2001): Connexin26 in adult rodent central nervous system: demonstration at astrocytic gap junctions and colocalization with connexin30 and connexin43. In *The Journal of comparative neurology* 441 (4), pp. 302–323. DOI: 10.1002/cne.1414.

Nasanbuyan, Naranbat; Yoshida, Masahide; Takayanagi, Yuki; Inutsuka, Ayumu; Nishimori, Katsuhiko; Yamanaka, Akihiro; Onaka, Tatsushi (2018): Oxytocin-Oxytocin Receptor Systems Facilitate Social Defeat Posture in Male Mice. In *Endocrinology* 159 (2), pp. 763–775. DOI: 10.1210/en.2017-00606.

Neumann, I.; Russell, J. A.; Landgraf, R. (1993): Oxytocin and vasopressin release within the supraoptic and paraventricular nuclei of pregnant, parturient and lactating rats: a microdialysis study. In *Neuroscience* 53 (1), pp. 65–75. DOI: 10.1016/0306-4522(93)90285-N.

Neumann, I. D.; Torner, L.; Wigger, A. (2000): Brain oxytocin: differential inhibition of neuroendocrine stress responses and anxiety-related behaviour in virgin, pregnant and lactating rats. In *Neuroscience* 95 (2), pp. 567–575. DOI: 10.1016/S0306-4522(99)00433-9.

Neumann, Inga D.; Slattery, David A. (2016): Oxytocin in General Anxiety and Social Fear: A Translational Approach. In *Biological psychiatry* 79 (3), pp. 213–221. DOI: 10.1016/j.biopsych.2015.06.004.

Nishida, Hideko; Okabe, Shigeo (2007): Direct astrocytic contacts regulate local maturation of dendritic spines. In *The Journal of neuroscience : the official journal of the Society for Neuroscience* 27 (2), pp. 331–340. DOI: 10.1523/JNEUROSCI.4466-06.2007.

Norenberg, M. D.; Martinez-Hernandez, A. (1979): Fine structural localization of glutamine synthetase in astrocytes of rat brain. In *Brain research* 161 (2), pp. 303–310. DOI: 10.1016/0006-8993(79)90071-4.

Nyuyki, Kewir D.; Waldherr, Martin; Baeuml, Sandra; Neumann, Inga D. (2011): Yes, I am ready now: differential effects of paced versus unpaced mating on anxiety and central oxytocin release in female rats. In *PloS one* 6 (8), e23599. DOI: 10.1371/journal.pone.0023599.

Ogata, K.; Kosaka, T. (2002): Structural and quantitative analysis of astrocytes in the mouse hippocampus. In *Neuroscience* 113 (1), pp. 221–233. DOI: 10.1016/s0306-4522(02)00041-6.

Ohayon, Maurice M.; Schatzberg, Alan F. (2010): Social phobia and depression: prevalence and comorbidity. In *Journal of psychosomatic research* 68 (3), pp. 235–243. DOI: 10.1016/j.jpsychores.2009.07.018.

Oliet, Stéphane H. R.; Mothet, Jean-Pierre (2006): Molecular determinants of D-serine-mediated gliotransmission: from release to function. In *Glia* 54 (7), pp. 726–737. DOI: 10.1002/glia.20356.

Oliet, Stéphane H. R.; Panatier, Aude; Piet, Richard; Mothet, Jean-Pierre; Poulain, Dominique A.; Theodosis, Dionysia T. (2008): Neuron-glia interactions in the rat supraoptic nucleus. In *Progress in brain research* 170, pp. 109–117. DOI: 10.1016/S0079-6123(08)00410-X.

Oliveira, Vinícius Elias de Moura; Lukas, Michael; Wolf, Hannah Nora; Durante, Elisa; Lorenz, Alexandra; Mayer, Anna-Lena et al. (2021): Oxytocin and vasopressin within the ventral and dorsal lateral septum modulate aggression in female rats. In *Nature communications* 12 (1), p. 2900. DOI: 10.1038/s41467-021-23064-5.

Opalka, Ashley N.; Wang, Dong V. (2020): Hippocampal efferents to retrosplenial cortex and lateral septum are required for memory acquisition. In *Learning & memory (Cold Spring Harbor, N.Y.)* 27 (8), pp. 310–318. DOI: 10.1101/lm.051797.120.

Orellana, Juan A.; Martinez, Agustín D.; Retamal, Mauricio A. (2013): Gap junction channels and hemichannels in the CNS: regulation by signaling molecules. In *Neuropharmacology* 75, pp. 567–582. DOI: 10.1016/j.neuropharm.2013.02.020.

Orellana, Juan A.; Stehberg, Jimmy (2014): Hemichannels: new roles in astroglial function. In *Frontiers in physiology* 5, p. 193. DOI: 10.3389/fphys.2014.00193.

Ostroff, Linnaea E.; Manzur, Mustfa K.; Cain, Christopher K.; LeDoux, Joseph E. (2014): Synapses lacking astrocyte appear in the amygdala during consolidation of Pavlovian threat conditioning. In *The Journal of comparative neurology* 522 (9), pp. 2152–2163. DOI: 10.1002/cne.23523.

Oyola, Mario G.; Handa, Robert J. (2017): Hypothalamic-pituitary-adrenal and hypothalamic-pituitary-gonadal axes: sex differences in regulation of stress responsivity. In *Stress (Amsterdam, Netherlands)* 20 (5), pp. 476–494. DOI: 10.1080/10253890.2017.1369523.

Pannasch, Ulrike; Dossi, Elena; Ezan, Pascal; Rouach, Nathalie (2019): Astroglial Cx30 sustains neuronal population bursts independently of gap-junction mediated biochemical coupling. In *Glia* 67 (6), pp. 1104–1112. DOI: 10.1002/glia.23591.

Pannasch, Ulrike; Freche, Dominik; Dallérac, Glenn; Ghézali, Grégory; Escartin, Carole; Ezan, Pascal et al. (2014): Connexin 30 sets synaptic strength by controlling astroglial synapse invasion. In *Nature neuroscience* 17 (4), pp. 549–558. DOI: 10.1038/nn.3662.

Pannasch, Ulrike; Rouach, Nathalie (2013): Emerging role for astroglial networks in information processing: from synapse to behavior. In *Trends in neurosciences* 36 (7), pp. 405–417. DOI: 10.1016/j.tins.2013.04.004.

Pannasch, Ulrike; Vargová, Lydia; Reingruber, Jürgen; Ezan, Pascal; Holcman, David; Giaume, Christian et al. (2011): Astroglial networks scale synaptic activity and plasticity. In *Proc. Natl. Acad. Sci. U.S.A.* 108 (20), pp. 8467–8472. DOI: 10.1073/pnas.1016650108.

Papouin, Thomas; Dunphy, Jaclyn; Tolman, Michaela; Foley, Jeannine C.; Haydon, Philip G. (2017): Astrocytic control of synaptic function. In *Philosophical transactions of the Royal Society of London. Series B, Biological sciences* 372 (1715). DOI: 10.1098/rstb.2016.0154.

Parfitt, Gustavo Morrone; Nguyen, Robin; Bang, Jee Yoon; Aqrabawi, Afif J.; Tran, Matthew M.; Seo, D. Kanghoon et al. (2017): Bidirectional Control of Anxiety-Related Behaviors in Mice: Role of Inputs Arising from the Ventral Hippocampus to the Lateral Septum and Medial Prefrontal Cortex. In *Neuropsychopharmacology : official publication of the American College of Neuropsychopharmacology* 42 (8), pp. 1715–1728. DOI: 10.1038/npp.2017.56.

Parpura, V.; Basarsky, T. A.; Liu, F.; Jeftinija, K.; Jeftinija, S.; Haydon, P. G. (1994): Glutamate-mediated astrocyte-neuron signalling. In *Nature* 369 (6483), pp. 744–747. DOI: 10.1038/369744a0.

Pasti, L.; Volterra, A.; Pozzan, T.; Carmignoto, G. (1997): Intracellular calcium oscillations in astrocytes: a highly plastic, bidirectional form of communication between neurons and astrocytes in situ. In *The Journal of neuroscience : the official journal of the Society for Neuroscience* 17 (20), pp. 7817–7830. DOI: 10.1523/JNEUROSCI.17-20-07817.1997.

Pedersen, C. A.; Prange, A. J. (1979): Induction of maternal behavior in virgin rats after intracerebroventricular administration of oxytocin. In *Proceedings of the National Academy of Sciences of the United States of America* 76 (12), pp. 6661–6665. DOI: 10.1073/pnas.76.12.6661.

Penninx, Brenda Wjh; Pine, Daniel S.; Holmes, Emily A.; Reif, Andreas (2021): Anxiety disorders. In *Lancet (London, England)* 397 (10277), pp. 914–927. DOI: 10.1016/S0140-6736(21)00359-7.

Perea, Gertrudis; Navarrete, Marta; Araque, Alfonso (2009): Tripartite synapses: astrocytes process and control synaptic information. In *Trends in neurosciences* 32 (8), pp. 421–431. DOI: 10.1016/j.tins.2009.05.001.

Phan, K. Luan; Fitzgerald, Daniel A.; Nathan, Pradeep J.; Tancer, Manuel E. (2006): Association between amygdala hyperactivity to harsh faces and severity of social anxiety in generalized social phobia. In *Biological psychiatry* 59 (5), pp. 424–429. DOI: 10.1016/j.biopsych.2005.08.012.

Pitman, Seth R.; Knauss, Daniel P. C. (2020): Contemporary Psychodynamic Approaches to Treating Anxiety: Theory, Research, and Practice. In *Advances in experimental medicine and biology* 1191, pp. 451–464. DOI: 10.1007/978-981-32-9705-0_23.

Pizzagalli, Diego A.; Roberts, Angela C. (2022): Prefrontal cortex and depression. In *Neuropsychopharmacol* 47 (1), pp. 225–246. DOI: 10.1038/s41386-021-01101-7.

Poitry-Yamate, Carol L.; Vutskits, Laszlo; Rauen, Thomas (2002): Neuronal-induced and glutamate-dependent activation of glial glutamate transporter function. In *Journal of neurochemistry* 82 (4), pp. 987–997. DOI: 10.1046/j.1471-4159.2002.01075.x.

Porsolt, R. D.; Le Pichon, M.; Jalfre, M. (1977): Depression: a new animal model sensitive to antidepressant treatments. In *Nature* 266 (5604), pp. 730–732. DOI: 10.1038/266730a0.

Poskanzer, Kira E.; Yuste, Rafael (2011): Astrocytic regulation of cortical UP states. In *Proceedings of the National Academy of Sciences of the United States of America* 108 (45), pp. 18453–18458. DOI: 10.1073/pnas.1112378108.

Ramirez, Franchesca; Moscarello, Justin M.; LeDoux, Joseph E.; Sears, Robert M. (2015): Active avoidance requires a serial basal amygdala to nucleus accumbens shell circuit. In *The Journal of neuroscience : the official journal of the Society for Neuroscience* 35 (8), pp. 3470–3477. DOI: 10.1523/JNEUROSCI.1331-14.2015.

Ramón y Cajal, Santiago (1909): Histologie du système nerveux de l'homme & des vertébrés. Paris: Maloine.

Reeves, Alexander M. B.; Shigetomi, Eiji; Khakh, Baljit S. (2011): Bulk loading of calcium indicator dyes to study astrocyte physiology: key limitations and improvements using morphological maps. In *The Journal of neuroscience : the official journal of the Society for Neuroscience* 31 (25), pp. 9353–9358. DOI: 10.1523/JNEUROSCI.0127-11.2011.

Reichenbach, Andreas; Derouiche, Amin; Kirchhoff, Frank (2010): Morphology and dynamics of perisynaptic glia. In *Brain research reviews* 63 (1-2), pp. 11–25. DOI: 10.1016/j.brainresrev.2010.02.003.

Ren, Runan; Zhang, Li; Wang, Min (2018): Specific deletion connexin43 in astrocyte ameliorates cognitive dysfunction in APP/PS1 mice. In *Life sciences* 208, pp. 175–191. DOI: 10.1016/j.lfs.2018.07.033.

Réus, Gislaine Z.; Dos Santos, Maria Augusta B.; Abelaira, Helena M.; Quevedo, João (2014): Animal models of social anxiety disorder and their validity criteria. In *Life sciences* 114 (1), pp. 1–3. DOI: 10.1016/j.lfs.2014.08.002.

Rickmann, M.; Wolff, J. R. (1995): S100 protein expression in subpopulations of neurons of rat brain. In *Neuroscience* 67 (4), pp. 977–991. DOI: 10.1016/0306-4522(94)00615-c.

Riedel, G.; Reymann, K. G. (1996): Metabotropic glutamate receptors in hippocampal long-term potentiation and learning and memory. In *Acta physiologica Scandinavica* 157 (1), pp. 1–19. DOI: 10.1046/j.1365-201X.1996.484231000.x.

Ring, Robert H.; Malberg, Jessica E.; Potestio, Lisa; Ping, Julia; Boikess, Steve; Luo, Bin et al. (2006): Anxiolytic-like activity of oxytocin in male mice: behavioral and autonomic evidence, therapeutic implications. In *Psychopharmacology* 185 (2), pp. 218–225. DOI: 10.1007/s00213-005-0293-z.

Risold, P. Y.; Swanson, L. W. (1997a): Chemoarchitecture of the rat lateral septal nucleus. In *Brain research. Brain research reviews* 24 (2-3), pp. 91–113. DOI: 10.1016/S0165-0173(97)00008-8.

Risold, P. Y.; Swanson, L. W. (1997b): Connections of the rat lateral septal complex. In *Brain research. Brain research reviews* 24 (2-3), pp. 115–195. DOI: 10.1016/S0165-0173(97)00009-X.

Rizzi-Wise, Candace A.; Wang, Dong V. (2021): Putting Together Pieces of the Lateral Septum: Multifaceted Functions and Its Neural Pathways. In *eNeuro* 8 (6). DOI: 10.1523/ENEURO.0315-21.2021.

Robertson, James M. (2014): Astrocytes and the evolution of the human brain. In *Medical hypotheses* 82 (2), pp. 236–239. DOI: 10.1016/j.mehy.2013.12.004.

Rodebaugh, Thomas L.; Holaway, Robert M.; Heimberg, Richard G. (2004): The treatment of social anxiety disorder. In *Clinical psychology review* 24 (7), pp. 883–908. DOI: 10.1016/j.cpr.2004.07.007.

Santabárbara, Javier; Lasheras, Isabel; Lipnicki, Darren M.; Bueno-Notivol, Juan; Pérez-Moreno, María; López-Antón, Raúl et al. (2021): Prevalence of anxiety in the COVID-19 pandemic: An updated meta-analysis of community-based studies. In *Progress in neuro-psychopharmacology & biological psychiatry* 109, p. 110207. DOI: 10.1016/j.pnpbp.2020.110207.

Sapolsky, R. M.; Romero, L. M.; Munck, A. U. (2000): How do glucocorticoids influence stress responses? Integrating permissive, suppressive, stimulatory, and preparative actions. In *Endocrine reviews* 21 (1), pp. 55–89. DOI: 10.1210/edrv.21.1.0389.

Sattler, R.; Rothstein, J. D. (2006): Regulation and dysregulation of glutamate transporters. In *Handbook of experimental pharmacology* (175), pp. 277–303. DOI: 10.1007/3-540-29784-7_14.

Scemes, Eliana; Spray, David C. (2012): Extracellular K^+ and astrocyte signaling via connexin and pannexin channels. In *Neurochemical research* 37 (11), pp. 2310–2316. DOI: 10.1007/s11064-012-0759-4.

Schiele, M. A.; Domschke, K. (2018): Epigenetics at the crossroads between genes, environment and resilience in anxiety disorders. In *Genes, brain, and behavior* 17 (3), e12423. DOI: 10.1111/gbb.12423.

Schneier, Franklin R. (2006): Clinical practice. Social anxiety disorder. In *The New England journal of medicine* 355 (10), pp. 1029–1036. DOI: 10.1056/NEJMcp060145.

Semyanov, Alexey; Henneberger, Christian; Agarwal, Amit (2020): Making sense of astrocytic calcium signals - from acquisition to interpretation. In *Nature reviews. Neuroscience* 21 (10), pp. 551–564. DOI: 10.1038/s41583-020-0361-8.

Shechner, Tomer; Hong, Melanie; Britton, Jennifer C.; Pine, Daniel S.; Fox, Nathan A. (2014): Fear conditioning and extinction across development: evidence from human studies and animal models. In *Biological psychology* 100, pp. 1–12. DOI: 10.1016/j.biopsycho.2014.04.001.

Sheehan, Teige; Numan, Michael: The Septal Region and Social Behavior. In, pp. 175–209.

Sheehan, Teige P.; Chambers, R. Andrew; Russell, David S. (2004): Regulation of affect by the lateral septum: implications for neuropsychiatry. In *Brain research. Brain research reviews* 46 (1), pp. 71–117. DOI: 10.1016/j.brainresrev.2004.04.009.

Shigetomi, Eiji; Koizumi, Schuichi (2023): The role of astrocytes in behaviors related to emotion and motivation. In *Neuroscience research* 187, pp. 21–39. DOI: 10.1016/j.neures.2022.09.015.

Shigetomi, Eiji; Patel, Sandip; Khakh, Baljit S. (2016): Probing the Complexities of Astrocyte Calcium Signaling. In *Trends in cell biology* 26 (4), pp. 300–312. DOI: 10.1016/j.tcb.2016.01.003.

Sierra-Mercado, Demetrio; Padilla-Coreano, Nancy; Quirk, Gregory J. (2011): Dissociable roles of prelimbic and infralimbic cortices, ventral hippocampus, and basolateral amygdala in the expression and extinction of conditioned fear. In *Neuropsychopharmacology : official publication of the American College of Neuropsychopharmacology* 36 (2), pp. 529–538. DOI: 10.1038/npp.2010.184.

Slattery, David A.; Uschold, Nicole; Magoni, Mauro; Bär, Julia; Popoli, Maurizio; Neumann, Inga D.; Reber, Stefan O. (2012): Behavioural consequences of two chronic psychosocial stress paradigms: anxiety without depression. In *Psychoneuroendocrinology* 37 (5), pp. 702–714. DOI: 10.1016/j.psyneuen.2011.09.002.

Smith, Caroline J. W.; Poehlmann, Max L.; Li, Sara; Ratnaseelan, Aarane M.; Bredewold, Remco; Veenema, Alexa H. (2017): Age and sex differences in oxytocin and vasopressin V1a receptor binding densities in the rat brain: focus on the social decision-making network. In *Brain structure & function* 222 (2), pp. 981–1006. DOI: 10.1007/s00429-016-1260-7.

Sofroniew, Michael V.; Vinters, Harry V. (2010): Astrocytes: biology and pathology. In *Acta neuropathologica* 119 (1), pp. 7–35. DOI: 10.1007/s00401-009-0619-8.

Somjen, G. G. (1988): Nervenkitt: notes on the history of the concept of neuroglia. In *Glia* 1 (1), pp. 2–9. DOI: 10.1002/glia.440010103.

Steenbergen, H. L.; Heinsbroek, R. P.; van Hest, A.; van de Poll, N. E. (1990): Sex-dependent effects of inescapable shock administration on shuttlebox-escape performance and elevated plus-maze behavior. In *Physiology & behavior* 48 (4), pp. 571–576. DOI: 10.1016/0031-9384(90)90302-K.

Stehberg, Jimmy; Moraga-Amaro, Rodrigo; Salazar, Christian; Becerra, Alvaro; Echeverría, Cesar; Orellana, Juan A. et al. (2012): Release of gliotransmitters through astroglial connexin 43 hemichannels is necessary for fear memory consolidation in the basolateral amygdala. In *FASEB journal : official publication of the Federation of American Societies for Experimental Biology* 26 (9), pp. 3649–3657. DOI: 10.1096/fj.11-198416.

Stein, Murray B.; Goldin, Philippe R.; Sareen, Jitender; Zorrilla, Lisa T. Eyler; Brown, Gregory G. (2002): Increased amygdala activation to angry and contemptuous faces in generalized social phobia. In *Archives of general psychiatry* 59 (11), pp. 1027–1034. DOI: 10.1001/archpsyc.59.11.1027.

Stein, Murray B.; Stein, Dan J. (2008): Social anxiety disorder. In *Lancet (London, England)* 371 (9618), pp. 1115–1125. DOI: 10.1016/S0140-6736(08)60488-2.

Steiner, Johann; Bernstein, Hans-Gert; Bielau, Hendrik; Berndt, Annika; Brisch, Ralf; Mawrin, Christian et al. (2007): Evidence for a wide extra-astrocytic distribution of S100B in human brain. In *BMC neuroscience* 8, p. 2. DOI: 10.1186/1471-2202-8-2.

Steinman, Michael Q.; Duque-Wilckens, Natalia; Trainor, Brian C. (2019): Complementary Neural Circuits for Divergent Effects of Oxytocin: Social Approach Versus Social Anxiety. In *Biological psychiatry* 85 (10), pp. 792–801. DOI: 10.1016/j.biopsych.2018.10.008.

Suadicani, S. O.; Flores, C. E.; Urban-Maldonado, M.; Beelitz, M.; Scemes, E. (2004): Gap junction channels coordinate the propagation of intercellular Ca2+ signals generated by P2Y receptor activation. In *Glia* 48 (3), pp. 217–229. DOI: 10.1002/glia.20071.

Sun, Jian-Dong; Liu, Yan; Yuan, Yu-He; Li, Jing; Chen, Nai-Hong (2012): Gap junction dysfunction in the prefrontal cortex induces depressive-like behaviors in rats. In *Neuropsychopharmacology : official publication of the American College of Neuropsychopharmacology* 37 (5), pp. 1305–1320. DOI: 10.1038/npp.2011.319.

Swanson, G. T.; Kamboj, S. K.; Cull-Candy, S. G. (1997): Single-channel properties of recombinant AMPA receptors depend on RNA editing, splice variation, and subunit composition. In *The Journal of neuroscience : the official journal of the Society for Neuroscience* 17 (1), pp. 58–69. DOI: 10.1523/JNEUROSCI.17-01-00058.1997.

Swanson, L. W.; Sawchenko, P. E.; Wiegand, S. J.; Price, J. L. (1980): Separate neurons in the paraventricular nucleus project to the median eminence and to the medulla or spinal cord. In *Brain research* 198 (1), pp. 190–195. DOI: 10.1016/0006-8993(80)90354-6.

Szuhany, Kristin L.; Simon, Naomi M. (2022): Anxiety Disorders: A Review. In *JAMA* 328 (24), pp. 2431–2445. DOI: 10.1001/jama.2022.22744.

Tafet, Gustavo E.; Nemeroff, Charles B. (2016): The Links Between Stress and Depression: Psychoneuroendocrinological, Genetic, and Environmental Interactions. In *The Journal of neuropsychiatry and clinical neurosciences* 28 (2), pp. 77–88. DOI: 10.1176/appi.neuropsych.15030053.

Tafet, Gustavo E.; Nemeroff, Charles B. (2020): Pharmacological Treatment of Anxiety Disorders: The Role of the HPA Axis. In *Frontiers in psychiatry* 11, p. 443. DOI: 10.3389/fpsyt.2020.00443.

Tanaka, K.; Watase, K.; Manabe, T.; Yamada, K.; Watanabe, M.; Takahashi, K. et al. (1997): Epilepsy and exacerbation of brain injury in mice lacking the glutamate transporter GLT-1. In *Science (New York, N.Y.)* 276 (5319), pp. 1699–1702. DOI: 10.1126/science.276.5319.1699.

Tang, F.; Lane, S.; Korsak, A.; Paton, J. F. R.; Gourine, A. V.; Kasparov, S.; Teschemacher, A. G. (2014): Lactate-mediated glia-neuronal signalling in the mammalian brain. In *Nature communications* 5, p. 3284. DOI: 10.1038/ncomms4284.

Taylor, Stephan F.; Liberzon, Israel (2007): Neural correlates of emotion regulation in psychopathology. In *Trends in cognitive sciences* 11 (10), pp. 413–418. DOI: 10.1016/j.tics.2007.08.006.

Taylor, Steven; Abramowitz, Jonathan S.; McKay, Dean (2012): Non-adherence and non-response in the treatment of anxiety disorders. In *Journal of anxiety disorders* 26 (5), pp. 583–589. DOI: 10.1016/j.janxdis.2012.02.010.

Theis, Martin; Giaume, Christian (2012): Connexin-based intercellular communication and astrocyte heterogeneity. In *Brain research* 1487, pp. 88–98. DOI: 10.1016/j.brainres.2012.06.045.

Theodosis, D. T.; Chapman, D. B.; Montagnese, C.; Poulain, D. A.; Morris, J. F. (1986a): Structural plasticity in the hypothalamic supraoptic nucleus at lactation affects oxytocin-, but not vasopressin-secreting neurones. In *Neuroscience* 17 (3), pp. 661–678. DOI: 10.1016/0306-4522(86)90038-2.

Theodosis, D. T.; Montagnese, C.; Rodriguez, F.; Vincent, J. D.; Poulain, D. A. (1986b): Oxytocin induces morphological plasticity in the adult hypothalamo-neurohypophysial system. In *Nature* 322 (6081), pp. 738–740. DOI: 10.1038/322738a0.

Theodosis, Dionysia T.; Poulain, Dominique A.; Oliet, Stéphane H. R. (2008): Activity-dependent structural and functional plasticity of astrocyte-neuron interactions. In *Physiological reviews* 88 (3), pp. 983–1008. DOI: 10.1152/physrev.00036.2007.

Thomas, Roji Philip (2014): CBT for Anxiety Disorders: A Practitioner Book - Gregoris Simos & Stefan G. Hofmann, Wiley-Blackwell, 2013, £29.99, pb, 268 pp. ISBN: 9780470975534. In *Psychiatr. Bull.* 38 (6), p. 312. DOI: 10.1192/pb.bp.113.044867.

Todd, Alison C.; Hardingham, Giles E. (2020): The Regulation of Astrocytic Glutamate Transporters in Health and Neurodegenerative Diseases. In *International journal of molecular sciences* 21 (24). DOI: 10.3390/ijms21249607.

Torres, Arnulfo; Wang, Fushun; Xu, Qiwu; Fujita, Takumi; Dobrowolski, Radoslaw; Willecke, Klaus et al. (2012): Extracellular Ca^{2+} acts as a mediator of communication from neurons to glia. In *Science signaling* 5 (208), ra8. DOI: 10.1126/scisignal.2002160.

Toth, Iulia; Neumann, Inga D. (2013): Animal models of social avoidance and social fear. In *Cell and tissue research* 354 (1), pp. 107–118. DOI: 10.1007/s00441-013-1636-4.

Toth, Iulia; Neumann, Inga D.; Slattery, David A. (2012): Social fear conditioning: a novel and specific animal model to study social anxiety disorder. In *Neuropsychopharmacology : official publication of the American College of Neuropsychopharmacology* 37 (6), pp. 1433–1443. DOI: 10.1038/npp.2011.329.

Toth, Iulia; Neumann, Inga D.; Slattery, David A. (2013): Social fear conditioning as an animal model of social anxiety disorder. In *Current protocols in neuroscience* Chapter 9, Unit9.42. DOI: 10.1002/0471142301.ns0942s63.

Trent, Natalie L.; Menard, Janet L. (2010): The ventral hippocampus and the lateral septum work in tandem to regulate rats' open-arm exploration in the elevated plus-maze. In *Physiology & behavior* 101 (1), pp. 141–152. DOI: 10.1016/j.physbeh.2010.04.035.

Ulrich-Lai, Yvonne M.; Herman, James P. (2009): Neural regulation of endocrine and autonomic stress responses. In *Nature reviews. Neuroscience* 10 (6), pp. 397–409. DOI: 10.1038/nrn2647.

Uschold-Schmidt, Nicole; Nyuyki, Kewir D.; Füchsl, Andrea M.; Neumann, Inga D.; Reber, Stefan O. (2012): Chronic psychosocial stress results in sensitization of the HPA axis to acute heterotypic stressors despite a reduction of adrenal in vitro ACTH responsiveness. In *Psychoneuroendocrinology* 37 (10), pp. 1676–1687. DOI: 10.1016/j.psyneuen.2012.02.015.

van den Burg, Erwin H.; Stindl, Julia; Grund, Thomas; Neumann, Inga D.; Strauss, Olaf (2015): Oxytocin Stimulates Extracellular Ca2+ Influx Through TRPV2 Channels in Hypothalamic Neurons to Exert Its Anxiolytic Effects. In *Neuropsychopharmacology : official publication of the American College of Neuropsychopharmacology* 40 (13), pp. 2938–2947. DOI: 10.1038/npp.2015.147.

van Haaren, F.; van Hest, A.; Heinsbroek, R. P. (1990): Behavioral differences between male and female rats: effects of gonadal hormones on learning and memory. In *Neuroscience and biobehavioral reviews* 14 (1), pp. 23–33. DOI: 10.1016/S0149-7634(05)80157-5.

Vasile, Flora; Dossi, Elena; Rouach, Nathalie (2017): Human astrocytes: structure and functions in the healthy brain. In *Brain structure & function* 222 (5), pp. 2017–2029. DOI: 10.1007/s00429-017-1383-5.

Velasco, E. R.; Florido, A.; Milad, M. R.; Andero, R. (2019): Sex differences in fear extinction. In *Neuroscience and biobehavioral reviews* 103, pp. 81–108. DOI: 10.1016/j.neubiorev.2019.05.020.

Verkhratsky, A. (2007): Calcium and cell death. In *Sub-cellular biochemistry* 45, pp. 465–480. DOI: 10.1007/978-1-4020-6191-2_17.

Verkhratsky, Alexei; Ho, Margaret S.; Parpura, Vladimir (2019): Evolution of Neuroglia. In *Advances in experimental medicine and biology* 1175, pp. 15–44. DOI: 10.1007/978-981-13-9913-8_2.

Verkhratsky, Alexei; Nedergaard, Maiken (2016): The homeostatic astroglia emerges from evolutionary specialization of neural cells. In *Philosophical transactions of the Royal Society of London. Series B, Biological sciences* 371 (1700). DOI: 10.1098/rstb.2015.0428.

Verkhratsky, Alexei; Nedergaard, Maiken (2018): Physiology of Astroglia. In *Physiological reviews* 98 (1), pp. 239–389. DOI: 10.1152/physrev.00042.2016.

Verkhratsky, Alexei; Parpura, Vladimir; Li, Baoman; Scuderi, Caterina (2021): Astrocytes: The Housekeepers and Guardians of the CNS. In *Advances in neurobiology* 26, pp. 21–53. DOI: 10.1007/978-3-030-77375-5_2.

Verkhratsky, Alexei; Untiet, Verena; Rose, Christine R. (2020): Ionic signalling in astroglia beyond calcium. In *The Journal of physiology* 598 (9), pp. 1655–1670. DOI: 10.1113/JP277478.

Volterra, Andrea; Meldolesi, Jacopo (2005): Astrocytes, from brain glue to communication elements: the revolution continues. In *Nature reviews. Neuroscience* 6 (8), pp. 626–640. DOI: 10.1038/nrn1722.

Vries, Geert J. de; Rissman, Emilie F.; Simerly, Richard B.; Yang, Liang-Yo; Scordalakes, Elka M.; Auger, Catherine J. et al. (2002): A model system for study of sex chromosome effects on sexually dimorphic neural and behavioral traits. In *The Journal of neuroscience : the official journal of the Society for Neuroscience* 22 (20), pp. 9005–9014. DOI: 10.1523/JNEUROSCI.22-20-09005.2002.

Wahis, Jérôme; Baudon, Angel; Althammer, Ferdinand; Kerspern, Damien; Goyon, Stéphanie; Hagiwara, Daisuke et al. (2021): Astrocytes mediate the effect of oxytocin in the central amygdala on neuronal activity and affective states in rodents. In *Nature neuroscience* 24 (4), pp. 529–541. DOI: 10.1038/s41593-021-00800-0.

Waldherr, Martin; Neumann, Inga D. (2007): Centrally released oxytocin mediates mating-induced anxiolysis in male rats. In *Proceedings of the National Academy of Sciences of the United States of America* 104 (42), pp. 16681–16684. DOI: 10.1073/pnas.0705860104.

Waldherr, Martin; Nyuyki, Kewir; Maloumby, Rodrigue; Bosch, Oliver J.; Neumann, Inga D. (2010): Attenuation of the neuronal stress responsiveness and corticotrophin releasing hormone synthesis after sexual activity in male rats. In *Hormones and behavior* 57 (2), pp. 222–229. DOI: 10.1016/j.yhbeh.2009.11.006.

Wang, Ping; Wang, Stephani C.; Li, Dongyang; Li, Tong; Yang, Hai-Peng; Wang, Liwei et al. (2019): Role of Connexin 36 in Autoregulation of Oxytocin Neuronal Activity in Rat Supraoptic Nucleus. In *ASN neuro* 11, 1759091419843762. DOI: 10.1177/1759091419843762.

Wang, Yu-Feng; Hatton, Glenn I. (2006): Mechanisms underlying oxytocin-induced excitation of supraoptic neurons: prostaglandin mediation of actin polymerization. In *Journal of neurophysiology* 95 (6), pp. 3933–3947. DOI: 10.1152/jn.01267.2005.

Wang, Yu-Feng; Hatton, Glenn I. (2007): Dominant role of betagamma subunits of G-proteins in oxytocin-evoked burst firing. In *The Journal of neuroscience : the official journal of the Society for Neuroscience* 27 (8), pp. 1902–1912. DOI: 10.1523/JNEUROSCI.5346-06.2007.

Wang, Yu-Feng; Hatton, Glenn I. (2009): Astrocytic plasticity and patterned oxytocin neuronal activity: dynamic interactions. In *The Journal of neuroscience : the official journal of the Society for Neuroscience* 29 (6), pp. 1743–1754. DOI: 10.1523/JNEUROSCI.4669-08.2009.

Watase, K.; Hashimoto, K.; Kano, M.; Yamada, K.; Watanabe, M.; Inoue, Y. et al. (1998): Motor discoordination and increased susceptibility to cerebellar injury in GLAST mutant mice. In *The European journal of neuroscience* 10 (3), pp. 976–988. DOI: 10.1046/j.1460-9568.1998.00108.x.

Weiss, Shirley; Clamon, Lauren C.; Manoim, Julia E.; Ormerod, Kiel G.; Parnas, Moshe; Littleton, J. Troy (2022): Glial ER and GAP junction mediated Ca2+ waves are crucial to maintain normal brain excitability. In *Glia* 70 (1), pp. 123–144. DOI: 10.1002/glia.24092.

Wied, d. de (1965): The influence of the posterior and intermediate lobe of the pituitary and pituitary peptides on the maintenance of a conditioned avoidance response in rats. In *International journal of neuropharmacology* 4, pp. 157–167. DOI: 10.1016/0028-3908(65)90005-5.

Williams, Alexia V.; Duque-Wilckens, Natalia; Ramos-Maciel, Stephanie; Campi, Katharine L.; Bhela, Shanu K.; Xu, Christine K. et al. (2020): Social approach and social vigilance are differentially regulated by oxytocin receptors in the nucleus accumbens. In *Neuropsychopharmacology : official publication of the American College of Neuropsychopharmacology* 45 (9), pp. 1423–1430. DOI: 10.1038/s41386-020-0657-4.

Williams, Alexia V.; Laman-Maharg, Abigail; Armstrong, Crystal V.; Ramos-Maciel, Stephanie; Minie, Vanessa A.; Trainor, Brian C. (2018): Acute inhibition of kappa opioid receptors before stress blocks depression-like behaviors in California mice. In *Progress in neuro-psychopharmacology & biological psychiatry* 86, pp. 166–174. DOI: 10.1016/j.pnpbp.2018.06.001.

Williams, Susan M.; Sullivan, Robert K. P.; Scott, Heather L.; Finkelstein, David I.; Colditz, Paul B.; Lingwood, Barbara E. et al. (2005): Glial glutamate transporter expression patterns in brains from multiple mammalian species. In *Glia* 49 (4), pp. 520–541. DOI: 10.1002/glia.20139.

Willner, P. (1984): The validity of animal models of depression. In *Psychopharmacology* 83 (1), pp. 1–16. DOI: 10.1007/BF00427414.

Wirtshafter, Hannah S.; Wilson, Matthew A. (2021): Lateral septum as a nexus for mood, motivation, and movement. In *Neuroscience and biobehavioral reviews* 126, pp. 544–559. DOI: 10.1016/j.neubiorev.2021.03.029.

Wong, Li Chin; Wang, Li; D'Amour, James A.; Yumita, Tomohiro; Chen, Genghe; Yamaguchi, Takashi et al. (2016): Effective Modulation of Male Aggression through Lateral Septum to

Medial Hypothalamus Projection. In *Current biology : CB* 26 (5), pp. 593–604. DOI: 10.1016/j.cub.2015.12.065.

Woolley, C. S. (1998): Estrogen-mediated structural and functional synaptic plasticity in the female rat hippocampus. In *Hormones and behavior* 34 (2), pp. 140–148. DOI: 10.1006/hbeh.1998.1466.

Xu, Haifeng; Liu, Ling; Tian, Yuanyuan; Wang, Jun; Li, Jie; Zheng, Junqiang et al. (2019): A Disinhibitory Microcircuit Mediates Conditioned Social Fear in the Prefrontal Cortex. In *Neuron* 102 (3), 668-682.e5. DOI: 10.1016/j.neuron.2019.02.026.

Yoon, Bo-Eun; Lee, C. Justin (2014): GABA as a rising gliotransmitter. In *Frontiers in neural circuits* 8, p. 141. DOI: 10.3389/fncir.2014.00141.

Zeug, Andre; Müller, Franziska E.; Anders, Stefanie; Herde, Michel K.; Minge, Daniel; Ponimaskin, Evgeni; Henneberger, Christian (2018): Control of astrocyte morphology by Rho GTPases. In *Brain research bulletin* 136, pp. 44–53. DOI: 10.1016/j.brainresbull.2017.05.003.

Zhang, Anao; Borhneimer, Lindsay A.; Weaver, Addie; Franklin, Cynthia; Hai, Audrey Hang; Guz, Samantha; Shen, Li (2019): Cognitive behavioral therapy for primary care depression and anxiety: a secondary meta-analytic review using robust variance estimation in meta-regression. In *Journal of behavioral medicine* 42 (6), pp. 1117–1141. DOI: 10.1007/s10865-019-00046-z.

Zhang, Ariel Y.; Elias, Elias; Manners, Melissa T. (2024): Sex-dependent astrocyte reactivity: Unveiling chronic stress-induced morphological changes across multiple brain regions. In *Neurobiology of disease* 200, p. 106610. DOI: 10.1016/j.nbd.2024.106610.

Zhang, Lili; Blackman, Brigitte E.; Schonemann, Marcus D.; Zogovic-Kapsalis, Tatjana; Pan, Xiaoyu; Tagliaferri, Mary et al. (2010): Estrogen receptor beta-selective agonists stimulate calcium oscillations in human and mouse embryonic stem cell-derived neurons. In *PloS one* 5 (7), e11791. DOI: 10.1371/journal.pone.0011791.

Zhang, Meng; Wang, Zhen-Zhen; Chen, Nai-Hong (2023): Connexin 43 Phosphorylation: Implications in Multiple Diseases. In *Molecules (Basel, Switzerland)* 28 (13). DOI: 10.3390/molecules28134914.

Zhao, Changjiu; Eisinger, Brian; Gammie, Stephen C. (2013): Characterization of GABAergic neurons in the mouse lateral septum: a double fluorescence in situ hybridization and immunohistochemical study using tyramide signal amplification. In *PloS one* 8 (8), e73750. DOI: 10.1371/journal.pone.0073750.

Zhou, Xinyi; Xiao, Qian; Xie, Li; Yang, Fan; Wang, Liping; Tu, Jie (2019): Astrocyte, a Promising Target for Mood Disorder Interventions. In *Frontiers in molecular neuroscience* 12, p. 136. DOI: 10.3389/fnmol.2019.00136.

Zlokovic, Berislav V. (2008): The blood-brain barrier in health and chronic neurodegenerative disorders. In *Neuron* 57 (2), pp. 178–201. DOI: 10.1016/j.neuron.2008.01.003.

Zoicas, Iulia; Slattery, David A.; Neumann, Inga D. (2014): Brain oxytocin in social fear conditioning and its extinction: involvement of the lateral septum. In *Neuropsychopharmacology : official publication of the American College of Neuropsychopharmacology* 39 (13), pp. 3027–3035. DOI: 10.1038/npp.2014.156.

Zuloaga, Damian G.; Zuloaga, Kristen L.; Hinds, Laura R.; Carbone, David L.; Handa, Robert J. (2014): Estrogen receptor β expression in the mouse forebrain: age and sex differences. In *The Journal of comparative neurology* 522 (2), pp. 358–371. DOI: 10.1002/cne.23400.